THE USE OF ORGANOTELLURIUM HETEROCYCLES AS PRECURSORS FOR NOVEL ORGANOMETALLIC COMPOUNDS

by

KARANBIR BADYAL

A thesis submitted for the degree of

Doctor of Philosophy

at

The University of Aston in Birmingham

September 1996

THE USE OF ORGANOTELLURIUM HETEROCYCLES AS PRECURSORS FOR NOVEL ORGANOMETALLIC COMPOUNDS

by
Karanbir Badyal

A thesis submitted for the degree of Doctor of Philosophy, September 1996
The University of Aston in Birmingham

Summary

The reactions of group 16 heterocycles with organometallic reagents are described. Thiophenes have been used as models for organic sulfur in coal and their reactivity towards triiron dodecacarbonyl has been investigated. Reaction of unsubstituted thiophene with $Fe_3(CO)_{12}$ results in desulfurisation of the heterocycle, with the organic fragment being recovered in the form of the ferrole, $C_4H_4.Fe_2(CO)_6$. In addition a novel organometallic compound of iron is isolated, the formula of which is shown to be $C_4H_4.Fe_3(CO)_8$. Benzothiophene reacts with $Fe_3(CO)_{12}$ to yield benzothiaferrole, $C_8H_6S.Fe_2(CO)_6$, in which the sulfur is retained in the heterocycle. Dibenzothiophene, a more accurate model for organic sulfur in coal, displays no reactivity towards the iron carbonyl, suggesting that the more condensed systems will desulfurise less readily. Microwave methodology has been successful in accelerating the reactions of thiophenes with $Fe_3(CO)_{12}$. However, reaction of benzothiophene does not proceed to the desulfurisation stage while dibenzothiophene is unreactive even under microwave conditions.

Tellurophenes (Te analogues of thiophenes) are shown to mimic the behaviour of thiophenes towards certain organometallic reagents with the advantage that their greater reactivity enables recovery of products in higher yields. Hence, reaction of tellurophene with $Fe_3(CO)_{12}$ again affords the ferrole but with an almost ten-fold increase in yield over thiophene. More significantly, dibenzotellurophene is also detellurated by the iron carbonyl affording the previously inaccessible dibenzoferrole, $C_{12}H_8.Fe_2(CO)_6$, thereby demonstrating the mechanistic feasibility of dechalcogenation of the more condensed aromatic molecules. The potential of tellurium heterocycles to act as precursors for novel organometallics is also recognised owing to the relatively facile elimination of the heteroatom from these systems. Thus, 2-telluraindane reacts with $Fe_3(CO)_{12}$ to yield a novel organometallic compound of formula $C_{16}H_{16}.Fe(CO)_3$, arising from the unsymmetric dimerisation of two organic fragments.

The inclusion of nitrogen in tellurium heterocycles provides access to an entirely new area of organometallic chemistry. The reaction of benzisotellurazole with $Fe_3(CO)_{12}$ gives rise to a symmetrical dimer of formula $(C_7H_5NTe)_2.Fe_3(CO)_7$, the x-ray crystal structure of which, shows the central Fe to be in a unique seven coordinate environment involving bonds to both Te and N. 2-methylbenzotellurazole in which the N is not adjacent to Te is, in contrast to benzisotellurazole, detellurated upon treatment with $Fe_3(CO)_{12}$ affording two novel iron organometallics; $C_8H_7N.Fe_2(CO)_6$ and $C_8H_7N.Fe3(CO)_{10}$. The former has a structure comparable to the previously reported ferrole while the crystal structure of the latter displays some unprecedented features, of particular note being the fact that the three Fe atoms possess six, seven and eight-fold coordination environments.

A further advantage enjoyed by tellurium heterocycles over their sulfur analogues is the availability of ^{125}Te NMR spectroscopy for following their reactions with organometallic reagents. This technique has been particularly useful in studying the reactions of tellurophenes with $[Cp^*RhCl_2]_2$. It has emerged that the mode of coordination of tellurophenes to rhodium can be established by observation of chemical shifts and, more importantly, the ^{125}Te-^{103}Rh spin-spin coupling constants. Hence η^5-coordination of the heterocycle to rhodium, in which a relatively weak π-interaction between Te and Rh exists, gives a much smaller coupling constant than that observed for η^1-coordination where a strong σ-bond is present. Furthermore, rhodium is effective in activating the heterocycles towards detelluration, achieved by further treatment with $Fe_3(CO)_{12}$. In the case of dibenzotellurophene a diverse range of products is obtained including some novel organorhodium complexes.

Key words: desulfurisation, tellurophenes, triiron dodecacarbonyl, pentamethylcyclopenatadienyl dichloride rhodium dimer

Acknowledgements

I would like to express my sincere gratitude to Professor W. R. McWhinnie for his supervision, encouragement and unfailing interest throughout the course of this work and his helpful remarks during the writing of this thesis.

I am grateful to Dr. T. A. Hamor (School of Chemistry, University of Birmingham) for his collaboration and valuable discussions in X-ray crystallography work. I also acknowledge with thanks, Dr. M. Perry (Department of Chemical Engineering & Applied Chemistry, University of Aston) for recording NMR spectra and members of the technical staff for the services rendered to me.

I thank Dr. P. Monsef-Mirzai for sharing her knowledge on aspects of Coal Science and all colleagues in the laboratory for their good company and co-operation.

I am also most grateful to every member of my family for their support throughout my studies.

Finally, I am grateful to EPSRC for the funding of this project.

LIST OF CONTENTS

LIST OF TABLES

LIST OF FIGURES

LIST OF SCHEMES

LIST OF ABBREVIATIONS

T	Thiophene
TMT	Tetramethylthiophene
THT	Tetrahydrothiophene
BT	Benzothiophene
DBT	Dibenzothiophene
HDS	Hydrodesulfurisation
Me	CH_3
Et	C_2H_5
n-Bu	n-C_4H_9
Ph	C_6H_5
R	Alkyl
Ar	Aryl
L	Ligand
M	Metal
THF	Tetrahydrofuran
dbte	Dibenzotellurophene
cod	1,5-cyclooctadiene
bipy	2,2-bipyridyl
diphos	1,2-bis(diphenylphosphino)ethane
Cp	Cyclopentadienyl, η^5-C_5H_5
Cp^*	Pentamethylcyclopentadienyl, η^5-C_5Me_5
OTf	Triflate, $CF_3OSO_2^-$
TLC	Thin Layer Chromatography
FT	Fourier Transform
IR	Infrared
NMR	Nuclear Magnetic Resonance
XPS	X-ray Photoelectron Spectroscopy
ESCA	Electron Spectroscopy for Chemical Analysis
EI-MS	Electron Impact Mass Spectrometry
FAB-MS	Fast Atom Bombardment Mass Spectrometry
NOBA	Nitrobenzyl Alcohol

CHAPTER 1

INTRODUCTION

INTRODUCTION

1.1 THE NEED FOR DESULFURISATION OF FOSSIL FUELS

Coal contains organic and inorganic sulfur and both forms contribute to the well documented and politically sensitive environmental issues when coal is combusted.

Concern over the extent of environmental damage that may be caused by acid deposition has prompted massive research programmes into the formation of sulfur dioxide and into the nature and cause of environmental damage attributed to it. It has also resulted in many governments passing regulations for the reduction of sulfur dioxide (and nitrogen oxides) emissions from both new and existing plants.

1.2 METHODS FOR REDUCTION OF SULFUR DIOXIDE EMISSIONS

Sulfur dioxide emissions can be reduced by the removal of sulfur from coal prior to combustion, by the removal of sulfur dioxide during the combustion process, or from flue gases after combustion.

1.2.1 Sulfur dioxide removal during combustion

Sulfur dioxide removal during combustion[1] involves the injection of dry alkali, usually slaked lime or limestone, into the hot boiler gases where it can react with sulfur oxides and is then removed after reaction. The problems associated with this process are that the maximum removal efficiency is unlikely to be greater than ~ 40% with a required limestone : sulfur stoichiometry of ~ 2. This means that large amounts of limestone would need to be imported into a station and large quantities of residual calcined reagent mixed with fly ash would need to be disposed of. Such a process would therefore not be very economically competitive for large stations.

1.2.2 Flue gas desulfurisation

Flue gas desulfurisation processes[2] involve the use of scrubbing systems that use lime or limestone to neutralise the sulfur dioxide and are capable of removing 90% or more of the released sulfur dioxide. The problems associated with this process are that it is relatively expensive as careful maintenance of scrubbers is required to prevent catastrophic scaling in the absorbers and also the disposal of the resulting reaction products (calcium sulfate / sulfite) leads to the build up of waste in disused land sites. However, research is ongoing in flue gas desulfurisation to improve efficiency of the scrubbers and also to create marketable reaction products e.g. gypsum (calcium sulfate dihydrate) which is useful in the building business.

Due to the problems associated with sulfur dioxide removal there is currently a lot of activity in research into the removal of sulfur from coal prior to combustion.

1.3 REMOVAL OF SULFUR FROM COAL

1.3.1 Coal structure

Coal is a highly heterogeneous solid originating from plant substance. It contains in varying amounts, essentially all the elements in the periodic table combined into nearly all of the minerals normally encountered in the earth's crust.

The organic matrix may be characterised as a cross-linked polymer and can also be viewed as an organic chemical substance containing classical organic functional groups e.g. mainly carbonyl and hydroxyl, aromatic and heterocyclic ring units and aliphatic bridges.

Inorganic coal structure comprises the minerals component of coal which is intimately associated with the organic matrix. This consists essentially of shale, kaolin, sulfides, carbonates and chlorides. The remainder of the inorganic material in coal consists of

ash (oxides of the minerals) which is mainly SiO_2, Al_2O_3, Fe_2O_3, CaO, MgO, TiO_2, Na_2O, K_2O, SO_3.

1.3.2 Occurrence of sulfur in coal

The total sulfur content in coal can be as much as 6%.[3]

Inorganic sulfur is mainly pyrite (FeS_2) with small amounts of sulfates and comprises between 0 to 4 % of the total sulfur content.

Organic sulfur is that which is intimately bound to the organic coal matrix and consists mainly of:
mercaptans or thiols (-SH) - alkyl, cyclic, aromatic
thioethers and dithioethers (-SR and -SSR) - alkyl, cyclic, alkyl-cycloalkyl
thiophenic - aromatic ring sulfur as exemplified by the thiophene, benzothiophene and dibenzothiophene systems.
Organic sulfur comprises between 0.3 to 4% of the total sulfur content.

1.3.3 Chemical desulfurisation methods

The number of desulfurisation chemicals is so large that some criteria must be established for evaluating promising chemical desulfurisation approaches for further investigation. The selected criteria may include the following important considerations:

(i) The reagent must be highly selective to either the pyritic (FeS_2) or organic sulfur content of coal (or both) and not significantly reactive with other coal components i.e. the coal matrix and hence calorific value should be retained.

(ii) The reagent must be rapid, cheap and regenerable.

(iii) The reagent should be either soluble or volatile in both its unreacted and reacted forms so that it can be near totally recovered from the coal matrix.

(iv) The system must operate at low(ish) temperature and pressure to avoid decomposition of the coal and also keep operating costs low.

1.3.3.1 Determination of sulfur in coal

The sulfur content in coal is determined by the British Standard (BS)[4] method or the American Standard (ASTM)[6] method both in which a hydrochloric acid extraction is used to determine sulfate sulfur and a nitric acid extraction method is used to determine pyritic sulfur. Alternative low-temperature and high-temperature methods are suggested in the BS[5] and ASTM[7] standards to determine the total sulfur in coal. Organic sulfur in the standards is then determined by difference. Elemental sulfur, which would be accounted for as "organic sulfur", has been mentioned only in a few references in the literature.[8]

1.3.3.2 Removal of inorganic sulfur

Inorganic sulfur is removed relatively easily and many methods have been reported in the literature. The reactions of the oxidants hydrogen peroxide, nitric acid, sulfuric acid and sodium hypochlorite have all been reported to effectively remove the inorganic sulfur from coals[9], giving varying mixtures of Fe^{2+}, Fe^{3+}, S and SO_4^{2-}. Caustic treatment is also well known[10] and oxidisative leaching is a common method of pyrite removal[11] e.g. via chlorinolysis in organic solvents, which requires the removal of chlorine at the end of the process. In both treatments the end product is SO_4^{2-}.

1.3.3.3 Removal of organic sulfur

Organic sulfur is more resistant to removal by chemical methods due to strong C-S bonds (see Table 1.1) in the coal matrix. A recent review in the literature has shown[12] that approximately 40-50% of organic sulfur can be removed from Chinese coals by

caustic treatment in methanolic or aqueous solutions at 350°C. Furthermore, it was shown that the stability of organic sulfur in coal could be roughly grouped as follows:

(i) Easily decomposed organic sulfur such as -SH, -SR and -SSR which are linked with aliphatic structure.

(ii) Relatively difficult decomposed organic sulfur such as -SH and -SR which are directly linked with aromatic rings.

(iii) Most difficult decomposed organic sulfur such as thiophenic sulfur.

Other reported methods of organic sulfur removal include solvent extraction[13] using trichloroethane and microbial desulfurisation using the micro-organisms *Thiobacillus thioxidans* [14] or *Thiobacillus ferrooxidans*[15] which obtain energy from oxidising the sulfur in coal. The downside with biological removal of sulfur is the large amount of time that is required to effect the desulfurisation. The chemical methods to remove organic sulfur that have so far been studied are too expensive and generally alter the coal characteristics. Hence, there is a need for a simple coal desulfurisation process which can satisfy the previously outlined criteria.

1.4 HYDRODESULFURISATION OF FOSSIL FUELS

Hydrodesulfurisation (HDS) of heavy crude oils and coal derived liquids is one of the most important catalytic processes in the petroleum refining industry. Sulfur is contained in these feedstocks in thiophene or thiophene derivatives such as benzothiophene or dibenzothiophene, and during HDS, sulfur is removed when the feedstock is passed at high temperature and hydrogen pressure over a transition metal sulfide catalyst. The actual industrial catalyst systems are quite complex (e.g. sulfided Co/Mo or Ni/Mo supported on Al_2O_3) and in spite of extensive research our knowledge of the mechanism of HDS remains quite limited. Understanding the HDS process requires a better understanding of how thiophenic molecules interact with, and are activated by transition metal centres.

1.5 MODEL COMPOUNDS FOR SULFUR IN COAL

Since thiophenic type organic sulfur is the most difficult to remove from coal, this work has concentrated on looking at the potential of certain organometallic reagents to desulfurise *model compounds* that best represent sulfur in an heterocyclic environment in coal. These models include:

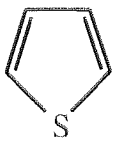

(I)

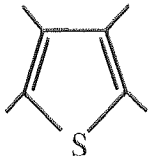

(II)

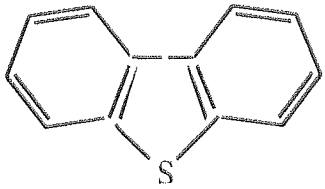

(III)

The latter two, more substituted heterocycles, provide better coal models.

1.5.1 Occurrence of thiophenes

Thiophenes are well known for their occurrence in fossil fuels[16] and thiophene itself was first discovered as an impurity in coal derived benzene. Benzo- and dibenzothiophenes are especially common in higher boiling fractions of petroleum. Thiophenes in fossil fuels arise by the action of elemental sulfur on hydrocarbons.

1.5.2 Properties of thiophenes

Thiophenes behave as aromatic compounds with respect to their structures, physical properties and reactivity. The coordinating properties of thiophenes are closer to arenes, not thioethers. In comparison to benzene, thiophene is somewhat more nucleophilic as suggested by its ionisation potential of 8.9 versus 9.3 eV for benzene. Ab initio calculations indicate accumulation of negative charge on the 2,5-carbon atoms and positive charge on sulfur. Hence, protonation and many other electrophilic reactions occur at the 2,5-carbon positions.

1.5.3 Coordination chemistry of thiophenes

Most publications on the interactions of thiophenes and transition metals deal with the heterogeneously catalysed hydrodesulfurisation of thiophenes. The elucidation of the mechanisms of such desulfurisation processes provides the impetus for much of the current work on thiophene complexes. With this motivation, a number of metal thiophene complexes have been synthesised and characterised in recent years, and several different bonding modes of thiophenic ligands have been identified. These modes (Figure 1.1) include η^5-bound, where thiophene binds much like the cyclopentadienyl (Cp^-) ligand, η^1(S)-bound, in which thiophene binds through the heteroatom only, η^4-bound, where the ring sulfur bends well out of the plane of the ring carbon atoms so that binding to the metal involves only the four ring carbon atoms, and a ring-opened form where a transition metal has inserted into a C-S bond of the thiophene ring. The attachment of thiophenes to metallic catalysts via sulfur is believed to be the first step in catalytic desulfurisation of coal.[17]

Figure 1.1

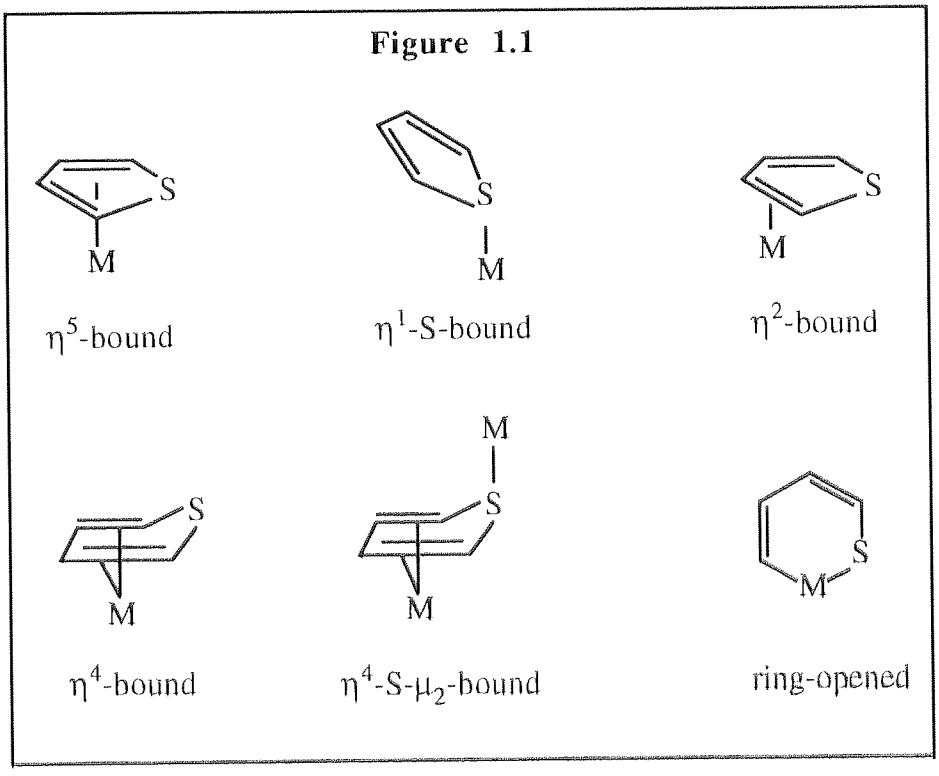

Figure 1.1 Common modes of binding of thiophene with transititon metals

1.5.3.1 η^1,S-Thiophene complexes

Until recently, few η^1(S)-bound thiophenic ligands were known in which thiophene acts as a two electron donor. The most general synthetic strategy involves the reaction of thiophene with "soft" $16e^-$ metal electrophiles, particularly those of the type $(C_5R_5)ML_2$. For example, $Cp^*Re(CO)_2(thf)$ reacts with simple thiophenes to give S-bound $Cp^*Re(CO)_2(C_4H_{4-x}Me_xS)$, as yellow air-stable solids[18] (where $Cp^* = \eta^5$-C_5Me_5).

By using $[CpFe(CO)_2(thf)]^+$, referred to as $Fp(thf)^+$, Kuhn et al[19] obtained an unstable red oil analysing as $[Fp(\eta^1\text{-}C_4H_4S)]BF_4$ while Selegue and co-workers[20] employed $[Fp(isobutene)]^+$ for the synthesis of $Fp(S\text{-ligand})^+$ complexes.

More recently, Angelici and Benson[21] carried out a kinetic study on the rate of displacement of η^1-coordinated thiophene ligands from a ruthenium complex (Eq. 1.1).

$$CpRu(CO)(PPh_3)(\eta^1(S)\text{-Th})^+ + L' \underset{CD_2Cl_2}{\overset{25^oC}{\rightleftharpoons}} CpRu(CO)(PPh_3)(L')^+ + Th$$

Eq. 1.1

It was noted that the equilibrium constant (K') increased in the following order: T (1.00) < 2,5-Me_2T (2.76) < 2-MeT (4.11) < 3-MeT (6.30) < BT (29.9) < Me_4T (57.4) < DBT (74.1) « THT (> 7.1 x 10^6). Thus, by comparison with THT (tetrahydrothiophene), all the thiophene ligands are weakly coordinating, thiophene being the most weakly binding. The addition of a methyl group increases the coordinating ability of thiophene; the electron releasing groups making the sulfur a stronger σ donor.

An alternative mode of η1–coordination has been demonstrated whereby the thiophene binds to the transition metal via a carbon rather than a sulfur atom. The ligand is then known as a σ- thienyl ligand, $C_4R_4S^-$, which reacts with electrophillic reagents. Recent mononuclear chemistry by Angelici[22], Jones[23] and co-workers has focused on the potential of the σ-2-thienyl ligand as an entry point to ring opening reactions, while Chisolm et al[24] have reported the stepwise activation of σ-thienyl ligands at di-tungsten centres.

1.5.3.2 η^5-Thiophene complexes

In the η^5 binding mode, thiophene can be viewed as a formal six-electron donor and numerous η^5-T complexes can be found in the literature. Virtually all known π-thiophene complexes are precedented by analogous arene complexes and η^5 binding of thiophene to a transition metal can readily be compared to η^5 binding in Cp^-.

The first transition metal thiophene complex, $Cr(T)(CO)_3$, was obtained in 1958 by Fischer[25] in low yields, from the thermal reaction of thiophene and $Cr(CO)_6$.

$$Cr(CO)_6 + C_4H_4S \xrightarrow{\Delta} Cr(\eta^5\text{-}C_4H_4S)(CO)_3 + 3CO \qquad \textbf{Eq. 1.2}$$

The isoelectronic relationship between $Cr(CO)_3$ and $Mn(CO)_3^+$ fragments was exploited by Singer[26] in his synthesis of $[Mn(\eta^5\text{-}C_4R_4S)(CO)_3]^+$ and has since led to the development of an extended range of thiophene π complexes. Hence, iron[27], ruthenium[28], rhodium and iridium[29] all form η^5-complexes with certain thiophenes, especially tetramethylthiophene in which the poor nucleophilicity of thiophene is improved by strong donor substituents to facilitate π complexation of the heterocycle.

1.5.3.3 η^2-Thiophene complexes

Generally, η^2-thiophene complexes are observed only for $16e^-$ metal centres that are exceptional π donors and which have only one coordination site available for ligand bonding.

The magnesium reduction of $[Os(NH_3)_5OTf](OTf)_2$ in the presence of thiophene gave $[Os(NH_3)_5(T)](OTf)_2$.[30] The ^1H NMR spectrum of this complex showed four doublets of doublets as expected for η^2 binding, (Eq. 1.3). These data did not, however, distinguish η^2 binding from the ring-opened isomer.

$$[Os^{III}(NH_3)_5(OTf)]^{2+} \xrightarrow{+1e^-,\ C_4H_4S} [Os^{II}(NH_3)_5(\eta^2\text{-}C_4H_4S)]^{2+} \qquad \text{Eq. 1.3}$$

The ring-opened isomer is by far the most common form of η^2 coordination of transition metals to thiophenes and several examples of insertion of iron[31,53], rhodium[32] and iridium[33] into the heterocycle have appeared in the literature.

1.5.3.4 η^4-Thiophene complexes

In η^4 bound complexes the thiophene acts as a four electron donor. The most common synthetic procedure involves a two-electron reduction of 18 electron η^5-thiophene complexes.

The first evidence for η^4-thiophene complexes arose from the studies of Huckett and Angelici[34] who observed that $[Cp^*Ir(\eta^5\text{-}C_4R_4S)]^{2+}$ reduced with 2M equivalents of $NaBHEt_3$. The unstable reduction product could also be prepared by using Cp_2Co as the reducing agent.

The 2e⁻ reduction of $[Cp^*M(\eta^5\text{-}C_4R_4S)]^{2+}$, where M = Rh[35] or Ir[36] resulted in major spectroscopic and geometric changes. The ^{13}C NMR shifts for the 2,5 ring carbon atoms moved ca. 50 ppm upfield upon reduction of the η^5 precursor. Crystallographic studies showed that the thiophene ring in $[Cp^*Rh(\eta^4\text{-TMT})]$ and $[Cp^*Ir(\eta^4\text{-2,5-}Me_2T)]$ was folded along the C2-C5 axis with long M-S distances of ~ 2.96Å.

Salts of the type $[Cp^*Ir(\eta^5\text{-}C_4R_4S)]^{2+}$ underwent 2e⁻ reductions upon treatment with two equivalents of $NaAlH_2(OCH_2CH_2OCH_3)_2$ (Red-Al)[36] which not only gave the η^4 complexes (**IV**) but also a novel isomeric ring-opened thiophene complex known as an "iridathiabenzene" (**V**), which had an unusual structure and properties of an aromatic ring.(Eq. 1.4).

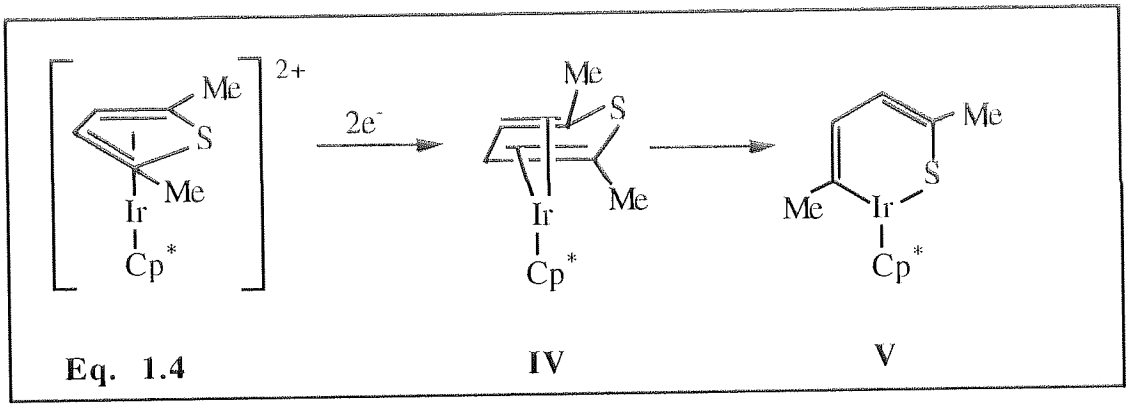

Eq. 1.4 **IV** **V**

1.5.3.5 Summary of thiophene coordination

The isolation and characterisation of complexes of thiophenes with transition metals provide structural models for the interaction of organic sulfur in coal with a metallic catalyst which may be considered a viable initial step in HDS. The following conclusions can be drawn from studies of these structural models:

(i) Under particular conditions, the η^5, η^1, and η^4 binding modes all activate the bound thiophene ring towards further reaction.

(ii) In η^1 complexes, substituted thiophenes coordinate more strongly to the metal owing to the electron releasing effects making sulfur a stronger σ donor.[21]

(ii) In cationic η^5 complexes the thiophene ring is susceptible to nucleophilic attack.[37,38]

(iii) In η^4 complexes the ring sulfur atom itself becomes strongly nucleophillic[36,39]

(iv) Both the η^4 and the η^1 binding modes can serve as precursors to insertion of a transition metal into a C-S bond of the thiophene ring.[32,36] This could eventually lead to its complete desulfurisation.

1.6 COORDINATION CHEMISTRY OF POLYCYCLIC THIOPHENES

Benzothiophene (BT) and dibenzothiophene (DBT) more closely correspond to the major sulfur components in fossil fuels than thiophene, hence the coordination chemistry of the polycyclic aromatic sulfur compounds is of special relevance.

1.6.1 Comparison of basicity of sulfur models

A recent review in the literature[40] has shown that the electron density on the sulfur heteroatom increases in the following order:

Dibenzothiophene (DBT) > Benzothiophene (BT) > Thiophene (T)

The greater delocalisation of the sulfur non-bonding electrons into the π system of the heterocycle accounts for the lower basicity (and nucleophillicity) of thiophene. Hence, the above order is true for ease of S-alkylation using alkylating agents such as tryalkyloxonium salts and methyl trifluoromethanesulfonate.[41]

1.6.2 Bonding modes in BT and DBT

Benzothiophene and dibenzothiophene commonly bind to transition metals through the η^1(S) or η^6 modes (Figure 1.2). Few examples of η^5 coordination have been reported,[47]while η^2 and η^4 complexes are unknown.

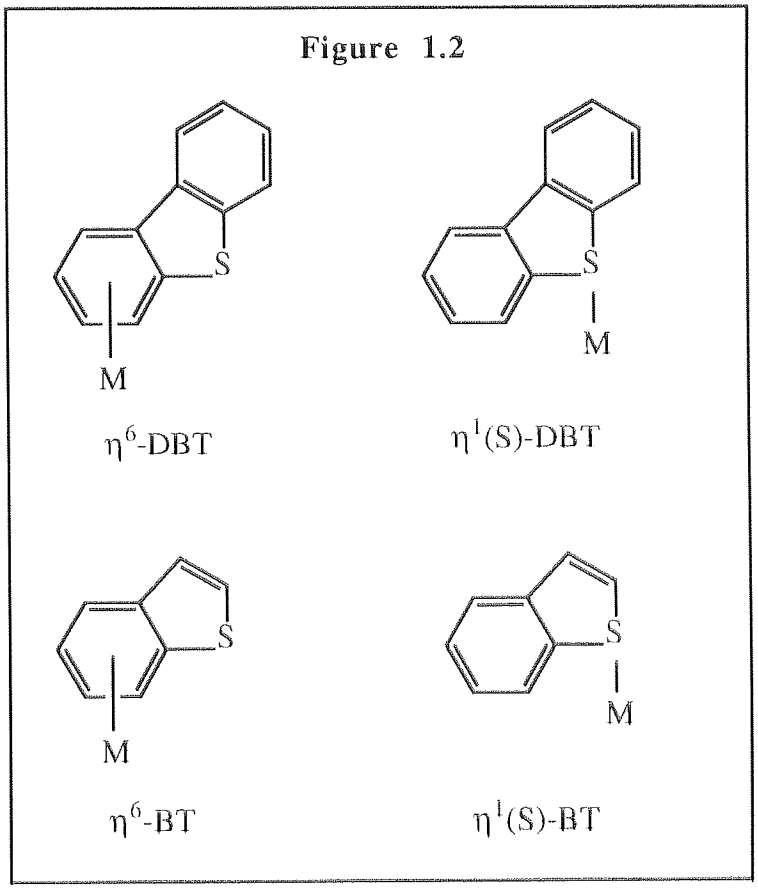

Figure 1.2 Common modes of binding for benzo- and dibenzothiophene with transition metals

1.6.2.1 η^1, S-Benzo- and Dibenzothiophene Complexes

In S-bound complexes the heterocycle acts as a two electron donor. The first well-characterised S-bound complex of any thiophene was $RuCl_2[Ar_2P\text{-}DBT]_2$ where Ar_2P-DBT is DBT substituted in the 4-position with di(p-tolyl)phosphino or diphenylphosphino groups, and the phosphine-DBT ligand chelates to the ruthenium through the S and P centres.[42] Dichloromethane solutions of $[CpFe(CO)_2(isobutene)]BF_4$ reacted with benzothiophene and dibenzothiophene to give $[Cp(CO)_2Fe(\eta^1(S)\text{-BT})^+$ and $[Cp(CO)_2Fe(\eta^1(S)\text{-DBT})^+$ respectively, which were shown to be more stable than the thiophene analogue.[20]

In a kinetic study[43] of the rate of dissociation of η^1(S)-thiophenes (Th) from $Cp(CO)_2Re(\eta^1(S)\text{-Th})$, it was observed that DBT dissociates more slowly than BT or

thiophene, thus suggesting that DBT coordinates through the sulfur to transition metals more strongly than other thiophenes. Further evidence for this was provided by Angelici and coworkers who reported the synthesis of η^1(S)-DBT complexes of Ir and Rh (Eq. 1.5).[44]

$$[Cp^*MCl_2]_2 + 2DBT \xrightarrow{CHCl_3} 2\,Cp^*MCl_2(\eta^1(S)\text{-DBT})$$

1: M = Ir
2: M = Rh

Eq. 1.5

This study demonstrated that the sulfur of DBT is sufficiently strongly coordinating to enable it to cleave the chloro bridging ligands in $[Cp^*MCl_2]_2$ to give Ir and Rh-DBT complexes; in contrast, BT, 2,5-dimethylthiophene and thiophene did not react under similar conditions. These observations can be accounted for by considering the higher basicity of DBT compared to that of BT and thiophene.

The η^1(S)-DBT complexes described here have been studied by crystallography and all show pyramidal sulfur coordination such that the metal does not lie in the plane of the DBT.

1.6.2.2 η^6-coordination of benzo- and dibenzothiophenes

In η^6 or π complexes of BT and DBT the heterocycle acts as a six electron donor in which the metal is bound to the arene.

Fischer et al[45] showed that BT and DBT react with $Cr(CO)_6$, or $Cr(MeCN)_3(CO)_3$ to give $Cr(CO)_3(\eta^6$-BT) and $Cr(CO)_3(\eta^6$-DBT) complexes in good yield where the metal is bound to the arene. Iron complexes of DBT were prepared by the Saskatoon group[46] by the reaction of an excess of the heterocycle with ferrocene, $AlCl_3$ and powdered aluminium metal yielding both $[CpFe(\eta^6$-DBT)$]^+$ and $[(CpFe)_2(\mu$-η^6,η^6-

DBT)]$^{2+}$. Analogous [CpRu(η^6-DBT)]$^+$ and [(CpRu)$_2$(μ-η^6,η^6-DBT)]$^{2+}$ were also prepared from the reaction of DBT with [CpRu(MeCN$_3$)]$^+$.[47] These cations reacted with hydride reagents to give a pair of yellow isomeric products CpRu(η^5-DBT-6-H) and CpRu(η^5-DBT-9-H), wherein the metal was bound to the hexadienyl ring.

Removal of the chlorine ligands from [Cp*MCl$_2$]$_2$ by AgBF$_4$ followed by reaction with DBT in acetone was a strategy employed by Angelici to produce η^6 complexes (Eq. 1.6).[44]

$$[Cp^*MCl_2]_2 + 4AgBF_4 \xrightarrow[\text{acetone}]{\text{DBT}} 2\,[Cp^*M(\eta^6\text{-DBT})](BF_4)_2 + 4\,AgCl$$

1: M = Ir
2: M = Rh

Eq. 1.6

There are however no reactions of these η^6 derivatives that suggest η^6 coordination activates BT or DBT to desulfurisation on HDS catalysts. It is the η^1(S) bonding mode believed to be the first step in catalytic desulfurisation.[17]

1.7 CLEAVAGE AND DESULFURISATION OF THIOPHENE RINGS BY TRANSITION METAL CENTRES

It is well known that certain organometallic reagents have an ability to cleave C-S bonds under relatively mild conditions. One of the earliest examples of this was demonstrated by the reaction of Fe(CO)$_5$ with alkyl sulfides,[48] which showed that the organometallic carbonyl cleaved the C-S bond. In another example a mixture of Fe(CO)$_5$ and Co$_2$(CO)$_8$ was shown to desulfurise thiophene under hydroformylation conditions - a mixed cobalt iron carbonyl sulfide, Co$_2$Fe(CO)$_9$S, (**VI**) being formed in 9.3% yield[49] (Eq. 1.7). Thiols were also desulfurised under these conditions.

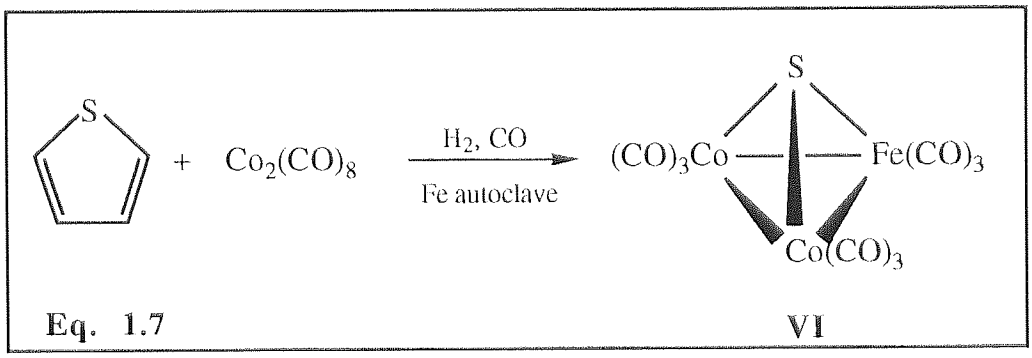

Eq. 1.7 **VI**

1.7.1 Desulfurisation of thiophenes by transition metal carbonyls

In 1960 Stone et al[50] demonstrated that the reaction of thiophene and tri-iron dodecacarbonyl, $Fe_3(CO)_{12}$, afforded the ferrole $Fe_2C_2H_4(CO)_6$ (**VII**).

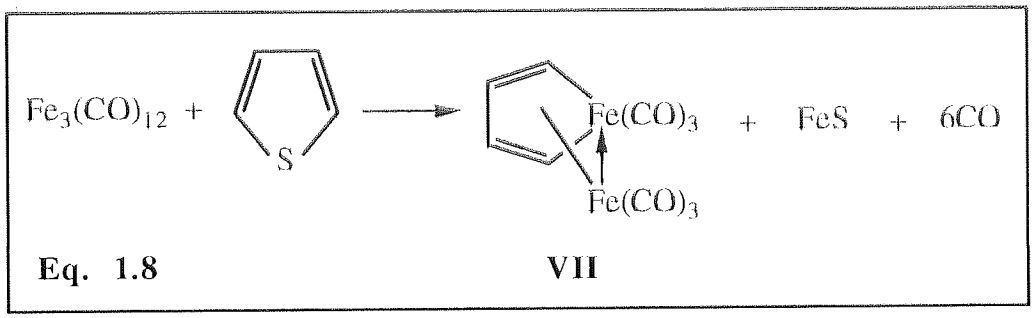

Eq. 1.8 **VII**

Ferroles are now a well established family of compounds featuring ferrocyclopentadiene species $C_4R_4Fe(CO)_3$ which are π bonded (η^5-) to a second $Fe(CO)_3$ centre. The initial yields were poor (5%) but more prolonged reaction of thiophene with $Fe_3(CO)_{12}$[51] (2 days) increased the yield of the ferrole to 17%. The use of substituted thiophenes gave yields in the range of 0.7 to 10.7% of appropriate ferroles.[52] Moreover, it was found that by reacting methylthiophenes with $Fe_3(CO)_{12}$, thiaferroles, $Fe_2(SC_4R_4)(CO)_6$, (**VIII**) as well as ferroles (**IX**) were formed. These compounds arose by the regiospecific insertion of an iron atom into the less hindered S-C bond (Eq.1.9).

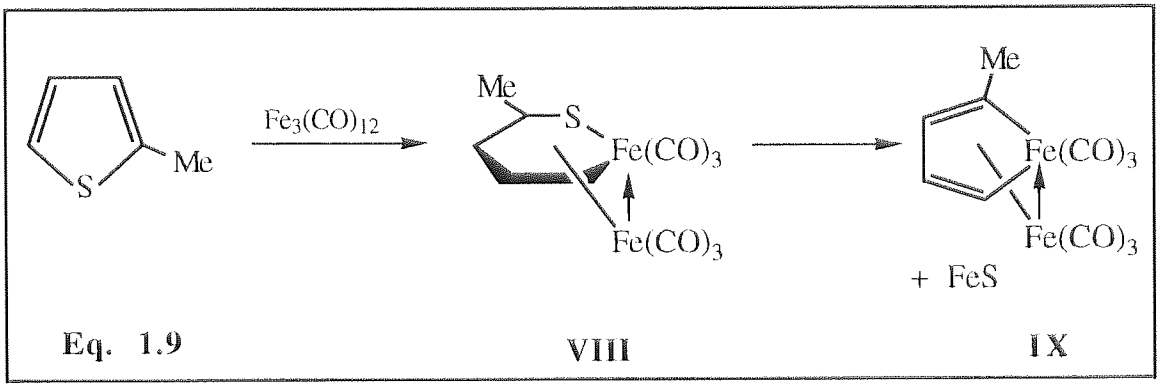

Eq. 1.9 **VIII** **IX**

Tri-iron dodecacarbonyl represents an attractive system for the modelling of coal desulfurisation since:

(i) sulfur is ultimately released in the form of iron sulfide - magnetically removable (convenient);

(ii) ferrole type products can be burnt with coal and removed as ash;

(iii) coal matrix is essentially retained hence minimum loss of calorific value is expected.

Practical aspects such as cost, quantities and handling of reagents, however, are not favourable for large scale operations.

In contrast to thiophene, the reaction of benzothiophene with $Fe_3(CO)_{12}$ in refluxing benzene[53] gave only the benzothiaferrole, $Fe_2(C_8H_6S)(CO)_6$ (**X**), which did not readily desulfurise. The iron atom again inserted regioselectively into the less hindered C-S bond.

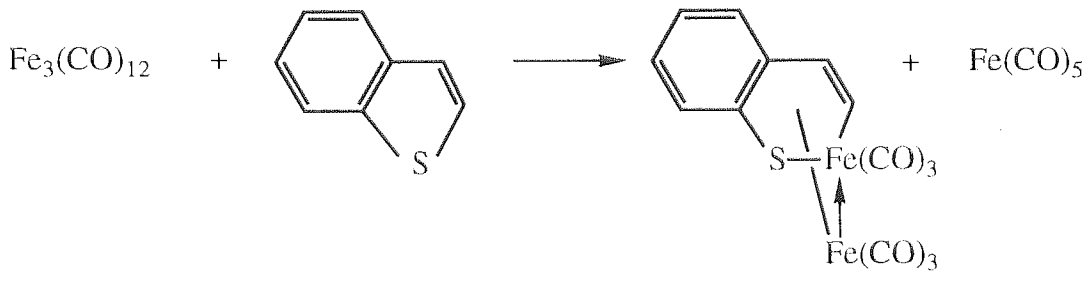

Eq. 1.10 **X**

On the basis of the stoichiometry of equation 1.10 the optimised yield of benzothiaferrole was 49%.

From this observation Rauchfuss and co-workers concluded that thiaferroles are precursors to ferroles, implying that insertion of a metal atom into the C-S bond is the initial step in the desulfurisation process.

Dibenzothiophene did not react under any conditions with $Fe_3(CO)_{12}$ thus the observed reactivity of thiophenes with $Fe_3(CO)_{12}$ increases in the order:

dibenzothiophene (no reaction) < thiophene (~5% yield of ferrole) < benzothiophene (~49% yield of benzothiaferrole).

Hence benzothiophene and thiophene have very different rates of reaction with $Fe_3(CO)_{12}$ in that the benzothiaferrole derivative is more readily formed than the thiaferrole from the respective heterocycles. Moreover, the thiaferroles and the benzothiaferroles have very different thermal stabilities. The thiaferroles are easily converted to the ferroles while the benzothiaferrole does not convert to a benzoferrole, although the latter is known.[53]

A similar study on the reaction of thiophene with $Ru_3(CO)_{12}$ has also been carried out[54] in which the sulfur free species $Ru_2(\mu\text{-}C_4H_4)(CO)_6$ was derived by C-S bond

cleavage as in the iron case, but in addition, the tetranuclear cluster $Ru_4(\mu_3\text{-}S)(\mu\text{-}C_4H_4)(CO)_{11}$ containing separate S and C_4H_4 ligands within the same molecule was also observed.

With osmium, C-H rather than C-S bonds were cleaved exclusively and $Os_3(CO)_{12}$ or $Os_3(CO)_{10}(MeCN)_2$ reacted with thiophene to give the thienyl isomers $(Os_3(\mu\text{-}H)(\mu\text{-}C_4H_3S)(CO)_{10}$ (exo and endo isomers in rapid equilibrium), which decarbonylated to the thiophyne cluster $Os_3(\mu\text{-}H)_2(\mu_3\text{-}C_4H_3S)(CO)_9$.[55]

Somewhat more exotic systems based on rhodium were studied by Rauchfuss et al,[39] in which stable tetramethylthiophene complexes of rhodium were reacted with iron carbonyls:

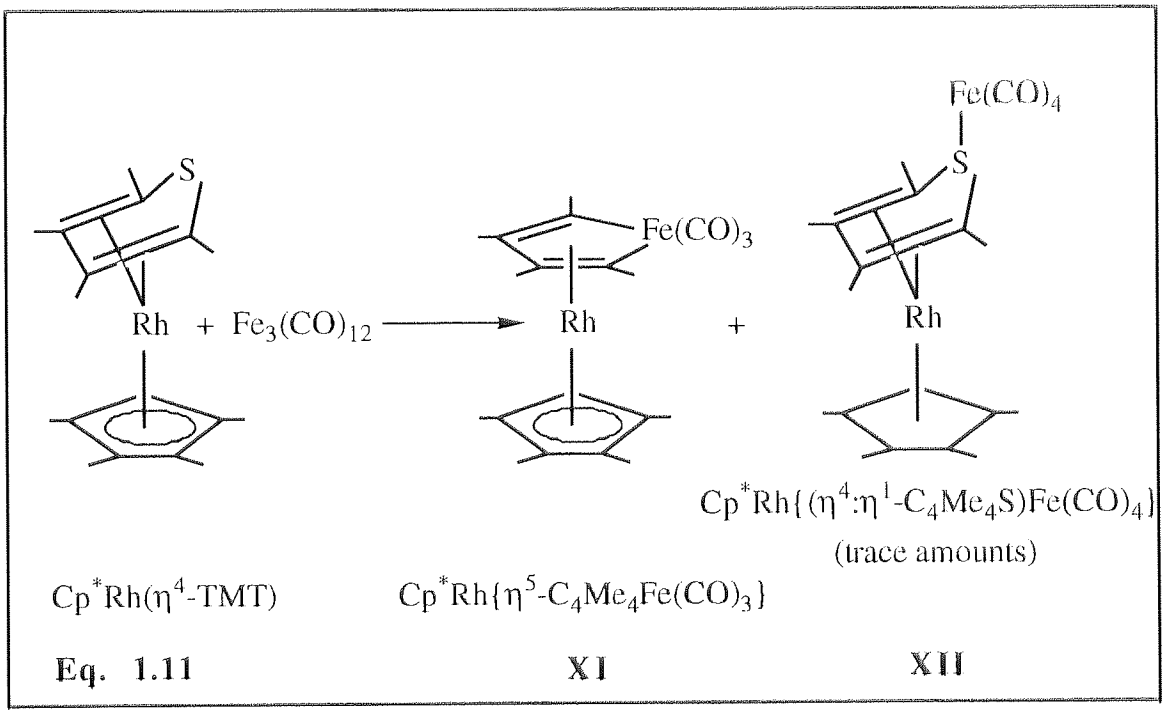

Thermolysis of (**XII**) in refluxing benzene yielded insoluble FeS and free TMT together with the following products:

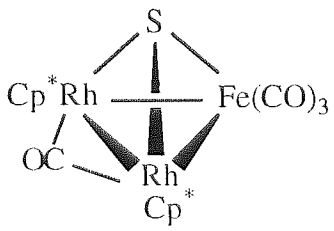

(XIII)

\+ 2

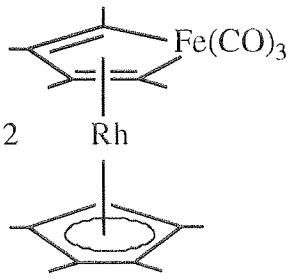

(XIV)

In the thermolysis of (**XII**) one set of metals stabilises the hydrocarbon residue in the form of a heterometallic ferrole (**XIV**), while a second group of metals binds to the extruded sulfur atom to give the cluster $Cp^*Rh_2(\mu\text{-}CO)SFe(CO)_3$ (**XIII**). This desulfurisation process illustrates the following vital mechanistic points:

(i) The insertion of an iron atom into a C-S bond activates the heterocycle towards desulfurisation.

(ii) Transition metals play a dual role in thiophene desulfurisation by separately stabilising the desulfurised hydrocarbon in the form of a metallacycle and accepting the sulfur.

Further evidence of these mechanistic views were provided by Angelici and co-workers in a recent publication[56], reporting the reaction of the iridathiabenzene complex with $Co_4(CO)_{12}$.

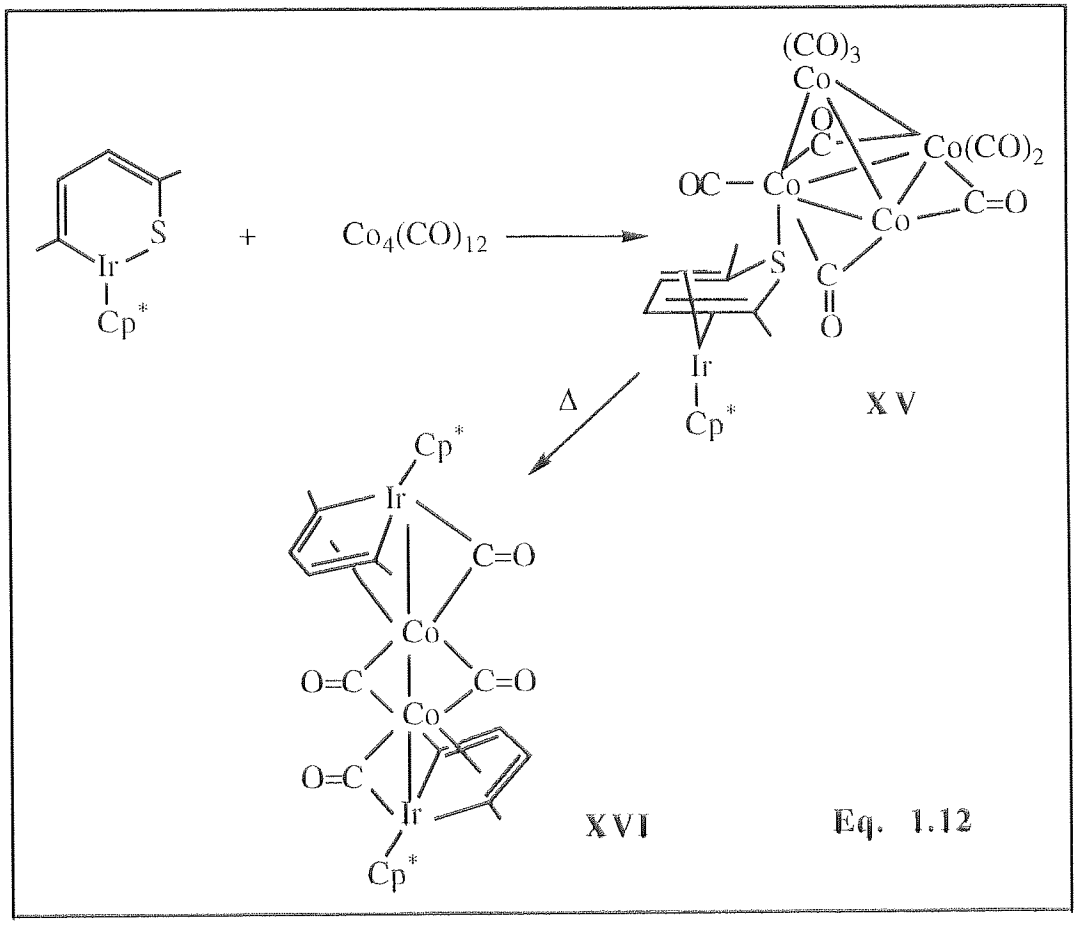

Eq. 1.12

As the reaction conditions became more rigorous, the amount of (**XV**) decreased and (**XVI**) increased. It was presumed that the removed sulfur combines with the excess Co in (**XV**) to give a cobalt sulfide, thereby demonstrating the dual role played by the transition metal.

Jones and Chin[57] reported the hydrodesulfurisation of thiophene to butadiene and butane by a homogeneous iridium complex. Thermolysis of the dimer $[(C_5Me_5)IrH_3]_2$ in neat thiophene in the presence of tert-butylethylene at 60°C gave the desulfurisation cleavage product $[(C_5Me_5)Ir]_2(\mu\text{-}S)(\mu\text{-}1,2\text{-}\eta^2\text{-}3,4\text{-}\eta^2\text{-}C_4H_6)$. (**XVII**)

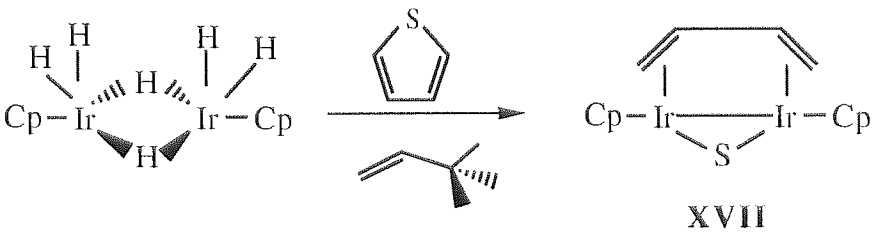

XVII

Eq. 1.13

Hydrogenation of the desulfurisation cleavage product (**XVII**) yielded butane or butadiene depending on the reaction conditions. This work supported the idea that two metal centres may be required for the cleavage of both C-S bonds. Earlier work by the same group with the mononuclear complex $Cp^*Rh(PMe)_3(Ph)H$ lead only to the cleavage of a single C-S bond.[32]

1.72 Desulfurisation of polycyclic thiophenes by transition metal reagents

Desulfurisation of the more condensed systems such as benzothiophene and dibenzothiophene has proved more difficult as already shown by Rauchfuss's work with $Fe_3(CO)_{12}$.[53] A few examples, however, can be found in the literature in which these systems have been desulfurised by transition metals.

Alper et al[58] demonstrated that molybdenum hexacarbonyl adsorbed onto silica provided an active desulfurisation agent for DBT. When the reaction was carried out in tetrahydrofuran over a period of 3-4 days at 50°C, the desulfurised product, biphenyl (**XVIII**), was formed in essentially quantitative yield (Eq.1.14).

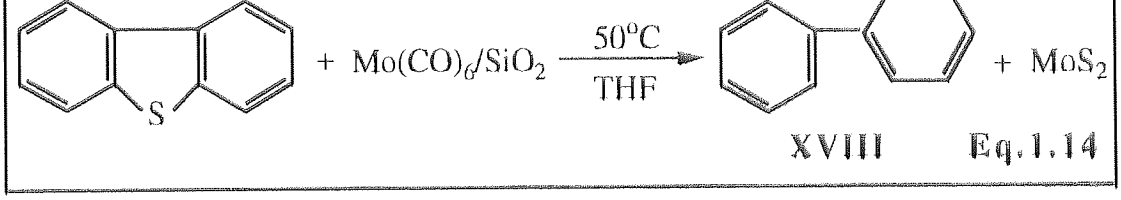

XVIII Eq.1.14

Eisch et al[59] developed methods for the desulfurisation of dibenzothiophene by soluble nickel reagents. The complex Ni(cod)(bipy), where cod is 1,5-cyclooctadiene and bipy is 2,2'-bipyridine, reacted at room temperature with DBT to give after acid hydrolysis, biphenyl. Optimal yields (45%) were obtained with two equivalents of the nickel reagent per heterocycle. The investigators suggested that the nearly 50% yield of the biphenyl arose from the dual role of the metal reagent (as previously highlighted), 1 equivalent accepting sulfur as NiS, and the other stabilising the hydrocarbon residue as a metallacycle. An alternative desulfurisation agent generated from Ni(cod)(bipy) and $LiAlH_4$, containing 1 equivalent of active hydrogen, converted DBT to biphenyl in greater than 90% yield.

A more recent publication[60] showed that BT was desulfurised when treated with $Ru_3(CO)_{12}$ in refluxing THF (Eq. 1.15).

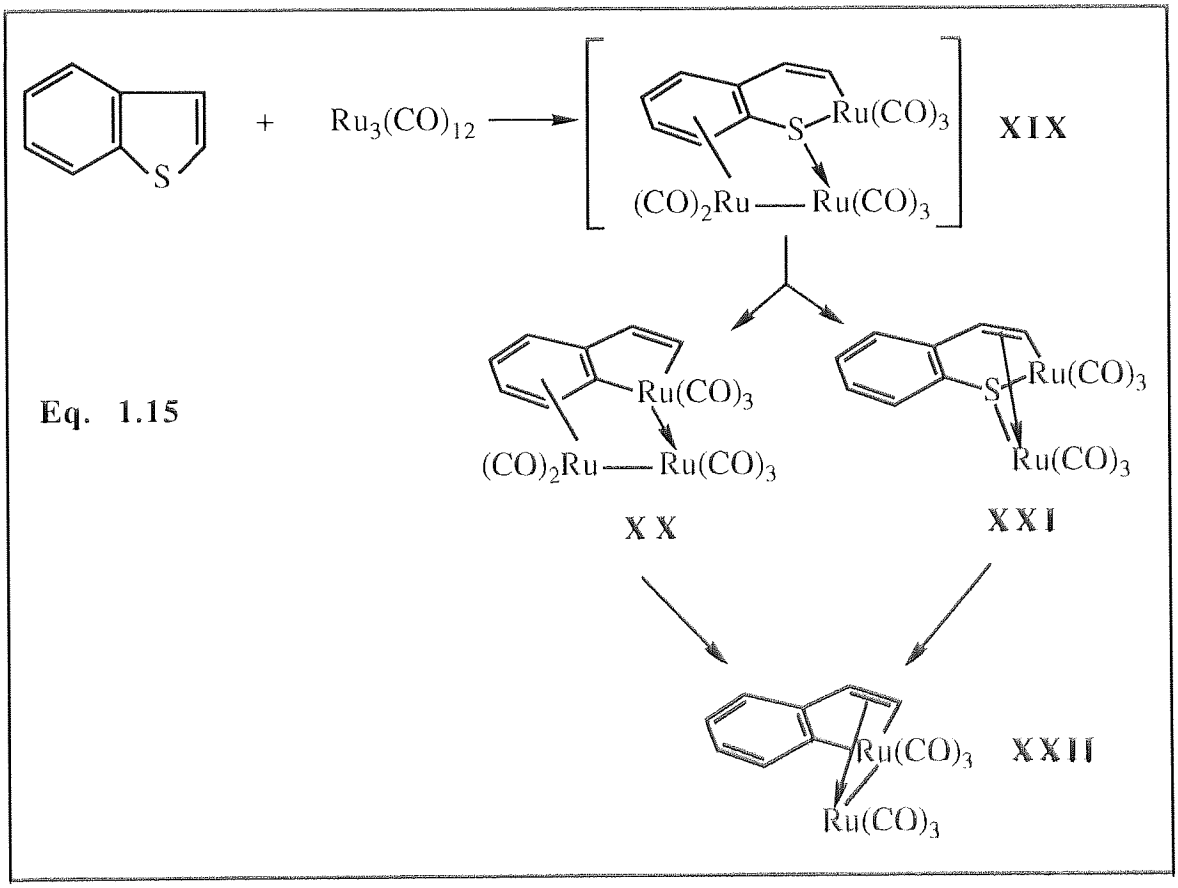

Eq. 1.15

Compounds (**XX**) (28% yield) and (**XXII**) (10%) were formed by C-S bond cleavage with subsequent extrusion of the sulfur atom in the form of RuS_2. Compound (**XXI**) (17%) is closely related to the benzothiaferrole obtained by Rauchfuss from the reaction of BT and $Fe_3(CO)_{12}$.[53]

Jones and Chin[61] reported the reaction of the monometallic reagent $Cp^*Co(C_2H_4)_2$ with dibenzothiophene (Eq. 1.16), which yielded the dinuclear C-S insertion adduct $[Cp^*Co]_2(\mu\text{-}\eta^2,\eta^3\text{-}C_{12}H_8S)$ (**XXIII**). However, desulfurisation of the heterocycle was not observed, thus providing further evidence that multimetallic reagents may be required for the cleavage of both C-S bonds necessary for desulfurisation.

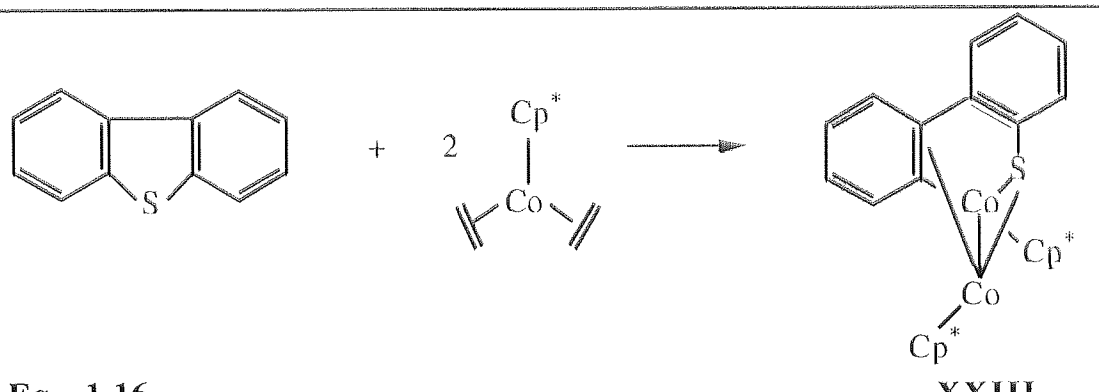

Eq. 1.16 **XXIII**

1.73 Summary of desulfurisation of thiophenes by transition metals

The following conclusions can be drawn from the studies of the desulfurisation of sulfur models facilitated by transition metal organometallics:

(i) The more condensed heterocyclic systems such as BT and DBT represent better sulfur models yet they are more difficult to activate towards desulfurisation than the simple thiophenes.

(ii) The initial step in the reaction pathway to desulfurisation is invariably the insertion of the metal atom into the C-S bond with subsequent removal of the heteroatom.

(iii) An electron rich metal centre is believed to be required for metal insertion into the thiophene ring and *multimetallic* reagents are expected to be the most effective desulfurising agents since they are capable of facilitating the cleavage of both C-S bonds in an aromatic ring.

(iv) The transition metal plays two distinct roles in the desulfurisation of the heterocycle by separately stabilising the hydrocarbon residues and accepting the extruded sulfur.

1.8 TELLURIUM HETEROCYCLES AS 'COAL SULFUR MODELS'

Electronically, tellurophenes are similar to thiophenes[62] and this is manifested in the similarity of their uv spectra. Hence the tellurium heterocyclic analogues of thiophenes are expected to display similar chemical reactivity towards transition metal organometallic reagents as the thiophenes themselves and may therefore be regarded as thiophene 'models'. Much of the work described here has concentrated on studying the reactivity of the tellurium heterocycles with transition metals since this has certain advantages over studying the thiophene systems. The advantages in using tellurium analogues are:

(i) The carbon-chalcogen bond strength will be less in tellurophenes hence they are expected to show a higher degree of reactivity compared to equivalent sulfur compounds. No suitable data can be found in the literature for C-Te bond strengths. However, a comparison of C-S and C-Se bond strengths (shown in Table 1.1) can be used and extrapolated to estimate C-Te bond strengths.

compound	C-E bond strength KJ mol^{-1}
Et_2S	293.5
Et_2Se	240.3
Ph_2S	348.0
Ph_2Se	285.3

Table 1.1 Mean bond dissociation energies in organosulfur and organoselenium compounds

By observing Table 1.1, it is clear that C-Se bond strengths, as expected, are considerably less than C-S bond strengths. The C-Te bond strength is therefore expected to be even weaker.

(ii) The weaker C-Te bond strength may facilitate detelluration reactions, even of dibenzotellurophene, and thereby demonstrate the *mechanistic feasibility* of the dechalcogenation reaction for the more condensed aromatic molecules.

(iii) A broader range of analytical techniques is available for following the reactions of tellurophenes e.g. ^{125}Te NMR spectroscopy. Indeed, Angelici and his group[64,65] have extended their investigations to selenophenes since ^{77}Se NMR spectroscopy allows direct observation of the ligand.

(iv) A new area of organometallic chemistry will be accessed thus providing routes to novel organometallic compounds.

1.8.1 Comparison of aromaticity in group 16 heterocycles

Selenophene and tellurophene complete with furan and thiophene a series of four stable heterocyclic systems which all obey the Hückel rule for aromaticity. These systems differ mainly in their degree of reactivity, but generally display similar reactions. Selenophene and tellurophene show typical aromatic behaviour; they are

more stable than the corresponding dienic compounds and tend to react by substitution rather than by addition. The geometry of these rings is planar[66,67] and similar to that of furan and thiophene. The more characteristic variations for the four congeners are an increase of the C(2)-E bond length from furan to tellurophene coupled with a decrease of the C(2)-E-C(5) bond angle (α).[68]

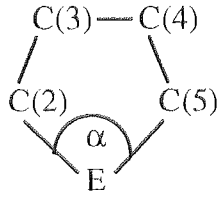

The ground-state aromaticity of the four systems has been studied[69] from which empirical values of resonance energy can be estimated for selenophene (121 KJ mol^{-1}) and tellurophene (105 KJ mol^{-1}) giving rise to the following order:

thiophene > selenophene > tellurophene > furan

This sequence can be explained by taking into account an interplay of two opposing factors; the decrease of electronegativity from O to Te, which should favour the contribution of the lone pair of the heteroatom to the aromatic sextet, and the corresponding increase of the covalent radius, which is unfavourable to good overlap between the p orbitals of C(2) and the heteroatom.

All four heterocycles undergo electrophilic substitution reactions[70] in the 2- and 5-position, one example being acetylation with acetic anhydride and $SnCl_4$. The reactivity sequence for these reactions is:

furan > tellurophene > selenophene > thiophene

Thus, the more aromatic system gives the lower substitution rate.

1.8.2 Comparison of binding properties of organochalcogen ligands

In general, the ligands R_2S, R_2Se and R_2Te can all be described as soft bases i.e. they have low electronegativity, high polarisability and are readily oxidised. Accordingly, they tend to form complexes with soft transition metal centres which tend to be large, of low charge or have valence shell electrons which are easily distorted or removed. Since the tellurium atom has a lower electronegativity (2.01) and higher single-bond covalent radius (1.37 Å) compared to the sulfur atom with an electronegativity of 2.44 and single-bond covalent radius of 1.04 Å, tellurium should be a softer donor than sulfur. In fact, most of the complexes of tellurium ligands have been reported to be with metal ions which have soft acid character.[71]

Selenophenes and tellurophenes are also expected to be better two-electron σ donors through the heteroatom to transition metals than thiophenes owing to their lower aromaticity. Evidence for this has been provided by Angelici and co-workers[68] who have demonstrated that selenophene in $[CpRu(CO)(PPh_3)(\eta^1(Se)\text{-}C_4H_4Se)]^+$ binds to Ru about 24 times more strongly than thiophene does in its analogous complex. Little work on the corresponding chemistry of tellurophenes can be found in the literature.

1.8.3 NMR properties of chalcogen nuclei

The development of FT NMR spectroscopy has enabled many elements of the periodic table to be studied. Among the group 16 elements the two most chemically prolific members, oxygen and sulfur, have NMR active isotopes (^{17}O and ^{33}S) which suffer from low natural abundance, relatively low sensitivity and are quadrupolar nuclei, while selenium and tellurium possess much more NMR favourable nuclei (^{77}Se, ^{123}Te and ^{125}Te) (Table 1.2). This has facilitated the application of ^{77}Se and ^{125}Te NMR spectroscopy to a wide range of organochalcogen compounds and indeed may be exploited to study their binding to transition metals.

Nucleus	Nuclear Spin	% Natural Abundance	Sensitivity	Receptivity
^{1}H	1/2	99.99	1	1
^{13}C	1/2	1.108	$1.59\ 10^{-2}$	$1.8\ 10^{-4}$
^{17}O	5/2	0.037	$2.91\ 10^{-2}$	$1.1\ 10^{-5}$
^{33}S	3/2	0.74	$2.26\ 10^{-3}$	$1.7\ 10^{-5}$
^{77}Se	1/2	7.50	$6.93\ 10^{-3}$	$5.2\ 10^{-4}$
^{123}Te	1/2	0.89	$1.80\ 10^{-2}$	$1.6\ 10^{-4}$
^{125}Te	1/2	7.03	$3.16\ 10^{-2}$	$2.2\ 10^{-3}$

Table 1.2 NMR properties of chalcogen nuclei compared to ^{1}H and ^{13}C

^{125}Te is about 4 times more sensitive and has longer relaxation times than ^{77}Se (4 to 6 times) and its negative gyromagnetic ratio can produce a negative nuclear Overhauser effect up to half of the normal signal intensity. For this reason together with the greater availability of organoselenium compounds ^{77}Se has been more widely investigated to date than ^{125}Te.

1.8.4 The coordination chemistry of heterocyclic tellurium compounds

The coordination chemistry of tellurium heterocycles with transition metals has been the subject of relatively little investigation and few examples of their reactivity with organometallics can be found in the literature.

The first example of the coordination of a tellurium heterocycle with a transition metal was reported in 1931 by Morgan and Burstall[72], who reacted cyclotelluropentane with mercury (II) chloride to yield a 1:1 complex (**XXIV**), (Eq. 1.17).

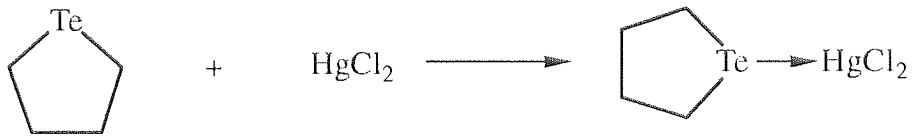

Eq. 1.17 **XXIV**

The telluracyclopentane displays strong lewis basicity compared with tellurophene due to non-delocalisation of the lone pair of electrons on the tellurium atom, enabling it to coordinate strongly to the "soft" Lewis acid, $HgCl_2$.

Activity in this field remained subdued for the next three decades, mainly due to the difficulties encountered by workers in attempting to synthesise the heterocyclic tellurium compounds, as well as to the general misconception that organotellurium compounds were extremely toxic and air sensitive. All attempts to prepare tellurophenes had been unsuccessful until 1961 when Braye *et al*[73] managed to isolate tetraphenyltellurophene by treating 1,4-dilithiotetraphenylbutadiene with $TeCl_4$. Further reaction with $Fe_3(CO)_{12}$ yielded a complex which was suggested by infrared spectroscopy as having the formula $(C_{28}H_{20}Te)$-$Fe(CO)_3$ (**XXV**), (Eq. 1.18). Due to the very low yields of the complex, further analyses were not performed and the structure was likened to the pentaphenylphosphole iron tricarbonyl which had previously been characterised.[74] It was further concluded in this publication that tellurophenes had an aromaticity similar to that of thiophenes and selenophenes.

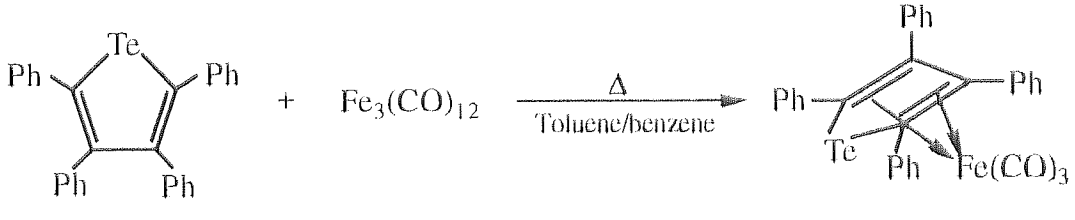

Eq. 1.18 **XXV**

Hieber and Kruck[75] reported in 1962 the reaction of manganese carbonylchloride with phenoxtellurine which lead to the formation of the disubstituted complex $Mn(CO)_3Cl(C_{12}H_8OTe)_2$ (**XXVI**).

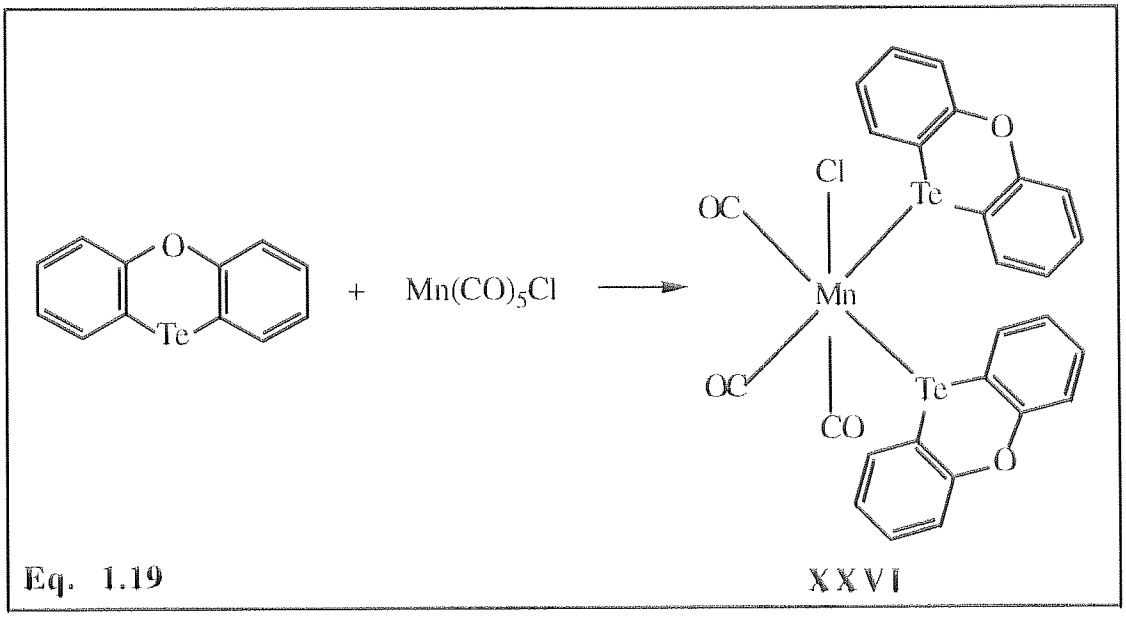

Eq. 1.19 **XXVI**

The first work done on the coordination of transition metals with unsubstituted tellurophene was published in 1972 by Öfele and Dotzauer.[76] Improvements in the synthesis of tellurophenes made these heterocycles more accessible with greater yields, thus enabling this group to react them with a variety of transition metals. Hence, the reaction of tellurophene with $(CH_3CN)_3Cr(CO)_3$ at 50-60°C (Eq. 1.20) yielded a purple-red crystalline solid having the molecular formula $C_7H_4CrO_3Te$. Similar reactions with thiophene[25], selenophene[77] and pyrole[78] had previously been carried out whereby IR, UV and NMR spectroscopy had suggested that a π complex between the heterocycle and the transition metal had been formed. The analogous structure for the tellurophene-chromium tricarbonyl was proposed (**XXVII**).

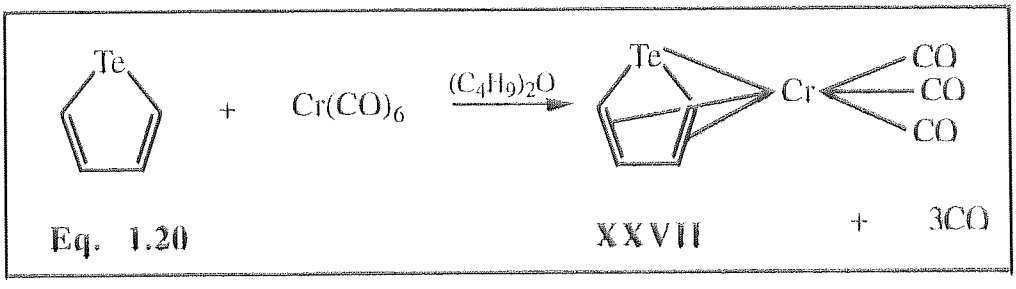

Eq. 1.20 **XXVII**

The tellurophene functions as a six-electron donor resulting in the formation of the η^5 complex as in the case of thiophene and selenophene.

The reaction of tellurophene with Na_2PdCl_4 in methanol at 25°C yielded two red-brown crystalline solids having the empirical formulas $C_8H_8Cl_2PdTe_2$ (70% yield) and $C_4H_4Cl_2PdTe$ (27% yield). The infrared spectra of the two complexes as well as that of the free heterocycle were very similar in the region between 4000 and 600 cm^{-1}. It was concluded that bonding in these complexes occurred only between the heteroatom and palladium i.e. η^1 coordination. Furthermore, the low frequency infrared spectra of the two complexes showed two bands corresponding to ν(Pd-Cl) at 303 and 287 cm^{-1} for the first and three bands at 359, 298 and 270 cm^{-1} for the second. The first complex was assigned a monomeric, square planar structure with cis-configuration (**XXVIII**) while the second was proposed to have a dimeric structure (**XXIX**).

Tetrachlorotellurophene was also reacted with $PdCl_2$ in methanol at 40-50°C yielding a solid having the molecular formula $(C_4Cl_4Te)_2PdCl_2$, formed in 61% yield which showed only one ν(Pd-Cl) band at 354 cm^{-1}. This complex was assigned the trans-configuration structure (**XXX**) which was preferred due to the big trans-effect of this ligand arising from the increased π-acceptor character of the chloro-substituted ring.

XXVIII

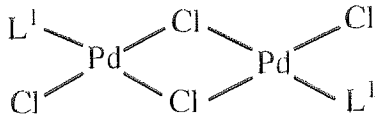

XXIX

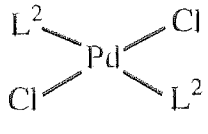

XXX

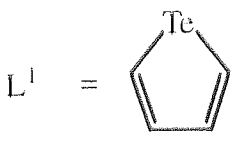

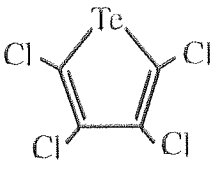

The analogous thiophene and selenophene complexes are not known, yet the stability of Pd^{II} complexes with dialkylchalcogenides increases in the order $R_2S > R_2Se > R_2Te$.[79]

The reaction of tellurophene with $Fe_3(CO)_{12}$, yielded the telluraferrole, $C_4H_4TeFe_2(CO)_6$ (**XXXI**), which on further heating converted to the ferrole, $C_4H_4Fe_2(CO)_6$, , accompanied with the formation of the cluster compound, $Te_2Fe_3(CO)_9$. The structure that was elucidated from the analytical data had similarities with a complex previously isolated from benzothiophene.[80]

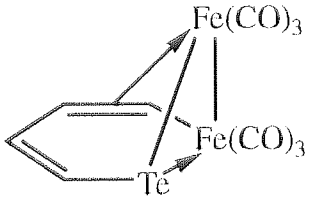

XXXI

From this work it was concluded that tellurophene has the greatest ability from the group 16 five-membered ring heterocycles to participate in coordinative bonding. This characteristic has a parallel in the fact that tellurophene is the only one that sustains addition of halogens at the heteroatom.[81]

In 1978 the synthesis and use of Ag(I) diaryl tellurides in photothermographic imaging elements was described. Complexes of the formula $(AgX)_2L$ (L = 1-oxa-4-telluracyclohexane, X = NO_3, Br[82]; L = dibenzotellurophene, X = Br[83]) were prepared (**XXXII**) and (**XXXIII**) by the addition of an aqueous solution of $AgNO_3$ or $AgBR_2$- to an acetone solution of the ligand. The ESCA data for these complexes showed a typical increase of 0.6-0.9 eV vs. the free ligand.

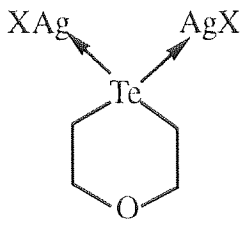

XXXII

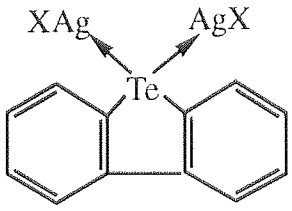

XXXIII

A similar study was carried out in 1980 in which a planar low-spin $Co^{(II)}L$ complex (where L = [N,N'-o-phenylenebis(salicilideneimidate)]) was reacted with telluracyclopentane and the analogous selenacyclopentane.[84] In both cases a 1:2 adduct was obtained in which the heteroatom was coordinated to the cobalt.

A more recent publication[85] demonstrated the ability of trinuclear transition metal carbonyls to extrude selenium and tellurium atoms from their respective heterocycles. Reactions of $Fe_3(CO)_{12}$, $Ru_3(CO)_{12}$ and $Os_3(CO)_{10}(MeCN)_2$ with selenophene and tellurophene were studied and compared with the analogous reactions of thiophenes.

It is common to find that when studying the chemistry of a group of elements, the first row is usually very different from the heavier analogues. However in the reaction of C_4H_4E with the triosmium cluster, a discontinuity in the chemistry was observed between thiophene and selenophene. It had been previously[86] noted that furan reacted with $Os_3(CO)_{10}(MeCN)_2$ by metallation at the 2-position to give the 2-furyl cluster in which the furyl ligand formed a μ,η^2-vinyl type bridge in $[Os_3H(\mu\text{-}\eta^2\text{-}C_4H_3O)(CO)_{10}]$ and acting as a three electron donor. The thiophene behaved in a totally analogous way but the heavier congeners gave stoichiometrically equivalent but non-hydridic compounds $[Os_3(CO)_{10}(C_4H_4E)]$ (E = Se or Te) in which a C-E rather than a C-H bond was broken (Eq. 1.21).

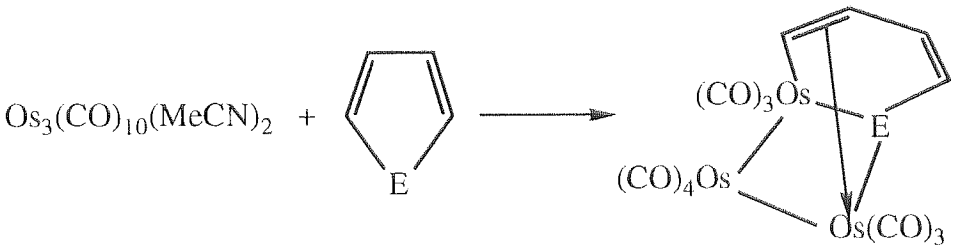

Eq. 1.21 **XXXIV**

$[Os_3(CO)_{10}(C_4H_4Te)]$ formed in 38% yield, was the only product that was isolated from the reaction with tellurophene. In contrast selenophene gave two additional products formulated as the bridging hydride complex $[Os_6(\mu\text{-}H)(\mu_3\text{-}Se)(\mu_4\text{-}C_4H_3)(CO)_{20}]$ (**XXXV**) and the dinuclear compound $Os_2(CO)_6(C_4H_4Se)$. (**XXXVI**).

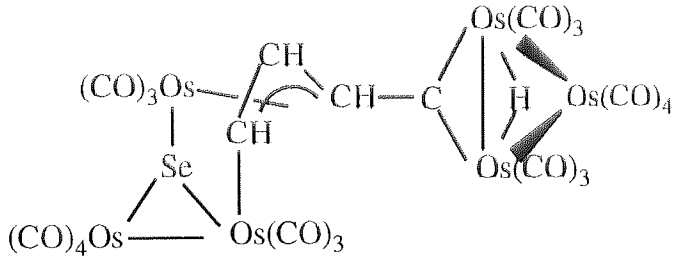

XXXV

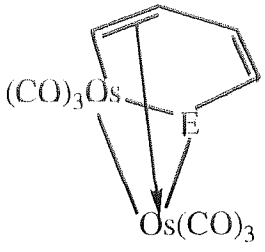

XXXVI

Reactions of the heterocycles with triruthenium carbonyl lead to the extrusion of the heteroatom from both selenophene and tellurophene giving rise to the dinuclear compound $[Ru_2(CO)_6(\mu\text{-}C_4H4)]$ (**XXXVII**). The fate of the heteroatom was not established but in the case of selenophene an additional product was observed whose structure was elucidated as the tetranuclear cluster $[Ru_4(\mu_3\text{-}Se)(\mu\text{-}C_4H_4)(CO)_{11}]$ (**XXXVIII**). Thiophene behaved in a similar way to selenophene giving rise to both dinuclear and tetranuclear compounds.[54]

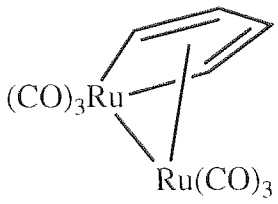

XXXVII

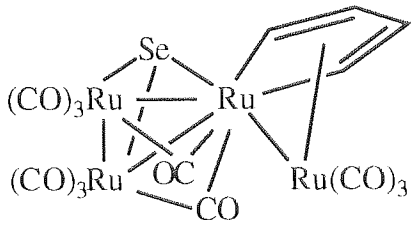

XXXVIII

Although no Te-containing product was obtained it seemed likely that a stepwise breaking of Te-C bonds had occurred to give the isolated metallacyclopentadiene complex (**XXXVII**). The presence of complex (**XXXVIII**) from the reaction with selenophene arose from the extrusion of selenium from the heteroatom which was subsequently held within the cluster.

In the same work,[85] $Fe_3(CO)_{12}$ was again shown to be effective in removing the heteroatom from selenophene and tellurophene, in both cases yielding the ferrole, $[Fe_2(CO)_6(\mu\text{-}C_4H_4)]$, which had previously been shown as being the desulfurisation product of thiophene.[50] In the reaction with selenophene, the intermediate selenaferrole, $[Fe_2(CO)_6(C_4H_4Se)]$, was isolated in 34% yield together with the ferrole (29%). However, in contrast to work reported by a previous group[76], no tellurium containing intermediate was observed and only the ferrole was isolated (25% yield). Thiophene behaved in a totally analogous way except that the ferrole was formed in much lower yields (5-10%) and again no thiaferrole intermediate was observed.

Most recently, Angelici has extended his work to look at the interactions of selenophenes with transition metals[64,65] with the objective of modelling the hydrodesulfurisation process. It is desirable to probe thiophene bonding on heterogeneous catalysts by comparing spectroscopic properties of adsorbed thiophene with those of thiophene in its fully characterised complexes, and solid-state NMR would be useful for making such comparisons. However, sulfur isotopes are not

generally suitable for NMR studies. The ^{77}Se nucleus has a 7.5% natural abundance and a nuclear spin of 1/2 making it very useful for studying by NMR spectroscopy. This valuable property has been exploited by Angelici and since selenophene has structural, bonding and reactivity properties that are very similar to those of thiophenes, his group has begun work on the studies of selenophene as a model for thiophene adsorbed on HDS catalysts.

A range of complexes have been prepared whereby selenophene is bonded to transition metals in a variety of modes and the ^{77}Se NMR spectra of the coordinated selenophenes have been compared. Figure 1.3 summarises the dependency of chemical shift in ^{77}Se NMR on the mode of binding in the selenophene complexes.

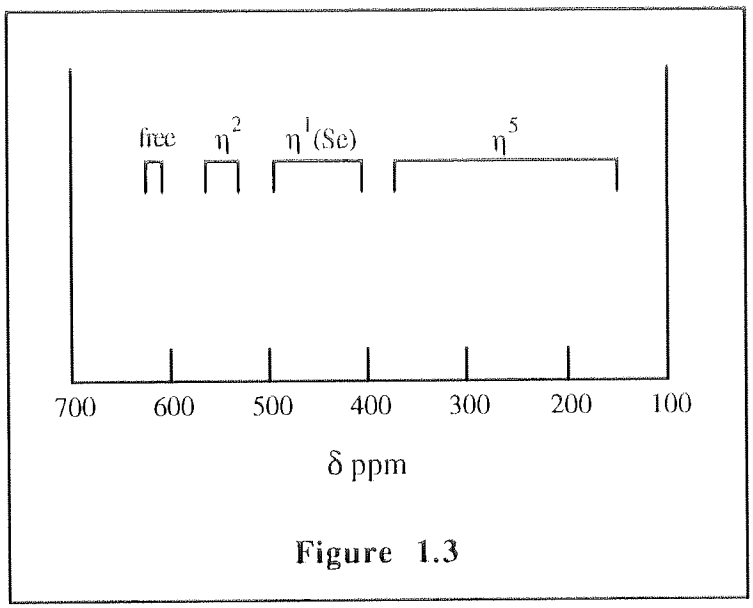

Figure 1.3

Figure 1.3 Variation of chemical shift in ^{77}Se NMR with mode of binding

In general, the various modes of selenophene coordination define certain ^{77}Se chemical shift regions. The free selenophenes are furthest downfield with chemical shift ranges of δ 621 for 2,5-Me_2Sel to δ 605 for Sel. Further upfield are the η^2 complexes in which selenophene is coordinated to two carbon atoms, of which only two compounds are known; $Cp^*Re(CO)_2(\eta^2$-Sel) (δ 524) and $Cp^*Re(CO)_2(\eta^2$-2-MeSel) (δ 549). Upfield still are the η^1(Se) ligands examples of which include

$ReCp^*(CO)_2(\eta^1(Se)\text{-}Sel)$ (δ 480) and $ReCp(CO)_2(\eta^1(Se)\text{-}Sel)$ (δ 402). The most upfield selenophenes are those displaying η^5 coordination to transition metals and these cover a broad range, increasing in the following order: $[IrCp^*(\eta^5\text{-}Sel)]^{2+}$ < $[Mn(CO)_3(\eta^5\text{-}Sel)]^+$ < $[RuCp^*(\eta^5\text{-}Sel)]^+$ < $Cr(CO)_3(\eta^5\text{-}Sel)$. In general, the ^{77}Se chemical shifts of the η^5-complexes move to higher field as the positive charge on the complex decreases but factors such as the metal and other ligands also have some influence. From these results it is clear that ^{77}Se NMR provides a powerful tool for establishing the mode of binding of selenophenes to catalyst surfaces.

No reports, rather surprisingly, can be found in the literature where analogous studies on the tellurophenes have been carried out. The ^{125}Te nucleus has a 7.03% natural abundance and a nuclear spin of 1/2, and therefore it would be interesting to study some transition metal complexes of tellurophenes with ^{125}Te NMR spectroscopy.

1.8.5 Summary of the coordination of tellurium heterocycles with transition metals

The following conclusions can be made about the reactions of tellurium heterocycles with transition metal organometallics:

(i) Tellurophenes can be considered as thiophene models since they are electronically similar.

(ii) Tellurophene ligands can be expected to coordinate more strongly to transition metals via the heteroatom compared to analogous sulfur compounds owing to their lower aromaticity (and therefore higher basicity).

(iii) Non-aromatic tellurium heterocycles display soft Lewis base character and coordinate strongly to soft transition metal centres.

(iv) The most illustrated mode of coordination of tellurophenes with transition metals is η^5 with few η^1 examples reported. No examples in the literature can

be found for similar complexes of the more condensed systems such as benzo- and dibenzotellurophene.

(v) In general thiophene, selenophene and tellurophene follow similar reaction pathways when reacted with transition metal organometallics, the main difference being that the heavier congeners are more reactive, thus giving products in higher yields. Moreover, tellurophene is more reactive than selenophene and a full range of products is not accessible for certain reactions.

(vi) The mode of binding of selenophenes to transition metals can be established using ^{77}Se NMR spectroscopy. In comparison ^{33}S NMR is difficult but it is feasible that ^{125}Te NMR can be employed in a parallel fashion.

1.9 MICROWAVE ACCELERATION OF REACTIONS

A wide range of organic and inorganic reactions have been accelerated using microwave techniques and the rapid synthesis of these compounds can be attributed primarily to superheating effects, which occur as the result of the effective coupling of microwaves to the polar solvent. For coupling of microwave radiation with molecules in solution, a dipole moment is required - on irradiation with microwaves, dielectric losses occur (due to dipolar polarisation in the microwave field) which cause friction and result in the build up of heat.

Microwave-driven reactions have been shown to be superior to conventional methods in their ability to dramatically reduce reaction times and in some cases give cleaner reactions - there is very little evidence to suggest that microwaves significantly alter the pathway of a reaction, as can happen with ultrasound. Microwave energy may be applied to solid, liquid or gaseous phases and even heterogeneous systems.

Indeed, microwave methodology developed within the research group has been shown to greatly accelerate a range of chemical reactions and also drive them more completely to equilibrium, and is a particularly attractive technique when applied to heterogeneous reactions involving coal.[87]

Since low yields are generally achieved in reactions involving desulfurization of model compounds by organometallic reagents, these are precisely the circumstances in which microwave acceleration could be most valuable. Also it would be interesting to see whether desulfurisation of the more condensed systems such as benzothiophene and dibenzothiophene can be effected by microwave heating.

Reactions that are to be carried out in the microwave oven require the use of microwave receptors to effect heating (Table 1.2). Thiophenes have low dielectric constants and therefore are not very good microwave receptors. Polar solvents (high dielectric constants) absorb microwave radiation most readily so most microwave reactions are done in a polar medium. It is also known[88] that several inorganic compounds will undergo remarkable heating in a simple microwave oven, e.g. oxides such as CuO and V_2O_5 may reach temperatures as high as 700°C in <1 min. Therefore, heat generated at the receptor sites can be transferred to the reactants, thereby encouraging a reaction.

	Receptor	**Receptibility**
Organic	acetonitrile	very good
	THF	moderate
Inorganic	water	very good
	Fe_3O_4	good

Table 1.3 Common receptors used for microwave heating

The chosen receptor must not interfere with the reaction in any way e.g. excess heat may decompose reactants or the receptor itself may react with the reactants.

1.10 OBJECTIVES

The objectives for this work can be defined as follows:

(i) To study the reactions of coal sulfur models such as thiophenes with organometallic reagents with the intent of desulfurising the heterocycle.

(ii) Attempt to drive these reactions more rapidly to equilibrium by employing microwaves rather than conventional heating methods. Also investigate whether microwave methodology can be used to effect the desulfurisation of the more condensed systems such as benzothiophene and dibenzothiophene which has to date proved most difficult.

(iii) To employ tellurophenes (the tellurium analogues of thiophenes) as coal sulfur models and study their reactivity towards certain organometallic reagents. This strategy will establish whether the difficulty encountered in desulfurising the more condensed heterocycles arises from a thermodynamic problem due to strong C-S bonds or whether it is simply not mechanistically feasible to remove a heteroatom from these systems. By switching to the tellurophenes we will be probing weaker C-Te bonds and therefore the activation energies for their cleavage will be lower.

(iv) By studying the reactivity of tellurium heterocycles with organometallic reagents a new area of chemistry should be accessed. It is therefore an aim of this work to react a diverse range of tellurium heterocycles with specific organometallic reagents in order to create novel organometallics which can then be spectroscopically and crystallographically studied.

CHAPTER 2

GENERAL EXPERIMENTAL AND PHYSICAL TECHNIQUES

2.1 GENERAL EXPERIMENTAL AND PHYSICAL TECHNIQUES

2.11 Reactions in an inert atmosphere

Experiments involving moisture sensitive or air sensitive reagents were performed under an atmosphere of pure argon using standard Schlenk line techniques.

2.12 Chemicals and solvents

Most chemicals were obtained from either the Aldrich Chemical Co., British Drug Houses (BDH) or Lancaster. Rhodium trichloride was supplied by Johnson and Matthey Ltd. Common solvents were supplied by the department and were dried where necessary prior to use. Analytically pure solvents were used without further purification.

2.13 Elemental analysis

Micro-elemental analyses for C, H and N were carried out by the Dept. of Chemistry, Brunel University.

2.14 Melting points

A Gallenkamp electrically heated melting point apparatus with a mercury thermometer was used to determine all melting points.

2.15 Infra-red spectroscopy

Infra-red spectra were recorded on a Bio-rad FTS-40A spectrometer incorporating a 600 microwatt 632.8nm CW class II laser. The spectra were obtained using a resolution of $8cm^{-1}$ and 16 scans. KBr discs were used for solid samples and liquids were analysed between NaCl cells. The range investigated was from 4000-400cm^{-1} (with a KBr beam splitter).

2.16 Nuclear magnetic resonance spectroscopy

NMR spectra (^{13}C and ^{1}H) were recorded using a Bruker AC-300 MHz instrument. Tetramethylsilane was used as the internal reference. Tellurium (^{125}Te) solution data were collected using bis(p-ethoxyphenyl) ditelluride as the reference.

2.17 Mass spectrometry

The electron impact (EI), chemical ionisation (CI), and fast atom bombardment (FAB) mass spectra of some compounds were obtained via the EPSRC mass spectrometry service, University College, Swansea. Some spectra were also obtained from The School of Chemistry at Birmingham University. Where appropriate, mass spectral peaks were assigned by considering ^{130}Te and ^{56}Fe as the most abundant isotopes.

2.18 X-ray photoelectron spectroscopy (XPS)

Spectra were recorded on a VG-Scientific ESCALAB 200-D instrument using MgK_{α} (1254eV) radiation.

2.19 Microwave reactions

Microwave reactions were carried out in a Sharp Carousel II R-84801 domestic microwave with a power rating of 650 watts and an operational frequency of 2.45 GHz. Part of the investigation was carried out in a CEM MES (microwave extraction system)-1000, delivering approximately 950±50 watts of microwave energy at a frequency of 2450 MHz at full power.

2.20 X-ray crystallography

Crystals of some compounds were obtained by recrystallisation from suitable solvents. Preliminary examinations of single crystals were performed using an optical microscope under cross polars in order to check the quality of the crystals.

Cell dimensions and intensity data were measured with an Enraf-Nonius CAD4 diffractometer operating in the ω-2θ scan mode using MoK_α radiation. The angular range for data collection was 2-25^o and three standard reflections were measured every two hours to check the stability of the system. The structures were determined by direct methods with SHELXS 86 and refined by least squares using anisotropic thermal parameters for the heavier atoms. Hydrogen atoms were placed in calculated positions, riding on their respective bonding atoms.

Data for some crystals was collected on a Rigaku R-axis II area-detector diffractometer using graphite monochromated MoK_α radiation.

CHAPTER 3

THE REACTIONS OF TELLURIUM HETEROCYCLES WITH IRON CARBONYLS

3.1 INTRODUCTION

As stated in chapter 1, Stone and co-workers[50] demonstrated in a classic contribution in 1960 that the reaction of thiophene and $Fe_3(CO)_{12}$ afforded the ferrole, $C_4H_4Fe_2(CO)_6$, together with FeS and other minor products. The same group went on to show that the C-S bonds of vinyl sulfides would cleave in the presence of $Fe_3(CO)_{12}$.[80] The initial yields of the ferrole were poor (5% after 15 hours), but others demonstrated that more prolonged reaction of thiophene with $Fe_3(CO)_{12}$ (2 days) increased the yield to 17%.[51]

This chemistry was believed potentially to provide useful mechanistic insight to the initial stages of hyrodesulfurisation reactions (HDS) of oils and of coal-derived liquids. Thiophene, however, is not an ideal molecular model for the bulk of organic sulfur in coal-derived liquids, rather benzothiophene and, more particularly dibenzothiophene, are superior models.[12] Benzothiophene gives a thiaferrole on reaction with $Fe_3(CO)_{12}$ which undergoes oxidative demetallation, but no removal of ring sulfur is noted.[53] Dibenzothiophene is unreactive under similar conditions.

The work done by Stone was initially repeated in order to see whether products could be more fully characterised and their yields improved before going on to investigate the reactivity of some tellurium heterocyclic compounds with $Fe_3(CO)_{12}$. Electronically, tellurophenes are similar to thiophenes and may therefore be regarded as thiophene 'models'. The carbon-chalcogen bond strength will be less in tellurophenes and this may facilitate detelluration reactions, even of dibenzotellurophene, and thereby demonstrate the mechanistic feasibility of the dechalcogenation reaction for the more condensed aromatic molecules. ^{125}Te NMR spectroscopy allows direct observation of the ligands and also a new area of organometallic chemistry is accessed.

3.2 EXPERIMENTAL

3.2.1 Reaction of thiophene with triiron dodecacarbonyl.

A 3-neck 250 cm^3 R.B flask was fitted with a Soxhlet extractor and reflux condenser, to the top of which was attached a calcium chloride guard tube. 150 cm^3 of thiophene was placed in the flask and 10g (19.8 mmol) of $Fe_3(CO)_{12}$ were placed in the thimble of the Soxhlet. A steady stream of nitrogen was continuously passed through the system. The flask and its contents were heated for 15 hours, during which time the iron carbonyl was extracted continuously. A black gloss formed around the edges of the flask and the green colour due to the iron carbonyl gradually changed to red. After cooling to room temperature, filtration afforded a red/orange filtrate from which excess thiophene was removed on a rotary evaporator leaving a dark red/brown oil. The oil was dissolved in 10 cm^3 pentane and a TLC trace was recorded on silica with pentane as the mobile phase solvent, revealing the presence of two components in the mixture (R_f values of 0.39 and 0.27 respectively). The two components were separated using dry flash column chromatography on a 2.5 x 20 cm column of TLC grade silica (without binder) with pentane as the eluting solvent. Removal of solvent afforded a red oil (trace) from the first eluate and an orange solid from the second eluate. The orange solid (yield, 0.35g) melted at 51°C.

3.2.2 Reactions of tellurium heterocycles with iron carbonyls

3.2.2.1 Preparation of heterocyclic tellurium compounds

Some tellurium heterocycles were prepared according to published literature methods as shown in Schemes 3.1-3.4. The identity and purity of the compounds was confirmed by comparison of melting points and spectroscopic data with the reported data.

(a) Tellurophene[62,89]

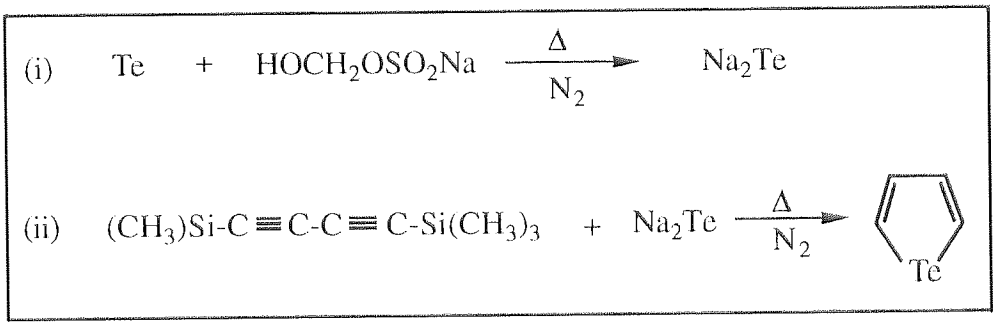

Scheme 3.1

Tellurophene was prepared in yields ranging from 38-59% (based on Te). The infrared data for the prepared tellurophene were consistent with those reported in the literature. The ^{13}C, ^{1}H and ^{125}Te NMR spectra are shown in Figures 3.10, 3.12 and 3.14 respectively. All coincide with the literature spectra.

(b) Dibenzotellurophene[90,91]

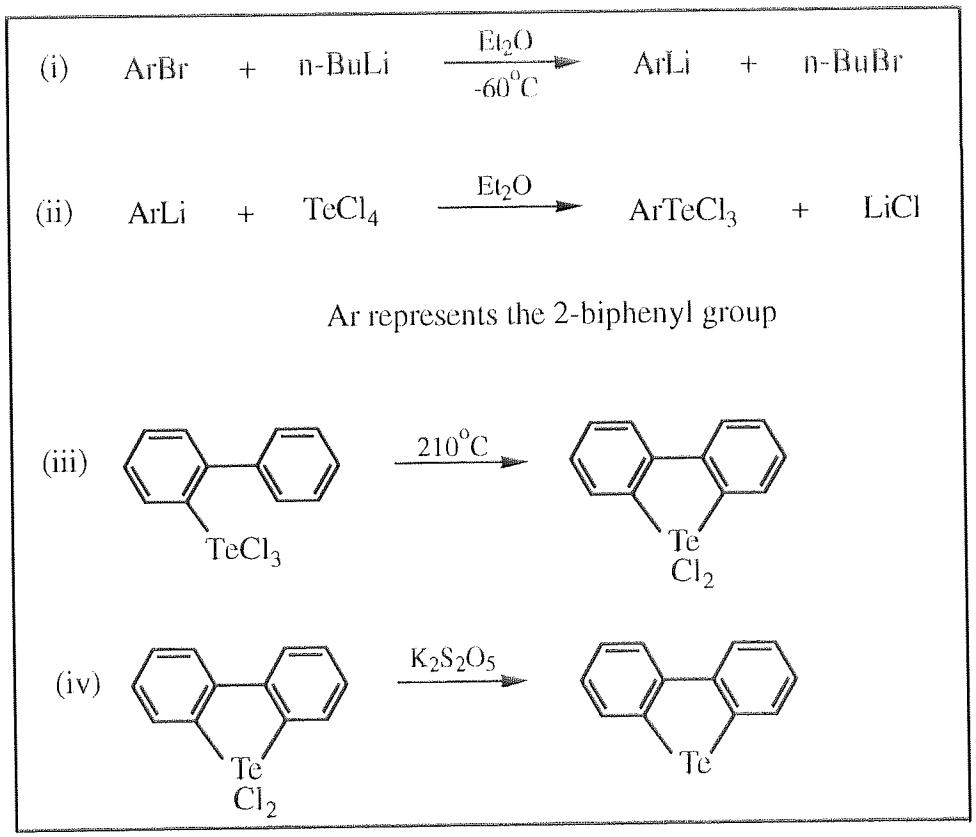

Scheme 3.2

The yield of dibenzotellurophene ranged from 36-43% (based on $TeCl_4$). The melting point was determined as 90-91°C which compared well with reported values (91-94°C). ^{13}C, ^{1}H and ^{125}Te NMR spectra are shown in Figures 3.16, 5.7 and 5.9 (chapter 5) respectively and all are in good agreement with the literature spectra.

(c) 2-telluraindane[92]

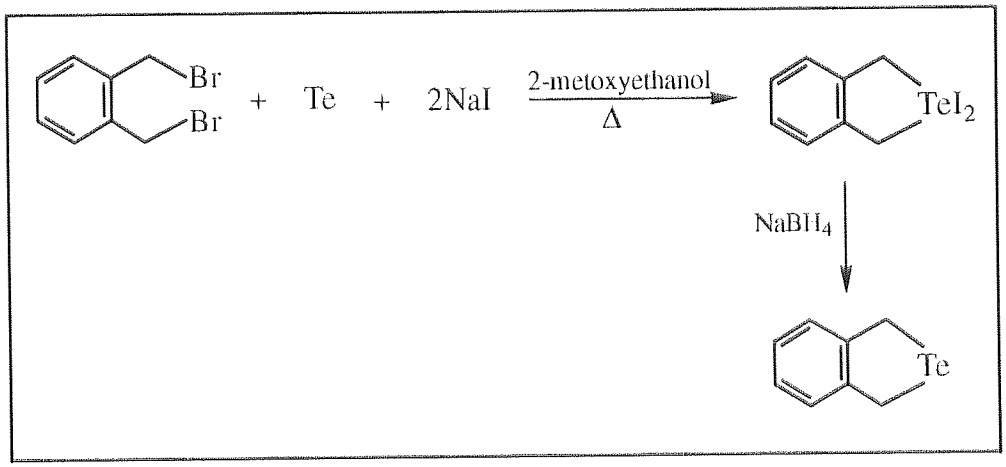

Scheme 3.3

2-telluraindane was prepared in 30-35% yield (based on Te). The melting point was determined as 44°C c.f lit. m.p 45°C. ^{1}H and ^{13}C NMR spectra are displayed in Figures 3.18 and 3.19 respectively and both correlate well with the reported spectral data.

(d) Phenoxtellurine[93]

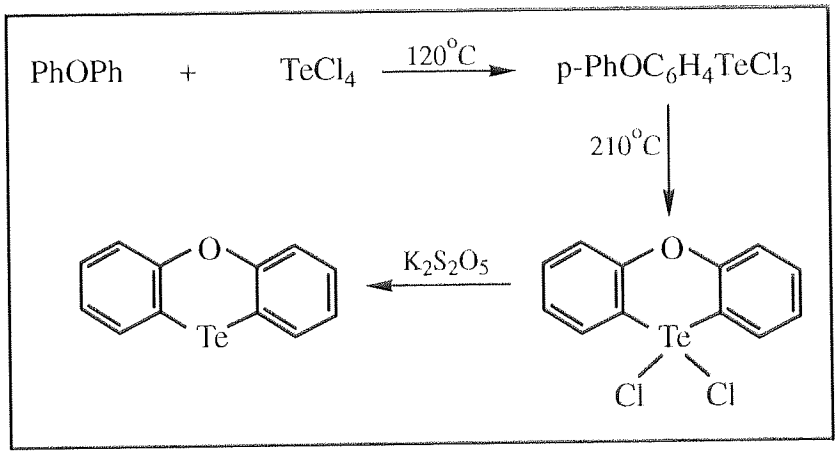

Scheme 3.4

Phenoxtellurine was prepared in 24% yield (based on $TeCl_4$). The melting point was determined as 78°C c.f lit. m.p 78-79°C.

3.2.2.2 Reaction of tellurophene with triiron dodecacarbonyl

Tellurophene (3.00g, 16.7 mmol) and $Fe_3(CO)_{12}$ (3.02g, 6.0 mmol) were refluxed in heptane (100 cm^3) with stirring for 2.5 hours. After 45 minutes the dark green colour due to the iron carbonyl gave way to an intense violet which in turn changed to orange after 1.5 hours. No further colour changes were observed during the next hour, after which the heating was stopped. The solution was filtered affording an orange filtrate and a black residue which adhered to the side of the flask. The solvent in the orange filtrate was evaporated under vacuum yielding orange flake-like crystals (0.89g), which melted at 51°C.

The whole experiment was repeated but this time the reaction was terminated at the intermediate stage (violet solution). Evaporation of heptane under vacuum left a deep violet almost black solid. TLC revealed the presence of 3 components in the reaction product (R_f values 0.30, 0.27 and 0.24), which were separated using dry flash column chromatography using a 2.5 x 20 cm column of TLC-grade silica (without binder) and pentane as the eluting solvent. Removal of solvent afforded a dark red powder from the first eluate, orange crystals from the second eluate and black solid (unreacted iron carbonyl) from the final eluate. The dark red material was recrystallised from boiling heptane, yielding shiny, violet, plate-like crystals which melted at 42°C; yield 1.82g. The crystals were characterised by infrared spectroscopy and mass spectrometry and a full NMR study (^1H, ^{13}C, ^{125}Te) was carried out. The orange crystals from the second eluate melted at 52°C and had an identical infrared spectrum to the compound isolated in the initial experiment.

3.2.2.3 Reaction of dibenzotellurophene with triiron dodecacarbonyl

Dibenzotellurophene (1.93g, 6.9 mmol) and $Fe_3(CO)_{12}$ (2.30g, 2.3 mmol), dissolved in heptane (100 cm^3), were heated and stirred under refluxed for 2.5 hours, during which time the colour of the solution gradually changed from dark green to orange.

After cooling, filtration afforded a brown residue and a deep orange filtrate from which the heptane was evaporated off under vacuum leaving a dark brown solid. TLC revealed the presence of two components (R_f values 0.05 and 0.16) which were separated using column chromatography as before, thereby giving a purple band preceded by a small yellow band. Elution with pentane and removal of solvent yielded yellow crystals from the first eluate (unreacted dibenzotellurophene) and a red powder from the second which on recrystallisation from boiling heptane gave violet crystals (0.28g) that melted at 176°C. The crystals were characterised using infrared spectroscopy and mass spectrometry and an NMR study (^1H, ^{13}C) was carried out. Crystals suitable for X-ray diffraction measurements were grown by slowly cooling a concentrated hexane solution.

3.2.2.4 Reaction of 2-telluraindane with triiron dodecacarbonyl

2-telluraindane (1.93g, 8.3 mmol) and $Fe_3(CO)_{12}$ (2.8g, 5.3 mmol) were dissolved in heptane (100 cm^3) and heated, with stirring, under reflux for 3 hours during which time the solution changed from dark green to deep purple. After cooling, the solution was filtered affording a black residue and an intense purple solution. The solution was evaporated to dryness under vacuum leaving a dark purple solid and a red oil. The mixture was dissolved in pentane (10 cm^3) and chromatographed on a 2.5 x 20 cm column of TLC-grade silica, thereby giving a small orange band preceded by a small yellow and large purple band. Elution with pentane and removal of solvent gave purple crystals (1.13g) from the first eluate and a red-brown solid (0.34g) from the third, m.p 76°C; a third component, an unstable yellow oil was also eluted. Infrared and NMR spectroscopy and mass spectrometry were used to characterise the three components. Crystals of the red-brown solid from the third eluate suitable for X-ray diffraction measurements were grown by slowly cooling a concentrated hexane solution.

3.2.2.5 Reaction of phenoxtellurine with triiron dodecacarbonyl

Phenoxtellurine (0.5g, 1.7 mmol) and $Fe_3(CO)_{12}$ (0.28g, 0.6 mmol) were dissolved in heptane (100 cm^3) and heated, with stirring, under reflux for 3 hours. The dark green colour due to the iron carbonyl gradually disappeared, giving way to an intense orange solution. After cooling, the reaction mixture was filtered yielding a black residue (0.16g) and the filtrate was evaporated to dryness to leave an orange-brown oily solid. The solid was shown by TLC to contain a mixture of a fast eluting component and a second component which was immobile on the silica TLC plate when pentane was used as the eluant. The oily solid was then shaken with pentane (15 cm^3) to give an orange solution and an insoluble pale pink solid (0.045g), m.p. 146°C which was removed by filtration. Evaporation of pentane from the filtrate left 0.21g of an orange oily solid. Mass spectrometry and infrared spectroscopy were used to characterise the isolated products.

3.2.3 Reactions of tellurium heterocycles with cyclopentadienyl iron carbonyls

The reactivity of the cyclopentadienyl iron carbonyls $CpFe(CO)_2I$ (cyclopentadienyl iron dicarbonyl iodide) and $Cp_2Fe_2(CO)_2$ (cyclopentadienyl iron dicarbonyl dimer) with tellurium heterocycles was studied. All the reactions were carried out under an argon atmosphere with the use of standard Schlenk techniques. The products were worked up as described previously and characterised by NMR and infrared spectroscopy and mass spectrometry. The following list summarises the reactions that were carried out using these organometallic reagents.

3.2.3.1 Reaction of tellurophene with cyclopentadienyl iron dicarbonyl iodide

Tellurophene (0.65g, 3.6 mmol) and $CpFe(CO)_2I$ (1.10g, 3.6 mmol) were dissolved in heptane (100 cm^3) and heated, with stirring, under reflux for 3 hours. Filtration yielded a black residue (0.32g) and a deep violet solution which after evaporation of heptane under vacuum gave violet crystals (0.36g), m.p. 118°C.

3.2.3.2 Reaction of 2-telluraindane with cyclopentadienyl iron dicarbonyl iodide

2-telluraindane (0.33g, 1.4 mmol) and $CpFe(CO)_2I$ (0.43g, 1.4 mmol) were dissolved in heptane (100 cm^3) and heated, with stirring, under reflux for 3 hours during which time the formation of a black crystalline precipitate was observed. The reaction mixture was then filtered to give a black crystalline residue (0.34g), m.p. 130°C and an intense brown solution which after removal of heptane yielded a brown solid (0.19g), m.p. 106°C.

3.2.3.3 Reaction of phenoxtellurine with cyclopentadienyl iron dicarbonyl iodide

Phenoxtellurine (0.50g, 1.7 mmol) and $CpFe(CO)_2I$ (0.52g, 1.7 mmol) were dissolved in heptane (75 cm^3) and heated, with stirring, under reflux for 3 hours. Filtration of the reaction mixture followed by evaporation of solvent from the filtrate yielded an orange solid (0.061g), m.p. 156°C and a brown residue (0.38g), m.p. >234°C.

3.2.3.4 Reaction of tellurophene with cyclopentadienyl iron dicarbonyl dimer

Tellurophene (2..00g, 11.1 mmol) and $Cp_2Fe_2(CO)_2$ (3.94g, 11.1 mmol) were dissolved in chloroform (100 cm^3) and heated, with stirring, under reflux for 7 hours. The reaction mixture was filtered to give a brown residue (1.77g) and an intense purple solution which after removal of solvent yielded a purple solid (2.06g).

3.3 RESULTS AND DISCUSSION

3.3.1 Techniques employed for characterisation of reaction products

All products were analysed by infrared spectroscopy and where possible by NMR spectroscopy and mass spectrometry. The IR and NMR spectra of selected compounds are displayed in Figures 3.2-3.20. Where suitable crystals were available, an X-ray crystallographic study of the compound was carried out (section 3.4).

IR spectroscopy has provided a useful preliminary method for examining whether a reaction has taken place by, in particular, looking at the carbonyl region. Successful reactions with iron carbonyls often lead to the inclusion of one or more $Fe(CO)_x$ fragments in the product which absorb strongly between 2100-1900 cm^{-1} (terminal CO stretch) or 1850-1700cm^{-1} (bridging CO stretch) in the infrared region. This provides a valuable fingerprint for the products and by comparison with the infrared spectrum of the precursor iron carbonyl, we can establish whether a reaction has occurred.

NMR spectroscopy has been useful for estimating the structure of products where crystallographic data cannot be obtained. By comparison of NMR data for reaction products to that of their precursor compounds, some useful information can be deduced. ^{13}C NMR is particularly useful here since the chemical shift is greatly influenced by the presence of tellurium and iron. The presence of tellurium also has further advantages in that the NMR active ^{125}Te nucleus is ~7.3% abundant and can therefore be seen in some ^{13}C and ^{1}H NMR spectra to be spin-spin coupled, which manifests itself in the form of satellites. ^{125}Te NMR itself is very useful since the chemical shift is highly sensitive to changes in the structure, and this provides useful information about the nature of bonding around the tellurium atom.

Mass spectrometry has been used to establish the presence (or absence) of tellurium in certain compounds since tellurium possesses a rich isotopic distribution, and can therefore be readily recognised on the mass spectrum. Used in conjunction with IR and NMR spectroscopy, mass spectrometry has helped in elucidating the structure for some compounds.

3.3.2 Reaction of thiophene with triiron dodecacarbonyl.

The reaction of thiophene with triiron dodecacarbonyl was first reported by Stone et al[50] in 1960. The end products from this reaction were an orange solid (m.p. 52-54°C) and a red oil. Elemental analysis revealed that the orange solid had the composition $C_{10}H_4O_6Fe_2$. Since it had been reported earlier[94,95] that under certain conditions acetylene and iron carbonyls reacted to give an orange solid (m.p. 54-55°C) of composition $C_{10}H_4O_6Fe_2$, which was assigned structure (**1**), Stone suspected that an identical product was formed from the reaction of thiophene and $Fe_3(CO)_{12}$. This was confirmed when he found that the two infrared spectra had peaks (3500-800cm^{-1}) which were exactly coincident. However, the red oil which was also isolated was not investigated any further, although it was thought to be a mixture.

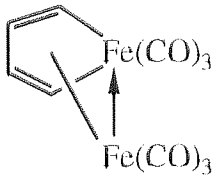

(**1**)

In the repeat experiment of this reaction carried out by ourselves two products were again formed - a red oil and an orange solid. The infrared bands in the carbonyl region are shown in Table 3.1 and peaks found in the mass spectrum are recorded in Table 3.2.

Red oil KBr, ν(CO) cm^{-1}	**Orange solid** KBr, ν(CO) cm^{-1}
2070(s)	2083(w)
2038(s)	2070(m)
1976(s)	2030(s)
	1985(s)

Table 3.1 Infrared bands in the carbonyl region of the products from the reaction of $Fe_3(CO)_{12}$ and thiophene

Red oil m/z	Orange solid m/z
444 (M^+) 220 (M^+ - 8CO)	332 (M^+)

Table 3.2 Significant peaks in the mass spectra (EI) of the products from the reaction of $Fe_3(CO)_{12}$ and thiophene

The infrared spectrum of the orange solid closely matches the infrared spectrum that was reported by Stone for his orange solid. The peak at m/z = 332 in the mass spectrum further confirms that this solid is in fact the ferrole product (RMM 332) that was previously reported.

The IR spectrum of the red oil also displays a rich carbonyl region but there is no indication of any bridging carbonyls. The mass spectrum peak at m/z = 444 suggests that the major component in this mixture has a structure in which the tri-iron ring has been retained, and indeed the peak at m/z = 220 provides a good fit for the $Fe_3CH_4^+$ fragment. These results have lead us to believe that the structure of this component resembles (**2**).

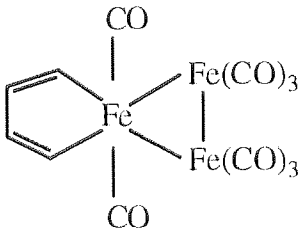

(**2**)

The solid black gloss which adhered to the side of the walls of the flask was treated with dilute hydrochloric acid resulting in the release of hydrogen sulfide (unpleasant smell). This suggested that the black residue was most likely to be FeS thus indicating that desulfurisation of thiophene had occurred.

In addition to Stone's findings it can therefore be concluded that the non-stoichiometric equation for the reaction between thiophene and triiron dodecacarbonyl is in fact:

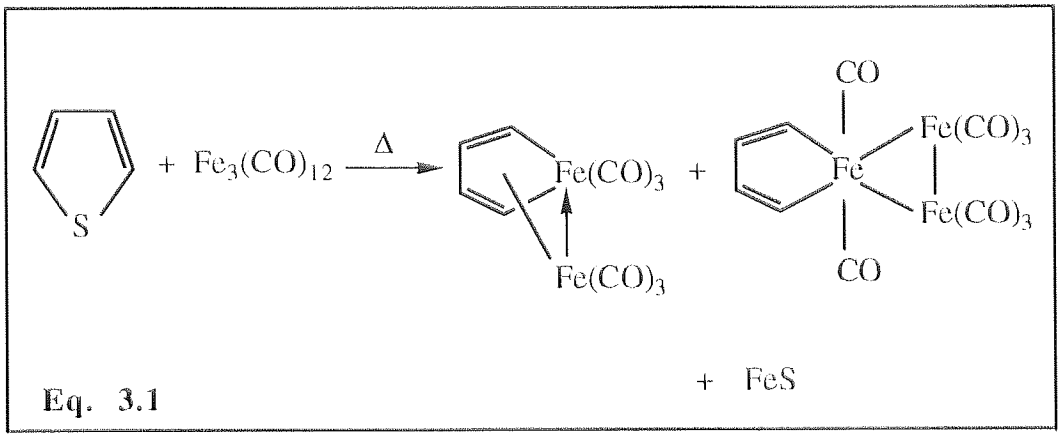

Eq. 3.1

3.3.3 Reaction of tellurophene with triiron dodecacarbonyl

From this reaction (2.5 hours) an orange crystalline product (m.p. 52°C) and a black solid residue were obtained. Data from the infrared spectrum in the carbonyl region for the orange crystals is recorded in Table 3.3. The CI mass spectrum registered a parent peak at m/z = 332.

Orange crystals KBr, ν(CO) cm^{-1}
2081 (m)
2072(m)
2029(s)
1985(s)
1940(s)

Table 3.3 Infrared bands in the carbonyl region for product from reaction of tellurophene and $Fe_3(CO)_{12}$

The infrared band pattern for the orange crystals in the carbonyl region together with the mass spectrum implies that the ferrole product, $C_4H_4Fe_2(CO)_6$ (**1**), has again been produced. This is further confirmed by elemental analysis;

Requires (%)	C, 36.1	H, 1.2	$C_{10}H_4O_6Fe_2$
Found (%)	C, 37.0	H, 1.4	

The yield of the ferrole was 0.89g or 45% based on $Fe_3(CO)_{12}$. Hence, although thiophene and tellurophene give identical products when reacted with $Fe_3(CO)_{12}$, the yield from the latter is much greater. This demonstrates that the tellurium analogues are in fact more reactive towards the iron carbonyl than their corresponding thiophenes yet both follow the same reaction pathway.

The elemental content of the black solid residue was investigated by X-ray photoelectron spectroscopy (XPS) and the Te 3d5 spectrum thus obtained is shown in Figure 3.1. Since XPS is predominantly a surface technique no conclusions about the environment of the Te atom in the residue should be drawn, suffice to say that tellurium is present, thus confirming its removal from the heterocycle. Other elements found in the residue by XPS analysis were C, O and Fe.

When the reaction was repeated but stopped after 45 minutes a dark violet crystalline product was obtained together with a black residue. The identity of the violet crystals was confirmed as the previously reported telluraferrole,[76] $C_4H_4TeFe_2(CO)_6$ (**3**); yield 1.82g, 66% based on $Fe_3(CO)_{12}$. Whereas only the ^1H NMR spectrum was reported by the previous workers, additional NMR data for ^{13}C and ^{125}Te nuclei is also presented here.

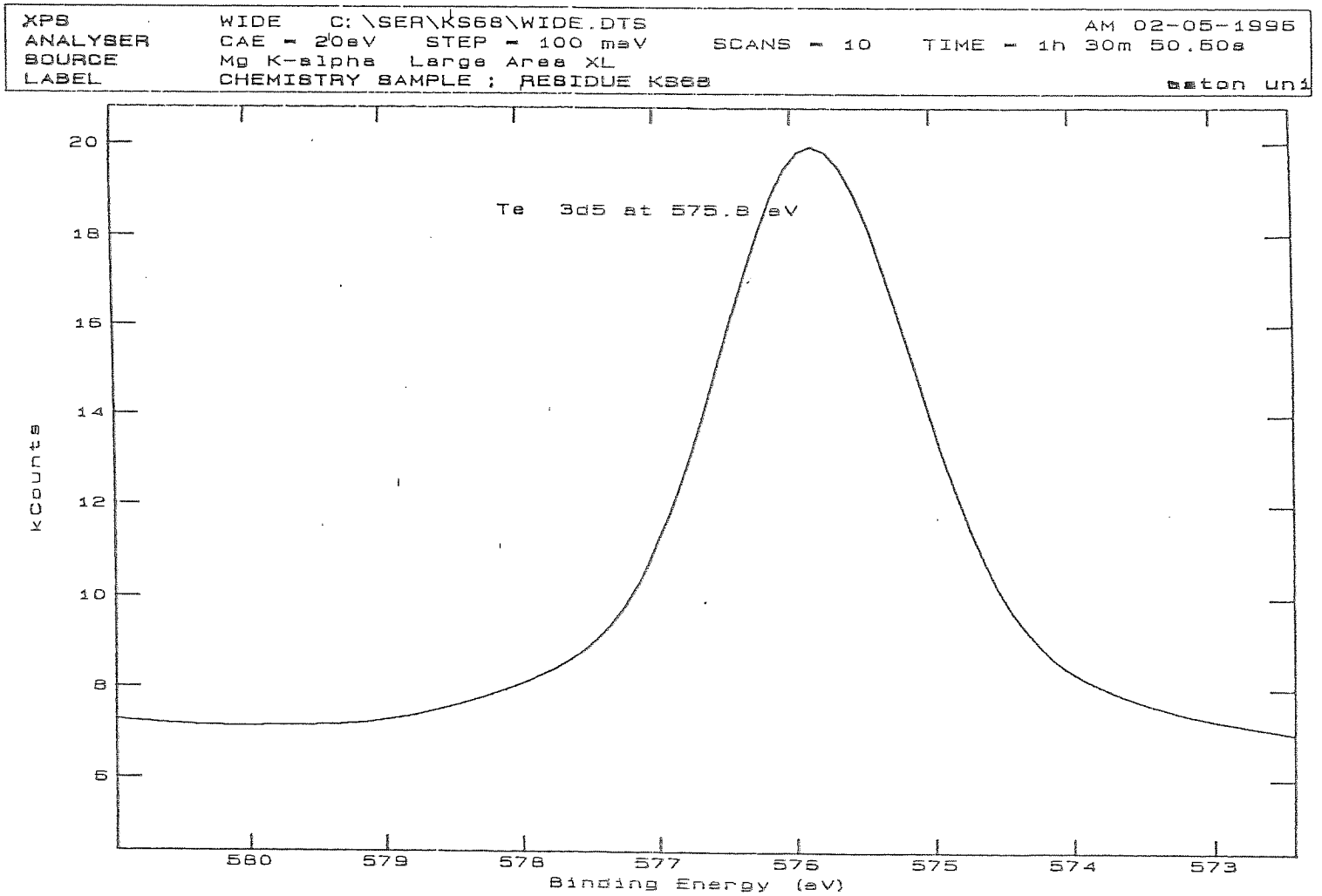

Figure 3.1 Te 3d5 XPS spectrum for residue from reaction of tellurophene with $Fe_3(CO)_{12}$

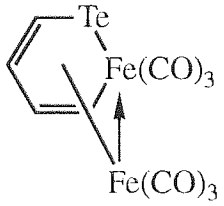

(**3**)

Requires (%)	C, 26.1	H, 0.9	$C_{10}H_4O_6Fe_2Te$
Found (%)	C, 26.0	H, 0.9	

A rich carbonyl region for (**3**) was again displayed in the infrared spectrum, the data from which is recorded in Table 3.4. The CI mass spectrum data is shown in Table 3.5 while NMR data is displayed in Tables 3.6, 3.7 and 3.8.

Telluraferrole KBr, ν(CO) cm^{-1}
2069(m)
2030(m)
1991(s)
1981(s)
1961(m)

Table 3.4 Infrared peaks in the carbonyl region for (**3**)

m/z	**assignment**
462	M^+
332	M^+ - Te
294	M^+ - 6 CO

Table 3.5 Mass spectrum (EI) peaks for (**3**)

compound	^{13}C ($CDCl_3$) δ, ppm J, Hz			
	C1	C2	C3	C4
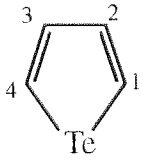	126.6 $J(C^1\text{-Te}) = 301.9$	137.9	137.9	126.6
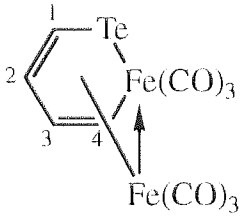	88.9	147.0	86.4	181.9

Table 3.6 ^{13}C NMR data collected for tellurophene and (**3**)

compound	^{1}H ($CDCl_3$) δ, ppm J, Hz			
	H1	H2	H3	H4
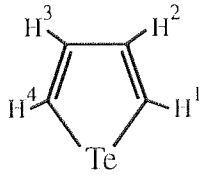	9.03(d) $J(H^1\text{-Te}) = 100.1$ $J(H^1\text{-}H^2) = 6.4$	7.94(q) $J(H^2\text{-}H^3) = 5.7$	7.94(q)	9.03(d)
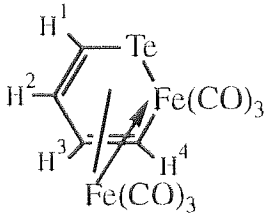	5.73(d) $J(H^1\text{-Te}) = 92.4$ $J(H^1\text{-}H^2) = 9.3$	7.36(q) $J(H^2\text{-}H^3) = 5.7$	5.23(q) $J(H^3\text{-}H^4) = 7.4$	9.55(d)

Table 3.7 ^{1}H NMR data collected for tellurophene and (**3**)

compound	^{125}Te ($CDCl_3$) δ, ppm J(Te-H), Hz
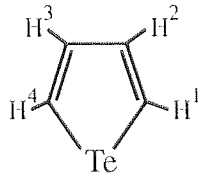	324.9 ppm J(Te-H^1) = 101.3 J(Te-H^2) = 20.0
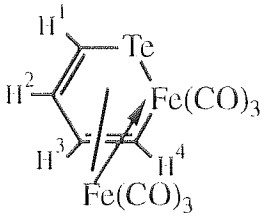	43.0 ppm J(Te-H^1) = 92.6 J(Te-H^2) = 18.9 J(Te-H^3) = 3.1

Table 3.8 ^{125}Te NMR data collected for tellurophene and (3)

The ^{1}H NMR spectrum of tellurophene is shown in Figure 3.12 on page 97. The low-field absorption is assigned to the 1 and 4 protons due to the presence of satellites arising from spin-spin coupling with the tellurium. This is analogous to the spectra of furan, thiophene and selenophene[62] in which the protons nearest to the heteroatom resonate at lower fields. Moreover, the protons of tellurophene resonate at much lower field than those of other heterocyclic compounds. This cannot be due to the inductive deshielding effect of the heteroatom; other effects (i.e. diamagnetic anisotropy and geometry of the ring) must be invoked. In contrast to the ^{1}H NMR spectrum, the carbons adjacent to tellurium, resonate at higher field than C(2) and C(3) as shown by the ^{13}C-^{125}Te satellites in the upfield signal of the ^{13}C NMR spectrum of tellurophene (Figure 3.10). This can be attributed to the shielding effect of the electropositive tellurium atom.

The ^{125}Te NMR spectrum of tellurophene, shown in Figure 3.14, displays a complex multiplet at 324.9 ppm arising from spin-spin coupling of Te with the aromatic ring protons.

The ^{1}H NMR spectrum of telluraferrole (**3**), shown in Figure 3.13, displays four absorptions corresponding to the four protons in the 6-membered ring. Assignments have been made by observation of splitting patterns and calculations of spin-spin coupling constants. The absorption due to the H(1) proton (closest to tellurium) is upfield compared to tellurophene and clearly displays satellites due to spin-spin coupling with ^{125}Te. The H(4) proton experiences a downfield shift relative to tellurophene caused by the insertion of the iron atom into the aromatic ring. This is consistent with the reported ^{1}H NMR spectrum of the analogous 3-methylthiaferrole in which the proton nearest to Fe absorbs furthest downfield.[52]

The ^{13}C NMR of (**3**), shown in Figure 3.11, again displays 4 absorptions corresponding to four C atoms in the 6-membered ring. The carbon adjacent to the iron experiences a considerable downfield shift relative to tellurophene (~55 ppm) with the C(2) carbon also resonating at lower field by ~9 ppm, while the carbon adjacent to tellurium and the C(3) carbon both resonate at higher fields.

The ^{125}Te NMR of (**3**) (Figure 3.15) shows an absorption for Te which is ~282 ppm upfield relative to tellurophene. The greater shielding can be explained by the fact that telluraferrole is diene-like in character whereas the tellurophene can be considered as aromatic. Hence, in telluraferrole, the non-delocalisation of the lone pair of electrons creates greater electron density at the tellurium nucleus which therefore resonates at higher field. The proposed structure, as implied by the NMR data, is shown below and is thought to be analogous to the structure reported for the 3-methylthiaferrole.[52]

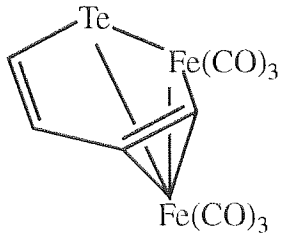

(3)

One $Fe(CO)_3$ unit is inserted into the tellurophene ring and this can be considered as an oxidative addition. The other $Fe(CO)_3$ is η^2-coordinated to two carbon atoms of the diene with a further two coordinative bonds to tellurium and iron.

3.3.4 Reaction of dibenzotellurophene with triiron dodecacarbonyl

The major product from this reaction was a violet crystalline compound, m.p. 176°C, and was identified as the dibenzoferrole (**4**), $C_{12}H_8Fe_2(CO)_6$, reported by ourselves in a recent publication[96]; yield 0.28g, 28% based on $Fe_3(CO)_{12}$.

Requires (%)	C, 50.1	H, 1.9	$C_{18}H_8Fe_2O_6$
Found (%)	C, 50.2	H, 2.0	

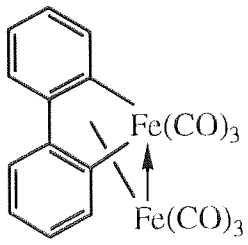

(4)

The data recorded on the infrared spectrum of this compound is shown in Table 3.9; CI mass spectrum data is shown in Table 3.10 while NMR data is displayed in Tables 3.11 and 3.12.

KBr, ν(CO) cm^{-1}
2060(m)
2027(s)
1992(s)
1973(s)
1884(m)

Table 3.9 Infrared bands in the carbonyl region for (**4**)

m/z	assignment
432	$C_{12}H_8Fe_2(CO)_6^+$
152	$C_{12}H_8^+$

Table 3.10 CI Mass spectrum (EI) peaks for (**4**)

compound	^{13}C ($CDCl_3$) δ, ppm					
	C1	C2	C3	C4	C5	C6
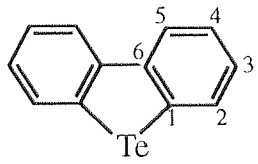	129.1	126.8	125.6	132.8	124.3	144.1
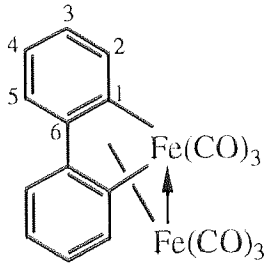	147.8	127.5	129.2	128.2	138.4	119.6

Table 3.11 ^{13}C NMR data for dibenzotellurophene and (**4**)

compound	^{1}H ($CDCl_3$) δ, ppm			
	H1	H2	H3	H4
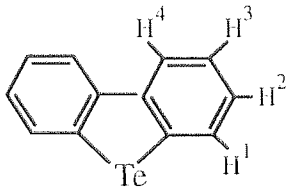	8.23(m)	7.32(m)	8.07(m)	7.47(m)
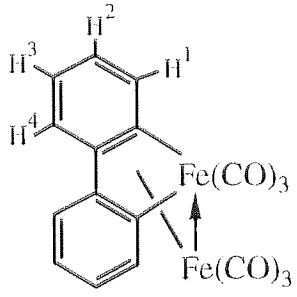	7.42(m)	7.82(m)	7.55(m)	8.23(m)

Table 3.12 ^{1}H NMR data for dibenzotellurophene and (**4**)

The ^{13}C NMR spectrum of dibenzotellurophene is shown in Figure 3.16. Assignments were made by observations of peak intensities and consideration of the shielding effect of the tellurium atom as well as the diamagnetic anisotropic effects in the benzene rings. Assignments for the proton NMR spectrum of dibenzotellurophene (Figure 5.7, chapter 5) were made accordingly.

The ^{13}C NMR spectrum of dibenzoferrole (**4**), shown in Figure 3.17, displays 6 absorptions. The carbon adjacent to iron experiences a downfield shift of ~19 ppm relative to dibenzotellurophene while the C(6) carbon resonates at higher field by ~25 ppm. This effect is also observed in the basic ferrole derived from tellurophene where the C(1) carbon shifts downfield by ~26 ppm, with C(2) resonating ~29 ppm upfield relative to tellurophene.[52]

The crystal structure of (**4**) has been elucidated and is discussed in section 3.4.

3.3.5 Reaction of 2-telluraindane with triiron dodecacarbonyl

Three components were obtained from this reaction after chromatography:

(i) The purple crystals were identified as the cluster compound $Fe_3Te_2(CO)_9$ (**5**); yield 1.13g, 40% based on C_8H_8Te.

Requires (%)	C, 16.0	H, 0.0	$C_9O_9Fe_3Te_2$
Found (%)	C, 16.6	H, 0.1	

(ii) The red-brown solid (m.p. 76°C) was shown to be a novel compound of the formula $C_{16}H_{16}Fe(CO)_3$ (**6**); yield 0.34g, 15.4% based on C_8H_8Te.

Requires (%)	C, 65.5	H, 4.6	$C_{19}H_{16}FeO_3$
Found (%)	C, 65.2	H, 4.8	

(iii) The identity of the yellow oil was not established but it did give an IR spectrum showing the presence of both organic fragments and carbonyl groups; yield 0.33g.

The cluster compound, $Fe_3Te_2(CO)_9$ (**5**) has been previously reported[97] while the novel, $C_{16}H_{16}Fe(CO)_3$ (**6**) was recently reported by ourselves[96] and was shown to have the structure illustrated below.

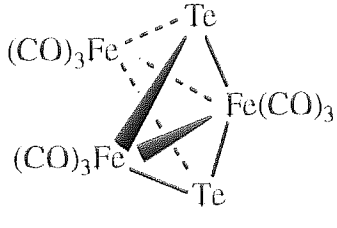

(**5**)

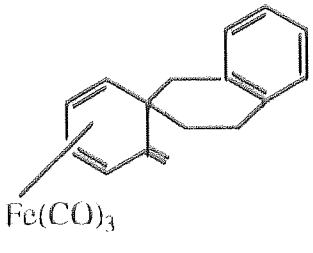

(**6**)

Infrared, NMR and mass spectral data for the three compounds are shown in Tables 3.13-3.18.

compound	KBr, ν(CO) cm^{-1}
$Fe_3Te_2(CO)_9$	2077, 2052, 2020, 1998, 1976, 1960
$C_{16}H_{16}Fe(CO)_3$	2048, 2019, 1978
yellow oil	2051, 1983, 1962

Table 3.13 Infrared bands in the carbonyl regions for products from reaction of 2-telluraindane with $Fe_3(CO)_{12}$

compound	m/z (FAB)	assignment
$Fe_3Te_2(CO)_9$	680	M^+
$C_{16}H_{16}Fe(CO)_3$	384	M^+
	300	$M^+ - 3CO$
yellow oil	unstable	

Table 3.14 FAB-MS (NOBA matrix) data for products from reaction of 2-telluraindane with $Fe_3(CO)_{12}$

compound	^1H ($CDCl_3$), δ ppm
$Fe_3Te_2(CO)_9$	- - - - -
yellow oil	7.45 (m, 2H), 7.36 (m, 2H), 2.44 (d, 2H), 0.22 (d, 2H)

Table 3.15 ^1H NMR data for products from reaction of 2-telluraindane with $Fe_3(CO)_{12}$

compound	^{13}C ($CDCl_3$), δ ppm
$Fe_3Te_2(CO)_9$ yellow oil	211.6, 209.3 132.0, 128.0, 100.0, 35.5, 29.3

Table 3.16 ^{13}C NMR data for products from reaction of 2-telluraindane with $Fe_3(CO)_{12}$

compound	^{13}C ($CDCl_3$) δ, ppm							
	C1	C2	C3	C4	C5	C6	C7	C8
	C9	C10	C11	C12	C13	C14	C15	C16
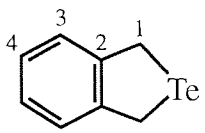	9.46	143.8	125.8	127.7			$J(C^1\text{-}Te) = 135.2$ Hz	
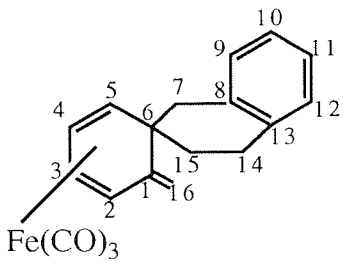	135.6	<-----	154.6	154.2	----->	40.5	29.8	155.0
	<-----	128.5	125.8	----->	155.0	32.8	33.2	102.2

Table 3.17 ^{13}C NMR data for 2-telluraindane and (**6**) obtained from reaction with $Fe_3(CO)_{12}$

compound	^{1}H ($CDCl_3$) δ, ppm					
	H1	H2	H3	H4	H5	H6
	H7	H8	H9	H10	H11	H12
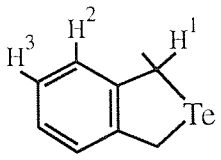	4.6(s)	7.06(q)	7.22(q)			
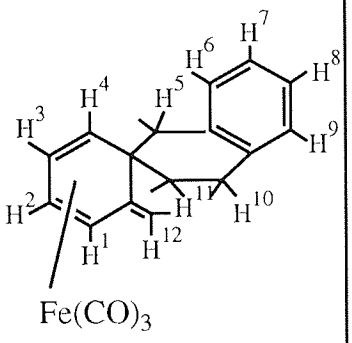	<--------	7.39	7.32(m)	-------->	0.28(s)	<--------
	7.48	7.42(m)	-------->	<---0.22	0.19---> (m)	2.44(s)

Table 3.18 ^{1}H NMR data for 2-telluraindane and (**6**) obtained from reaction with $Fe_3(CO)_{12}$

The ^{1}H and ^{13}C NMR spectra of 2-telluraindane are shown in Figures 3.18 and 3.19 respectively.

The ^{13}C NMR spectrum of compound (**6**) formed from the reaction of 2-telluraindane with $Fe_3(CO)_{12}$ displays absorptions at 154.6-154.2 ppm for the diene carbons, C(1), C(2), C(3) and C(4), resonating further downfield than might be expected due to donation of π-electron density to the iron atom with only slight back-donation. The resonance absorptions for the exocyclic double bond carbons C(1) and C(16) are clearly defined at 135.6 and 102.2 ppm respectively, while the chiral carbon C(6) displays an absorption peak at 40.5 ppm. The ^{1}H NMR assignments have been made by correlation with ^{13}C NMR data.

The structure of compound (**6**) has been elucidated by X-ray crystallography and is discussed in section 3.4.

3.3.6 Reaction of phenoxtellurine with triiron dodecacarbonyl

Two major products were obtained from this reaction; a pale pink solid and an oily orange solid. The pale pink solid was identified as a carbonyl insertion product of formula, $C_{13}H_8O_2$, the structure of which is shown below (**7**); yield 0.045g. The identity of the oily orange solid (yield 0.21g) was not confirmed, but mass spectrometry suggested that it may be an intermediate, telluraferrole-type product as was observed in the reaction of tellurophene with $Fe_3(CO)_{12}$. Table 3.19 shows IR data obtained for these products while mass spectrometry data is displayed in Table 3.20. Suitable NMR data was not collected.

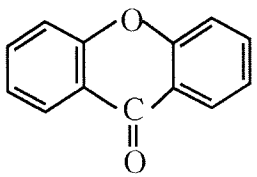

(**7**)

compound	KBr, ν(CO) cm^{-1}
$C_{13}H_8O_2$	1681, 1617, 1608
oily orange	2054, 2018, 1984
solid	

Table 3.19 Infrared bands in the carbonyl regions for products from reaction of phenoxtellurine with $Fe_3(CO)_{12}$

compound	m/z (FAB)	assignment
$C_{13}H_8O2$	196	M^+
oily orange solid	536	not identified
	372	

Table 3.20 FAB-MS (NOBA matrix) data for products from reaction of phenoxtellurine with $Fe_3(CO)_{12}$

The reaction of phenoxtellurine with $Fe_3(CO)_{12}$ results in the removal of tellurium from the heterocyclic ring to eventually yield a carbonyl insertion product. The oily orange solid may well be an intermediate in which an $Fe(CO)_3$ fragment has inserted into the C-Te bond of phenoxtellurine, as suggested by the presence of a rich carbonyl region in its infrared spectrum.

3.3.7 Summary of reactions of tellurium heterocycles with $Fe_3(CO)_{12}$

The reactions of the tellurium heterocycles with $Fe_3(CO)_{12}$ are summarised in Scheme 3.5

$Fe_3(CO_{12}$ is effective in removing the tellurium from all the heterocylic systems that have been studied leading to the formation of some novel organometallic compounds of iron. Reaction with tellurophene yields the ferrole (**1**) as observed with thiophene, but in addition, the intermediate telluraferrole (**3**) is also isolated. Dibenzotellurophene is also detellurated to yield the dibenzoferrole (**4**) which is inaccesible via reaction with the analogous sulfur heterocycle. This is an important observation since it proves the mechanistic feasibility of dechalcogenation of the more condensed systems. 2-telluraindane reacts with $Fe_3(CO)_{12}$ to afford the novel organometallic compound (**6**) while phenoxtellurine is detellurated to yield an organic carbonyl compound (**7**).

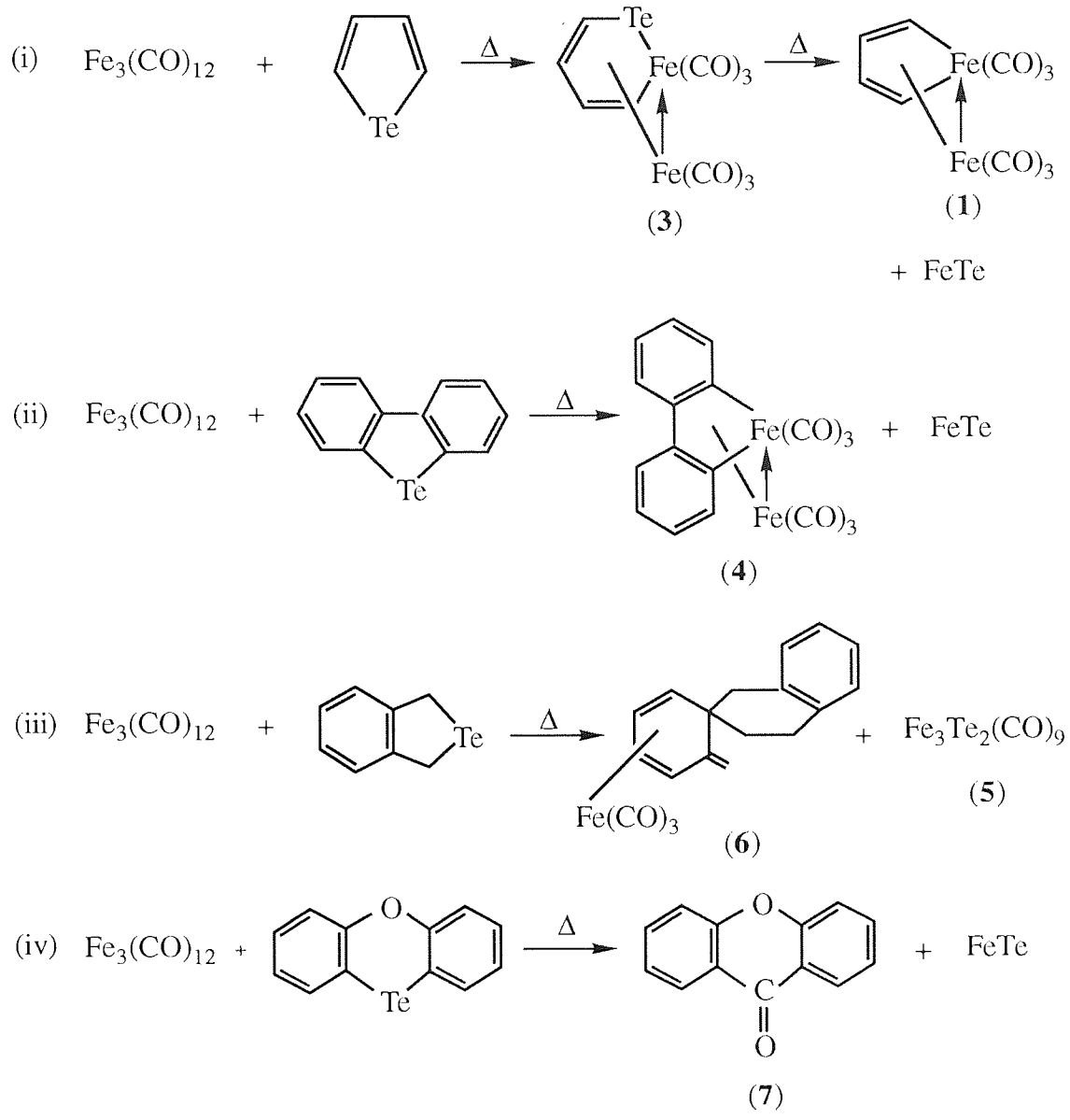

Scheme 3.5 Reactions of tellurium heterocycles with $Fe_3(CO)_{12}$

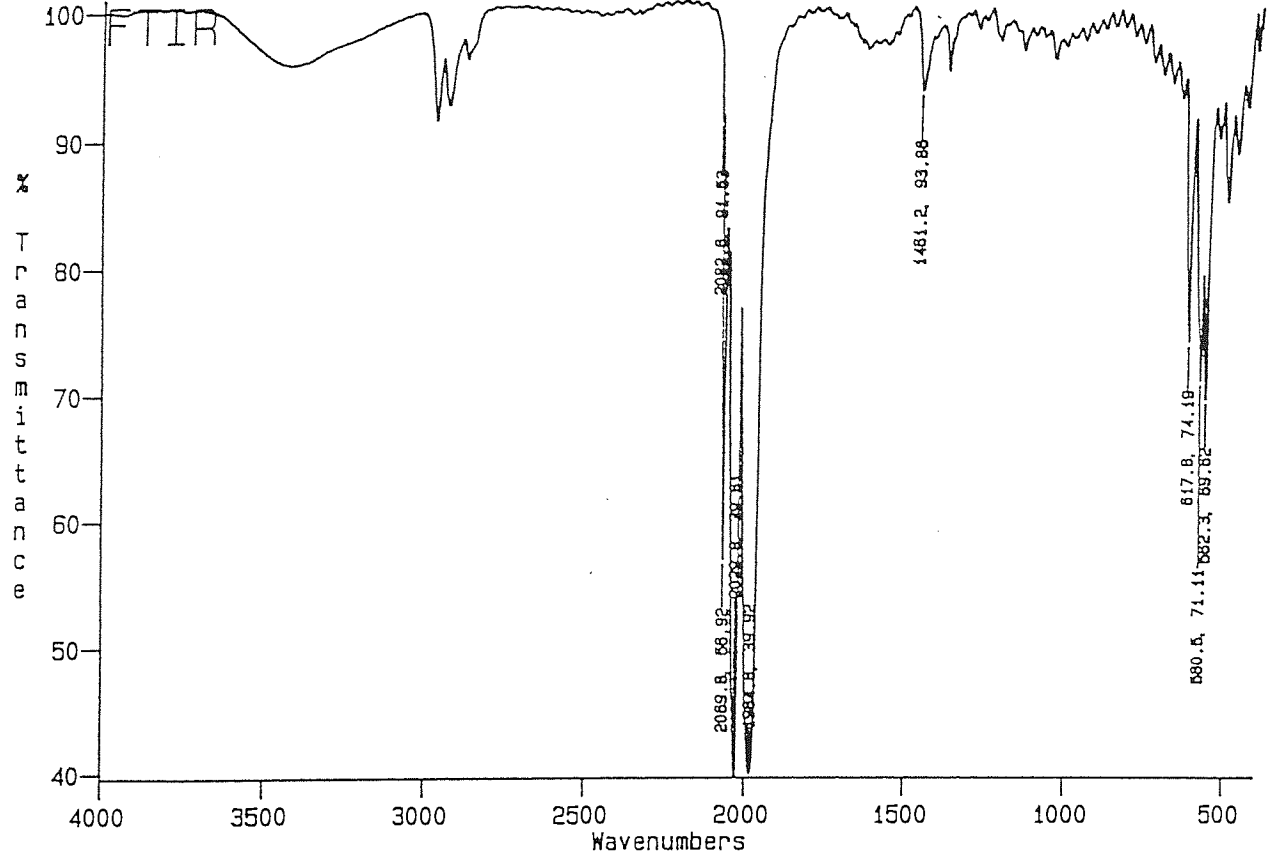

Figure 3.2 IR spectrum of ferrole, $C_4H_4.Fe_2(CO)_6$ (1)

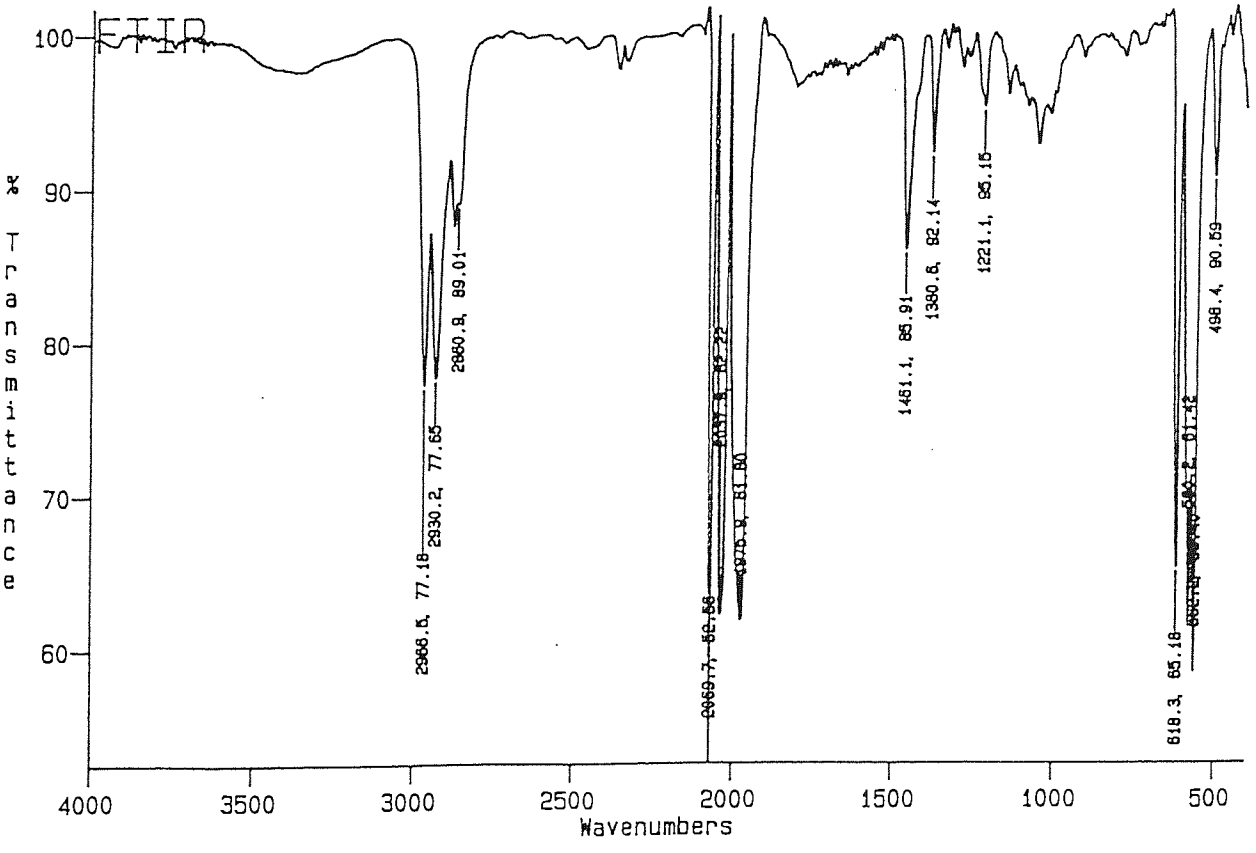

Figure 3.3 IR spectrum of $C_4H_4.Fe_3(CO)_8$ (2)

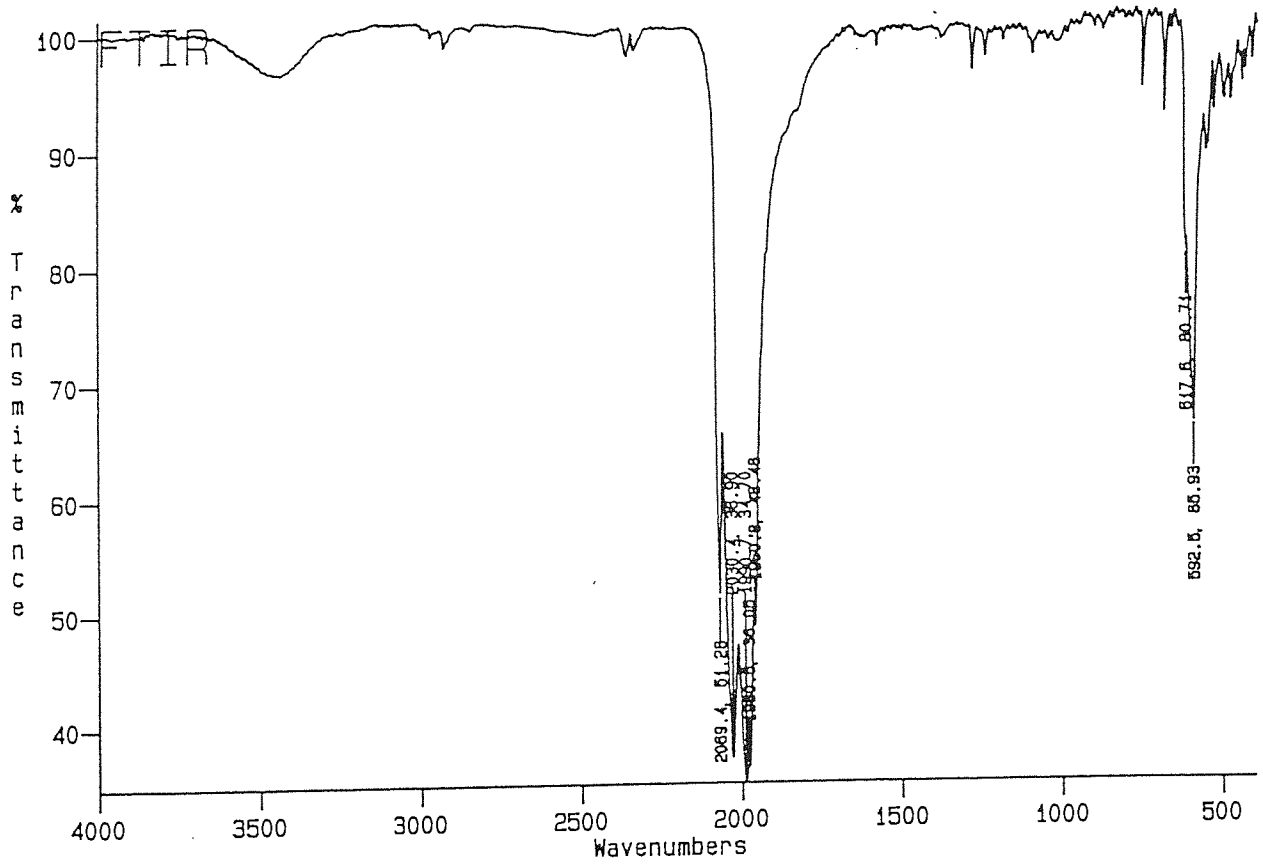

Figure 3.4 IR spectrum of telluraferrole, $C_4H_4Te.Fe_2(CO)_6$ (3)

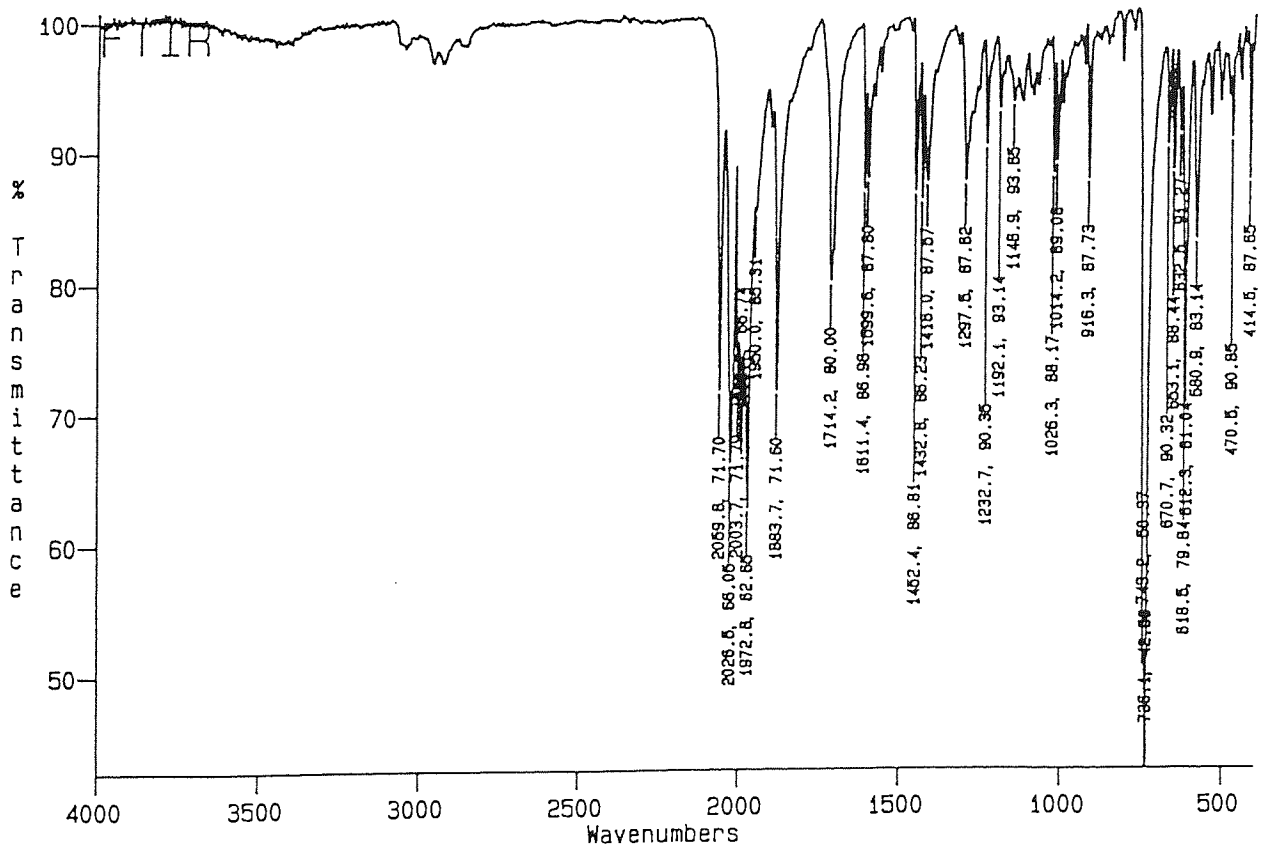

Figure 3.5 IR spectrum of dibenzoferrole, $C_{12}H_8.Fe_2(CO)_6$ (4)

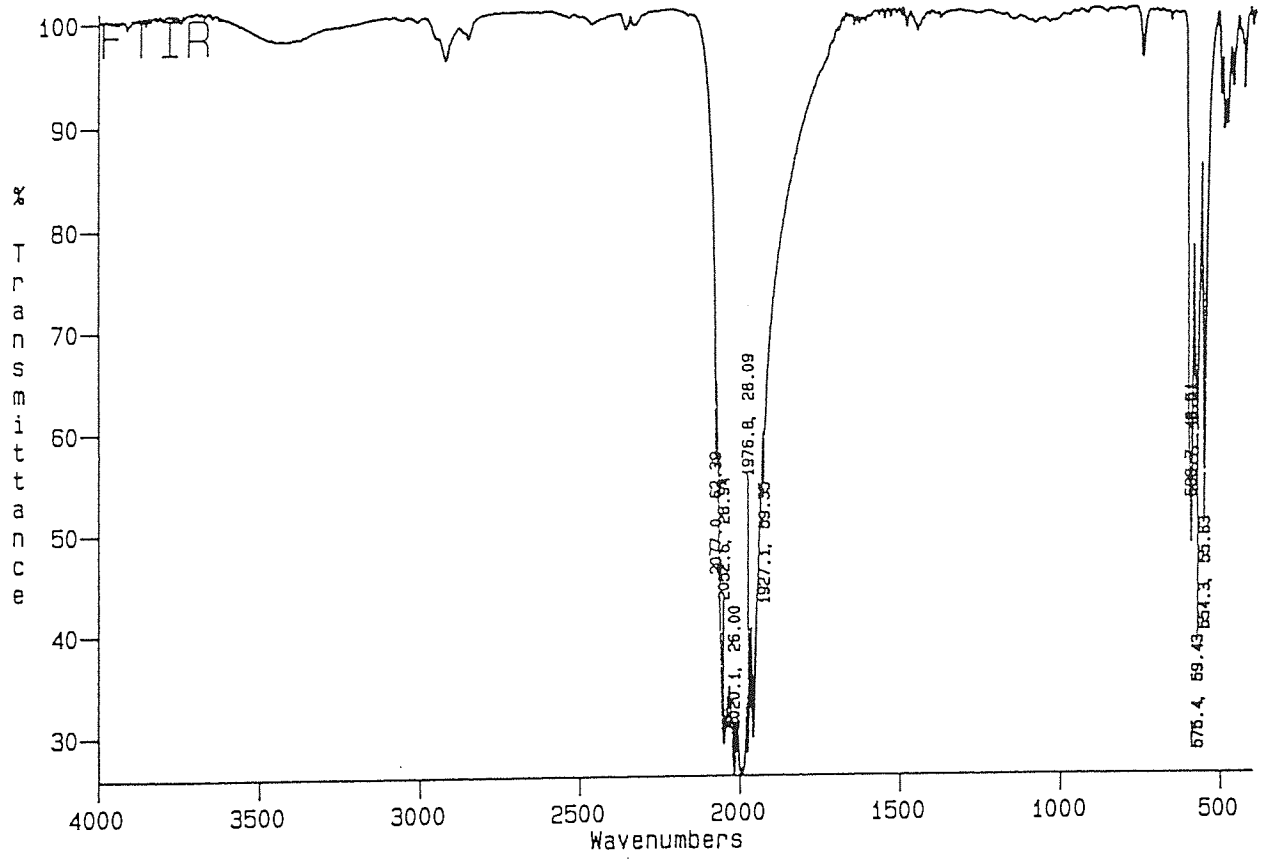

Figure 3.6 IR spectrum of $Fe_3Te_2(CO)_9$ (**5**)

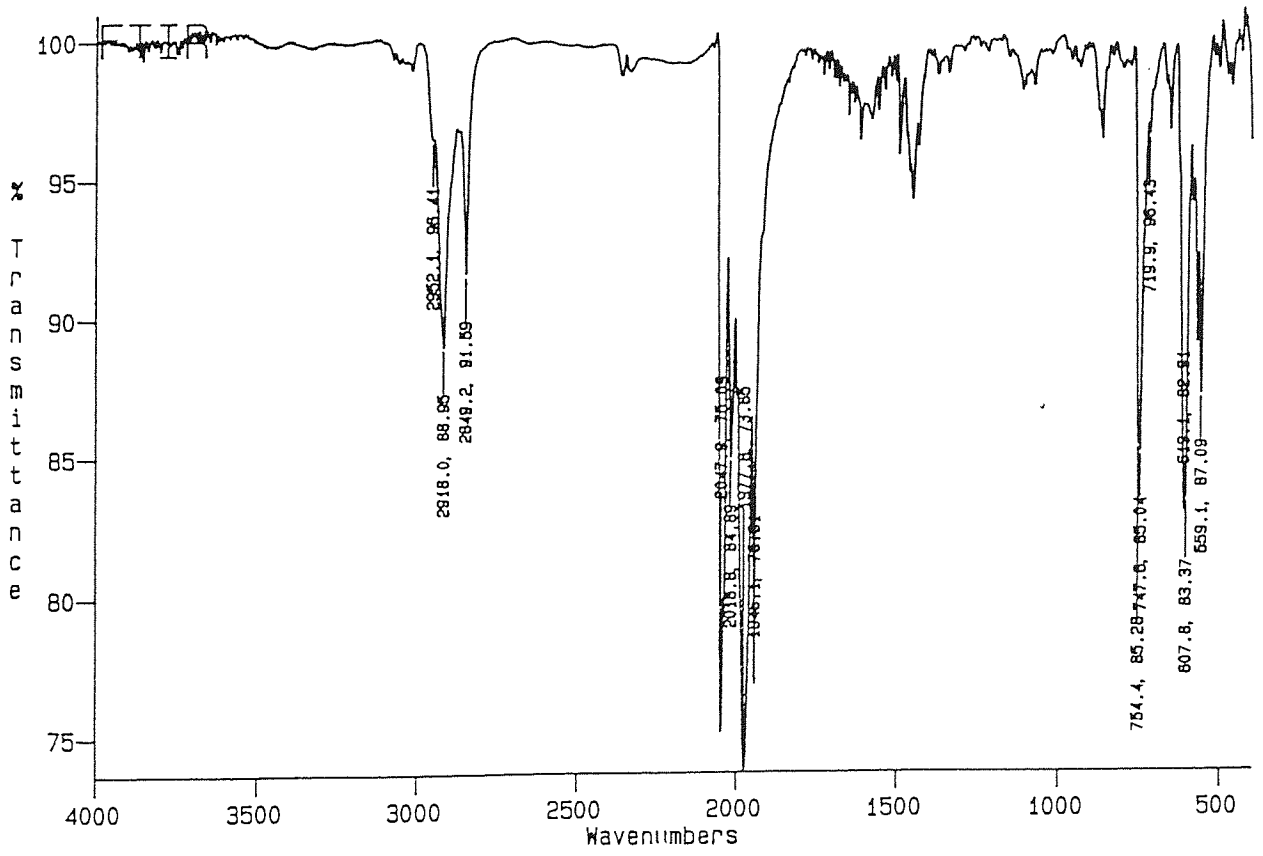

Figure 3.7 IR spectrum of $C_{16}H_{16}.Fe(CO)_3$ (**6**)

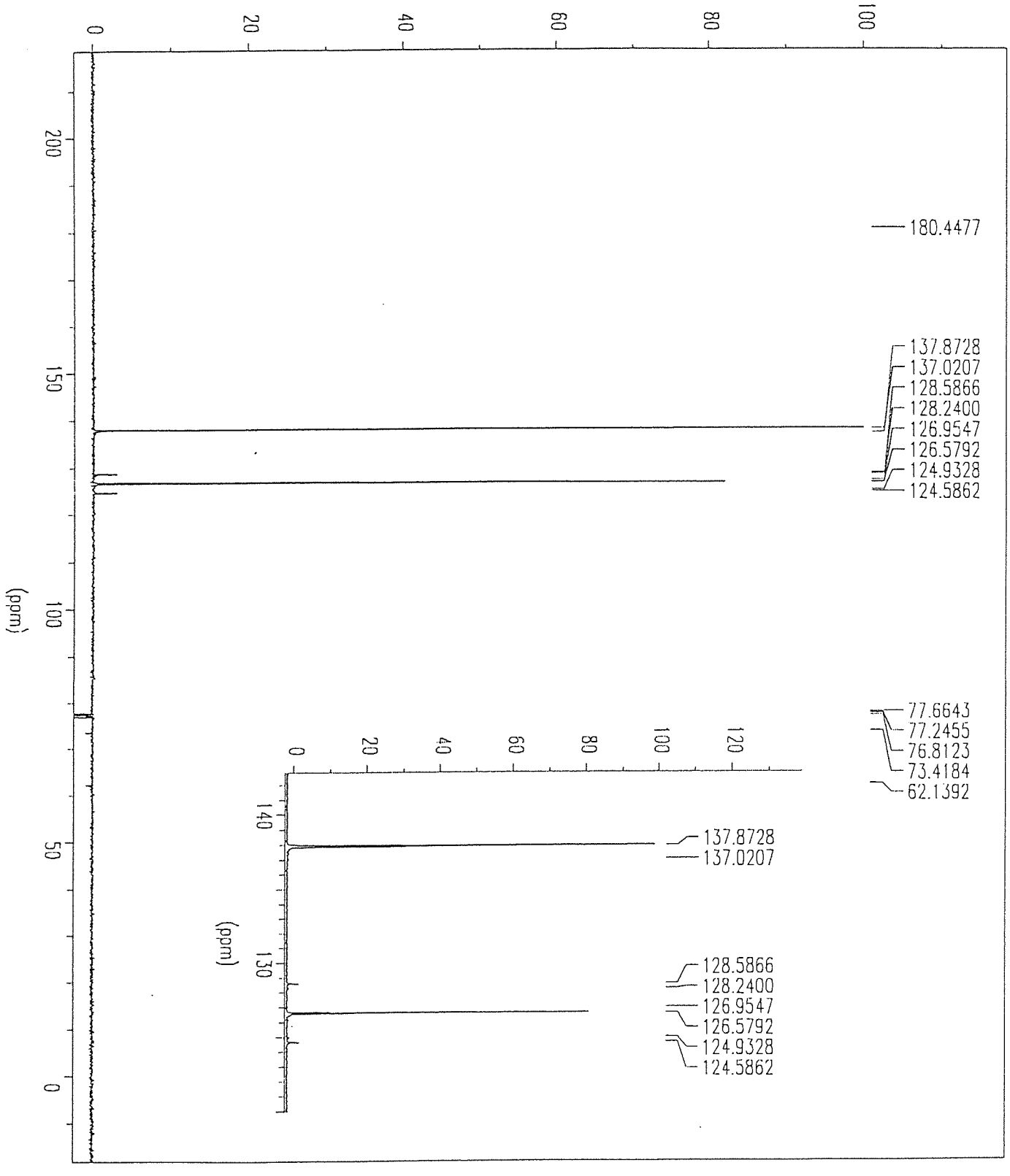

Figure 3.10 ^{13}C NMR spectrum of tellurophene

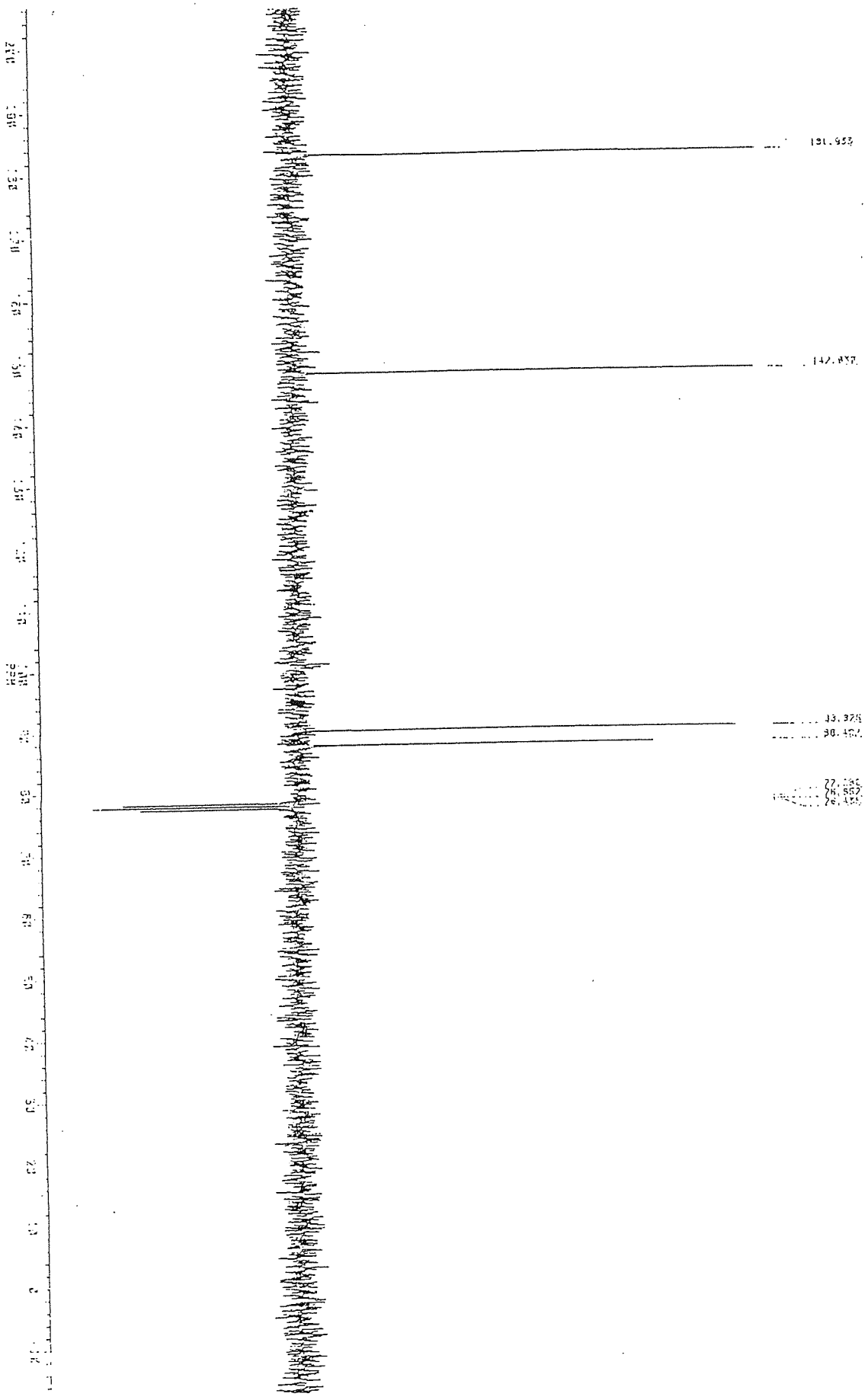

Figure 3.11 ^{13}C NMR spectrum of telluraferrole, $C_4H_4Te.Fe_2(CO)_6$ (**3**)

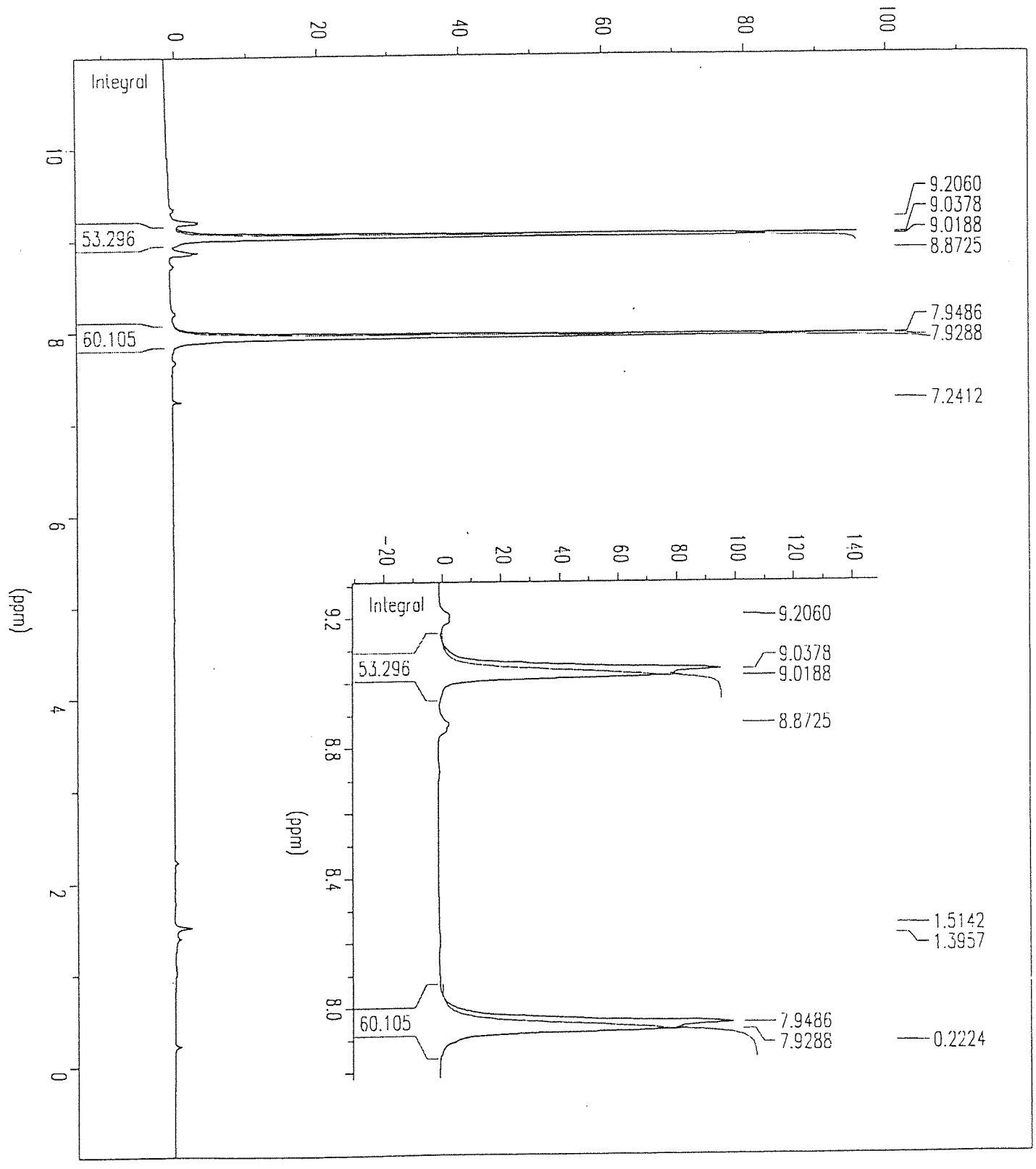

Figure 3.12 ^{1}H NMR spectrum of tellurophene

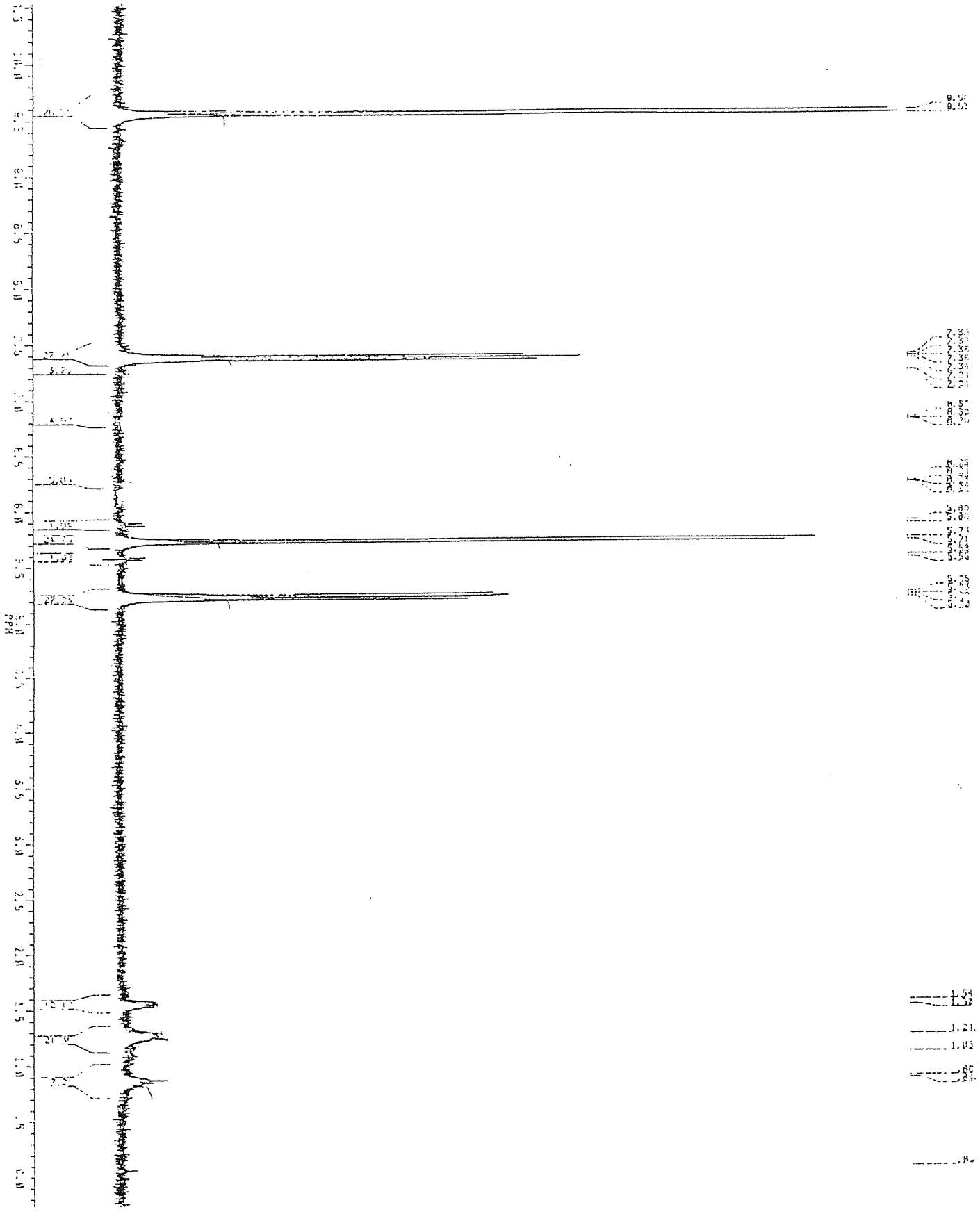

Figure 3.13 ^{1}H NMR spectrum of telluraferrole, $C_4H_4Te.Fe_2(CO)_6$ (3)

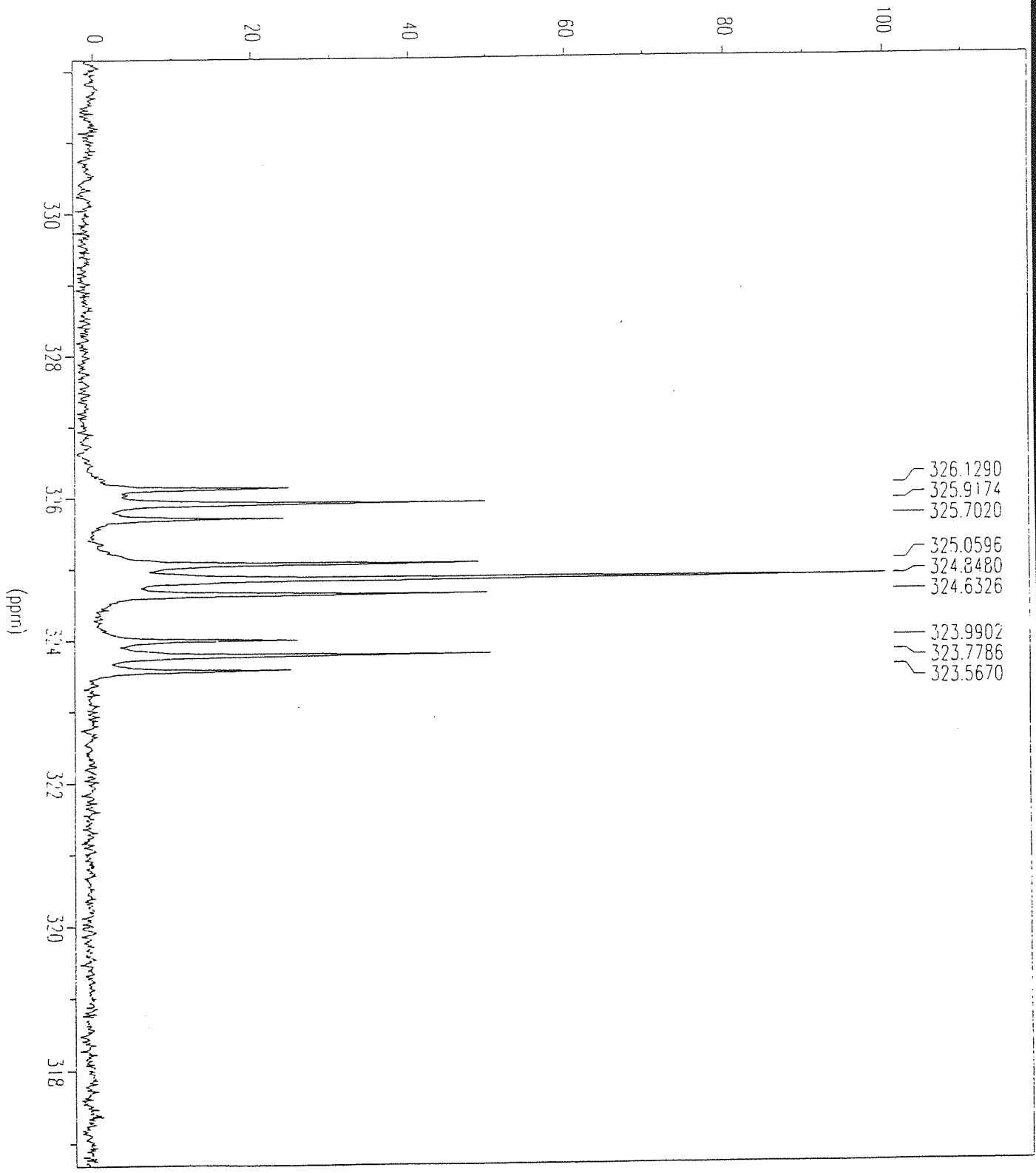

Figure 3.14 ^{125}Te NMR spectrum of tellurophene

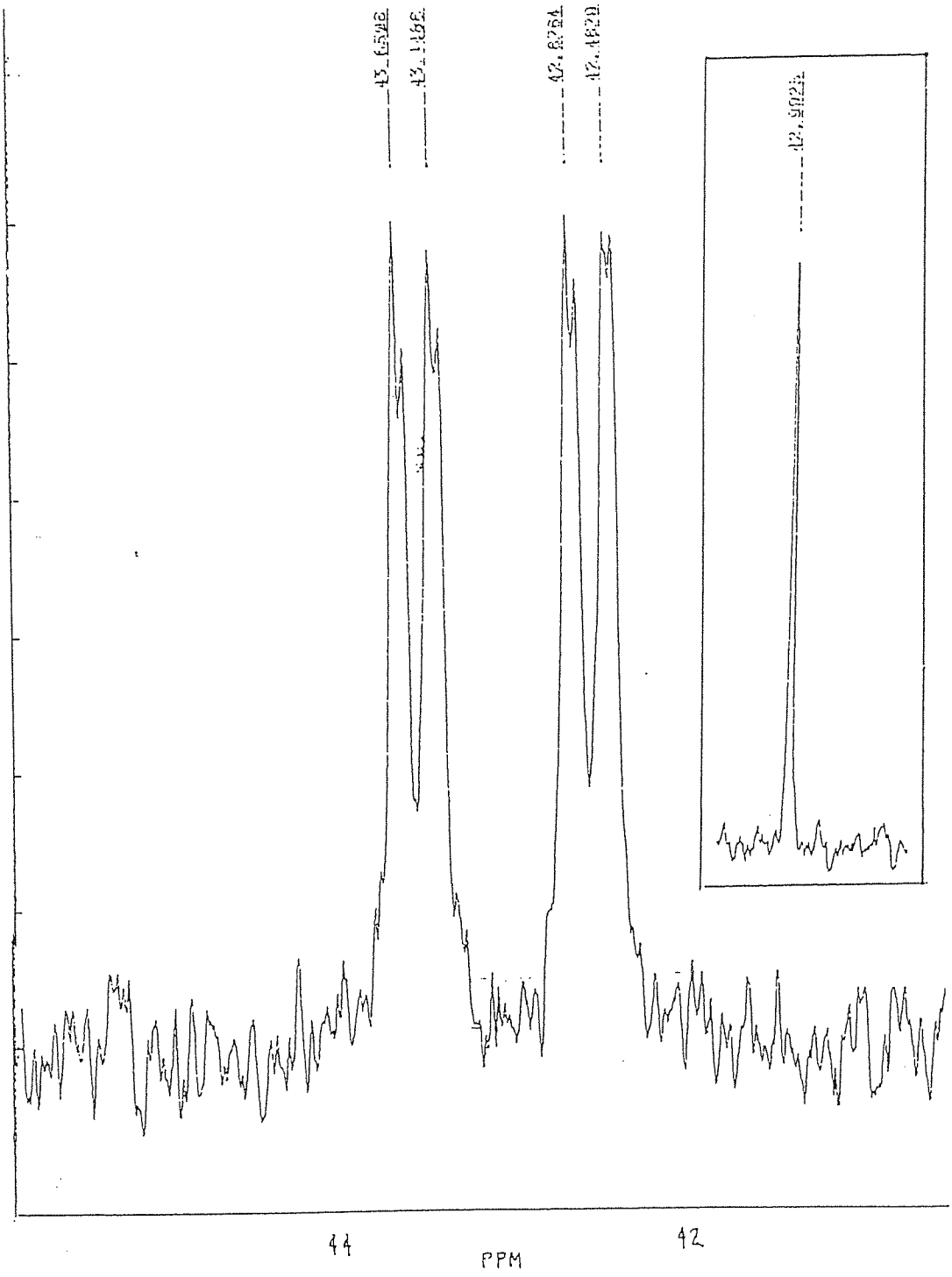

Figure 3.15 ^{125}Te NMR spectrum of telluraferrole, $C_4H_4Te.Fe_2(CO)_6$ (3)
Inset shows proton decoupled spectrum

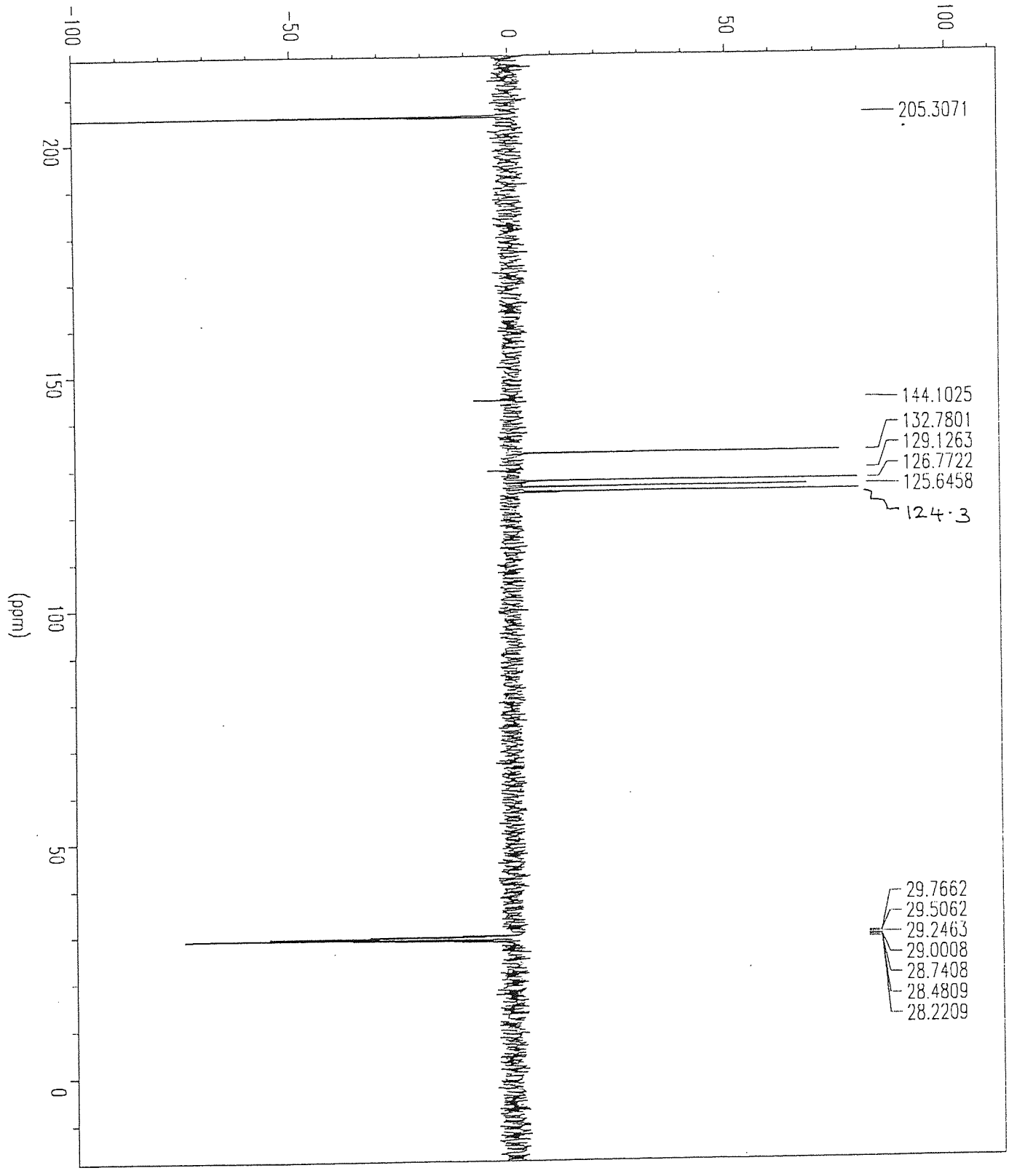

Figure 3.16 ^{13}C NMR spectrum of dibenzotellurophene

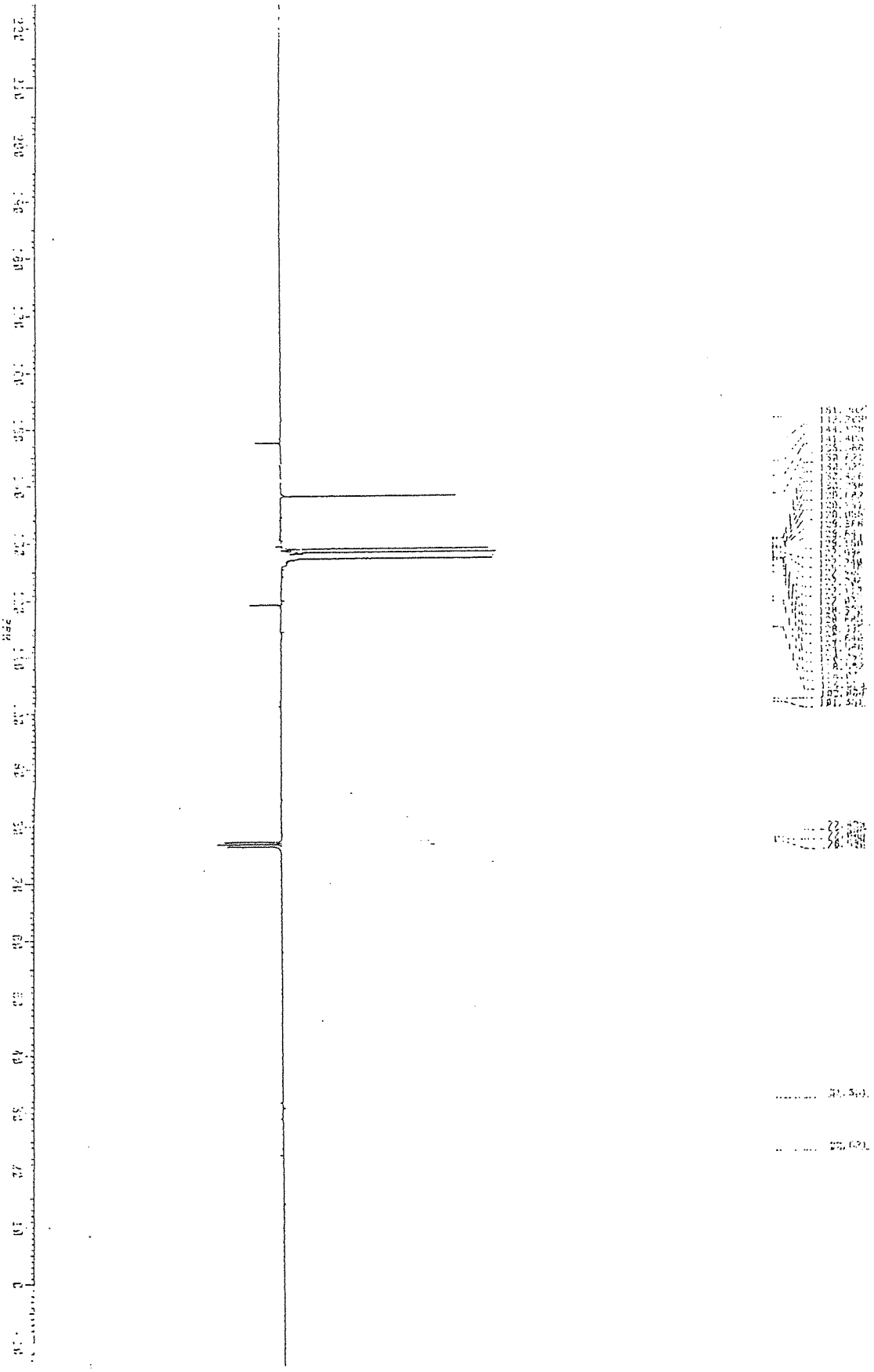

Figure 3.17 ^{13}C NMR spectrum of dibenzoferrole, $C_{12}H_8.Fe_2(CO)_6$ (**4**)

3.3.8 Reaction of tellurophene with cyclopentadienyl iron dicarbonyl iodide

No significant reaction was observed. The violet crystals that were recovered were found to be unreacted starting material, $CpFe(CO)_2I$. The black residue, however, did contain small amounts of tellurium when analysed by XPS.

3.3.9 Reaction of 2-telluraindane with cyclopentadienyl iron dicarbonyl iodide

The brown solid that was isolated was analysed as unreacted starting materials. The black crystalline precipitate that formed during the reaction (m.p. 130°C) gave strong absorption peaks in the carbonyl region of the infrared spectrum which did not coincide with those of $CpFe(CO)_2I$ and it also gave a positive test for iodide. The proposed structure of this solid, shown below (**8**), is thought to be a simple coordination compound ; yield 0.34g, 45.6% based on C_8H_8Te.

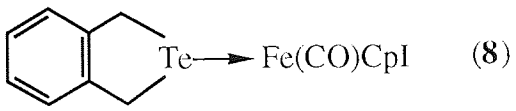

(**8**)

Requires (%)	C, 33.0	H, 2.6	$C_{14}H_{13}OFeTeI$
Found (%)	C, 32.7	H, 2.4	

Infrared, NMR and mass spectrometry data for this compound are shown in Tables 3.21-3.24.

$CpFe(CO)_2I$ KBr, ν(CO) cm^{-1}	$C_8H_8TeFe(CO)CpI$ KBr, ν(CO) cm^{-1}
2046 (m)	2033 (m)
1974 (w)	1990 (m)
1950 (w)	1941 (s)

Table 3.21 Infrared bands in the carbonyl region for $CpFe(CO)_2I$ and (**8**)

compound	m/z (FAB)	assignment
$C_8H_8TeFe(CO)CpI$	510	M^+
	482	M^+ - CO
	355	M^+ - CO - I
	234	$C_8H_8Te^+$
	104	$C_8H_8^+$

Table 3.22 Mass spectrometry data for (**8**)

compound	^{13}C ($CDCl_3$) δ, ppm	Δδ, ppm	assignment
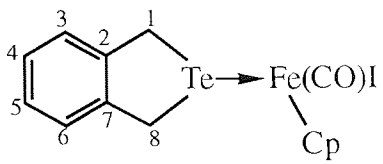	141.5	-2.3	C7
	141.2	-2.6	C2
	128.3	+0.6	C4, C5
	127.0	+1.2	C3, C6
	81.2	-	Cp
	24.6	+15.1	C8
	21.5	+12.0	C1

Table 3.23 ^{13}C NMR data for (**8**)

Δδ represents shift from parent 2-telluraindane; - = upfield shift, + = downfield shift

compound	^1H ($CDCl_3$) δ, ppm					
	H1	H2	H3	H4	H5	H6
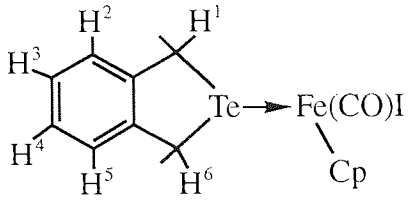	5.02(s)	<-------	7.24	7.08(m)	------->	5.43(s)

Table 3.24 ^1H NMR data for product from reaction of $CpFe(CO)_2I$ and 2-telluraindane

The ^{13}C NMR spectrum for (**8**) is shown in Figure 3.20. It clearly shows that the presence of iron has the greatest influence on the saturated carbons C(1) and C(8), both of which experience a downfield shift. This is indicative of the coordination of tellurium to the iron atom, resulting in an inductive deshielding effect on the adjacent carbons. The non-identical resonances of the C(1) and C(8) nuclei can be attributed to the unsymmetrical coordination environment of iron. The aromatic ring carbons show a small deviation in chemical shift from the parent compound, with the tertiary C(2) and C(7) carbons resonating at slightly higher fields. The ^1H NMR assignments have been made in correlation to the ^{13}C spectrum and again they show downfield shifts for protons on the carbons adjacent to tellurium. The available analytical data are all consistent with the proposed structure shown below.

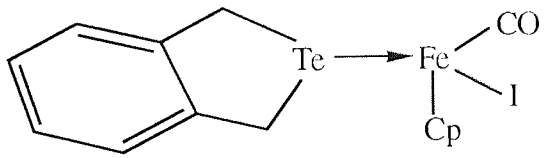

(**8**)

3.3.10 Reaction of phenoxtellurine with cyclopentadienyl iron dicarbonyl iodide

The orange solid (m.p. 158°C) showed a band in the infrared spectrum at 1636 cm^{-1}, suggesting the presence of an organic carbonyl group. No absorption peaks corresponding to inorganic carbonyl groups were detected, hence it is unlikely that iron is present. The test for iodide proved negative but its mass spectrum did indicate, by observation of isotopic patterns, that tellurium is retained. Suitable NMR data was not collected hence accurate predictions of the structure of this product cannot be made. It is evident, however, that a carbonyl insertion reaction has taken place and the mass spectral peak (EI) at m/z = 326 fits M^+ for the molecular formula $C_{13}H_8O_2Te$, the possible structure of which is shown below.

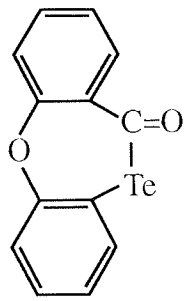

(**9**)

The identity of the brown residue that was also formed in this reaction was not confirmed.

3.3.11 Reaction of tellurophene with cyclopentadienyl iron dicarbonyl dimer

The purple solid obtained from this reaction was found to be unreacted $Cp_2Fe_2(CO)_2$. A comparison of the absorption peaks in the carbonyl region of the infrared spectrum for the brown residue and $Cp_2Fe_2(CO)_2$ is shown in Table 3.25.

$Cp_2Fe_2(CO)_2$ KBr, ν(CO) cm^{-1}	brown residue KBr, ν(CO) cm^{-1}
1972 (m)	2048 (m)
1938 (w)	2000 (m)
1906 (w)	

Table 3.25 Comparison of IR data in the carbonyl region for $Cp_2Fe_2(CO)_2$ and its reaction product with tellurophene

The brown residue did not show the presence of any organic groups in the IR spectrum and XPS showed that iron was present but tellurium was absent. Further analysis of the residue (NMR and mass spectrometry) proved inconclusive, hence its identity was not established.

3.3.12 Summary of reactions of tellurium heterocycles with $CpFe(CO)_2I$

The reactions of the tellurium heterocycles with $CpFe(CO)_2I$ are summarised in Scheme 3.6.

Both $Cp_2Fe_2(CO)_2$ and $CpFe(CO)_2I$ show no reactivity towards tellurophene. $CpFe(CO)_2I$ does, however, react with 2-telluraindane affording a coordination complex (**8**), in which the gretater Lewis basicity of tellurium (c. f. tellurophene) is utilised. Cleavage of the C-Te bonds does not occur, even with prolonged reaction times, hence no detelluration of the heterocycle is observed. $CpFe(CO)_2I$ is, however, effective in cleaving one of the C-Te bonds in phenoxtellurine to yield a carbonyl insertion product (**9**), although again, no detelluration of the heterocycle is effected. Hence it is clear that the monometallic $CpFe(CO)_2I$ displays some success in the breaking C-Te bonds, but further treatment is required for the complete removal of the heteroatom.

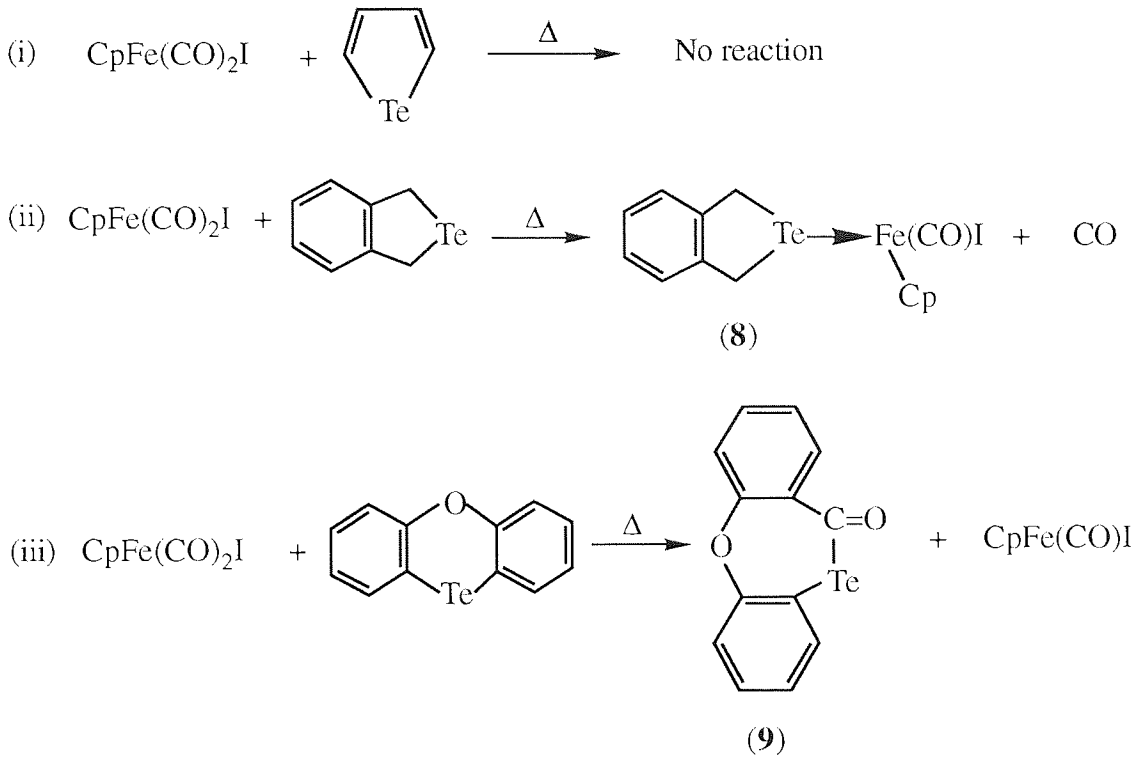

Scheme 3.6 Reactions of tellurium heterocycles with $CpFe(CO)_2I$

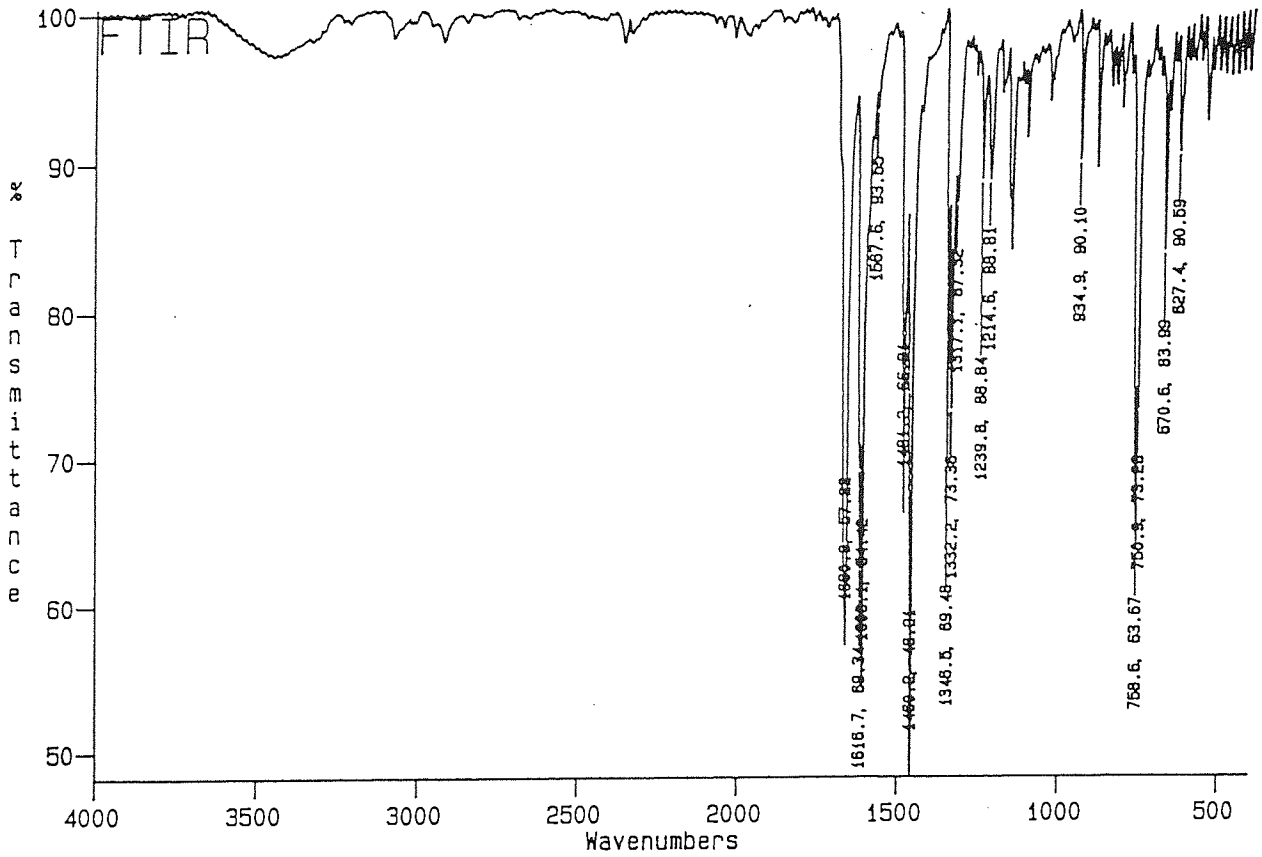

Figure 3.8 IR spectrum of $C_{12}H_8O.CO$ (7)

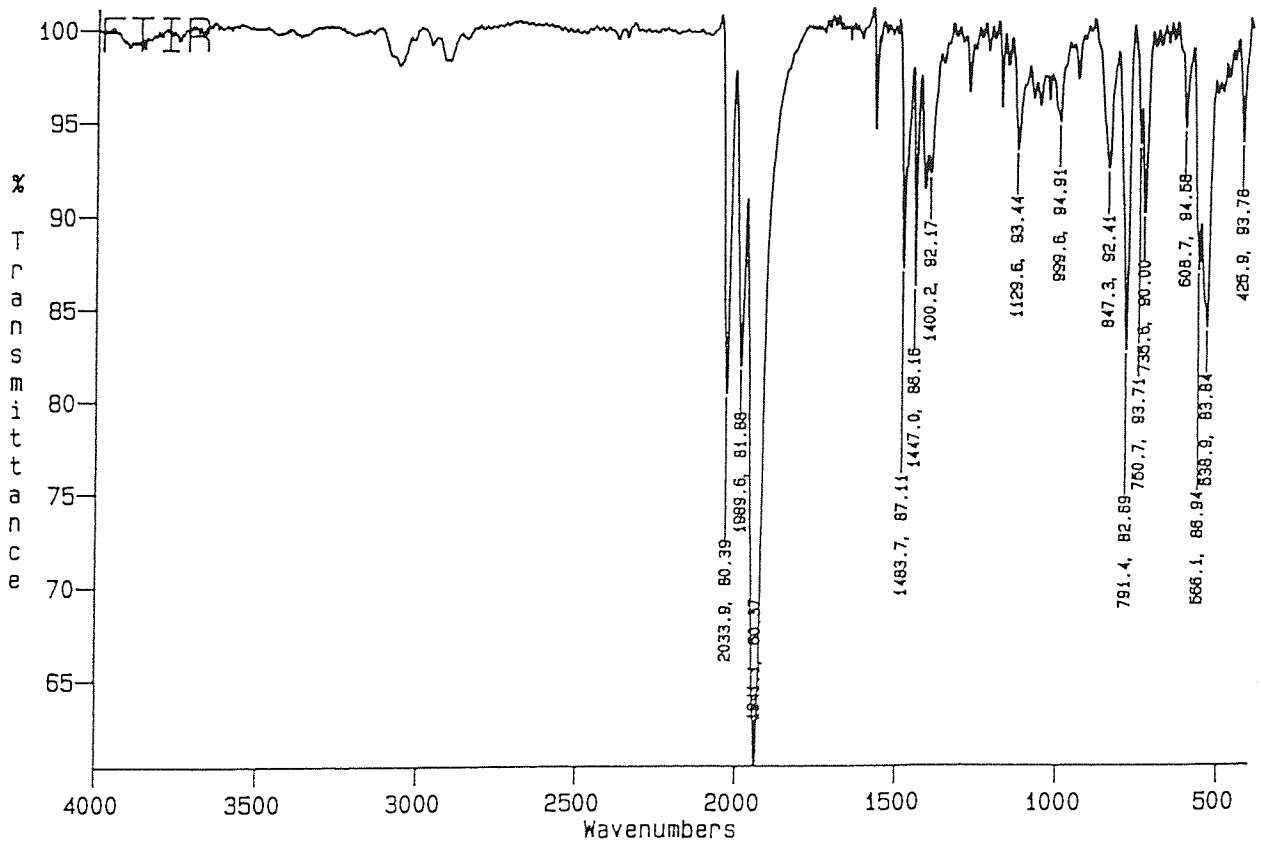

Figure 3.9 IR spectrum of $C_8H_8Te.Fe(CO)CpI$ (8)

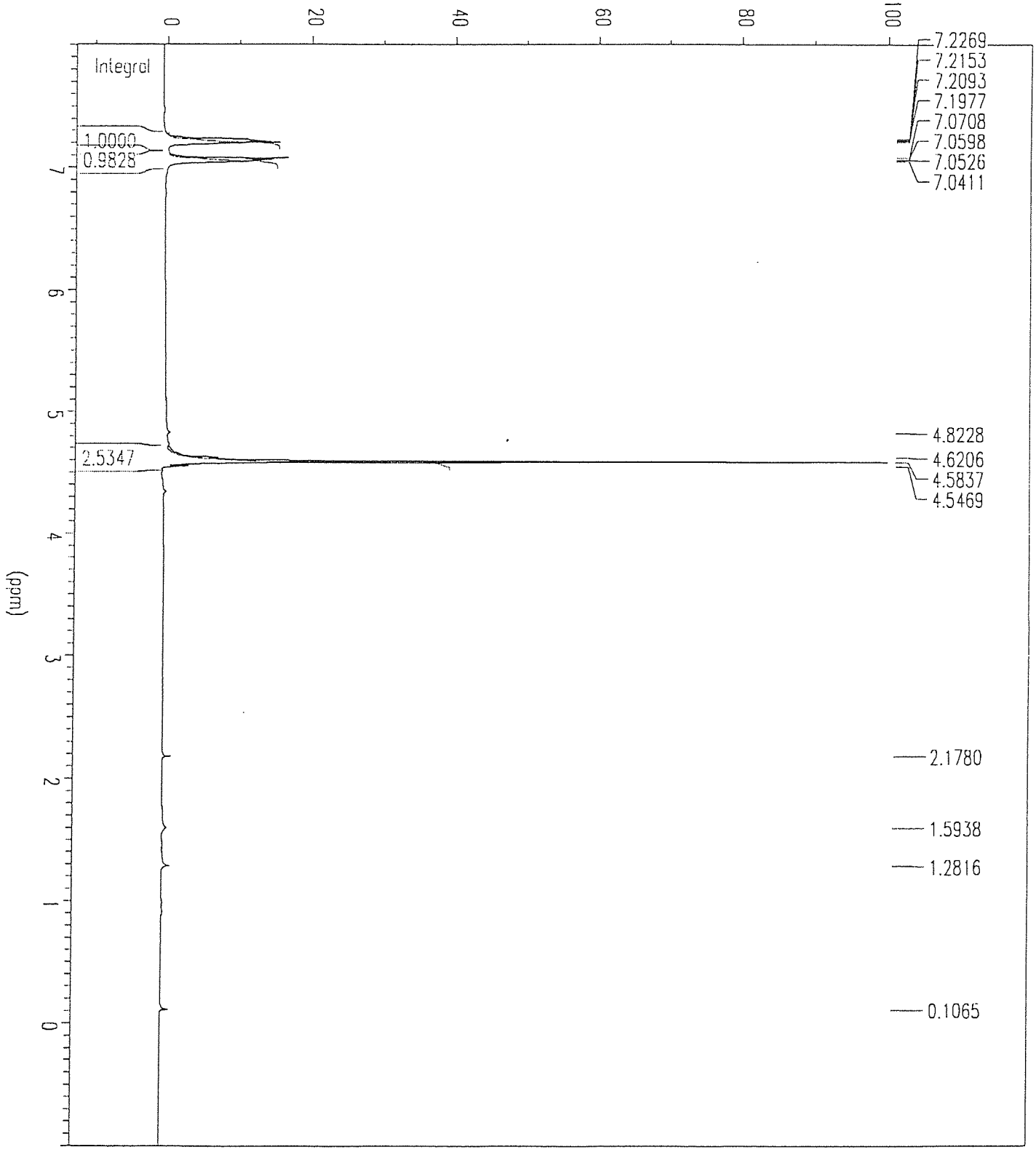

Figure 3.18 ^{1}H NMR spectrum of 2-telluraindane

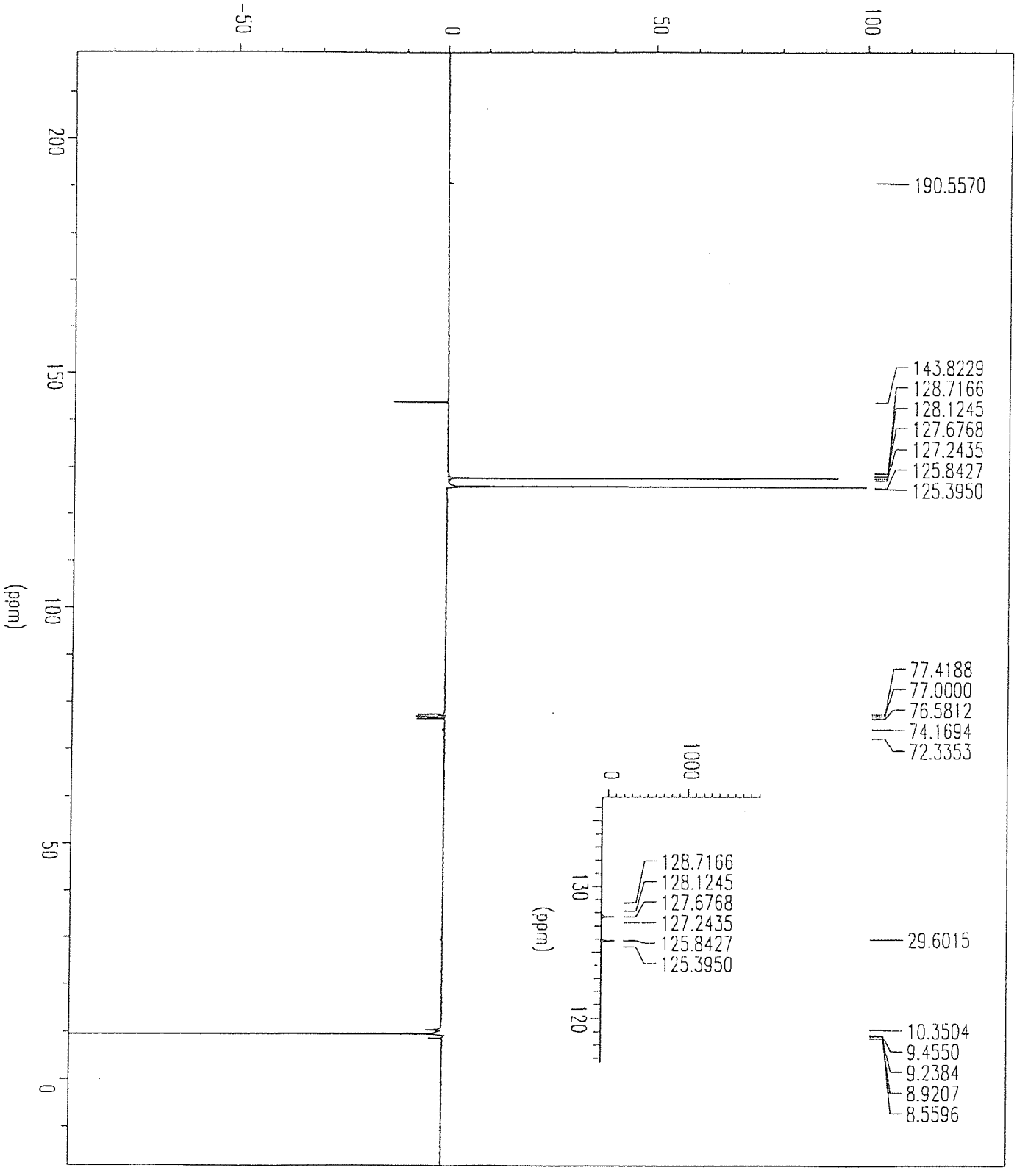

Figure 3.19 ^{13}C NMR spectrum of 2-telluraindane

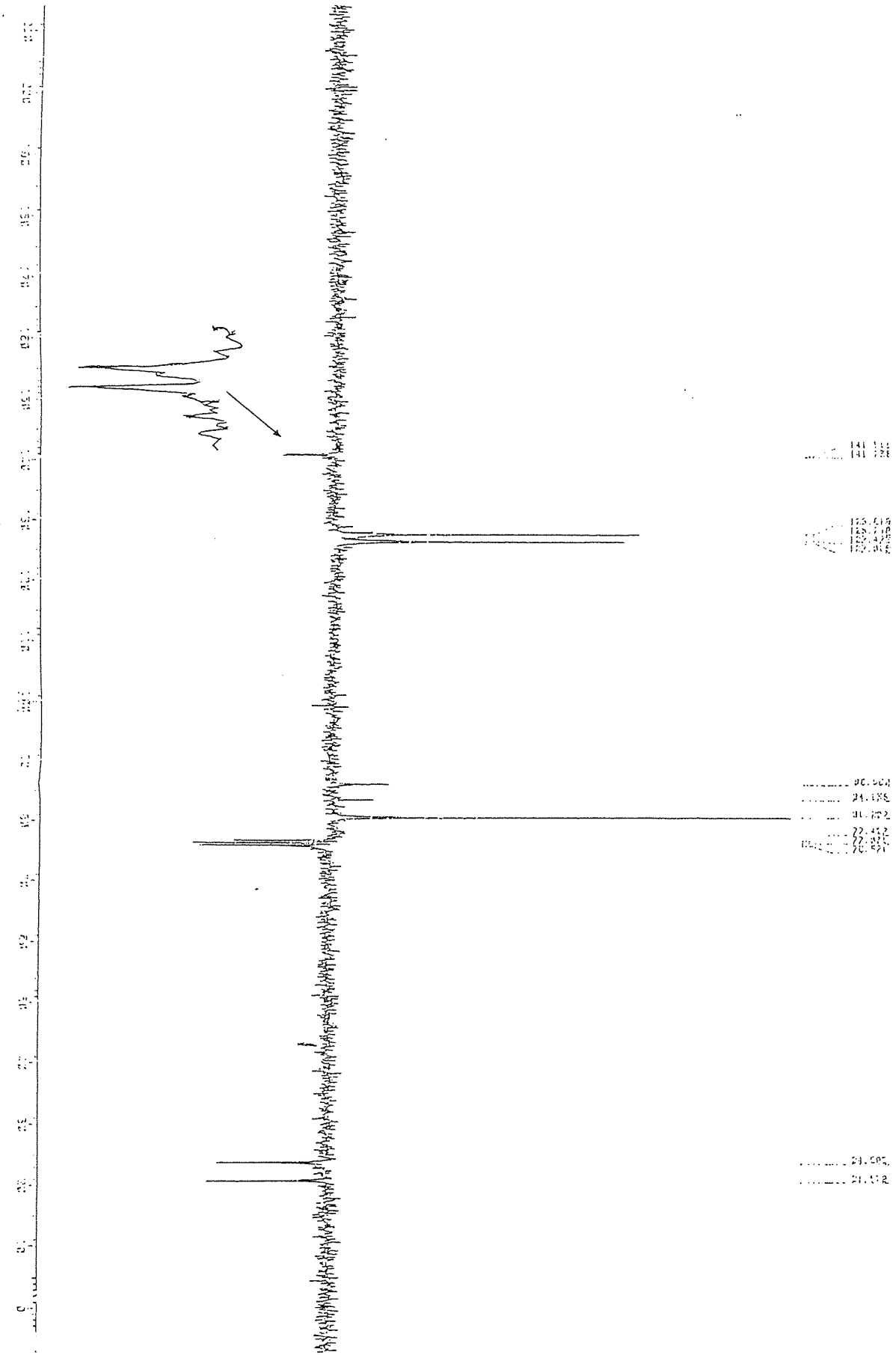

Figure 3.20 ^{13}C NMR spectrum of $C_8H_8Te.Fe(CO)CpI$ (**8**)

3.4 X-RAY CRYSTALLOGRAPHY

The crystal structures of compounds (**4**) and (**6**) were established and are shown in Figures 3.21 and 3.22 respectively. The crystal parameters are included in Table 3.26.

Three standard reflections were measured every 2 hours to check the stability of the systems. Small (1%) decay corrections were applied to the data. Both structure were determined by direct methods with SHELXS 86[98] and refined by least squares using anisotropic thermal parameters for Fe, C and O atoms. Hydrogen atoms were placed in calculated positions riding on their respective bonding atoms. Structure (**4**) was refined using the TEXSAN package[99] while structure (**6**) was refined using SHELXL 93.[100] Empirical absorption corrections were applied using DIFABS[101] and diagrams were drawn with PLUTO[102] (shown in Figures 3.21 and 3.22). Atomic coordinates are listed in Tables 3.27 and 3.28 with bond lengths and selected angles shown in Tables 3.29 and 3.30.

	compound 4	compound 6
Molecular formula	$C_{18}H_8Fe_2O_6$	$C_{19}H_{16}FeO$
Molecular weight	431.95	348.17
Cell constants (Å) a	7.357(2)	19.748(1)
b	8.386(8)	6.904(1)
c	13.585(3)	12.342(3)
(°) α	91.49(4)	90
β	92.10(10)	107.34
γ	102.21(2)	90
Cell volume ((Å^3)	818	1606
Space group	P1 (triclinic)	$P2_1/c$ (monoclinic)
Density (g cm^{-3}) calc.	1.753	1.1440
μ(Mo-K_α) mm^{-1}	1.806	0.950
Data collection		
Angular range (°)	2-25	2-25
Total data measured	5733	5877
Significant data [I>2.5σ(I)]	2474	5877
Least square weights		
Function minimised	$\Sigma w(\|F_o\| - \|F_c\|)^2$	$\Sigma w(F_o^2 - F_c^2)^2$
	$w = 1/\sigma^2(F_o)$	$w = 1/[\sigma^2(F_o^2) +$
		$0.004P^2 + 0.13P]$
Final R (%)	4.80	5.00
Final R´ (%)	4.90	12.70
Z	2	2
Residual electron density in final difference map (eÅ^{-3})	+0.9 to -0.9	+0.23 to -0.42

Table 3.26 Crystal and experimental parameters for compounds (**4**) and (**6**)

Atom	x	y	z
Fe(1)	1770(1)	7250(1)	2558(1)
Fe(2)	1991(1)	4394(1)	2218(1)
O(1)	5028(2)	2682(2)	2234(1)
O(2)	388(2)	3061(2)	274(1)
O(3)	-660(3)	1917(3)	3225(2)
O(4)	-1881(2)	5439(2)	1886(2)
O(5)	273(4)	8739(4)	4214(2)
O(6)	1466(2)	9883(2)	1259(1)
C(1)	4368(3)	7063(3)	3383(2)
C(2)	5243(3)	7981(3)	4224(2)
C(3)	4701(4)	7514(4)	5139(2)
C(4)	3288(4)	6135(4)	5252(2)
C(5)	2396(3)	5247(3)	4456(2)
C(6)	2910(3)	5663(3)	3474(2)
C(7)	4783(3)	7430(3)	2364(2)
C(8)	3666(2)	6337(3)	1679(2)
C(9)	3990(3)	6646(3)	640(2)
C(10)	5327(3)	7928(3)	381(2)
C(11)	6406(3)	8968(3)	1083(2)
C(12)	6154(3)	8764(3)	2064(2)
C(13)	3852(3)	3354(3)	2282(2)
C(14)	1020(3)	3606(3)	1018(2)
C(15)	357(3)	2913(3)	2836(2)
C(16)	-340(3)	5871(3)	2130(2)
C(17)	859(4)	8179(3)	3552(2)
C(18)	1564(3)	8854(3)	1773(2)

Table 3.27 Atomic coordinates (x 10^4) for complex (**4**)

Atom	x	y	z
Fe	1156(1)	1687(1)	1534(1)
O(1)	1789(1)	4653(3)	3221(2)
O(2)	-248(1)	1421(4)	1854(2)
O(3)	628(2)	4070(5)	-495(2)
C(1)	1538(2)	3523(4)	2557(2)
C(2)	295(2)	1523(4)	1723(2)
C(3)	831(2)	3120(5)	285(2)
C(4)	2335(1)	-127(3)	3183(2)
C(5)	1585(1)	-601(4)	2701(2)
C(6)	1294(2)	-1267(4)	1565(2)
C(7)	1578(1)	-417(4)	769(2)
C(8)	2118(1)	942(4)	1219(2)
C(9)	2701(1)	430(3)	2308(2)
C(10)	3120(2)	-1345(4)	2070(3)
C(11)	3427(2)	-946(4)	1098(3)
C(12)	3829(1)	921(4)	1260(2)
C(13)	4324(2)	1263(5)	656(3)
C(14)	4709(2)	2935(5)	794(3)
C(15)	4618(2)	4324(5)	1547(3)
C(16)	4134(1)	4040(4)	2134(2)
C(17)	3737(1)	2349(4)	1996(2)
C(18)	3227(2)	2076(4)	2695(2)
C(19)	2643(2)	-178(5)	4297(2)

Table 3.28 Atomic coordinates (x 10^4) for complex (**6**)

Fe(1)-C(17)	1.767(5)	O(4)-C(16)	1.149(5)
Fe(1)-C(18)	1.767(5)	O(5)-C(17)	1.140(6)
Fe(1)-C(16)	1.796(5)	O(6)-C(18)	1.136(6)
Fe(1)-C(6)	2.122(4)	C(1)-C(6)	1.424(7)
Fe(1)-C(8)	2.126(4)	C(1)-C(2)	1.416(6)
Fe(1)-C(1)	2.216(4)	C(1)-C(7)	1.454(6)
Fe(1)-C(7)	2.216(4)	C(2)-C(3)	1.362(7)
Fe(1)-Fe(2)	2.468(1)	C(3)-C(4)	1.398(9)
Fe(2)-C(13)	1.773(5)	C(4)-C(5)	1.361(7)
Fe(2)-C(15)	1.787(5)	C(5)-C(6)	1.431(6)
Fe(2)-C(14)	1.807(4)	C(7)-C(12)	1.418(7)
Fe(2)-C(8)	2.002(4)	C(7)-C(8)	1.409(6)
Fe(2)-C(6)	2.005(4)	C(8)-C(9)	1.448(5)
Fe(2)-C(16)	2.320(5)	C(9)-C(10)	1.358(7)
O(1)-C(13)	1.129(5)	C(10)-C(11)	1.382(7)
O(2)-C(14)	1.139(5)	C(11)-C(12)	1.363(6)
O(3)-C(15)	1.150(5)		
Fe(2)-Fe(1)-C(1)	76.9(1)	Fe(2)-Fe(1)-C(17)	131.7(2)
Fe(2)-Fe(1)-C(7)	76.6(1)	Fe(1)-C(7)-C(8)	67.6(2)
Fe(2)-Fe(1)-C(16)	63.7(2)	Fe(2)-C(14)-O(2)	177.8(5)
Fe(2)-Fe(1)-C(18)	132.1(1)	Fe(2)-C(16)-O(4)	129.2(4)
Fe(1)-Fe(2)-C(6)	55.5(1)	Fe(1)-C(16)-O(4)	158.4(5)
Fe(1)-Fe(2)-C(13)	133.5(1)	Fe(1)-C(17)-O(5)	177.6(5)
Fe(1)-Fe(2)-C(15)	114.6(2)	Fe(1)-C(7)-C(1)	70.8(2)
Fe(1)-Fe(2)-C(14)	113.4(2)	Fe(1)-C(8)-Fe(2)	73.4(1)

Table 3.29 Bond lengths (Å) and selected bond angles (°)for complex(**4**)

Fe-C(3)	1.783(3)	C(6)-C(7)	1.397(4)
Fe-C(2)	1.788(3)	C(7)-C(8)	1.404(4)
Fe-C(1)	1.789(3)	C(8)-C(9)	1.529(3)
Fe-C(7)	2.042(3)	C(9)-C(18)	1.519(3)
Fe-C(6)	2.056(3)	C(9)-C(10)	1.544(3)
Fe-C(8)	2.112(2)	C(10)-C(11)	1.523(4)
Fe-C(5)	2.135(2)	C(11)-C(12)	1.496(4)
O(1)-C(1)	1.133(3)	C(12)-C(17)	1.389(4)
O(2)-C(2)	1.134(4)	C(12)-C(13)	1.414(4)
O(3)-C(3)	1.135(3)	C(13)-C(14)	1.365(5)
C(4)-C(19)	1.327(4)	C(14)-C(15)	1.383(5)
C(4)-C(5)	1.459(4)	C(15)-C(16)	1.374(4)
C(4)-C(9)	1.517(3)	C(16)-C(17)	1.389(4)
C(5)-C(6)	1.424(4)	C(17)-C(18)	1.520(4)
O(1)-C(1)-Fe	178.4(2)	C(7)-C(8)-C(9)	118.5(2)
O(2)-C(2)-Fe	179.3(2)	C(4)-C(9)-C(18)	113.1(2)
O(3)-C(3)-Fe	178.4(3)	C(4)-C(9)-C(8)	106.9(2)
C(19)-C(4)-C(5)	120.8(3)	C(18)-C(9)-C(10)	111.7(2)
C(19)-C(4)-C(9)	125.1(3)	C(4)-C(9)-C(10)	109.2(2)
C(5)-C(4)-C(9)	114.1(2)	C(18)-C(9)-C(10)	107.3(2)
C(6)-C(5)-C(4)	122.4(2)	C(8(-C(9)-C(10)	108.7(2)
C(6)-C(7)-C(8)	114.7(2)		

Table 3.30 Bond lengths (Å) and selected angles (°) for complex(6)

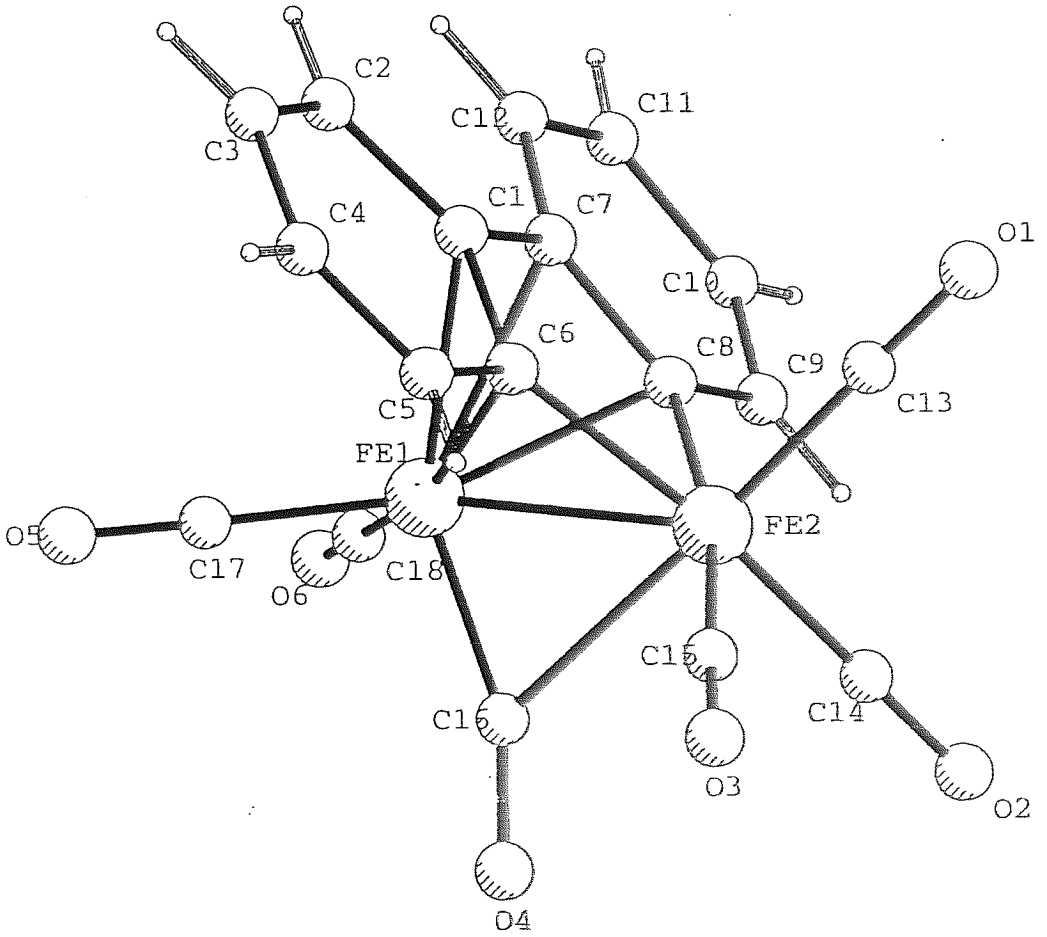

Figure 3.21 The molecular structure of dibenzoferrole, $C_{12}H_8.Fe_2(CO)_6$ (4)

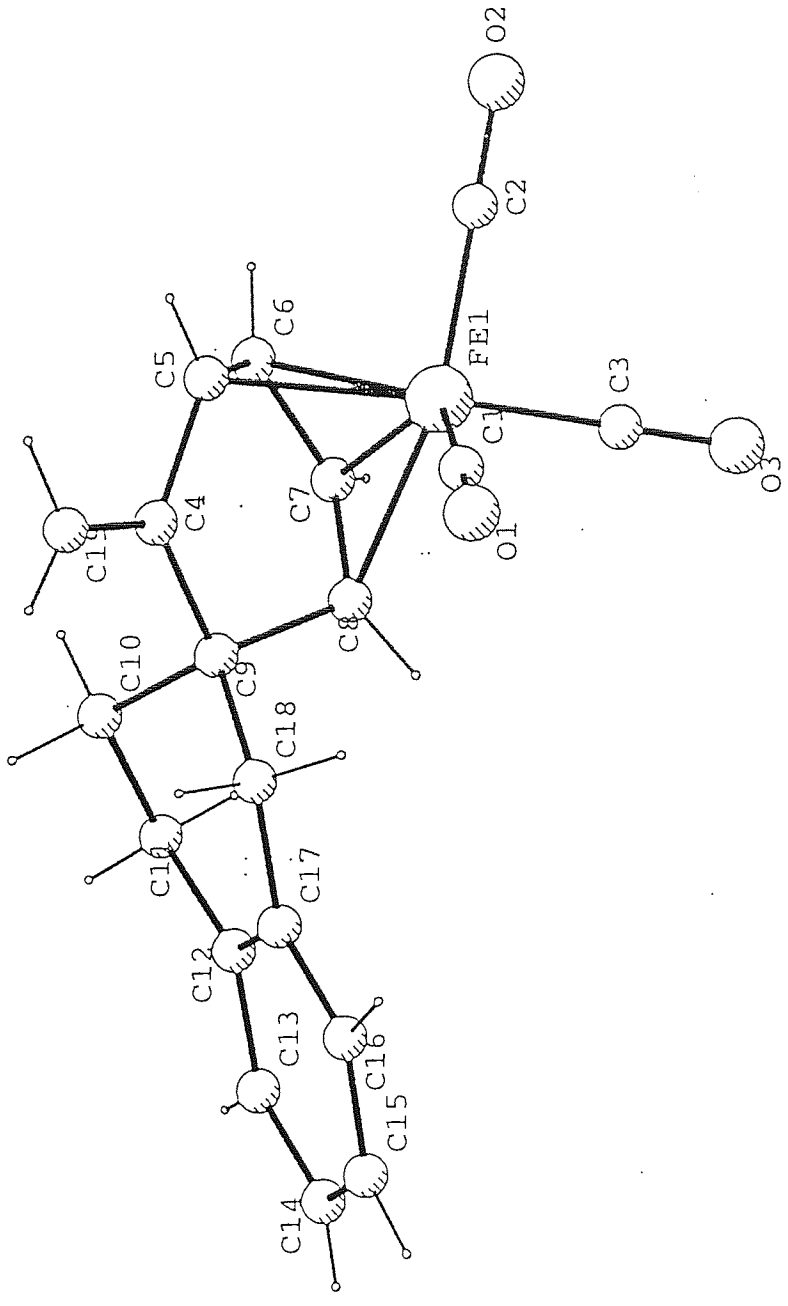

Figure 3.22 The molecular structure of $C_{16}H_{16}.Fe(CO)_3$ (**6**)

3.4.1 Structural studies of complexes (4) and (6)

The structure of the $C_{18}H_8Fe_2O_6$ (**4**) is shown in Figure 3.21; bond lengths and selected angles are in Table 3.29. The biphenyl residue is planar to within ± 0.018 Å. One of the iron atoms, Fe(1) is displaced by 1.67 Å from the plane and is π-bonded to the aromatic bonds C(6)-C(1) and C(7)-C(8). The Fe(1)-C distances involving inner carbon atoms, C(1) and C(7), at 2.216(4) Å are significantly longer than those involving the outer atoms, C(6) and C(8), at 2.122(4) and 2.126(4) Å respectively. Atom Fe(2) lies close to the biphenyl plane, displacement 0.22 Å, and is σ-bonded to C(6) and C(8), forming a metallocyclic ring. The Fe(2)-C bonds at 2.005(4) and 2.002(4) Å are shorter than the π interactions observed between Fe(1) and the ring carbon atoms.

The central C(1)-C(7) bond is 1.454(6) Å, some 0.03-0.05 Å shorter than is commonly found in biphenyls, and may indicate some inter-ring electron delocalisation, presumably triggered by the π-bonded atom. The Fe(1)-Fe(2) distance is 2.468(1) Å, corresponding to a bonding interaction. The carbonyl group C(16)-O(4) is involved in bonding to both Fe(1) and Fe(2), Fe(1)-C(16); 1.796(5) and Fe(2)-C(16); 2.320(5) Å, forming an unsymmetrical bridge. This Fe_2CO iron carbonyl system is bent, angles Fe(1)-C(16)-O(4) and Fe(2)-C(16)-O(4); 158.4(5) and 129.2(4)° respectively. The other iron carbonyl groupings have normal dimensions, Fe-C 1.767-1.807, C-O 1.129-1.150 Å, Fe-C-O 177.5-179.0°. The longest Fe-CO bonds, apart from those of the bridging carbonyl group, are those *trans* to the C(6)-Fe(2) and C(8)-Fe(2) σ bonds, indicating a possible weak *trans* influence of these bonds. The C-O bond of the bridging carbonyl group at 1.149(5) Å falls within the range of lengths of the other, non-bridging carbonyl groups. Both iron atoms obey the 18-electron rule.

The central $Fe_2C_4(CO)_6$ residue bears a striking resemblance to the corresponding residue in (hexacarbonylcyclododeca-1,7-diyne)diiron the crystal structure of which

has been determined.[103] Here the Fe-Fe separation is 2.462(3) Å and the Fe-CO (bridging) distances are 1.75(2) and 2.32(2) Å with Fe-C-O angles 162(3) and 125(3)°.

The structure of the $C_{19}H_{16}FeO_3$ (**6**) molecule is shown in Figure 3.22. Bond lengths and angles are in Table 3.30. The iron atom is coordinated to three carbonyl groups and to the C(5)-C(6) and C(7)-C(8) double bonds of the organic system. The Fe-Co distances average 1.787(3) Å. The Fe-C(5), -C(6), C(7) and C(8) distances are 2.135(2), 2.056(3), 2.042(3) and 2.112(2) Å respectively. These distances may be compared with those found in a selection of 21 structures containing the cyclohexadiene-$Fe(CO)_3$ system extracted from the Cambridge Structural Database.[104] In 18 of these structures the Fe-C(diene) bond lengths follow the pattern observed in our structure, with bonds to the inner carbon atoms (mean over all 21 structures 2.05 Å) shorter than those to the outer carbon atoms (mean 2.11 Å). The C-O lengths average 1.134(1) Å and the Fe-C-O angles are all within 1.6° of being linear. As in (**4**), the iron atom here also obeys the 18-electron rule.

The bonds C(5)-C(6), C(6)-C(7) and C(7)-C(8) involving the complexed diene moiety are 1.424(4), 1.397(4) and 1.404(4) Å respectively, essentially all equal, intermediate between single and double bond distances. It is nevertheless, of interest that in 17 of the 21 structures cited above the central bond of the diene system is slightly shorter (mean over 21 structures 1.40 Å) than the outer two bonds (mean 1.42 Å), in good agreement with our results, indicating a tendency to bond alternation of the opposite sense to that of the parent free ring system. This effect had been noted[105] previously, but not considered to be significant. Reverse bond alternation is more pronounced in structures where there is a cyclopentadienyl ligand coordinated to the iron atom *trans* to the cyclohexadiene.[106] Bonds C(8)-C(9) and C(4)-C(9) are purely single, while C(4)-C(5) (1.459 Å) is slightly shorter than a single bond and C(19)-C(4) (1.327 Å) is very slightly longer than a double bond. Thus the C(19)-C(4) double bond appears to be partly conjugated with the iron-diene system.

The complexed cyclohexadiene-like ring has atoms C(5)-C(8) coplanar to within ±0.005 Å with C(4) and C(9) displaced on the same side of this plane by 0.725 and 0.974 Å, respectively. The iron atom lies 1.655 Å on the opposite side of this plane. The cyclohexene ring C(9)-C(18) adopts the half-chair conformation. Atoms C(11), C(12), C(17) and C(18) are coplanar to within ±0.004 Å and C(9), C(10) are located on opposite sides of this plane at distances of 0.35 and 0.44 Å.

3.5 CONCLUSIONS

The classic reaction of Stone and co-workers[50] was repeated and found to proceed precisely as reported, although chromatography did reveal a trace of compound not previously reported (identified by mass spectroscopy), namely $C_4H_4Fe(CO)_2.Fe(CO)_6$ (**2**). The yield of the ferrole (**1**), however, could not be improved and attention was directed to reactions of tellurium heterocycles, given their known advantages, in order to 'model' the reactivity of thiophenes.

Öfele and Dotzauer[76] were the first to consider reactions of tellurophene with metal carbonyls. In particular they treated tellurophene with $Fe_3(CO)_{12}$ in benzene to obtain black $Fe_3Te_2(CO)_9$ and the orange ferrole $C_4H_4.Fe_2(CO)_6$ (**1**), together with an 18% yield of a third material believed to be $C_4H_4FeTe.Fe_2(CO)_6$ (**3**). On repeating the reaction ourselves under slightly modified conditions a 45% yield of ferrole was obtained. Earlier termination of the reaction gave the telluraferrole (**3**) in 66% yield, of which a multinuclear NMR analysis was carried out, enabling us to more accurately predict its structure. The black residue from the reaction in our case was FeTe which doubtless arose from $Fe_3Te_2(CO)_9$ via loss of CO and $Fe(CO)_5$.

All attempts to desulfurise the dibenzothiophene using iron carbonyl have proved unsuccessful.[53] The analogous dibenzotellurophene, however, was shown to react with $Fe_3(CO)_{12}$, yielding the novel dibenzoferrole, $C_{18}H_8Fe_2O_6$ (**4**), in 28% yield. No

intermediate was isolated, but analysis of the black residue remaining in the reaction flask by XPS showed it to contain only Fe and Te. This result has great significance in that it demonstrates the mechanistic feasibility of the dechalcogenation reaction for the more condensed aromatic molecules. Therefore, the resistance of dibenzothiophene to desulfurisation appears to be due to unfavourable thermodynamics arising from the strength of the C-S bond.

To maintain the theme of reactions of heterocyclic compounds of tellurium with $Fe_3(CO)_{12}$, but to model a thioether rather than an aromatic environment, 2-telluraindane was used as a substrate. Tellurium was removed from the ring and , in this case, recovered as the cluster compound $Fe_3Te_2(CO)_9$ initially reported by Hieber and Gruber.[97] In addition, a 15% yield of a novel complex $C_{19}H_{16}FeO_3$ (**6**) was obtained which was shown by X-ray crystallography to contain an organic moiety derived from the unsymmetrical coupling of two C_8H_8 fragments. This is in contrast to the formation of benzocyclobutane following thermochemical extrusion of tellurium from 2-telluraindane.[107] It is expected that 2-telluraindane will be a better Lewis base than tellurophene, hence it is possible that the initial stage of the reaction is the monodentate coordination of two molecules of the base to the two equivalent iron atoms of $Fe_3(CO)_{12}$ thus providing a starting point from which the observed products might plausibly emerge. The retention of an exocyclic double bond is of interest; doubtless the coordination of that fragment of the molecule to the iron tricarbonyl unit is responsible for the stabilisation of this form. Indeed, it is possible that in an intermediate stage the C_8H_8 unit is coordinated as 1,6-dimethylenecyclohexa-2,4-diene thus facilitating the addition of a similar fragment across one exocyclic double bond.

Phenoxtellurine also underwent detelluration on treatment with $Fe_3(CO)_{12}$ resulting in the formation of the carbonyl insertion compound $C_{13}H_8O_2$ (**7**), which is thought to have arisen from a telluraferrole-type intermediate

The treatment of tellurophene with the monometallic $CpFe(CO)_2I$ proved less successful, as no significant reaction was observed. However, when reacted with 2-telluraindane, a reaction did occur in which the tellurium coordinated to the iron to give a simple complex (**8**). The difference in reactivities of tellurophene and 2-telluraindane towards $CpFe(CO)_2I$, can be explained by the greater Lewis basicity of tellurium in the latter. No detelluration, however, is observed even with prolonged reaction times. The same is true for the reaction of phenoxtellurine with $CpFe(CO)_2I$, in which a carbonyl insertion reaction takes place, whilst retaining the tellurium in the heterocycle. These results are in contrast to reactions with $Fe_3(CO)_{12}$ in which the heterocycles are detellurated, even though tellurium containing intermediates are isolated for some systems. These observations suggest that multimetallic reagents are more effective in removing the chalcogen from a heterocyclic environment. Hence, insertion of a metallic centre activates the heterocycle, but more than one metal within the same organometallic molecule is required for cleavage of the second C-Te bond to effect detelluration. Indeed, Rauchfuss has reported similar findings on his work with the sulfur systems[39] suggesting that the metal plays a dual role by separately stabilising the hydrocarbon residue and accepting the removed sulfur.

CHAPTER 4

MICROWAVE ACCELERATED REACTIONS OF THIOPHENES

4.1 INTRODUCTION

Coal, like many materials of natural origin, is a difficult substance with which to work. Recently however, it has been established that microwave heating can be used with benefit in some aspects of coal science. For example, derivitisation reactions of coal functional groups have been greatly accelerated leading to the development of new analytical methods.[108] At the outset of this work it was debated that similar acceleration of the desulfurisation reactions of thiophene rings using, $Fe_3(CO)_{12}$ might be possible and, further, that in the case of benzothiophene the reaction might be driven to the desulfurisation stage. It was also hoped that a reaction between dibenzothiophene and $Fe_3(CO)_{12}$ could be induced.

4.2 MICROWAVE EQUIPMENT

4.2.1 Sharp Carousel II R-84801

This is a domestic microwave oven with a power rating of 650 watts and an operational frequency of 2.45 GHz. The Carousel II R-84801 was not modified or adapted in any way for use in the laboratory, but for safety reasons it was used under a fume hood.

The containment vessels used in conjunction with the Carousel II consisted of Teflon® PFA digestion vessels incorporating safety relief valves and venting nuts. These digestion vessels had a volume of 100 cm^3 and were transparent to microwave energy.

4.2.2 CEM MES-1000 microwave system

For some experiments an MES (microwave extraction system) -1000 was used. The main features of this system are; a fluoropolymer coated cavity fitted with a cavity

exhaust fan, a direct drive alternating turntable, a tin oxide semiconductor gas sensor designed for detecting organic solvents, exhaust tubing to vent fumes, a digital programmable computer and 3 inlet/outlet ports to accommodate control lines. The MES-1000 delivers approximately 950±50 watts of microwave energy at a frequency of 2450 MHz at full power. The % power may be programmed in at 1% increments to control the rate of heating and a microcomputer controls and monitors operations. The MES-1000 is also equipped with a pressure monitoring device and a fibreoptic temperature probe, allowing heating to stop when set temperatures and pressures are attained.

The reaction vessel used in conjunction with the MES-1000 is manufactured from Teflon and encased in an Ultem® polyethermide outer body and cap. The cap has three outlets, the first of which is located at the top and is for the thermowell which accommodates the fibreoptic probe. The other two outlets for the pressure sensing line and the rupture membrane are both located at the side of the cap. The vessel, transparent to microwaves, can be used at temperatures up to 200°C and pressures up to 200 psi.

The notable advantage of using this microwave control system over a domestic microwave is that the user has precise control of operating conditions i.e. temperature and pressure, thereby introducing a whole new set of reaction parameters. The safety considerations are also greatly enhanced when using this system.

4.2.3 Microwave procedure

(i) Sharp Carosel II R-84801

The reactants were weighed into the Teflon digestion vessels and the lid was screwed on and tightened using capping stations. The containment vessel was then placed into the microwave cavity and the power level was selected. In reactions where very good microwave receptors e.g. CH_3CN were used, the total heating time was achieved by

irradiating the sample with microwaves (setting at medium/high) for one minute periods with intermittent cooling in a beaker of cold water. When only moderate receptors were used e.g. Fe_3O_4 and THF, the microwave power setting was on high and irradiation periods of five minutes with intermittent cooling were used. After completion of microwave heating, the digestion vessel was allowed to cool before opening the cap to ensure that the gas pressure inside the container had reduced to a safe level.

(ii) CEM MES-1000

The reactants were weighed into the open Teflon vessel which was then placed in its polyethermide sleeve. The cap was then screwed on hand-tight and the apparatus was placed inside the microwave cavity. The pressure sensing line, pressure rupture line, and fibreoptic probe were then attached to the containment vessel and the required temperature and pressure together with % power were programmed into the computer before starting microwave heating. With this procedure there was no need for intermittent cooling of the reagents because of the in-built control and safety features of the MES-1000.

4.3 EXPERIMENTAL

4.3.1 The microwave reaction of thiophene with triiron dodecacarbonyl

Microwave reactions were carried out by sealing $Fe_3(CO)_{12}$ and thiophene together with a chosen receptor in a Teflon container and heating the contents in a Sharp Carousel II R-84801 microwave oven operating at various power settings. Several experiments were carried out using different microwave receptors and varying reaction times. The total volume of solution was made up to 10 cm^3 where necessary by addition of heptane (inert solvent and non-receptor of microwaves) to the reaction mixture. Table 4.1 summarises the reactions that were performed.

Expt. No.	Thiophene (cm^3)	$Fe_3(CO)_{12}$ (g)	Receptor	Heating time (min)	Power setting
M1	10	0.50	-	100	HIGH
M2	2.5	6.00	CH_3CN (7.5 cm^3)	15	MED/HIGH
M3	-	1.00	CH_3CN (10 cm^3)	30	MED/HIGH
M4	-	0.50	-	30	HIGH
M5	9	2.00	CH_3CN (1 cm^3)	50	MED/HIGH
M6	10	1.00	THF (4 cm^3)	55	HIGH
M7	10	1.00	Fe_3O_4 (0.5g)	50	HIGH
M8	10	-	Fe_3O_4 (0.5g)	50	HIGH
M9	10	1.00	Fe_3O_4 (0.5g)	50	HIGH
M10	10	1.00	Fe_3O_4 (1g)	50	HIGH

Table 4.1 Microwave reactions of thiophene with $Fe_3(CO)_{12}$

After completion of microwave heating the reaction mixtures were filtered and the solvents removed by rotary evaporation. The recovered products were chromatographed on TLC-grade silica with pentane as the eluant and then characterised using infrared spectroscopy.

4.3.2 The microwave reaction of benzothiophene with triiron dodecacarbonyl

Benzothiophene (0.4g, 3.0 mmol) was placed in a Teflon container together with heptane (10 cm^3) and Fe_3O_4 (1.0g) and the mixture was heated in the Sharp Carousel II R-84801 microwave at high power for a total time of 1 hour with varying amounts of $Fe_3(CO)_{12}$. Table 4.2 summarises the reactions that were performed.

Expt. No.	BT (g)	$Fe_3(CO)_{12}$ (g)	Ratio BT:$Fe_3(CO)_{12}$	Product yield (g)
M11	0.40	0.50	3:1	0.14
M12	0.40	1.00	1.5:1	0.32
M13	0.40	1.50	1:1	0.37
M14	0.40	2.25	1:1.5	0.39

Table 4.2 Microwave reactions of benzothiophene with $Fe_3(CO)_{12}$

For each experiment the reaction mixture was filtered and then chromatographed on silica with pentane as the eluting solvent, thereby yielding one major band. Collection of the major fraction followed by removal of solvent under vacuum yielded orange-red crystals which were characterised by infrared spectroscopy and mass spectrometry.

4.3.3 The microwave reaction of dibenzothiophene with triiron dodecacarbonyl

These experiments were performed in the CEM MES-1000 microwave system equipped with a pressure monitoring device and a fibreoptic temperature probe. Dibenzothiophene was placed in a Teflon container in varying quantities together with $Fe_3(CO)_{12}$ and various receptor/solvent systems. The total volume of solution was made up to 10 cm^3 by the addition of heptane (where necessary) and the mixtures were heated under a variety of microwave conditions as summarised in Table 4.3.

Expt No.	DBT (g)	iron carbonyl (g)	Ratio DBT:iron carbonyl	Receptor	Total heating time (min)	Power setting (% of max)
M15	1.10	1.00	3:1	Fe_3O_4 (1g)	120	100
M16	1.10	1.00	3:1	CH_3CN 5 cm^3	120	50
M17	0.37	1.00	1:1	Fe_3O_4 (1g)	120	100
M18	0.37	1.00	1:1	CH_3CN 10 cm^3	60	20
M19	0.37	1.00	1:1	MoS_2 (1g)	60	100
M20	0.37	1.00	1:1	MoS_2 (1g)	120	50

Table 4.3 Microwave reactions of dibenzothiophene with $Fe_3(CO)_{12}$

The reaction mixtures were filtered after each experiment and the filtrate was evaporated to dryness under vacuum. The solids obtained were analysed by infrared spectroscopy.

4.4 RESULTS AND DISCUSSION

4.4.1 The microwave reaction of thiophene with triiron dodecacarbonyl

Several microwave experiments were carried out in which varying amounts of thiophene and $Fe_3(CO)_{12}$ were reacted in a range of microwave receptors. The identity of the products was determined by comparison of chromatographic and infrared spectroscopic data with previously isolated compounds. Hence, it was shown that where a reaction had occurred, identical products (**1** and **2**) to those formed from conventional heating methods, discussed in chapter 3, were obtained when microwave heating was employed.

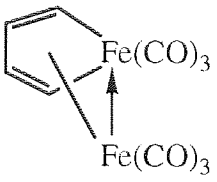

(1)

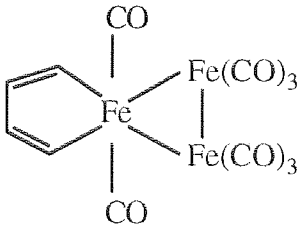

(2)

The yields of (**1**) and (**2**) ranged from 5 to 10% (based on $Fe_3(CO)_{12}$) and were formed in varying quantities depending on the reaction conditions.

Table 4.4 summarises the products that were obtained from these reactions.

No.	Expt.	Product appearance	Product identity
M1	10 cm^3 thiophene, 0.50g $Fe_3(CO)_{12}$ Heat- 100 min, High	orange oily solid brown powder (residue)	(1) FeS and iron oxides
M2	2.5 cm^3 thiophene 6.00g $Fe_3(CO)_{12}$ 7.5 cm^3 CH_3CN Heat- 15 min, Med/High	orange oil (traces) black residue	(1) iron/iron oxides
M3	0 cm^3 thiophene 1.00g $Fe_3(CO)_{12}$ 10 cm^3 CH_3CN Heat- 30 min, Med/High	black residue	iron oxides
M4	0 cm^3 thiophene 0.50g $Fe_3(CO)_{12}$ Heat- 30 min, High	black solid	$Fe_3(CO)_{12}$
M5	9 cm^3 thiophene 2.00g $Fe_3(CO)_{12}$ 1 cm^3 CH_3CN Heat- 50 min, Med/High	red oil brown powder (residue)	(1) & (2) iron oxides
M6	10 cm^3 thiophene 1.00g $Fe_3(CO)_{12}$ 4 cm^3 THF Heat- 55 min, High	brown/red oil black residue	(1) & (2) FeS and iron oxides
M7	10 cm^3 thiophene 1.00g $Fe_3(CO)_{12}$ 1.0g Fe_3O_4 Heat- 50 min, High	orange/red oil black gloss	(1) & (2) FeS
M8	10 cm^3 thiophene 0g $Fe_3(CO)_{12}$ 0.5g Fe_3O_4 Heat- 50 min, High	black residue	Fe_3O_4
M9	10 cm^3 thiophene 1.00g $Fe_3(CO)_{12}$ 0.5g Fe_3O_4 Heat- 50 min, High	orange/red oil black residue	(1) & (2) Fe_3O_4/FeS
M10	10 cm^3 thiophene 1.00g $Fe_3(CO)_{12}$ 1.0g Fe_3O_4 Heat- 50 min, High	orange/red oil black residue	(1) & (2) Fe_3O_4/FeS

Table 4.4 Products obtained from microwave reactions of thiophene with $Fe_3(CO)_{12}$

In experiment M1, no microwave receptor was used and the ferrole product (**1**) was formed in very low yields. Thiophene absorbs microwaves very weakly, hence effective heating could not have been achieved in this experiment.

In experiment M2 acetonitrile (7.5 cm^3) was used as the microwave receptor. After heating for 15 minutes it was found that $Fe_3(CO)_{12}$ had in fact decomposed to yield metallic iron and iron oxides. In the control experiment M3, where thiophene was excluded, it was found that the iron carbonyl decomposed in the presence of acetonitrile but in experiment M4 where the iron carbonyl was heated on its own no decomposition was observed under conditions of microwave heating. Hence it was concluded that excessive heat induced by the acetonitrile receptor was responsible for iron carbonyl decomposition. In experiment M5 a much smaller quantity of acetonitrile was used (1 cm^3) to overcome the problem of iron carbonyl decomposition, thus enabling an improved yield of the products.

In experiment M6 THF was used as the receptor solvent (moderate microwave absorption) and again both products (**1**) and (**2**) were obtained.

Experiments M7-M10 involved the use of magnetite (Fe_3O_4 solid) as the microwave receptor (moderate absorption). The highest yield of products (**1** and **2**) was obtained from experiment M7, in which 10 cm^3 of thiophene was reacted with 1g of triiron dodecacarbonyl using 0.5g of Fe_3O_4 as internal receptor. The total reaction time in this case was 50 minutes. The presence of FeS was again confirmed by treatment of the insoluble residue with dilute HCl. The control experiment M8 in which the iron carbonyl was excluded confirmed that thiophene did not react with the receptor.

The key results from the microwave reaction of thiophene and triiron dodecacarbonyl may be summarised as follows:

(i) The most efficient reaction (in terms of yield of ferrole) is achieved when magnetite is used as the microwave receptor. Identical products are obtained

as when the reaction is carried out using conventional heating method. However, there is a significant difference in the time taken to achieve equivalent stages in the reaction when performed under microwave conditions (50 min) and conventional refluxing (15 hours). Hence, the use of microwave heating is successful in accelerating the reaction between thiophene and $Fe_3(CO)_{12}$.

(ii) The yields of the products obtained from the microwave reactions of thiophene and $Fe_3(CO)_{12}$) are not significantly improved over reactions carried out using conventional heating methods.

(iii) Very good microwave receptors (e.g. acetonitrile) appear to create conditions which are too aggressive for the iron carbonyl leading to its decomposition, hence loss in reaction efficiency.

4.4.2 The microwave reaction of benzothiophene with triiron dodecacarbonyl

Having established optimum microwave conditions for reactions of thiophenes with iron carbonyl, four separate microwave experiments were carried out (M11-M14) in which the ratio of benzothiophene:$Fe_3(CO)_{12}$ was varied whilst keeping the solvent (heptane) and microwave receptor (Fe_3O_4) constant throughout. For each experiment, the same product (orange-red crystals) was produced as indicated by comparison of IR (Figure 4.1)) and mass spectra. The identity of the product was confirmed as the benzothiaferrole, $C_8H_6S.Fe_2(CO)_6$, previously reported by Rauchfuss *et al* in 1988,[53] the structure of which is shown below (**3**).

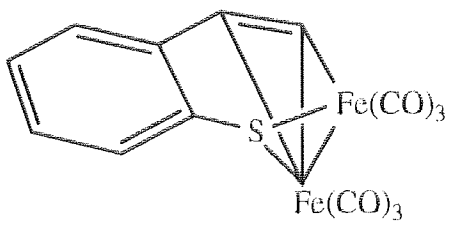

(**3**)

Requires (%)	C, 40.62	H, 1.46	$C_{14}H_6Fe_2O_6S$
Found (%)	C, 41.01	H, 1.67	

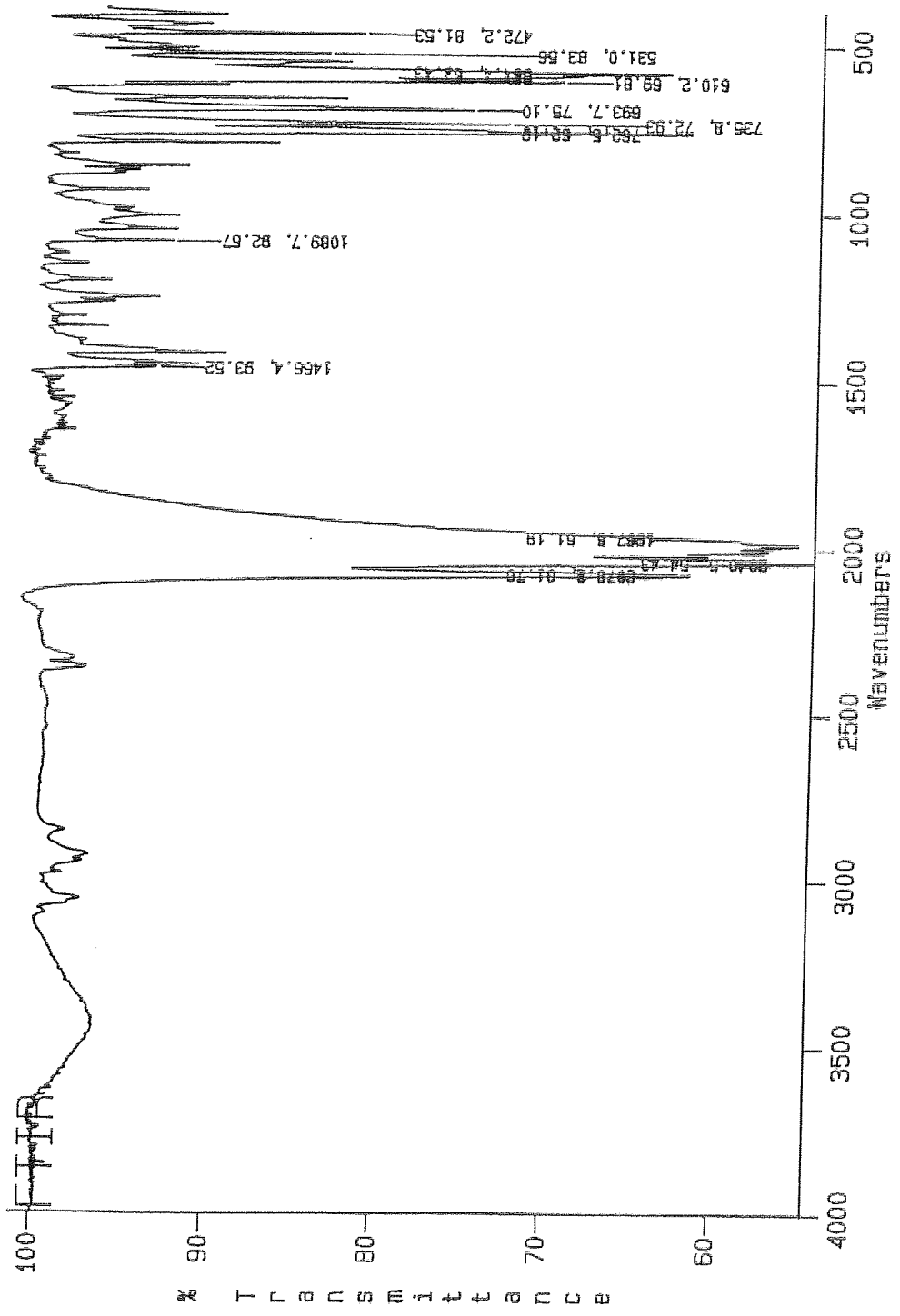

Figure 4.1 IR spectrum of benzothiaferrole, $C_8H_6S.Fe_2(CO)_6$ (3)

The infrared bands in the carbonyl region for benzothiaferrole are recorded in Table 4.5 while mass spectral data (EI) is displayed in Table 4.6.

Benzothiaferrole KBr, ν(CO) cm^{-1}
2080 (m)
2040 (s)
2030 (m)
2017 (s)
2006 (s)
1986 (m)
1976 (s)
1967 (m)

Table 4.5 Infrared bands in the carbonyl region for benzothiaferrole

m/z	**assignment**
414	M^+
246	M^+ - 6 CO

Table 4.6 Mass spectrum peaks for benzothiaferrole

The yields of benzothiaferrole for each experiment are recorded in Table 4.7

Expt. No.	Ratio BT:iron carbonyl	benzothiaferrole yield (g)	% yield $Fe_3(CO)_{12}$ based	% yield BT based
M11	3:1	0.14	34	11
M12	1.5:1	0.32	39	25
M13	1:1	0.37	30	29
M14	1:1.5	0.39	21	31

Table 4.7 Yields of benzothiaferrole from microwave reactions of BT and $Fe_3(CO)_{12}$

The variation in the % yield of benzothiaferrole with BT:$Fe_3(CO)_{12}$ ratio is depicted graphically in Fig. 4.2

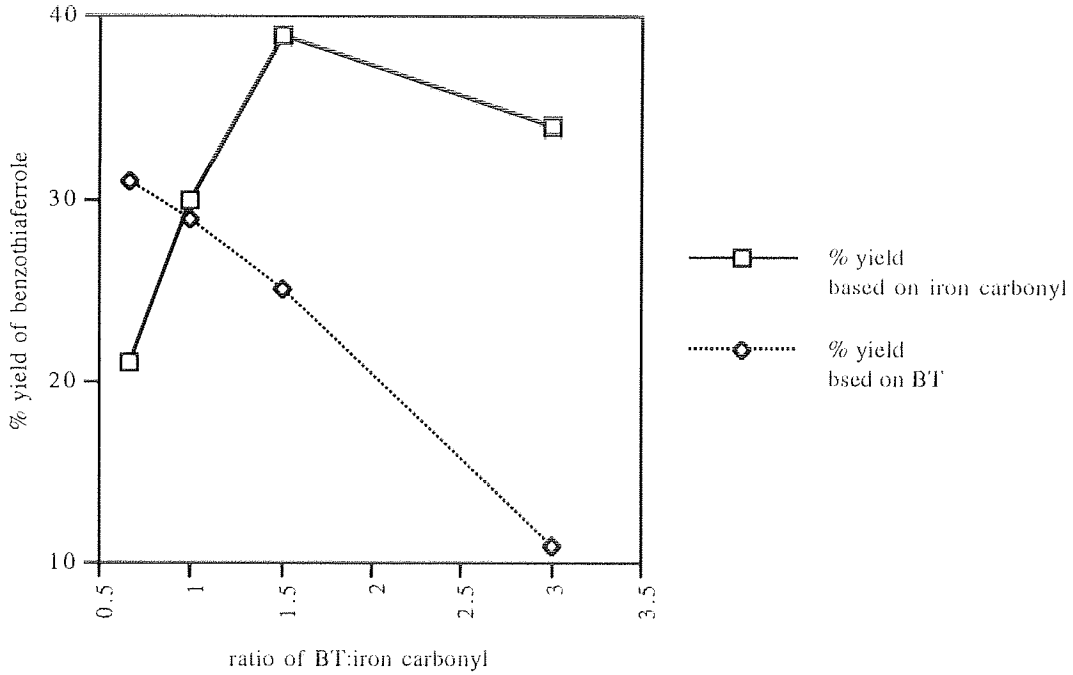

Figure 4.2 Variation in % yield of benzothiaferrole with BT:$Fe_3(CO)_{12}$ ratio

From Fig. 4.1 it can be seen that the optimum yield (based on iron carbonyl) of benzothiaferrole is achieved when a BT:$Fe_3(CO)_{12}$ ratio of 1.5:1 is used. The previous group obtained[53] a 49% yield of benzothiaferrole by treating benzothiophene with $Fe_3(CO)_{12}$ in refluxing benzene for 18 hours. Microwave heating was able to produce

similar yields in less than 1 hour and can therefore be considered to greatly accelerate this particular reaction. However, as observed previously, no desulfurisation of benzothiophene could be effected under microwave conditions.

4.4.3 The microwave reaction of dibenzothiophene with triiron dodecacarbonyl

Several microwave experiments (M15-M20) were carried out in an attempt to induce a reaction between dibenzothiophene and $Fe_3(CO)_{12}$. All previous efforts employing conventional heating methods had been unsuccessful and therefore the known advantages enjoyed by microwave heating were thought to be particularly favourable for this reaction. However, even under the most aggressive microwave conditions, dibenzothiophene, disappointingly, failed to show any signs of reactivity towards the iron carbonyl. This further outlines the difficulties encountered in attempting to cleave the C-S bonds where the sulfur is bonded to a carbon which is part of an aromatic ring as found in the more condensed heterocycles.

4.5 CONCLUSIONS

This work explored the question of the reactivity of materials such as thiophene and benzothiophene with $Fe_3(CO)_{12}$ under the influence of microwave heating. Since this methodology has been shown to be capable of greatly accelerating the passage to equilibrium of a large number of chemical reactions[109] it was interesting to examine whether, under these conditions, the benzothiophene reaction would proceed to the ferrole stage or indeed whether a reaction with dibenzothiophene could be induced.

When the reaction of thiophene and $Fe_3(CO)_{12}$ was performed under conditions of microwave heating, identical products to those reported for the reaction done under conventional heating (chapter 3) were obtained i.e. the ferrole, $C_4H_4.Fe_2(CO)_6$, and the tri-iron complex, $C_4H_4Fe(CO)_2.Fe_2(CO)_6$ with the sulfur being released in the form of FeS. Thiophene does not heat rapidly in a microwave field of 2.45 GHz but

the addition of 0.5g of otherwise inert Fe_3O_4 to the reaction mixture ensured rapid heating. The yield of products obtained after 50 minutes of microwave heating was equal to that obtained after 15 hours of bench reflux. Increasing the microwave heating time, however, did not improve the yields of products obtained. Equivalent experiments with benzothiophene also produced similar yields of the thiaferrole after 50 minutes to that obtained by the Rauchfuss group[53] after 18 hours, however, no desulfurisation of the benzothiophene was noted. Dibenzothiophene displayed no reactivity towards the iron carbonyl even under microwave conditions.

The use of microwave heating evidently leads to the acceleration of previously reported reactions of thiophene and derivatives with $Fe_3(CO)_{12}$. Since benzothiophene and dibenzothiophene are better models for sulfur in coal and coal-derived liquids, the failure to observe the desulfurisation of these polycyclic heterocycles under microwave conditions is somewhat disappointing. The order of reactivity of thiophenes towards $Fe_3(CO)_{12}$ under the influence of microwave heating (50 min) can be summarised as follows:

benzothiophene (~40% yield of thiaferrole) > thiophene (~10% yield of ferrole) > dibenzothiophene (no reaction)

CHAPTER 5

THE REACTIONS OF TELLURIUM HETEROCYCLES WITH CYCLOPENTADIENYL RHODIUM COMPLEXES

5.1 INTRODUCTION

The aim of this work was to synthesise a range of rhodium complexes of tellurium heterocycles and study them using ^{125}Te NMR. A further objective was to investigate whether once activated by coordination to rhodium, the tellurophenes would undergo detelluration reactions on further treatment with the previously successful triiron dodecacarbonyl.

Angelici has already shown that ^{77}Se NMR provides a useful tool for establishing the mode of binding of selenophenes to transition metals.[64,65] Hence free selenophenes give an ^{77}Se NMR signal which is more downfield compared to η^1 and η^2 selenophenes with η^5 coordination giving the most upfield signal. It was thought that ^{125}Te NMR could be used in a parallel fashion and therefore the primary objective was to synthesise rhodium complexes of tellurophenes with a variety of coordination modes, i.e. η^1, η^2, η^4 and η^5 for unsubstituted tellurophene and η^1 and η^6 for dibenzotellurophene.

5.11 Synthetic strategies

The $[Cp^*RhCl_2]_2$ dimer represents an attractive system for forming complexes given the known behaviour with thiophenes. It behaves as a "soft" sixteen e^- electrophile and the mode of bonding can be controlled by freeing coordination sites on the rhodium by removal of the labile Cl ligands.

Hence, for the formation of η^5 complexes it is desirable that all the Cl ligands are removed, thereby generating a highly reactive $[Cp^*Rh(solvent)_3]^{2+}$ cation in solution containing weakly coordinating solvent molecules. The solvent molecules are easily displaced when reacted with excess ligand and in the case of tetramethylthiophene an η^5 complex results,[39] thus satisfying the coordination requirements of rhodium.

The most common synthetic procedure for the formation of η^4 complexes involves a two-electron reduction of 18 electron η^5 complexes.[34-36] It is also proposed here that rhodium complexes such as $Cp^*RhCl_2PPh_3$ and $Cp^*Rh(diphos)Cl_2$ containing two labile chlorides may be used to prepare η^4 complexes. A similar synthetic strategy was thought viable for the formation of η^2 complexes, hence $[Cp^*Rh(diphos)Cl]PF_6$ containing only one labile chloride was used.

The general synthetic strategy employed for the formation of η^1 complexes involves the direct reaction of the $[Cp^*RhCl_2]_2$ dimer with excess ligand.[44] Thus, the Cl ligands are retained on the rhodium, whose coordination requirements will then be satisfied by the formation of a single σ bond to the heterocycle.

The analogous work done on thiophenic derivatives has provided useful models for the hetrogeneously catalysed hydrodesulfurisation reactions of oils and coal derived liquids. In that context, Rauchfuss and his co-workers[39] have shown that the $[Cp^*RhCl_2]_2$ dimer will react with tetramethylthiophene to give a product containing an η^4-bonded complex which, following reaction with $Fe_3(CO)_{12}$, gives further products some of which contain organic fragments arising from the loss of sulfur from the thiophene ring.

A further paper from the same laboratory[110] provided fascinating insight into the mechanism of the thermolysis of $Cp^*Rh(\eta^4\text{-}C_4Me_4S)$ which produces a characterised intermediate involving a trimeric rhodium cluster containing two $(\eta^4,\eta^1\text{-}C_4Me_4S)$ moieties. This intermediate undergoes thermal decomposition resulting in the formation of $[Cp^*Rh]_2(C_4Me_4S)$ in which the heterocycle is in a ring-opened form (Scheme 5.1).

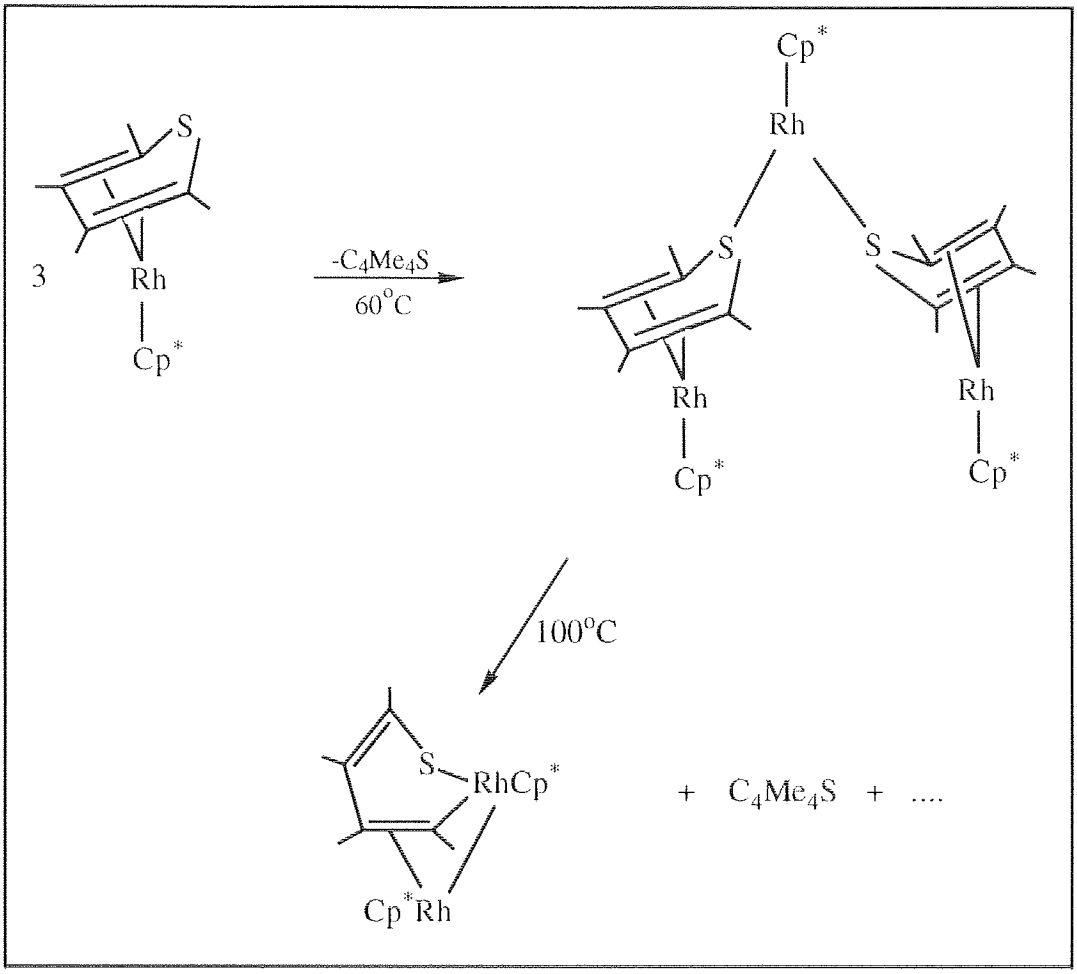

Scheme 5.1 Redistribution of thiophene ligands under thermal conditions

It is believed that this chemistry has particular relevance to the results presented in this work.

5.2 EXPERIMENTAL

$[Cp^*RhCl_2]_2$, $Cp^*RhCl_2PPh_3$, $Cp^*Rh(diphos)Cl_2$ and $[Cp^*Rh(diphos)Cl]PF_6$[111] were prepared from the indicated literature method using $RhCl_3.3H_2O$ as the starting material. The tellurium heterocycles were prepared as previously outlined in chapter 3, together with the additional heterocycle, cyclotelluropentane[72] which was prepared from the published method. The identity and purity of the starting materials was confirmed by comparison of IR and NMR spectra with published spectral data.

5.2.1 Synthesis of $[Cp^*Rh(\eta^5\text{-}C_4H_4Te)](OTf)_2$

An acetone solution (20 cm^3) of AgOTf (1.88g, 7.30 mmol) was added in one portion to an acetone suspension (30 cm^3) of $[Cp^*RhCl_2]_2$ (1.12g, 1.81 mmol) and tellurophene (1.15g, 6.42 mmol). The homogeneous red solution gradually changed to yellow with concomitant precipitation of AgCl. After 2 hours stirring at room temperature, the mixture was filtered through celite in air to remove the AgCl precipitate and the yellow filtrate was concentrated under vacuum to approximately 10 cm^3. Slow addition of $CHCl_3$ to the concentrated filtrate resulted in the precipitation of yellow, flaky crystals shown to have the formula $[Cp^*Rh(\eta^5\text{-}C_4H_4Te)](OTf)_2$ (**1**); yield 1.69g, 86% based on $[Cp^*RhCl_2]_2$.

Requires (%)	C, 26.8	H, 2.7	S, 9.0	$C_{16}H_{19}O_6RhTeF_6S_2$
Found (%)	C, 26.9	H, 2.7	S, 9.0	

5.2.2. Reduction of $[Cp^*Rh(\eta^5\text{-}C_4H_4Te)](OTf)_2$ with Cp_2Co : attempted synthesis of $Cp^*Rh(\eta^4\text{-}C_4H_4Te)$

An acetone suspension (20 cm^3) of $[Cp^*Rh(\eta^5\text{-}C_4H_4Te)](OTf)_2$ (1.08g, 1.62 mmol) was cooled to -78°C and a solution of Cp_2Co (0.62g, 3.28 mmol) in acetone (15 cm^3) was added in small portions over a period of 0.5 hours. The reaction mixture was warmed slowly to room temperature and then stirred for 2 hours followed by concentration to approximately 10 cm^3 under vacuum. The concentrated solution was diluted with an equal volume of hexane and filtered to remove a black solid, thought to be a mixture of elemental tellurium and $\{[Cp_2Co][CF_3SO_3]\}$. The cycle of hexane addition followed by concentration was repeated until no further solid was obtained. The resulting dark red solution was then evaporated to dryness, yielding a purple solid identified as the mixed oxidation state compound, $Cp^*Rh(\eta^5\text{-}C_4H_4RhCp^*)$ (**2**); yield 0.2g, 47% based on $[Cp^*Rh(\eta^5\text{-}C_4H_4Te)](OTf)_2$.

Requires (%)	C, 54.5	H, 6.4	$C_{24}H_{34}Rh_2$
Found (%)	C, 53.6	H, 6.7	

5.2.3 Reaction of $Cp^*Rh(\eta^5\text{-}C_4H_4RhCp^*)$ with $Fe_3(CO)_{12}$

$Cp^*Rh(\eta^5\text{-}C_4H_4RhCp^*)$ (0.13g, 0.25 mmol) and $Fe_3(CO)_{12}$ (0.18g, 0.36 mmol) were dissolved in 35 cm^3 toluene and heated and stirred under reflux for 3 hours during which time the solution gradually changed from dark green to deep orange. After cooling the solution was filtered to remove a black residue and the deep orange filtrate was evaporated to dryness affording a dark orange solid. The solid was chromatographed on a 2.5 x 12 cm column of TLC-grade silica gel, thereby giving a small yellow band preceded by a small purple band and a larger yellow band. Elution with 2:1 hexane/CH_2Cl_2 and removal of solvent gave yellow crystals from the first eluate and small traces of a purple solid and a yellow solid from the second and third eluates respectively. The yellow crystals melted at 146°C and were identified as the ferrarhodocene, $Cp^*Rh\{\eta^5\text{-}C_4H_4Fe(CO)_3\}$ (**3**); yield 50mg, 47% based on $Cp^*Rh(\eta^5\text{-}C_4H_4RhCp^*)$.

Requires (%)	C, 47.4	H, 4.4	$C_{17}H_{19}RhFeO_3$
Found (%)	C, 47.2	H, 4.4	

5.2.4 Synthesis of $[Cp^*Rh(C_{12}H_8Te)](OTf)_2$

An acetone solution (20 cm^3) of AgOTf (1.67g, 6.48 mmol) was added in one portion to an acetone suspension (30 cm^3) of $[Cp^*RhCl_2]_2$ (1.00g, 1.62 mmol).The dark red solution immediately changed to yellow and the precipitated AgCl was removed by filtration through celite. Dibenzotellurophene (1.00g, 3.57 mmol) was then added to the yellow filtrate which gradually changed to dark orange and a red-orange precipitate formed. The reaction mixture was stirred for 3 hours at room temperature after which precipitation was completed by concentration of the solution under

vacuum to 5 cm^3 followed by the addition of 20 cm^3 of ether. The red-orange precipitate was collected by filtration and shown to have the formula $[Cp^*Rh(C_{12}H_8Te)](OTf)_2$ (**4**); yield 1.66 g, 63% based on $[Cp^*RhCl_2]_2$.

Requires (%)	C, 35.3	H, 2.8	$C_{24}H_{23}RhTeO_6S_2F_6$
Found (%)	C, 35.4	H, 3.1	

5.2.5 Reduction of $[Cp^*Rh(C_{12}H_8Te)](OTf)_2$ with Cp_2Co: subsequent reaction with $Fe_3(CO)_{12}$

An acetone suspension (20 cm^3) of $[Cp^*Rh(C_{12}H_8Te)](OTf)_2$ (1.00g, 1.23 mmol) was cooled to -78°C and a solution of Cp_2Co (0.48g, 2.54 mmol) in 15 cm^3 acetone was added dropwise over a period of 0.5 hours. The reaction mixture was warmed slowly to room temperature and then stirred for 2 hours followed by evaporation under vacuum to dryness, yielding a dark brown solid, 1.03 g. The dark brown solid was dissolved in 50 cm^3 of toluene together with (0.70g, 1.39 mmol) of $Fe_3(CO)_{12}$ and then heated and stirred under reflux for 4 hours, during which time the dark green solution gradually changed to deep purple. After cooling, the mixture was filtered to remove a black residue (0.82g) and the deep purple filtrate was evaporated to dryness under vacuum, affording a dark purple solid. The solid was chromatographed on a 2.5 x 15 cm column of silica gel, thereby giving five distinct bands. Elution with 2:1 hexane/CH_2Cl_2 followed by removal of solvent gave yellow crystals from the first eluate, a dark brown solid from the second, purple crystals from the third, yellow crystals from the fourth and orange crystals from the fifth.

The identity of the yellow crystals from the first eluate was confirmed by infrared spectroscopy as dibenzotellurophene (**5**). The brown solid from the second eluate was shown to be dibenzoferrole, $C_{12}H_8Fe_2(CO)_6$ (**6**); yield 44mg, 17% based on $[Cp^*Rh(C_{12}H_8Te)](OTf)_2$. The purple crystals from the third eluate were identified as the dimeric mixed ligand compound, $[Cp^*Fe(CO)_2]_2$ (**7**). The yellow crystals from the

fourth eluate melted at 206°C (dec.) and were shown to have the formula $Cp^*RhC_{12}H_8(CO)$ (**8**); yield 55mg, 21% based on $[Cp^*Rh(C_{12}H_8Te)](OTf)_2$. The orange crystals from the fifth eluate (trace) had a melting point >234°C and were shown to be the reduction product of $[Cp^*Rh(C_{12}H_8Te)](OTf)_2$ having the formula $Cp^*C_{12}H_8Rh(\eta^1\text{-}C_{12}H_8Te)$ (**9**). Crystals of (**8**) and (**9**) suitable for X-ray diffraction measurements were grown by slowly cooling concentrated CH_2Cl_2 solutions.

5.2.6 Synthesis of $Cp^*RhCl_2(\eta^1\text{-}C_{12}H_8Te)$

$[Cp^*RhCl_2]_2$ (0.25g, 0.41 mmol) was dissolved in 2.5 cm^3 of $CHCl_3$ and dibenzotellurophene (0.28g, 1.00 mmol) was rapidly added resulting in the gradual formation of a red precipitate. After 30 minutes stirring the precipitate was collected by filtration and washed with 20 cm^3 of ether. The identity of the precipitate was confirmed as $Cp^*RhCl_2(\eta^1\text{-}C_{12}H_{12}Te)$ (**10**); yield, 0.47g, 98% based on $[Cp^*RhCl_2]_2$.

Requires (%)	C, 44.9	H, 3.9	$C_{22}H_{23}RhCl_2Te$
Found (%)	C, 44.9	H, 3.9	

Crystals of (**10**) suitable for X-ray diffraction measurements were grown by slowly cooling a concentrated toluene solution.

5.2.7 Synthesis of $[Cp^*RhPPh_3(\eta^4\text{-}C_4H_4Te)](OTf)_2$

An acetone solution (10 cm^3) of AgOTf (0.34g, 1.36 mmol) was added in one portion to an acetone suspension (15 cm^3) of $Cp^*RhCl_2PPh_3$ (0.45g, 0.79 mmol) and tellurophene (0.35g, 1.94 mmol). The orange solution gradually became lighter with concomitant precipitation of AgCl. The mixture was stirred for 3 hours at room temperature and then filtered through celite in air to remove the AgCl precipitate. The orange filtrate was concentrated under vacuum to approximately 5 cm^3. Slow addition of $CHCl_3$ to the concentrated filtrate followed by further concentration under vacuum

resulted in the precipitation of an orange/yellow solid of formula $[Cp^*RhPPh_3(C_4H_4Te)](OTf)_2$ (**11**); yield, 0.26g, 34% based on $Cp^*RhCl_2PPh_3$.

Requires (%)	C, 41.7	H, 3.5	$C_{34}H_{34}O_6RhPTeS_2F_6$
Found (%)	C, 38.5	H, 3.7	

5.2.8 Attempted synthesis of $[Cp^*Rh(diphos)(\eta^4\text{-}C_4H_4Te)](BF_4)_2$

A CH_2Cl_2 solution (10 cm^3) of $AgBF_4$ (0.12g, 0.63 mmol) was added in one portion to a CH_2Cl_2 suspension (15 cm^3) of $Cp^*Rh(diphos)Cl_2$ (0.20g, 0.28 mmol) and tellurophene (0.15g, 0.83 mmol). AgCl was gradually precipitated from the orange solution. After 3 hours stirring at room temperature, the mixture was filtered through celite in air to remove the AgCl precipitate and the orange filtrate was evaporated to dryness under vacuum, leaving an orange solid. The solid was redissolved in approximately 2 cm^3 of CH_2Cl_2 followed by addition of diethyl ether (20 cm^3) resulting in the precipitation of an orange crystalline solid; yield, 0.19g.

Requires (%)	C, 48.5	H, 4.3	P, 6.3	$C_{40}H_{43}RhP_2TeB_2F_8$
Found (%)	C, 52.5	H, 4.8	P, 7.9	

5.2.9 Attempted synthesis of $[Cp^*Rh(diphos)(\eta^2\text{-}C_4H_4Te)](BF_4)(PF_6)$

$[Cp^*Rh(diphos)Cl]PF_6$ (0.20g, 0.25 mmol) was dissolved in CH_2Cl_2 (20 cm^3) together with $AgBF_4$ (0.05g, 0.26 mmol) and tellurophene (0.15g, 0.84 mmol) and the mixture was stirred for 2 hours at room temperature. A small quantity of AgCl precipitated during the reaction and the solution colour changed from orange to yellow. The mixture was then filtered through celite in air to remove the AgCl precipitate and the yellow filtrate was evaporated to dryness under vacuum, leaving a yellow solid. Dissolution of the solid in CH_2Cl_2 (~ 2 cm^3) followed by addition of diethyl ether (20 cm^3) resulted in the precipitation of a yellow solid; yield, 0.14g.

Requires (%)	C, 45.8	H, 4.1	P, 8.9	$C_{40}H_{43}RhP_3TeBF_{10}$
Found (%)	C, 49.2	H, 4.3	P, 10.2	

5.2.10 Reaction of 2-telluraindane with $[Cp^*RhCl_2]_2$ in the presence of AgOTf

An acetone solution (10 cm^3) of AgOTf (0.83g, 3.23 mmol) was added in one portion to an acetone suspension (30 cm^3) of $[Cp^*RhCl_2]_2$ (0.50g, 0.81 mmol) and 2-telluraindane (0.38g, 1.64 mmol). AgCl gradually precipitated from the dark orange solution. After 2 hours stirring at room temperature, the mixture was filtered through celite in air to remove the AgCl precipitate and the orange filtrate was concentrated under vacuum to approximately half volume. Addition of an equal volume of hexane to the concentrated filtrate resulted in the precipitation of an orange solid shown to have the formula $[Cp^*Rh(C_8H_8Te)](OTf)_2$ (**12**); yield 0.59g, 47% based on $[Cp^*RhCl_2]_2$.

Requires (%)	C, 31.3	H, 3.0	$C_{20}H_{23}O_6RhTeS_2F_6$
Found (%)	C, 31.7	H, 3.4	

5.2.11 Direct reaction of 2-telluraindane with $[Cp^*RhCl_2]_2$

2-telluraindane (0.38g, 1.64 mmol) was dissolved in toluene (40 cm^3) together with $[Cp^*RhCl_2]_2$ (0.50g, 0.81 mmol) and heated, with stirring, under reflux for 3 hours. The reaction mixture was then filtered, affording a brown residue (0.11g) and a deep red-brown filtrate. Removal of toluene under vacuum from the filtrate yielded a dark red solid (m.p. >234°C), thought to have the formula $Cp^*RhCl_2(C_8H_8Te)$ (**13**); yield 0.54g, 62% based on $[Cp^*RhCl_2]_2$.

Requires (%)	C, 39.9	H, 4.3	$C_{18}H_{23}RhTeCl_2$
Found (%)	C, 40.2	H, 4.3	

5.2.12 Reaction of cyclotelluropentane with $[Cp^*RhCl_2]_2$ in the presence of AgOTf

An acetone solution (10 cm^3) of AgOTf (0.26g, 1.01 mmol) was added in one portion to an acetone suspension (10 cm^3) of $[Cp^*RhCl_2]_2$ (0.15g, 0.24 mmol).The dark red solution immediately changed to yellow and the precipitated AgCl was removed by filtration. Cyclotelluropentane (0.10g, 0.54 mmol) dissolved in $CHCl_3$ (25 cm^3) was then added dropwise via syringe to the yellow filtrate and the mixture was stirred for 3 hours at room temperature. The orange precipitate that formed was removed by filtration and the filtrate was evaporated to dryness under vacuum to give a red solid, shown by infrared spectroscopy to be unreacted $[Cp^*RhCl_2]_2$. The orange precipitate was also shown to be a mixture of unreacted starting materials.

5.2.13 Reaction of cyclotelluropentane with $[Cp^*RhCl_2]_2$

Cyclotelluropentane (0.27g, 1.50 mmol) dissolved in $CHCl_3$ (25 cm^3) was added dropwise via syringe to solution of $[Cp^*RhCl_2]_2$ (0.25g, 0.40 mmol) in $CHCl_3$ (2 cm^3) and the mixture was stirred under reflux for 2 hours. The dark red solution was filtered and then evaporated to dryness under vacuum, yielding a dark red solid (0.20g), shown to be unreacted $[Cp^*RhCl_2]_2$.

5.3 RESULTS AND DISCUSSION

NMR spectra of selected compounds are displayed in Figures 5.1-5.4 (pages 159-162), Figures 5.6-5.14 (pages 173-180) and Figures 5.15-5.18 (pages 190-193).

5.3.1 Synthesis of $[Cp^*Rh(\eta^5\text{-}C_4H_4Te)](OTf)_2$

$[Cp^*Rh(\eta^5\text{-}C_4H_4Te)](OTf)_2$ (**1**) was prepared by treating $[Cp^*RhCl_2]_2$ with tellurophene in the presence of silver triflate. The silver salt is capable of removing the chlorides from the rhodium complex thus generating a highly reactive $[Cp^*Rh(acetone)_3]^{2+}$ cation in which the solvent molecules are only weakly

coordinated. The acetone ligands are easily displaced by the more basic tellurophene to yield the η^5-complex. The final product is formed as yellow, flaky crystals in 86% yield (based on $[Cp^*RhCl_2]_2$). The infrared spectrum shows strong absorption at 1265 and 1223 cm^{-1} indicating the presence of the triflate cation. The structure of this complex, shown below, is thought to be analogous to that reported for the tetramethylthiophene complex, $[Cp^*Rh(\eta^5\text{-}C_4Me_4S)](OTf)_2$.[39]

(1) 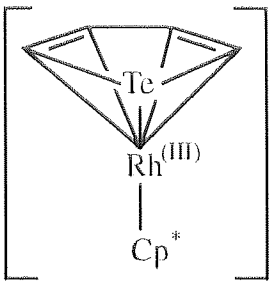

Data obtained from the FAB mass spectrum (NOBA matrix) is shown in Table 5.1, while NMR data is displayed in Tables 5.2-5.4.

m/z	assignment
569	$\{[Cp^*Rh(\eta^5\text{-}C_4H_4Te)]OTf\}^+$
420	$[Cp^*Rh(\eta^5\text{-}C_4H_4Te)]^+$

Table 5.1 FAB-MS (NOBA matrix) peaks for $[Cp^*Rh(\eta^5\text{-}C_4H_4Te)](OTf)_2$

compound	^{13}C δ, ppm (CD_3OCD_3)	J, Hz	assignment
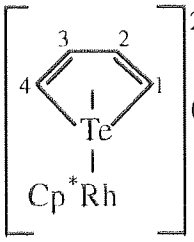	121.6	(^{19}F, ^{13}C) = 322	$(CF_3SO_3)^-$
	114.2 (-23.7)	(^{103}Rh, ^{13}C) = 7.6	C2, C3
	112.0 (-14.6)	(^{103}Rh, ^{13}C) = 4.4	C1, C4
	110.9	(^{103}Rh, ^{13}C) = 7.6	Cp^*
	10.82	-	Cp^* (CH_3)

Table 5.2 ^{13}C NMR data for $[Cp^*Rh(\eta^5\text{-}C_4H_4Te)](OTf)_2$
Figures in parenthesis indicate upfield shift from parent tellurophene

compound	^{1}H δ, ppm (CD_3OCD_3)	Δδ, ppm	assignment
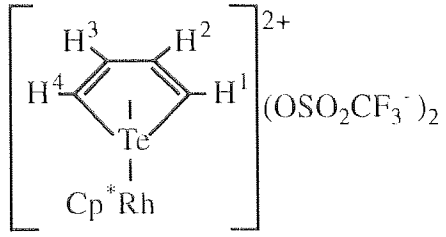	8.31 (q, 2H) 8.20 (q, 2H) 2.41 (s, 15H)	-0.72 +0.26	H1, H4 H2, H3 Cp* (CH_3)

Table 5.3 ^{1}H NMR data for $[Cp^*Rh(\eta^5\text{-}C_4H_4Te)](OTf)_2$

Δδ represents shift from parent tellurophene; - = upfield shift, + = downfield shift

compound	^{125}Te δ, ppm (CD_3OCD_3)	Δδ, ppm	J, Hz
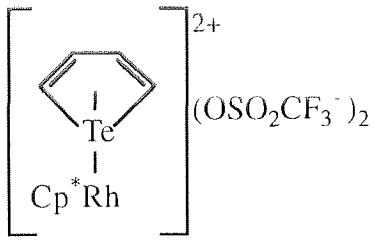	121.0	-203.9	(^{103}Rh, ^{125}Te) = 20.0

Table 5.4 ^{125}Te NMR data for $[Cp^*Rh(\eta^5\text{-}C_4H_4Te)](OTf)_2$

Δδ represents shift from parent tellurophene; - = upfield shift, + = downfield shift

The ^{13}C NMR spectrum for $[Cp^*Rh(\eta^5\text{-}C_4H_4Te)](OTf)_2$, shown in Figure 5.1, strongly supports the proposed structure of this complex. The observed ^{13}C-^{103}Rh coupling constants are in close agreement with those reported for the analogous tetramethylthiophene complex, $[Cp^*Rh(\eta^5\text{-}C_4Me_4S)](OTf)_2$ reported by Rauchfuss.[39] There are pronounced upfield shifts for all carbons of the tellurophene ligand on complexation with the rhodium. This increased shielding can be attributed to the greater electron density around the carbon nuclei in the complex. The enhanced electron density can in turn be associated with the formation of a "covalent

delocalised multicentre bond" often described for η^5 coordination.[112] Furthermore, the C2 and C3 carbons experience a significantly larger upfield shift than the C1 and C4 carbons adjacent to the tellurium atom implying an unequal strength of interaction between rhodium and the four carbons.

The ^{1}H NMR spectrum for $[Cp^*Rh(\eta^5\text{-}C_4H_4Te)](OTf)_2$ (Figure 5.2) displays absorptions for H1 and H4 protons on the carbons adjacent to the tellurium resonating at higher field compared to free tellurophene. This is in correlation with the shielding experienced by the C1 and C4 carbons on complexation with rhodium. The H2 and H3 protons, however, are deshielded on complexation, in contrast to the carbons C2 and C3 bearing them implying depleted electron density at these protons.

The proton decoupled ^{125}Te NMR spectrum (Figure 5.4) clearly displays a doublet arising from ^{125}Te-^{103}Rh spin-spin coupling. The magnitude of this coupling constant is much smaller than is expected for σ-coordination (see Table 5.29), thus providing further evidence for η^5-complexation. Moreover, the chemical shift of Te in the complex occurs at much higher field than that of the free heterocycle, in agreement with results obtained by Angelici, employing ^{77}Se NMR.

5.3.2. Reduction of $[Cp^*Rh(\eta^5\text{-}C_4H_4Te)](OTf)_2$ with Cp_2Co : attempted synthesis of $Cp^*Rh(\eta^4\text{-}C_4H_4Te)$

Reduction of $[Cp^*Rh(\eta^5\text{-}C_4H_4Te)](OTf)_2$ with Cp_2Co resulted in the formation of a mixed oxidation state compound having the formula $Cp^*Rh(\eta^5\text{-}C_4H_4RhCp^*)$ (**2**), the structure of which is shown below.

(2)

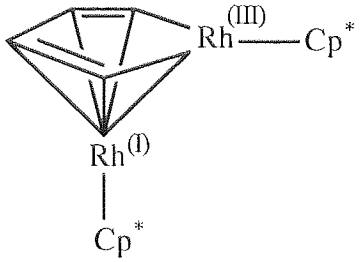

(2) was formed in 47% yield based on $[Cp^*Rh(\eta^5\text{-}C_4H_4Te)](OTf)_2$. The expected product from this reaction was the η^4-complex, $Cp^*Rh^{(I)}(\eta^4\text{-}C_4H_4Te)$ since the analogous $Cp^*Rh(\eta^4\text{-}C_4R_4S)$ is isolated when the reduction of $[Cp^*Rh(\eta^5\text{-}C_4R_4S)](OTf)_2$ is carried out.[39] However, in the tellurophene case, no η^4-complex was isolated although it can be postulated as an intermediate to the obtained compound (see Scheme 5.2). Although no crystals of (2) suitable for X-ray crystallography were obtained, both mass spectrometric (Table 5.5) and infrared spectroscopic data are consistent with the formulation given. Suitable NMR data was not collected for this compound.

m/z	assignment
528	M^+
135	$(Cp^*)^+$

Table 5.5 EI-MS peaks for $Cp^*Rh(\eta^4\text{-}C_4H_4RhCp^*)$

5.3.3 Reaction of $Cp^*Rh(\eta^5\text{-}C_4H_4RhCp^*)$ with $Fe_3(CO)_{12}$

The major product from this reaction was the ferrarhodocene, $Cp^*Rh\{\eta^5\text{-}C_4H_4Fe(CO)_3\}$ (3), which was formed in 47% yield based on $Cp^*Rh(\eta^5\text{-}C_4H_4RhCp^*)$. The crystal structure of the analogous $Cp^*Rh\{\eta^5\text{-}C_4Me_4Fe(CO)_3\}$ has been previously determined[39] by the Rauchfuss group and is shown in Figure 5.5.

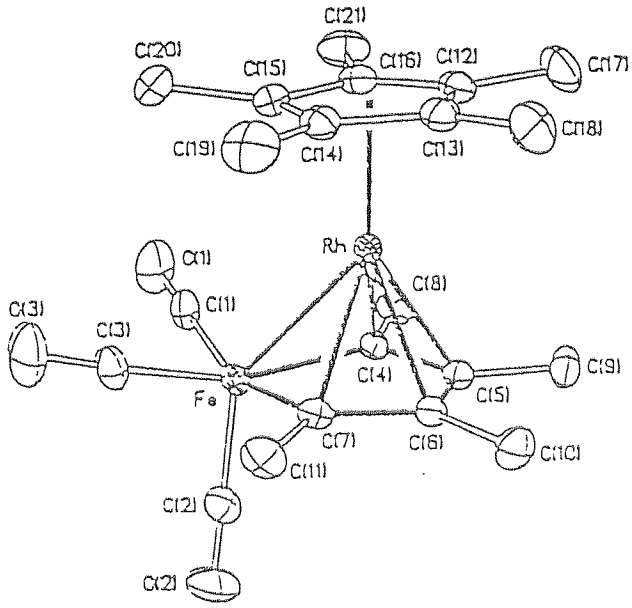

Figure 5.5 Structure of $Cp^*Rh\{\eta^5\text{-}C_4Me_4Fe(CO)_3\}$

The structure of $Cp^*Rh\{\eta^5\text{-}C_4H_4Fe(CO)_3\}$ is expected to be similar to that shown in Figure 5.5 and its mass spectrometric and infrared spectroscopic data are displayed in Tables 5.6 and 5.7 respectively.

m/z	assignment
430	M^+
346	M^+ - 3CO

Table 5.6 EI-MS peaks for $Cp^*Rh(\eta^5\text{-}C_4H_4Fe(CO)_3)$

KBr, ν(CO) cm^{-1}
2011(s)
1944(m)
1922(s)
1890(w)

Table 5.7 Infrared peaks in the carbonyl region for $Cp^*Rh(\eta^5\text{-}C_4H_4Fe(CO)_3)$

Other minor products were also obtained from this reaction and were separated by chromatography. A purple solid, the identity of which was not established, gave an infrared spectrum showing the presence of terminal carbonyl groups (Table 5.8) as well as organic functional groups whilst the mass spectrum showed a dominant peak at m/z = 373, indicative of $(Cp^*)_2Rh^+$. It is most likely, therefore that this is an intermediate to the eventual product from this reaction. The yellow solid that was also isolated (trace) did not display absorption in the carbonyl region of the infrared spectrum whilst mass spectrometry proved inconclusive as to its identity

KBr, ν(CO) cm^{-1}
2014(s)
1984(m)
1924(m)
1891(w)

Table 5.8 Infrared peaks in the carbonyl region for intermediate product from reaction of $Cp^*Rh(\eta^5\text{-}C_4H_4RhCp^*)$ with $Fe_3(CO)_{12}$

5.3.4 Summary of reactions of tellurophene with $[Cp^*RhCl_2]_2$

The reactions of tellurophene with $[Cp^*RhCl_2]_2$ are summarised in Scheme 5.2. The scheme is speculative, but precedents for the intermediates (**a**), (**b**) and (**c**) are known from the work of the groups of both Angelici[34] and Rauchfuss.[110] The difficulty in isolating these intermediates demonstrates the greater reactivity of the tellurium heterocycle compared to its sulfur analogue, since in the thiophene case the $(\eta^4\text{-}C_4Me_4S)RhCp^*$ would be isolable. The conversion of (**a**) to (**2**) appears to occur very rapidly at room temperature through intermediates (**b**) and (**c**) with the release of free tellurophene but in the analogous sulfur systems these transformations require a period of several days.[110] In contrast to the weak nucleophilicity and basicity of free tellurophene and $\eta^5\text{-}C_4H_4Te$ ligands, η^4-complexes such as (**a**) are expected to be strongly nucleophilic as the heteroatom is bent out of the plane. The proposed

transformation of (**a**) to (**b**) therefore reflects the strong tendency of η^4-ligands to more fully utilise their complement of non-bonding electrons. Complex (**b**) can be considered as possessing an η^4,η^1-C_4H_4Te coordination which eventually leads to C-Te bond cleavage giving rise to the isolated complex (**2**). In contrast to this, thiophenes are not desulfurised but stop at the stage where the complex analogous to (**c**) is formed.

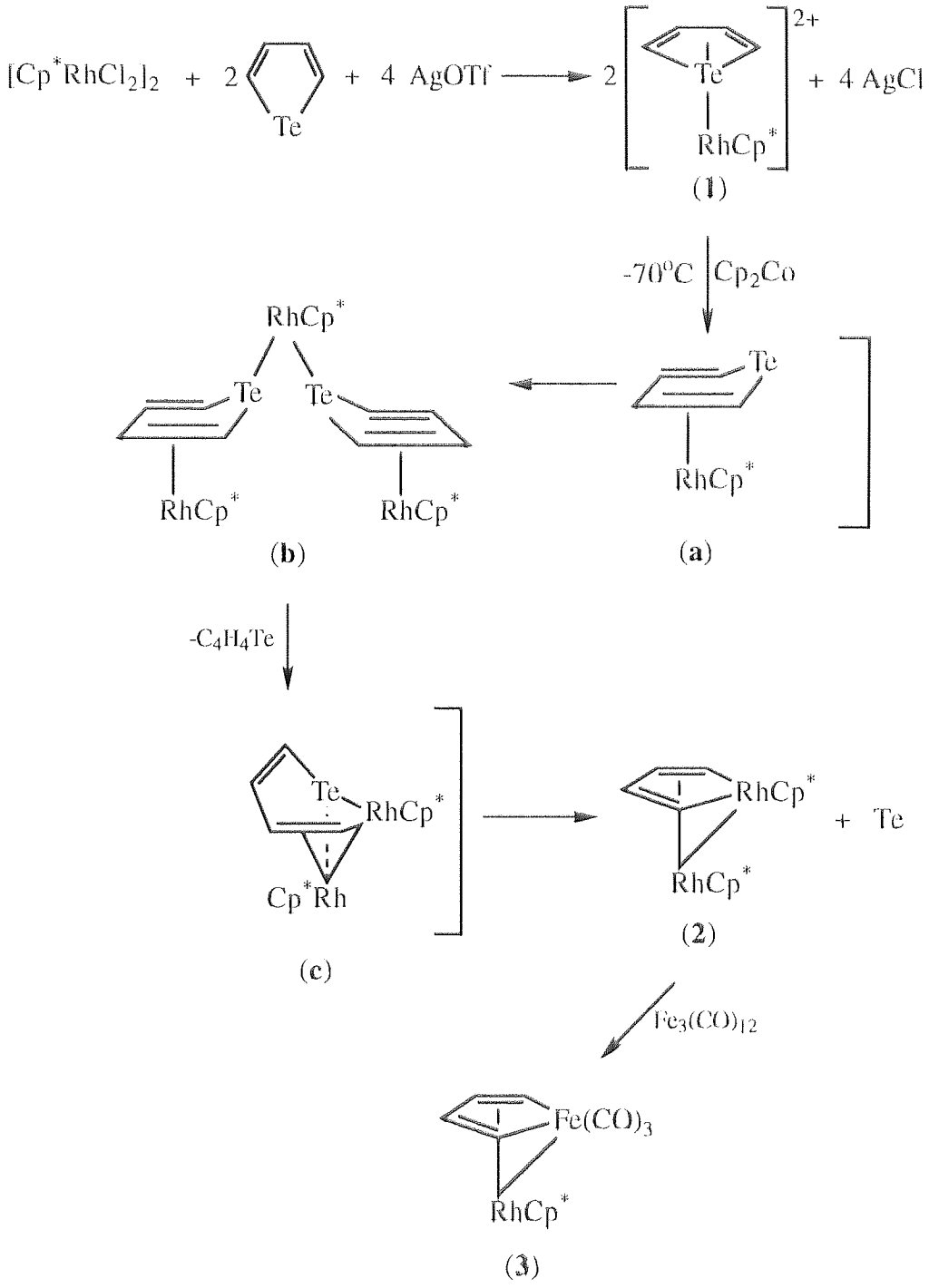

Scheme 5.2 The reactivity of tellurophene with $[Cp^*RhCl_2]_2$

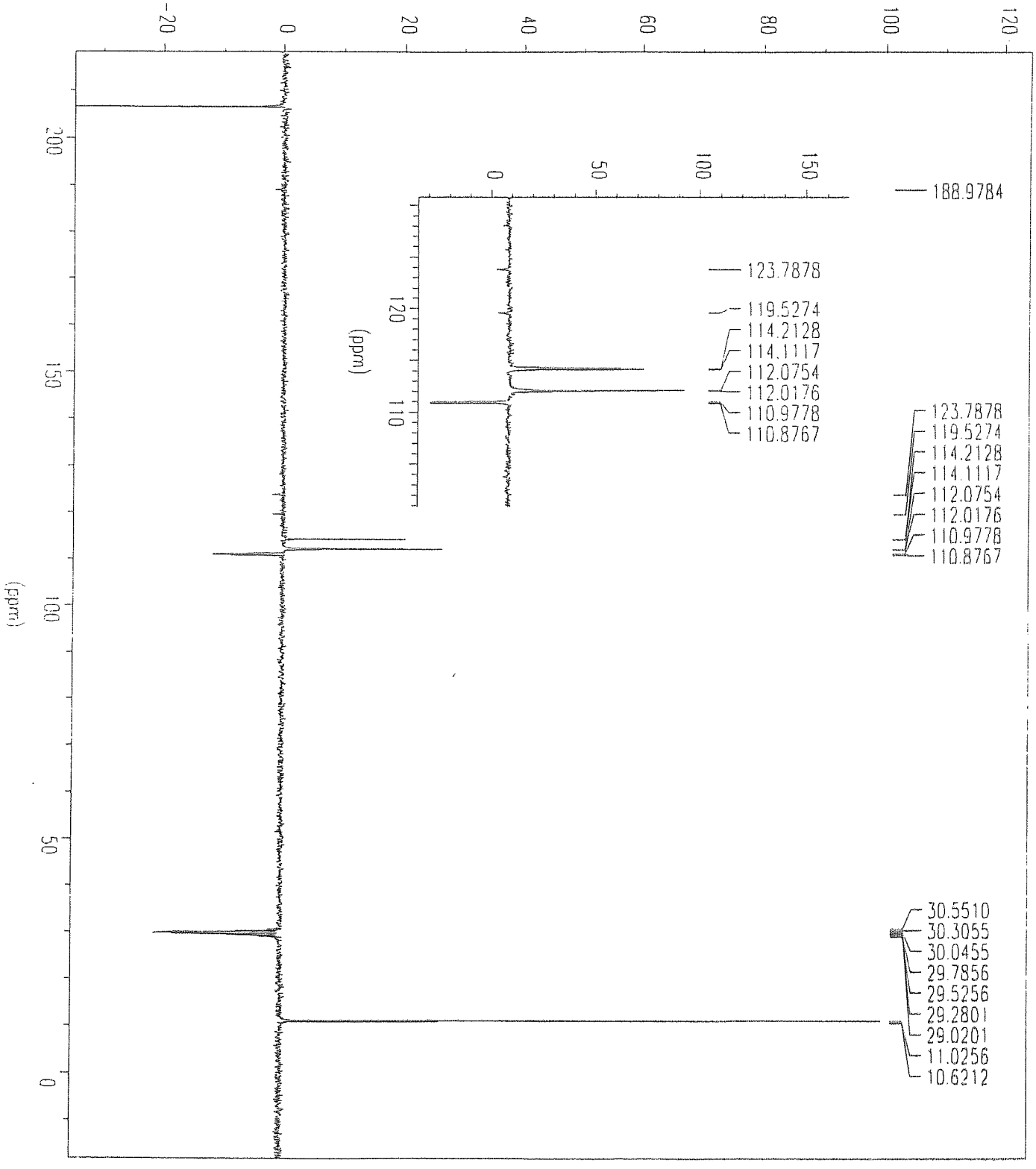

Figure 5.1 ^{13}C NMR spectrum of $[Cp^*Rh(\eta^5\text{-}C_4H_4Te)](OTf)_2$ (1)

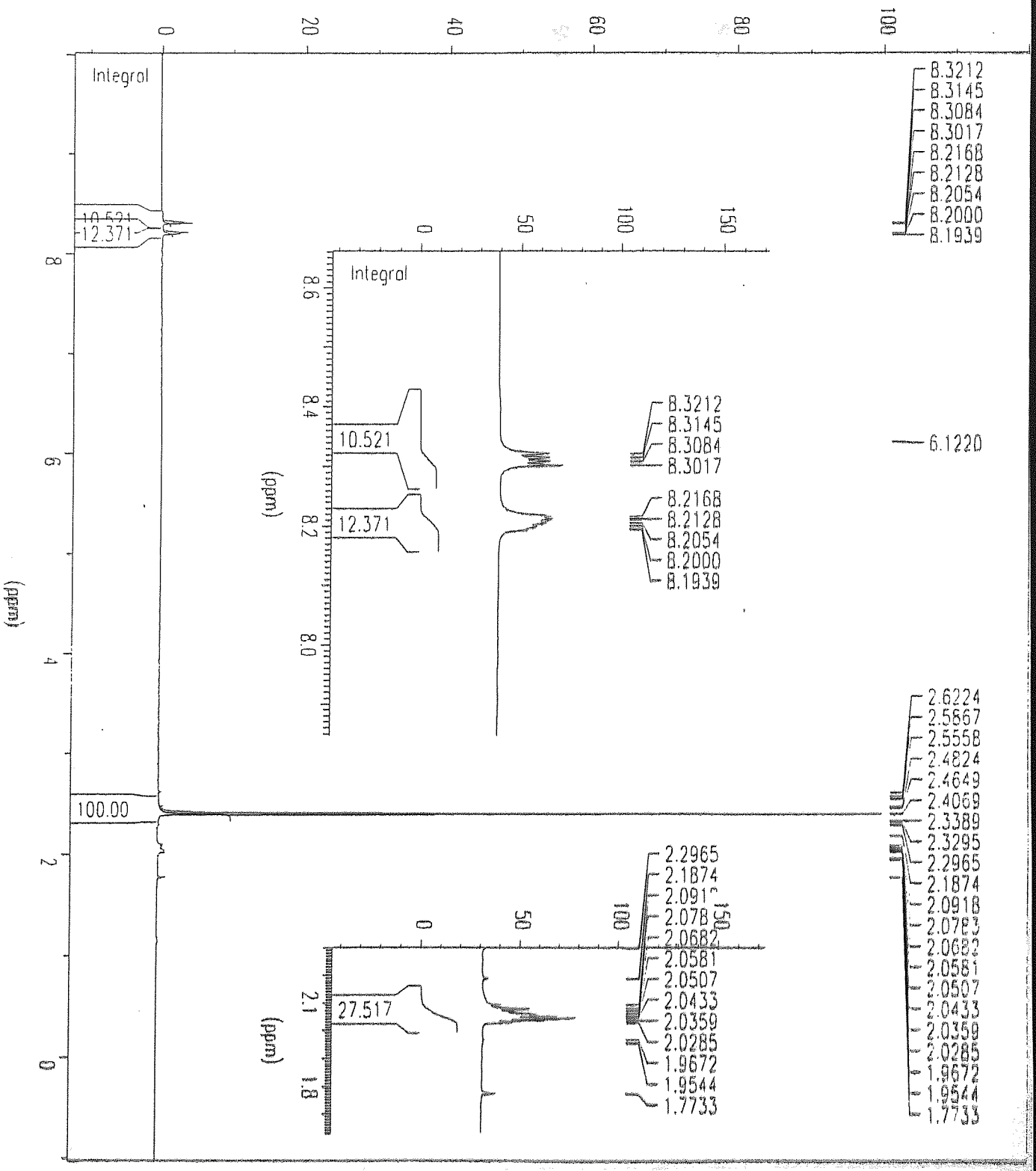

Figure 5.2 ^{1}H NMR spectrum of $[Cp^*Rh(\eta^5\text{-}C_4H_4Te)](OTf)_2$ (1)

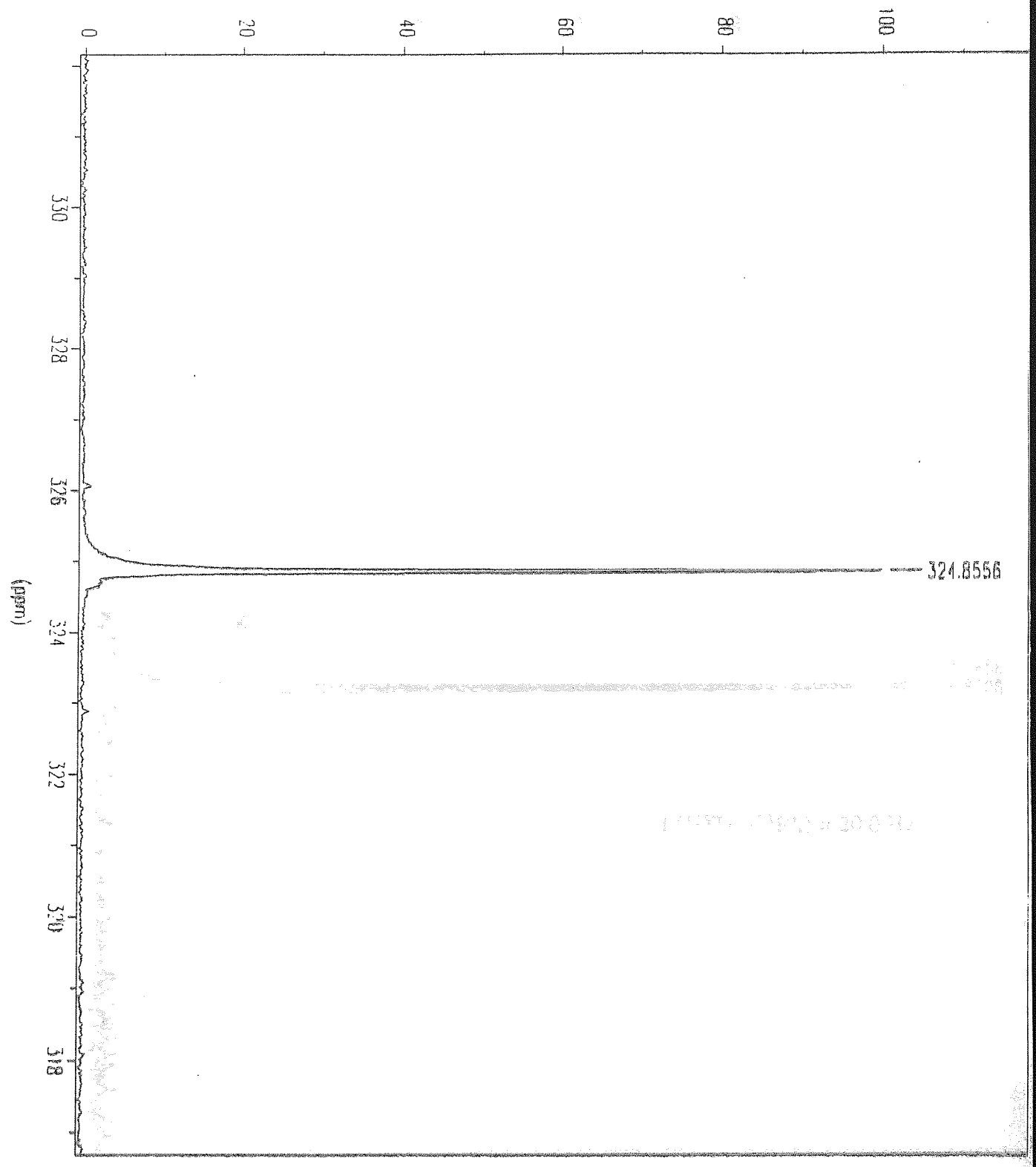

Figure 5.3 Proton decoupled^{125}Te NMR spectrum of tellurophene

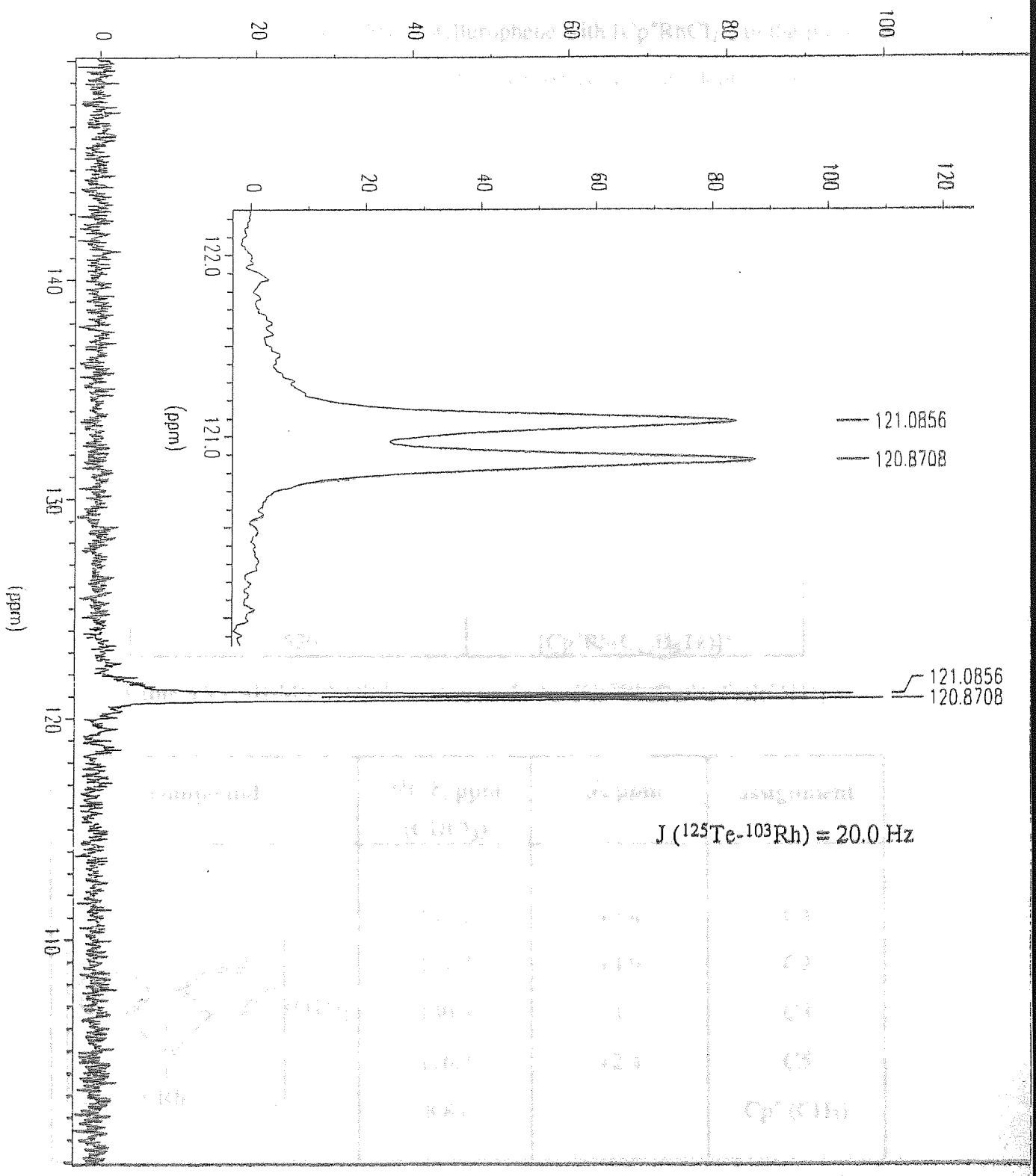

Figure 5.4 ^{125}Te NMR spectrum of $[Cp^*Rh(\eta^5\text{-}C_4H_4Te)](OTf)_2$ (1)

5.3.5 Synthesis of $[Cp^*Rh(C_{12}H_8Te)](OTf)_2$

A solid having the molecular formula $[Cp^*Rh(C_{12}H_8Te)](OTf)_2$ (4) was obtained in 63% yield from the reaction of dibenzotellurophene with $[Cp^*RhCl_2]_2$ in the presence of silver triflate. The presence of the triflate cation is again evident in the infrared spectrum, displaying absorption peaks ranging from 1307 to 1171 cm^{-1}. Free dibenzotellurophene displays two absorption peaks in its infrared spectrum at 742 and 735 cm^{-1} corresponding to bending vibrations in the ortho-disubstituted benzene rings. On complexation with rhodium these peaks undergo a shift in absorption to higher frequency appearing at 748 and 742 cm^{-1} respectively. Further evidence for the formation of this complex is provided by NMR spectroscopy and FAB-MS data, shown in Tables 5.9 to 5.12.

m/z (FAB)	assignment
669	$\{[Cp^*Rh(C_{12}H_8Te)]OTf\}^+$
520	$[Cp^*Rh(C_{12}H_8Te)]^+$

Table 5.9 FAB-MS (NOBA matrix) peaks for $[Cp^*Rh(C_{12}H_8Te)](OTf)_2$

compound	^{13}C δ, ppm ($CDCl_3$)	Δδ, ppm	assignment
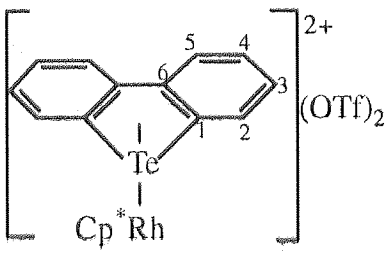	135.2	+2.4	C4
	131.7	+4.9	C2
	130.3	+4.7	C3
	126.7	+2.4	C5
	8.83		Cp^* (CH_3)

Table 5.10 ^{13}C NMR data for $[Cp^*Rh(C_{12}H_8Te)](OTf)_2$

Δδ represents shift from parent dibenzotellurophene; - = upfield shift, + = downfield shift

compound	^{1}H δ, ppm ($CDCl_3$)	Δδ, ppm	assignment
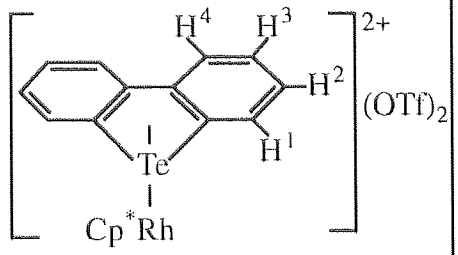	8.35 (m, 2H)	+0.12	H1
	8.13 (m, 2H)	+0.06	H3
	7.75 (m, 2H)	+0.28	H4
	7.56 (m, 2H)	+0.24	H2
	2.04 (s, 15H)		Cp* (CH_3)

Table 5.11 ^{1}H NMR data for $[Cp^*Rh(C_{12}H_8Te)](OTf)_2$

Δδ represents shift from parent dibenzotellurophene; - = upfield shift, + = downfield shift

compound	^{125}Te δ, ppm ($CDCl_3$)	Δδ, ppm	J, Hz
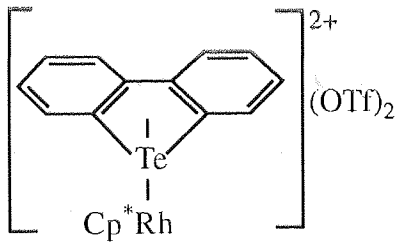	166.1	-56.5	(^{103}Rh, ^{125}Te) = 87.2

Table 5.12 ^{125}Te NMR data for $[Cp^*Rh(C_{12}H_8Te)](OTf)_2$

Δδ represents shift from parent dibenzotellurophene; - = upfield shift, + = downfield shift

The mode of attachment of dibenzotellurophene to rhodium in the complex $[Cp^*Rh(C_{12}H_8Te)](OTf)_2$ is a matter of some interest and since suitable crystals for X-ray crystallography could not be grown, NMR is particularly useful here for establishing whether η^1, η^4, η^5 or η^6 coordination exists.

The ^{13}C NMR spectrum of $[Cp^*Rh(C_{12}H_8Te)](OTf)_2$ (Figure 5.6) shows just four absorptions ruling out the possibility of η^6-coordination. Due to the low solubility of

this complex, the quarternary carbons, C1 and C6 were not detected. These carbons are expected to experience the greatest shift upon coordination of the rhodium and may indeed be split due to ^{103}Rh-^{13}C coupling.

The ^{1}H NMR spectrum (Figure 5.8) shows absorptions for protons which are not significantly shifted from the free dibenzotellurophene protons.

The proton decoupled ^{125}Te NMR spectrum (Figure 5.10) shows a doublet at 166.1 ppm arising from ^{125}Te-^{103}Rh spin-spin coupling. The magnitude of the coupling constant (~87 Hz) is indicative of a stronger interaction than that observed for the tellurophene complex $Cp^{*}Rh(\eta^{5}\text{-}C_4H_4Te)](OTf)_2$ (J, ^{125}Te-^{103}Rh ~20 Hz). This reflects a lesser degree of conjugation of tellurium lone pair electron density in the case of dibenzotellurophene than in the tellurophene case, and consequently a stronger Rh-Te interaction in η^{5}-coordination (in a sense, $\eta^{4} + \eta^{1}$). With η^{1}-coordination alone the rhodium would be coordinatively unsatisfied, therefore this mode of binding of the heterocycle is less likely. In simple η^{4}-coordination, the tellurium atom is expected to be bent out of the plane of the ring away from the rhodium atom thus producing no interaction and therefore no splitting of the proton decoupled ^{125}Te signal. The proton and ^{13}C NMR data clearly indicate the presence of a plane of symmetry thereby eliminating the need to consider an η^{6}-interaction in which the heterocycle is bound to rhodium through a benzene ring. A much smaller (or zero) ^{125}Te-^{103}Rh coupling constant would also be expected for this mode of attachment. Hence, the most likely coordination mode of dibenzotellurophene to rhodium in this complex is η^{5}, the structure of which is shown below (**4**). The fact that a larger coupling constant for $[Cp^{*}Rh(\eta^{5}\text{-}C_{12}H_8Te)](OTf)_2$ is observed than for $Cp^{*}Rh(\eta^{5}\text{-}C_4H_4Te)](OTf)_2$ can be rationalised by considering the greater electron density at the tellurium for the dibenzo system resulting in stronger Rh-Te interaction. The analogous sulfur systems exhibit very similar behaviour, whereby dibenzothiophene coordinates more strongly through the sulfur to metals than thiophene.[43]

(4)

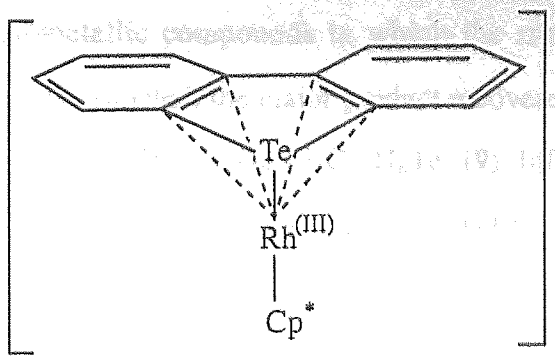

5.3.6 Reduction of $[Cp^*Rh(C_{12}H_8Te)](OTf)_2$ with Cp_2Co: subsequent reaction with $Fe_3(CO)_{12}$

Due to difficulties in isolating the product from the reduction of $[Cp^*Rh(C_{12}H_8Te)](OTf)_2$ the subsequent reaction with $Fe_3(CO)_{12}$ was done in situ giving rise to a diverse range of products. Yellow crystals of dibenzotellurophene (5) as well as the previously reported[96] dibenzoferrole (6) were both obtained as confirmed by their respective infrared spectra. The dimeric mixed ligand compound $[Cp^*Fe(CO)_2]_2$ (7) recovered from this reaction has also been previously reported[132] and peaks recorded in the carbonyl region of its infrared spectrum are shown in Table 5.13. The structure of (7) as determined by X-ray crystallography is shown in Figure 5.11 below.

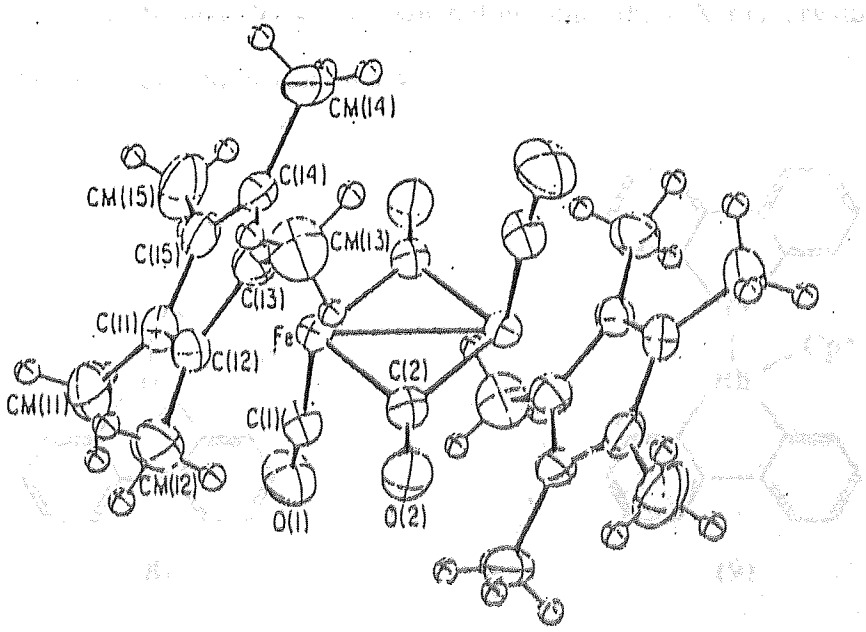

Figure 5.11 The molecular structure of $[Cp^*Fe(CO)_2]_2$ (7)

Two novel organometallic compounds in which the rhodium is inserted into the dibenzo ring were also isolated, the major product recovered being $Cp^*RhC_{12}H_8(CO)$ (**8**) with small traces of $Cp^*RhC_{12}H_8(\eta^1\text{-}C_{12}H_8Te)$ (**9**). Infrared data for (**8**) is shown in Table 5.13 while mass spectrometric data recorded for (**8**) and (**9**) is displayed in Table 5.14. Insufficient product yields were obtained for NMR analysis.

compound	KBr, ν(CO) cm^{-1}
$[Cp^*Fe(CO)_2]_2$	1920, 1884, 1745
$Cp^*RhC_{12}H_8(CO)$	2004, 1996, 1953

Table 5.13 Infrared bands in the carbonyl region for compounds (**7**) and (**8**)

compound	m/z (EI)	assignment
$Cp^*RhC_{12}H_8(CO)$	418	M^+
	390	M^+ - CO
$Cp^*RhC_{12}H_8(\eta^1\text{-}C_{12}H_8Te)$	672	M^+

Table 5.14 Mass spectral peaks (EI) recorded for compounds (**8**) and (**9**)

The structures of (**8**) and (**9**) are shown below and their X-ray crystallographic structural data is discussed in section 5.4.

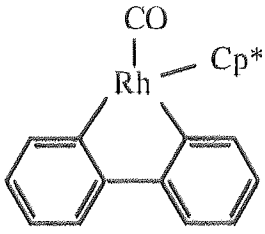

(**8**)

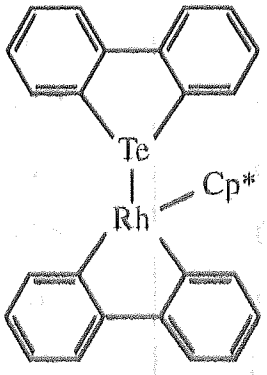

(**9**)

5.3.7 Synthesis of $Cp^*RhCl_2(\eta^1\text{-}C_{12}H_8Te)$

It was desirable to obtain a complex in which the mode of coordination of the dibenzotellurophene to rhodium was unambiguously η^1, thus a direct reaction between $[Cp^*RhCl_2]_2$ and dibenzotellurophene was carried out (a similar complex is known with dibenzothiophene) leading to the formation of $Cp^*RhCl_2(\eta^1\text{-}C_{12}H_8Te)$ (**10**) obtained in almost quantitative yield. The absence of silver triflate ensures that the chloride ligands are retained on the rhodium whose coordination requirements are then satisfied by the formation of a single coordinative bond to the tellurium in dibenzotellurophene. Mass spectral data for (**10**) is shown in Table 5.15 while NMR data is displayed in Tables 5.16-5.18.

m/z (FAB)	assignment
555	$\{[Cp^*RhCl(C_{12}H_8Te)]^+$
520	$[Cp^*Rh(C_{12}H_8Te)]^+$

Table 5.15 FAB-MS (NOBA matrix) peaks for $[Cp^*RhCl_2(\eta^1\text{-}C_{12}H_8Te)]$

compound	^{13}C δ, ppm ($CDCl_3$)	Δδ, ppm	assignment
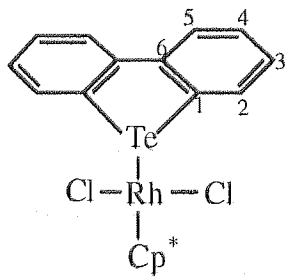	--	--	C6
	133.4	+0.6	C4
	129.0	+2.2	C2
	128.3	-0.8	C1
	128.1	+2.5	C3
	124.3	0	C5
	95.9		Cp^*
	8.83		Cp^* (CH_3)

Table 5.16 ^{13}C NMR data for $[Cp^*RhCl_2(\eta^1\text{-}C_{12}H_8Te)]$

Δδ represents shift from parent dibenzotellurophene; - = upfield shift, + = downfield shift

compound	^{1}H δ, ppm ($CDCl_3$)	Δδ, ppm	assignment
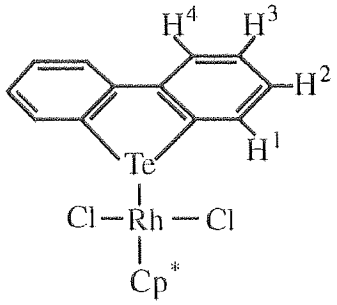	8.01 (m, 2H)	-0.22	H1
	7.94 (m, 2H)	-0.13	H3
	7.56 (m, 2H)	-0.09	H4
	7.35 (m, 2H)	-0.03	H2
	1.18 (s, 15H)		Cp* (CH_3)

Table 5.17 ^{1}H NMR data for $[Cp^*RhCl_2(\eta^1\text{-}C_{12}H_8Te)]$

Δδ represents shift from parent dibenzotellurophene; - = upfield shift, + = downfield shift

compound	^{125}Te δ, ppm ($CDCl_3$)	Δδ, ppm	J, Hz
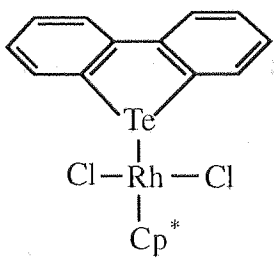	155.4	-67.2	(^{103}Rh, ^{125}Te) = 142.9

Table 5.18 ^{125}Te NMR data for $[Cp^*RhCl_2(\eta^1\text{-}C_{12}H_8Te)]$

Δδ represents shift from parent dibenzotellurophene; - = upfield shift, + = downfield shift

The ^{13}C NMR spectrum for $[Cp^*RhCl_2(C_{12}H_8Te)]$ (Figure 5.12) shows absorptions for carbons which are not significantly shifted from the parent dibenzotellurophene carbons. This is expected since the rhodium is bonded only to the tellurium atom in the heterocycle and therefore does not greatly affect the shielding experienced by the carbon nuclei. Similarly, the protons of the η^1-complex (Figure 5.13) absorb close to the protons of the free dibenzotellurophene.

The proton-decoupled ^{125}Te spectrum, shown in Figure 5.14, clearly shows a large splitting of the signal arising from spin-spin coupling of the rhodium and tellurium nuclei. The large observed splitting is consistent with the strong interaction between rhodium and tellurium in an η^1-complex. The chemical shift for the complex is further upfield than the free heterocycle by ~67 ppm, and this can be attributed to the attraction of the delocalised π-electrons in the heterocycle, when it is bound to rhodium.

The crystal structure of $[Cp^*RhCl_2(C_{12}H_8Te)]$ has been elucidated and is discussed in section 5.4.

5.3.8 Summary of reactions of dibenzotellurophene with $[Cp^*RhCl_2]_2$

The essential findings of the reactions of dibenzotellurophene with $[Cp^*RhCl_2]_2$ are summarised in Scheme 5.3.

Initial reaction of dibenzotellurophene (dbte) with the rhodium dimer in the presence of silver triflate affords $[Cp^*Rh(C_{12}H_8Te)](OTf)_2$ (**4**) in which an η^5 attachment of the heterocycle to the metal has been postulated. Attempted reduction of this 2+ complex followed by treatment with $Fe_3(CO)_{12}$ leads to a complex sequence of reactions taking place. There are clearly a number of reactions which have progressed in parallel, thus the dibenzoferrole (**6**) reasonably arises from the direct reaction of $Fe_3(CO)_{12}$ and dbte released from (**9**). It is probable that conversion of (**4**) to (**9**) takes place via an intermediate of formula $[Cp^*Rh(\eta^1\text{-dbte})_2]$ which in turn converts to a tellurarhodacyclic compound prior to (**9**) being formed. The formation of complex (**8**) can then be considered as a simple ligand exchange reaction in which dbte is replaced by a CO group originating from $Fe_3(CO)_{12}$. The presence of $[Cp^*Fe(CO)_2]_2$ (**7**) in the reaction mixture is indicative of some ligand scrambling since the Cp^* groups must have originated from the rhodium.

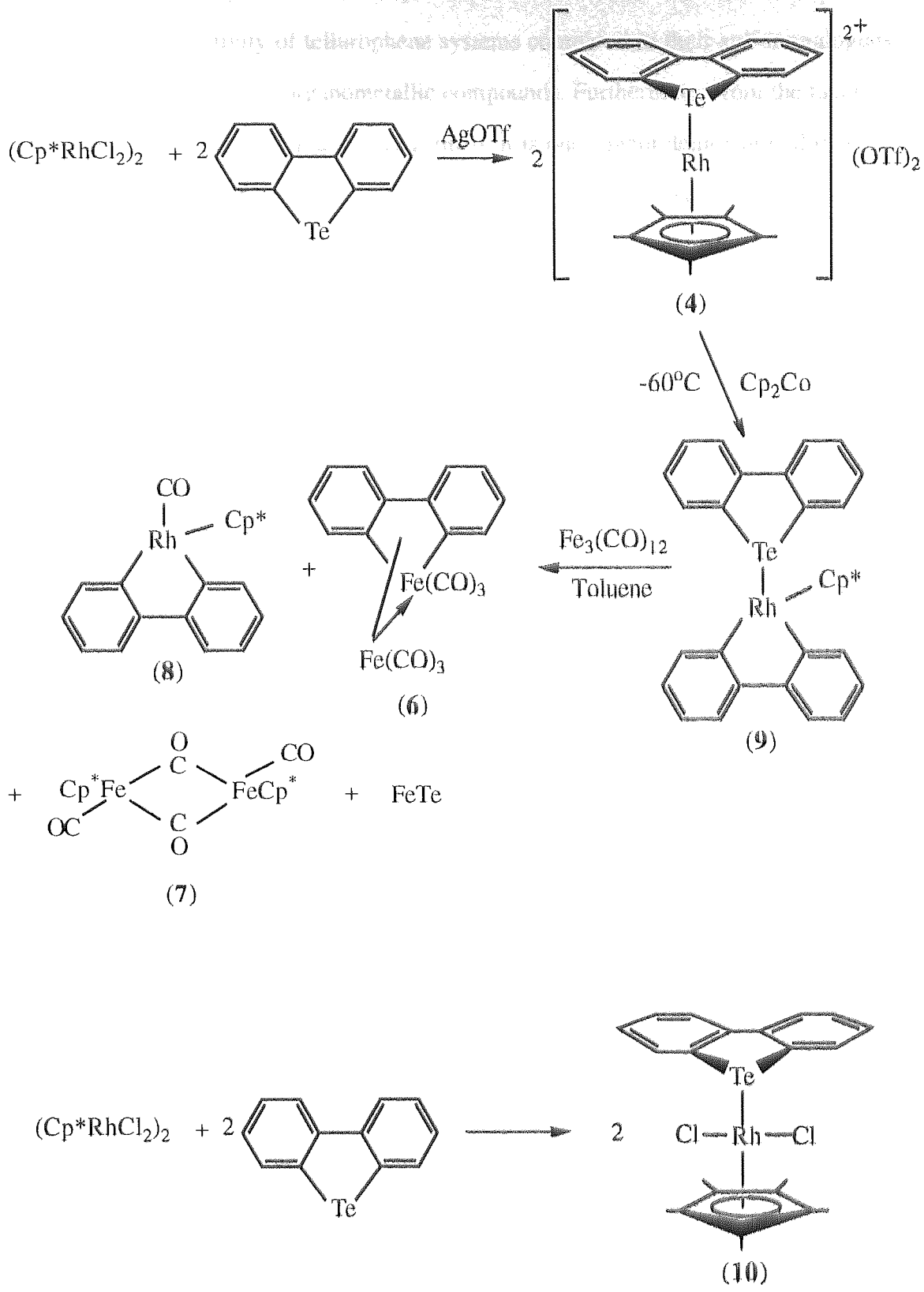

Scheme 5.3 Reactions of dibenzotellurophene with $[Cp^*RhCl_2]_2$

Further mechanistic speculation is not justified, however, what has been established is that the greater reactivity of tellurophene systems compared to their sulfur analogues provide pathways to novel organometallic compounds. Furthermore, from the fact that compounds of the type (**6**) and (**8**) are formed, it is once again demonstrated that the removal of a group 16 heteroatom from condensed systems, using organometallic reagents, is *mechanistically feasible*. Thus the initial step is the activation of the heterocycle by the rhodium, with further reaction with iron carbonyl being required to achieve complete detelluration. The fate of the removed tellurium is not certain, but ESCA analysis does show the presence of Fe and Te in the reaction residue. Rh and Co are also observed to be present in the residue.

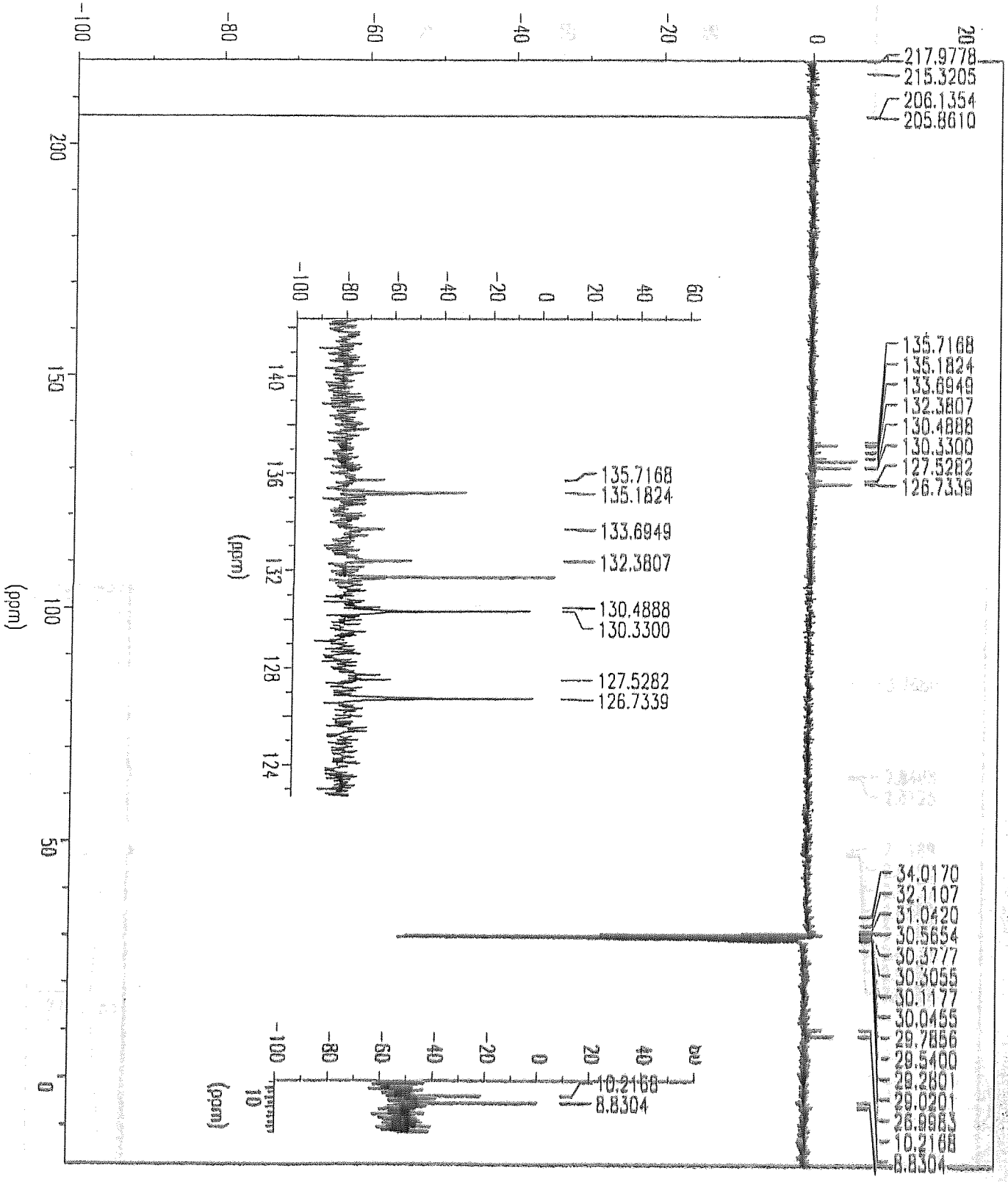

Figure 5.6 ^{13}C NMR spectrum of $[Cp^*Rh(C_{12}H_8Te)](OTf)_2$ (4)

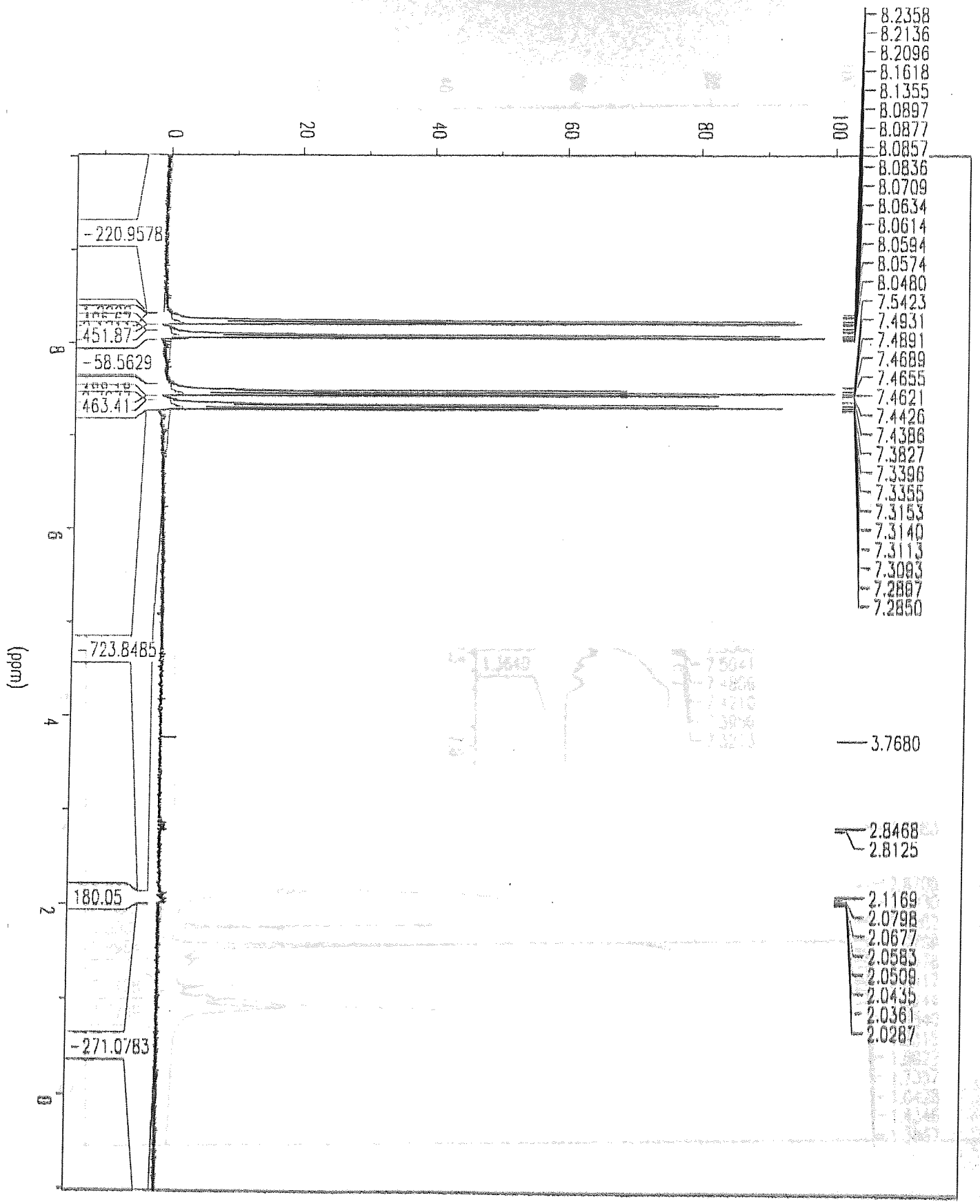

Figure 5.7 ^{1}H NMR spectrum of dibenzotellurophene

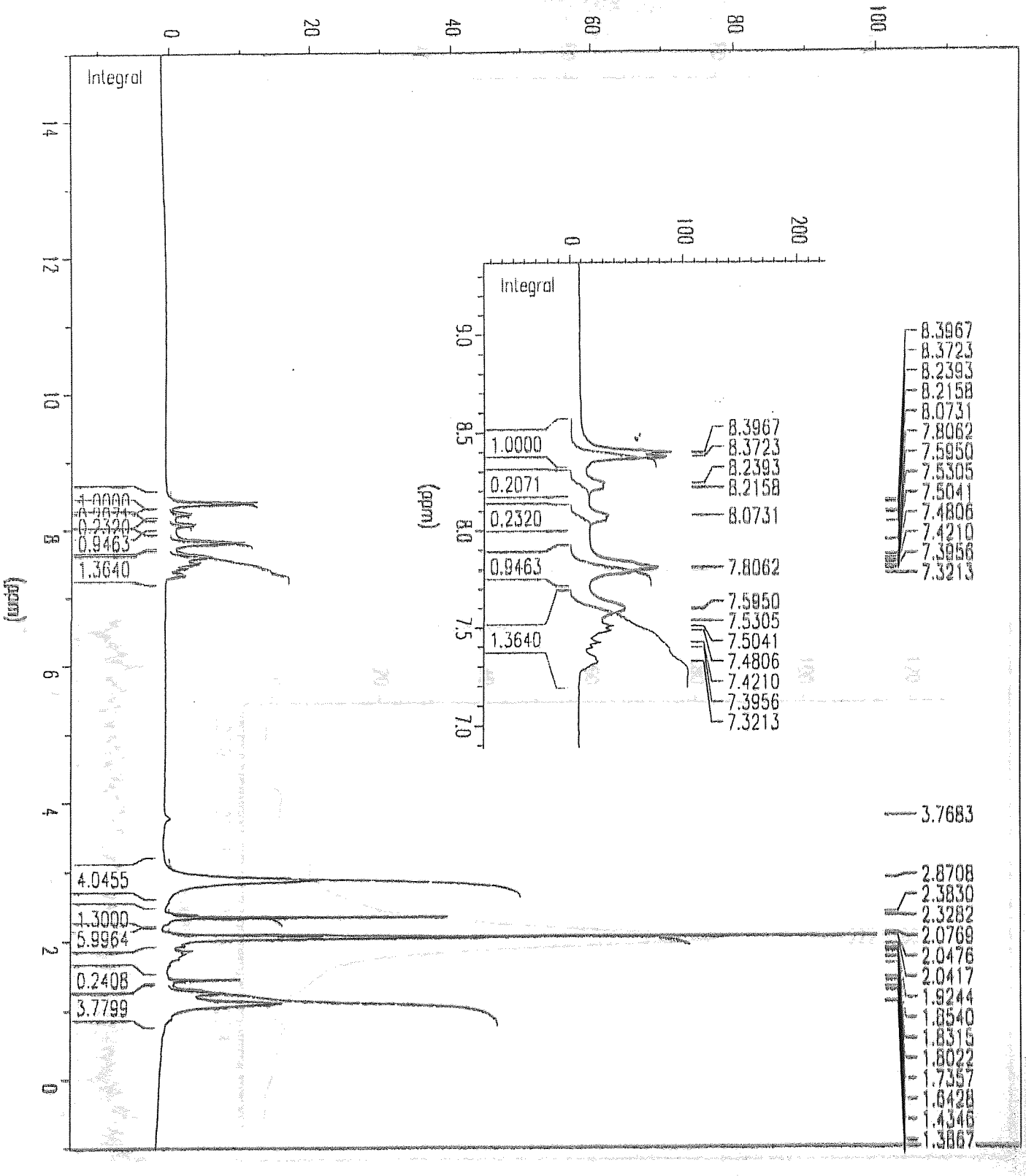

Figure 5.8 ^{1}H NMR spectrum of $[Cp^{*}Rh(C_{12}H_{8}Te)](OTf)_{2}$ (4)

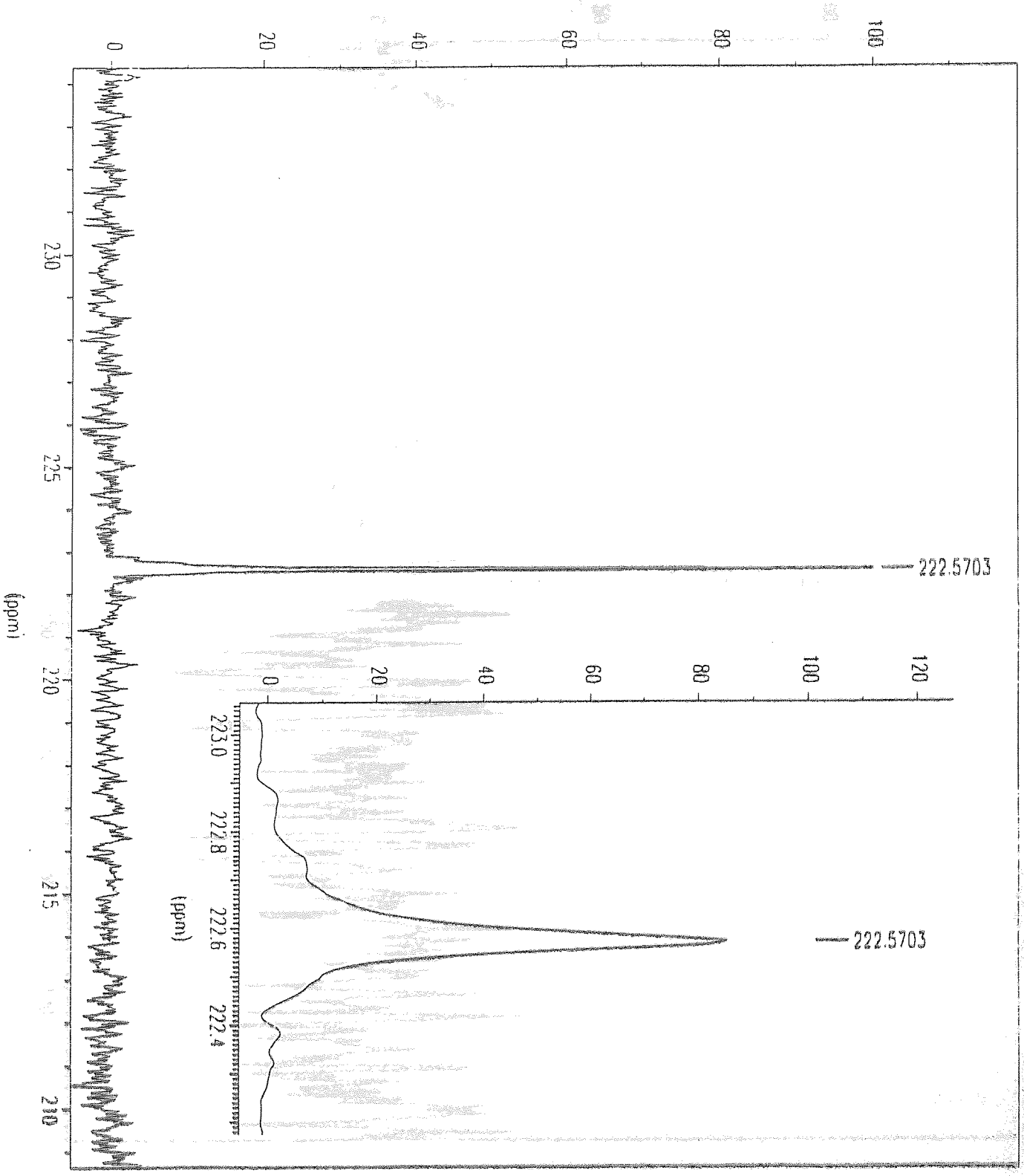

Figure 5.9 Proton decoupled ^{125}Te NMR spectrum of dibenzotellurophene

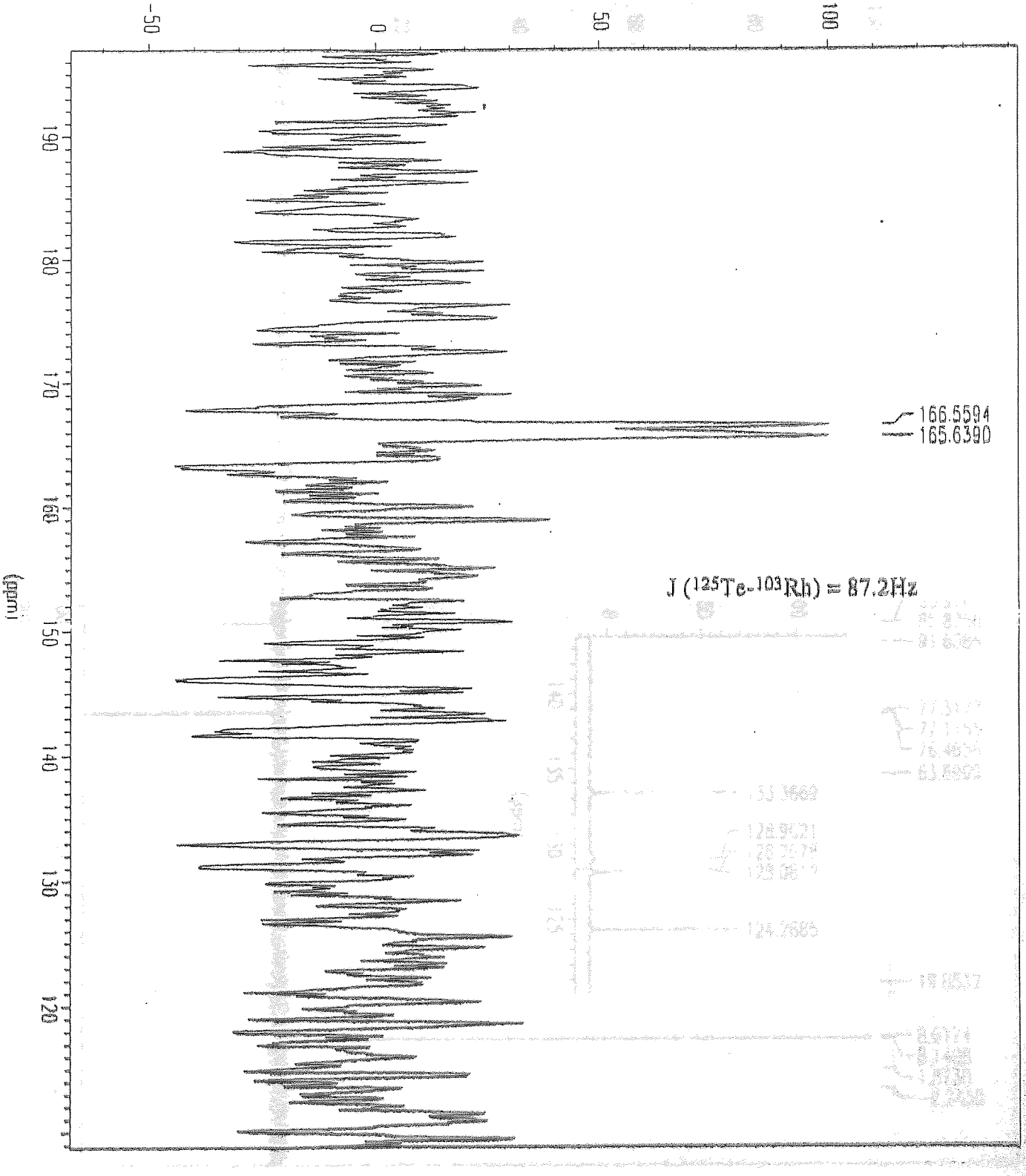

Figure 5.10 ^{125}Te NMR spectrum of $[Cp^*Rh(C_{12}H_8Te)](OTf)_2$ (4)

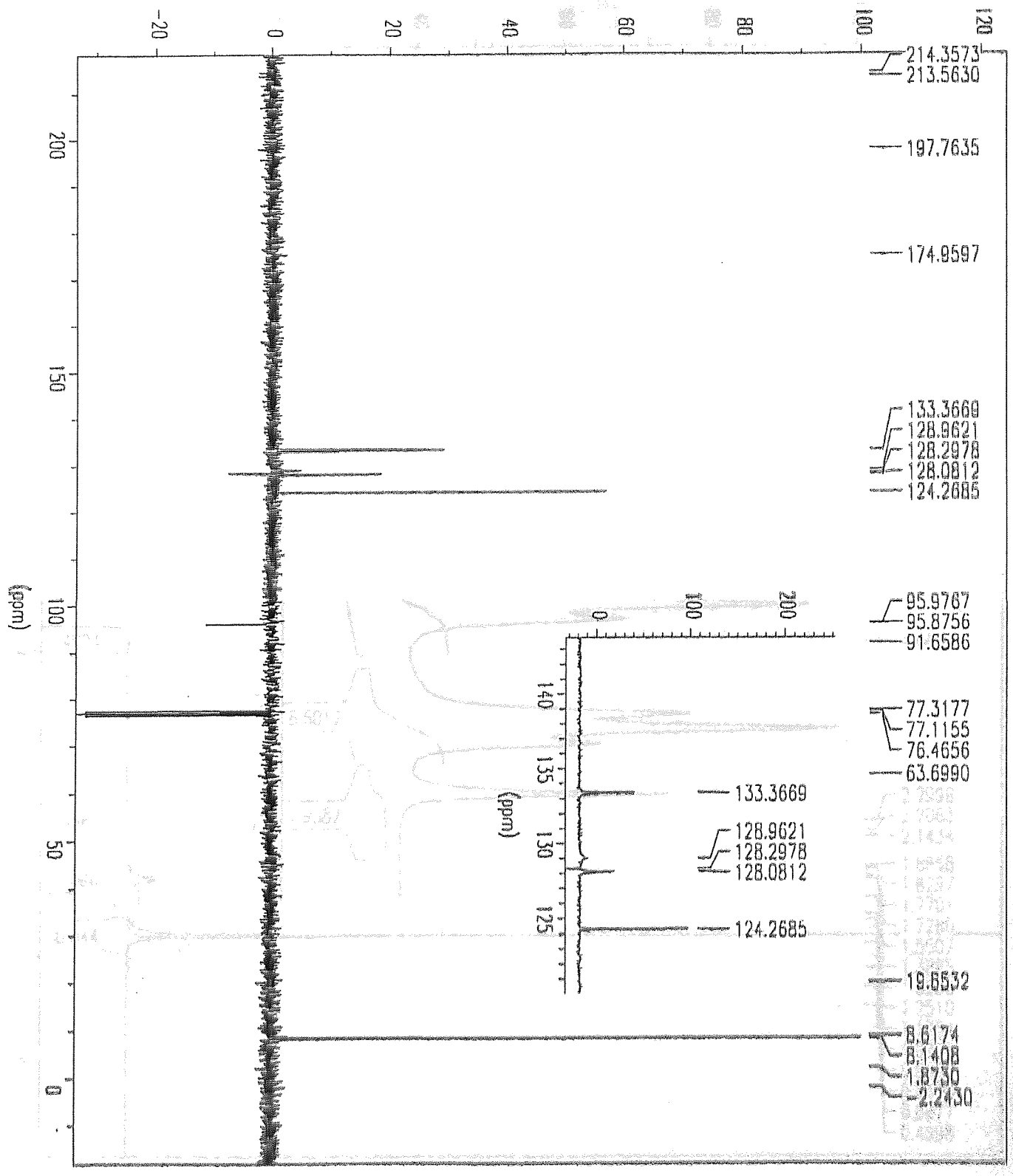

Figure 5.12 ^{13}C NMR spectrum of $[Cp^*RhCl_2(\eta^1\text{-}C_{12}H_8Te)]$ (10)

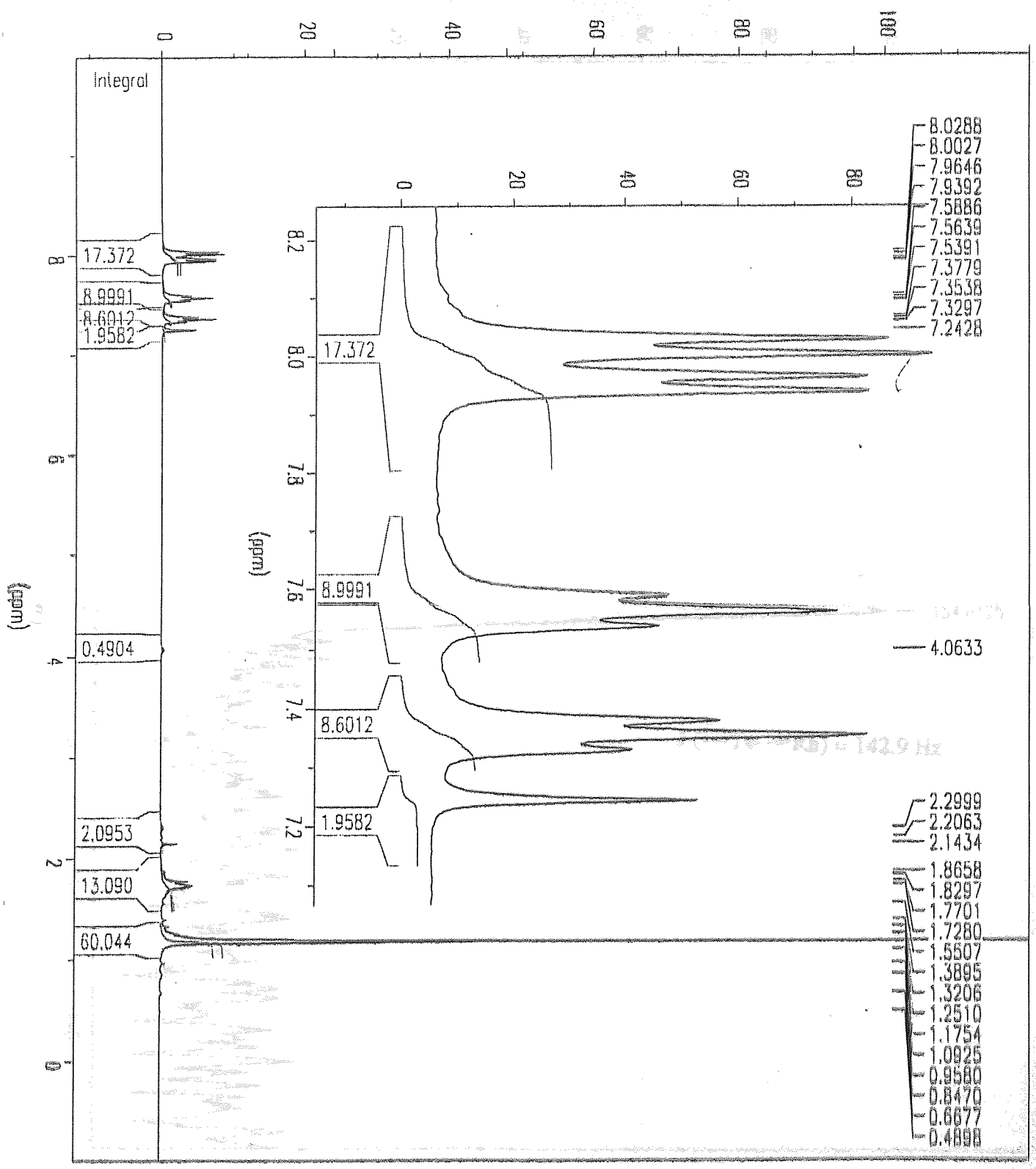

Figure 5.13 ^{1}H NMR spectrum of $[Cp^{*}RhCl_2(\eta^1\text{-}C_{12}H_8Te)]$ (10)

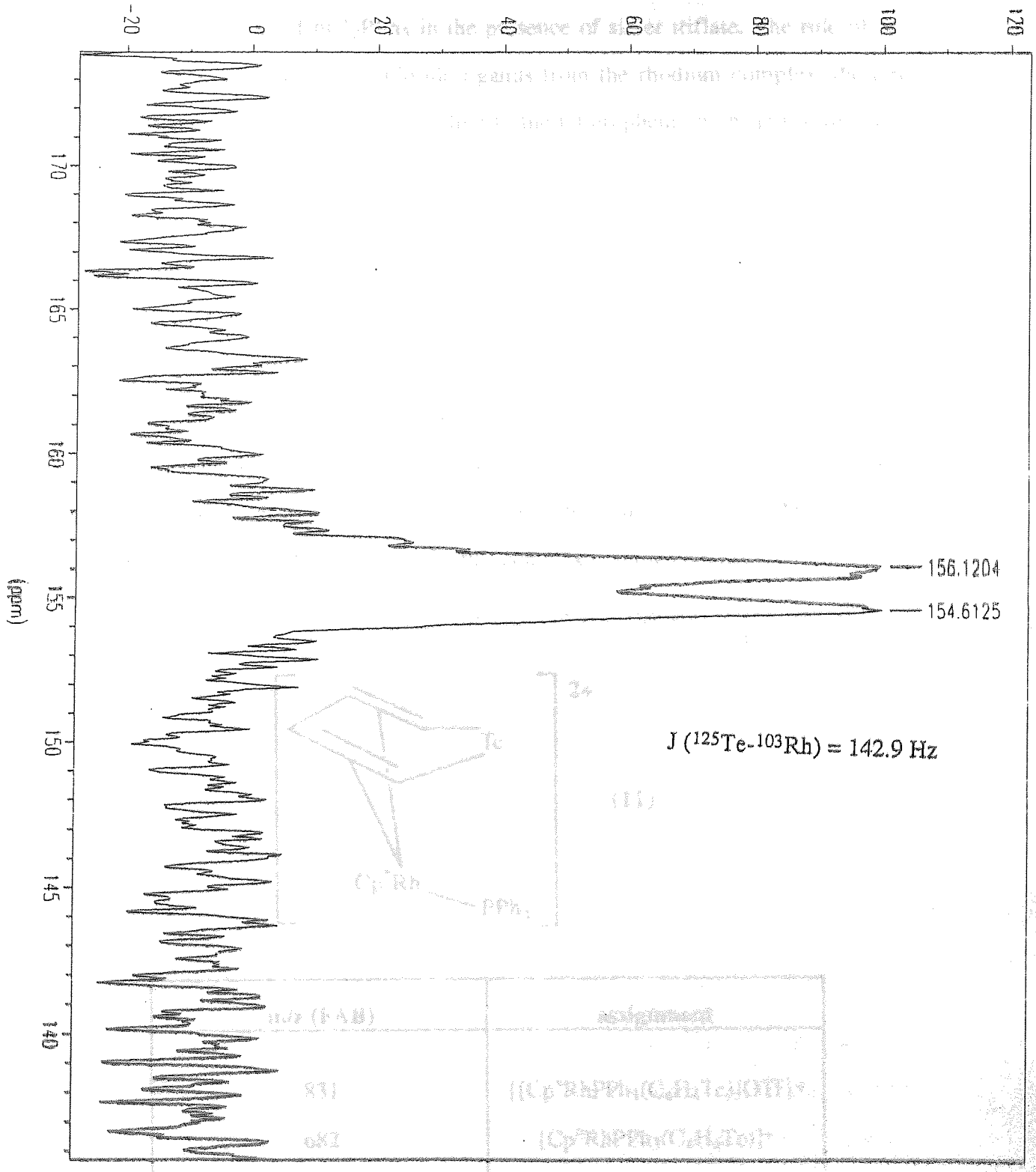

Figure 5.14 ^{125}Te NMR spectrum of $[Cp^*RhCl_2(\eta^1\text{-}C_{12}H_8Te)]$ (10)

5.3.9 Synthesis of $[Cp^*RhPPh_3(\eta^4\text{-}C_4H_4Te)](OTf)_2$

The synthesis of $[Cp^*RhPPh_3(C_4H_4Te)](OTf)_2$ (**11**) was achieved by reacting tellurophene with $Cp^*RhCl_2PPh_3$ in the presence of silver triflate. The role of the silver salt was to remove the chloride ligands from the rhodium complex, thereby freeing two coordination sites for binding to the tellurophene in an η^4 fashion. The final yield of the product was 34%. The infrared spectrum showed intense absorptions at 1264 and 1224 cm^{-1} arising from the presence of the triflate anion in the complex. Further evidence for the suggested formula of the complex was provided by mass spectrometry (Table 5.19) and ^{13}C and ^{1}H NMR spectroscopy (Tables 5.20 and 5.21 respectively). The presence of an η^4-linkage of the tellurophene ligand to the rhodium however, was not confirmed due to the low solubility of the complex in all suitable solvents making it difficult to produce crystals for X-ray diffraction experiments. For the same reason, despite several attempts, suitable data for ^{125}Te NMR was not obtained. The proposed η^4 structure for this complex is shown below.

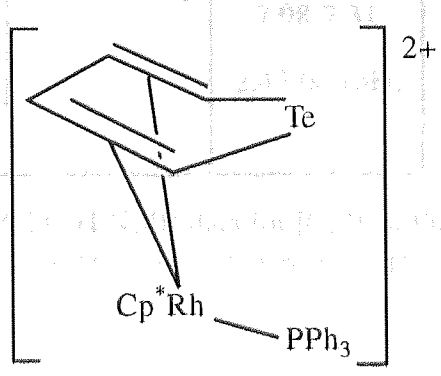

(11)

m/z (FAB)	assignment
831	$\{[Cp^*RhPPh_3(C_4H_4Te)]OTf\}^+$
682	$[Cp^*RhPPh_3(C_4H_4Te)]^+$
500	$[Cp^*RhPPh_3]^+$

Table 5.19 FAB-MS (NOBA matrix) peaks for $[Cp^*RhPPh_3(C_4H_4Te)](OTf)_2$

compound	^{13}C δ, ppm (CD_3OCD_3)	assignment
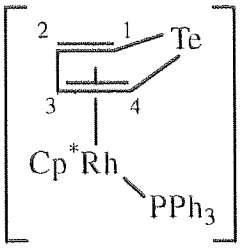 $(OSO_2CF_3^-)_2$	135.2-128.9	Ph
	114.4 (-23.5)	C2, C3
	112.1 (-14.5)	C1, C4
	102.0	Cp^*
	9.67	Cp^* (CH_3)

Table 5.20 ^{13}C NMR data for $[Cp^*RhPPh_3(C_4H_4Te)](OTf)_2$
Figures in parenthesis indicate upfield shift from parent tellurophene

compound	^1H δ, ppm (CD_3OCD_3)	Δδ, ppm	assignment
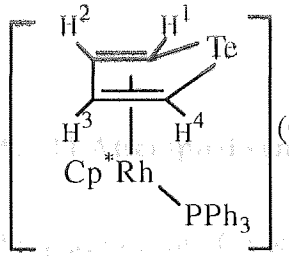 $(OSO_2CF_3^-)_2$	8.35 (q, 2H)	-0.68	H1, H4
	8.24 (q, 2H)	+0.28	H2, H3
	7.98-7.31		Ph
	2.43 (s, 15H)		Cp^* (CH_3)

Table 5.21 ^1H NMR data for $[Cp^*RhPPh_3(C_4H_4Te)](OTf)_2$
Δδ represents shift from parent tellurophene; - = upfield shift, + = downfield shift

Evidence for complexation of tellurophene to $[Cp^*RhPPh_3]^{2+}$ is provided by both the ^{13}C (Figure 5.15) and ^1H NMR spectra for the complex. The ^{13}C spectrum displays significant upfield coordination shifts for the ligand carbons. The large upfield shifts can be attributed to extensive backbonding from the metal, enhancing the electron density on the ligand carbon nuclei. The proposed mode of binding of tellurophene to rhodium is η^4 since one coordination site on the metal is occupied by the PPh_3 group therefore eliminating the need for bonding with the tellurium atom.

5.3.10 Attempted synthesis of $[Cp^*Rh(diphos)(\eta^4\text{-}C_4H_4Te)](BF_4)_2$

The synthesis of $[Cp^*Rh(diphos)(\eta^4\text{-}C_4H_4Te)](BF_4)_2$ was attempted by treating $Cp^*Rh(diphos)Cl_2$ with tellurophene in the presence of $AgBF_4$. The silver salt was expected to remove the chloride ligands from the rhodium complex to free two coordination sites making the rhodium available for η^4-complexation to tellurophene. Although a silver chloride precipitate was recovered from this reaction it is apparent by observation of NMR spectra of the orange solid product that tellurophene did not complex with the resultant rhodium species. The infrared spectrum of the orange solid showed the presence of the BF_4^- anion (intense absorption at 1097, 1088 and 1057 cm^{-1}) but peaks due to complexed tellurophene were absent. The remainder of the peaks did not coincide with starting materials, hence a reaction appears to have occurred, possibly dimerisation of $[Cp^*Rh(diphos)]^{2+}$ generated by the removal of the chlorides. Mass spectral data proved inconclusive as to the true identity of this product.

5.3.11 Attempted synthesis of $[Cp^*Rh(diphos)(\eta^2\text{-}C_4H_4Te)](BF_4)(PF_6)$

Preparation of $[Cp^*Rh(diphos)(\eta^2\text{-}C_4H_4Te)](BF_4)(PF_6)$ was attempted by treating $[Cp^*Rh(diphos)Cl]PF_6$ with tellurophene in the presence of $AgBF_4$. Removal of a single chloride ligand from the rhodium was expected, thereby providing a coordination site for complexation with tellurophene in an η^2 fashion. Small traces of AgCl precipitate were formed during the reaction but no evidence of complexed tellurophene was apparent in the final product. The infrared spectrum of the yellow solid that was obtained indicated a mixture of starting materials hence no reaction had occurred.

It therefore appears that the presence of the diphos group (bidentate $(PPh_2CH_2)_2$) in the initial complex suppresses the ability of the rhodium to coordinate with the heterocyclic ligand.

5.3.12 Reaction of 2-telluraindane with $[Cp^*RhCl_2]_2$ in the presence of AgOTf

The aim here was to investigate the reactivity of a heterocycle towards the rhodium complex in which the tellurium is in a non-aromatic environment. Thus 2-telluraindane was reacted with the $[Cp^*RhCl_2]_2$ dimer in the presence of silver triflate. A complex of formula $[Cp^*Rh(C_8H_8Te)](OTf)_2$ (**12**) was formed as an orange solid in 47% yield. The infrared spectrum showed intense absorptions at 1275 and 1262 cm^{-1} confirming the presence of the triflate anion. Further evidence for the proposed formula is provided by mass spectrometry (Table 5.22) and NMR spectroscopy (Tables 5.23-5.25). The mode of coordination of the heterocycle to rhodium, however, is not certain, although a strong interaction between the rhodium and tellurium atoms is indicated by the NMR data.

m/z (FAB)	assignment
621	$[Cp^*Rh(C_8H_8Te)](OTf)^+$
472	$[Cp^*Rh(C_8H_8Te)]^+$
387	$[Cp^*Rh](OTf)^+$

Table 5.22 FAB-MS (NOBA matrix) peaks for $[Cp^*Rh(C_8H_8Te)](OTf)_2$

compound	^{13}C δ, ppm ($CDCl_3$)	Δδ, ppm	assignment
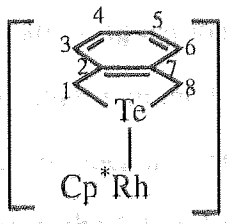 2+	140.2	-3.6	C2,C7
	128.5	+0.8	C4,C5
	128.2	+2.4	C3,C6
	20.92	+11.5	C1,C8
	9.97		$Cp^*(CH_3)$

Table 5.23 ^{13}C NMR data for $[Cp^*Rh(C_8H_8Te)](OTf)_2$
Δδ represents shift from parent 2-telluraindane; - = upfield shift, + = downfield shift

compound	^{1}H δ, ppm ($CDCl_3$)	Δδ, ppm	assignment
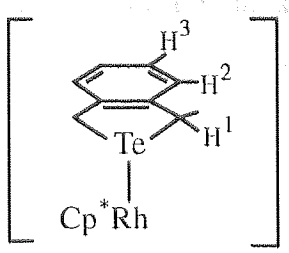	7.16 (m, 2H)	-0.09	H3
	7.14 (m, 2H)	-0.03	H2
	4.37 (q, 4H) J_{AB} = 16.0 Hz	+0.03	H1
	1.60 (s, 15H)		Cp* (CH_3)

Table 5.24 ^{1}H NMR data for $[Cp^*Rh(C_8H_8Te)](OTf)_2$
Δδ represents shift from parent 2-telluraindane; - = upfield shift, + = downfield shift

compound	^{125}Te δ, ppm (CD_3NO_2)	Δδ, ppm	J, Hz
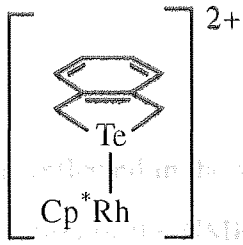	74.8	+260	(^{103}Rh, ^{125}Te) = 65.9

Table 5.25 ^{125}Te NMR data for $[Cp^*Rh(C_8H_8Te)](OTf)_2$
Δδ represents shift from parent 2-telluraindane; - = upfield shift, + = downfield shift

The ^{13}C NMR spectrum of $[Cp^*Rh(C_8H_8Te)](OTf)_2$, displays absorption peaks due to the aromatic ring carbons, C2-C7, resonating close to those for the free heterocycle. This, together with the fact that no splitting of these carbons is observed suggests that the rhodium does not interact significantly with the aromatic part of the heterocycle. In contrast, the C1 and C8 carbons adjacent to tellurium experience a more notable downfield shift indicating that it is the non-aromatic part of the ligand where interaction with rhodium exists.

The proton NMR spectrum (Figure 5.16) supports the idea that an η^1-coordination between rhodium and the tellurium heterocycle is present, as indicated by the AB quartet observed for the saturated ring protons. No fluxional behaviour about the pyramidal telluium is evident at room temperature.

The ^{125}Te signal is observed as a doublet arising from spin-spin coupling of the tellurium-rhodium nuclei. Furthermore, the size of the coupling constant (~75 Hz) appears to lie midway between those observed for η^5 (~20 Hz) and η^1 (~140 Hz) complexes of the aromatic tellurophenes (see Table 5.29). Also, in contrast to the tellurophene complexes, the tellurium in this complex is greatly *deshielded* relative to the free heterocycle. If an η^1 complex is invoked here, then this implies that the tellurium acts as a simple 2-electron donor (Lewis base), and therefore the Te nucleus experiences depleted electron density, with very little contribution of back-donation from the rhodium. This further implies that a weaker bond between rhodium and tellurium is formed compared with the analogous dibenzotellurophene η^1 complex, and this is reflected in the smaller value of the ^{125}Te-^{103}Rh coupling constant. Hence, by observation of the NMR spectra it is most likely that we have an η^1 complex, the structure of which is shown below (**12**).

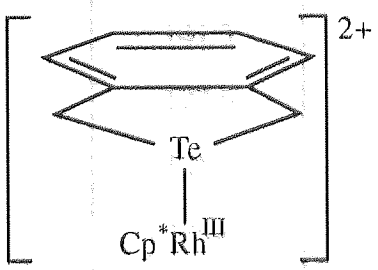

(**12**)

This structure, however, does not account for the full coordination requirements of the rhodium in the solid state although in solution further coordination with solvent molecules is likely to satisfy this deficiency.

5.3.13 Direct reaction of 2-telluraindane with $[Cp^*RhCl_2]_2$

The aim here was to produce an indisputable η^1-complex of the heterocycle which would arise by retaining the chloride ligands on the rhodium, thus limiting its capacity for coordination. A compound having the formula $Cp^*RhCl_2(C_8H_8Te)$ (**13**) was recovered as indicated by the mass spectrum (Table 5.26) but, disappointingly, no ^{125}Te spectrum of the complex could be obtained due to its very poor solubility in all solvents. The ^{13}C (Table 5.27) and ^1H NMR (Table 5.28) spectra, however, are very similar to those of compound (**12**) suggesting that the heterocycle binds to the rhodium in a similar η^1 fashion.

m/z (FAB)	assignment
507	$[Cp^*RhCl(C_8H_8Te)]^+$
472	$[Cp^*Rh(C_8H_8Te)]^+$

Table 5.26 FAB-MS (NOBA matrix) peaks for $[Cp^*RhCl_2(C_8H_8Te)]$

compound	^{13}C δ, ppm ($CDCl_3$)	Δδ, ppm	assignment
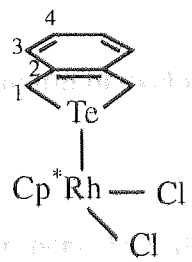	141.3	-2.5	C2
	127.6	0	C4
	126.7	+0.9	C3
	96.2		Cp^*
	21.63	+12.2	C1
	9.47		$Cp^*(CH_3)$

Table 5.27 ^{13}C NMR data for $[Cp^*RhCl_2(C_8H_8Te)]$

Δδ represents shift from parent 2-telluraindane; - = upfield shift, + = downfield shift

compound	^{1}H δ, ppm ($CDCl_3$)	Δδ, ppm	assignment
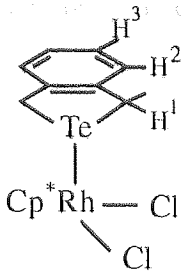	7.13 (m, 2H)	-0.09	H3
	7.03 (m, 2H)	-0.03	H2
	4.60 (4H) b.s at r. temp q at < 245 K J_{AB} = 13.4 Hz	+0.01	H1
	1.68 (s, 15H)		Cp^* (CH_3)

Table 5.28 ^{1}H NMR data for $[Cp^*RhCl_2(C_8H_8Te)]$

Δδ represents shift from parent 2-telluraindane; - = upfield shift, + = downfield shift

In the ^{13}C NMR spectrum of $[Cp^*RhCl_2(C_8H_8Te)]$, the carbons adjacent to the tellurium are significantly deshielded relative to the free heterocycle, whilst the aromatic carbons experience little variation on complexation. This is consistent with the η^1 formulation as previously suggested for complex (**12**). The proton NMR spectrum of (**13**) at room temperature (Figure 5.18) displays a broad singlet for the saturated ring protons, which resolve into an AB quartet at temperatures below 245 K. This indicates fluxional behaviour about the pyramidal tellurium at room temperature, and is in contrast to the behaviour observed for complex (**12**).

5.3.14 Reaction of cyclotelluropentane with $[Cp^*RhCl_2]_2$ in the presence of AgOTf

Cyclotelluropentane, C_4H_8Te, is a saturated five-membered heterocycle and therefore in contrast to the previously studied heterocycles it has no capacity for forming π-complexes with metals. It is expected to be a better Lewis base than the aromatic heterocycles since the lone pairs on the tellurium are not delocalised, hence any complexation that occurs must involve simple σ-coordination. The product obtained from this reaction, however, showed that no complexation had occurred and only starting materials were recovered.

5.3.15 Direct reaction of cyclotelluropentane with $[Cp^*RhCl_2]_2$

By reacting cyclotelluropentane directly with $[Cp^*RhCl_2]_2$ it was thought that the complex, $Cp^*RhCl_2(\eta^1\text{-}C_4H_4Te)$ would be produced, since analogous compounds had been prepared previously using a similar procedure. However, on examination of the recovered product, it was found that only a mixture of starting materials was obtained.

This is a rather surprising result considering that cyclotelluropentane is expected to be a good Lewis base, and therefore should more readily complex with rhodium than the previously studied systems. In fact, it implies that the presence of a π-system within the heterocycle, encourages its complexation to the rhodium.

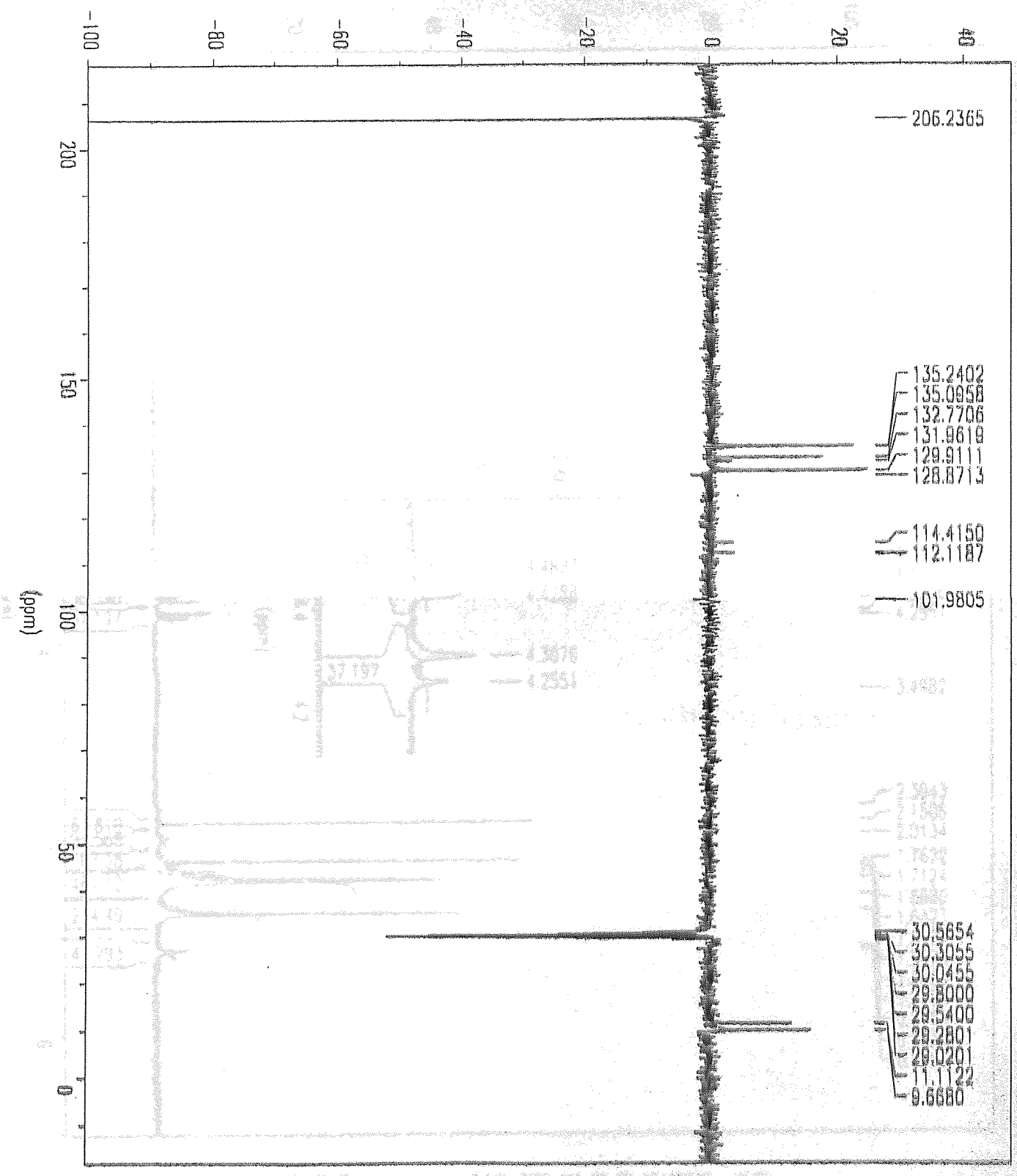

Figure 5.15 ^{13}C NMR spectrum of $[Cp^*RhPPh_3(C_4H_4Te)](OTf)_2$ (11)

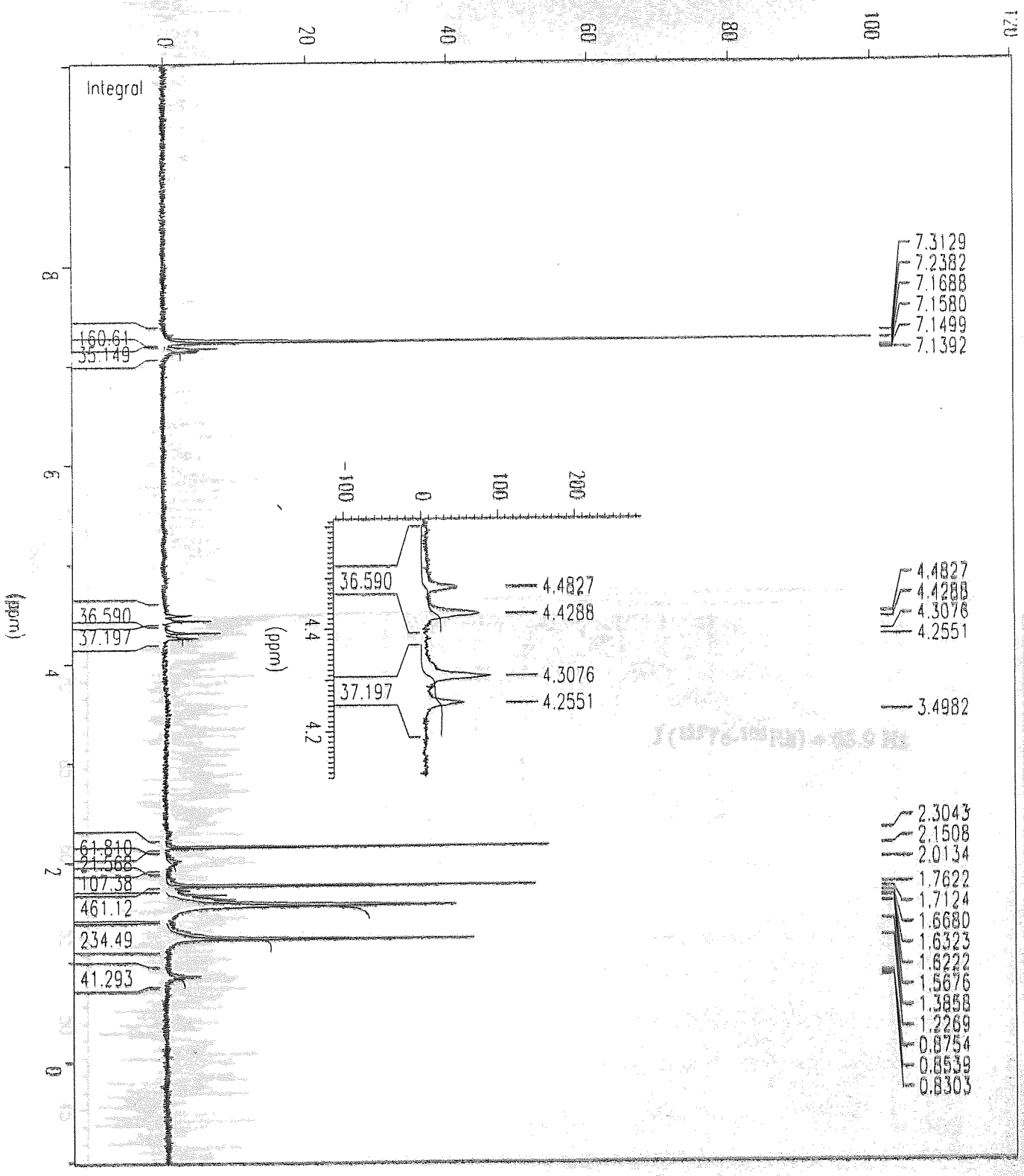

Figure 5.16 ^{1}H NMR spectrum of $[Cp^{*}Rh(C_8H_8Te)](OTf)_2$ **(12)**

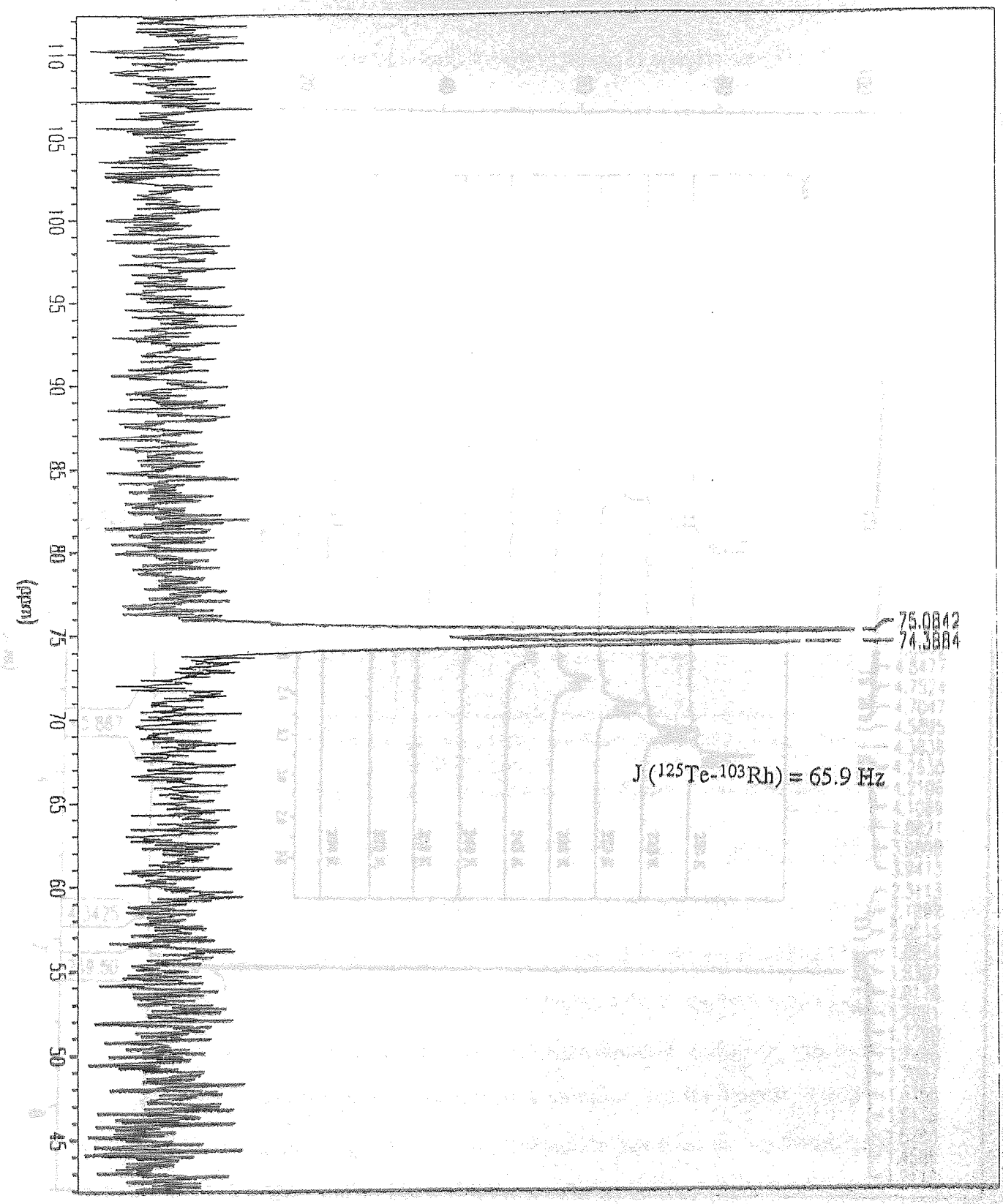

Figure 5.17 ^{125}Te NMR spectrum of $[Cp^*Rh(C_8H_8Te)](OTf)_2$ (12)

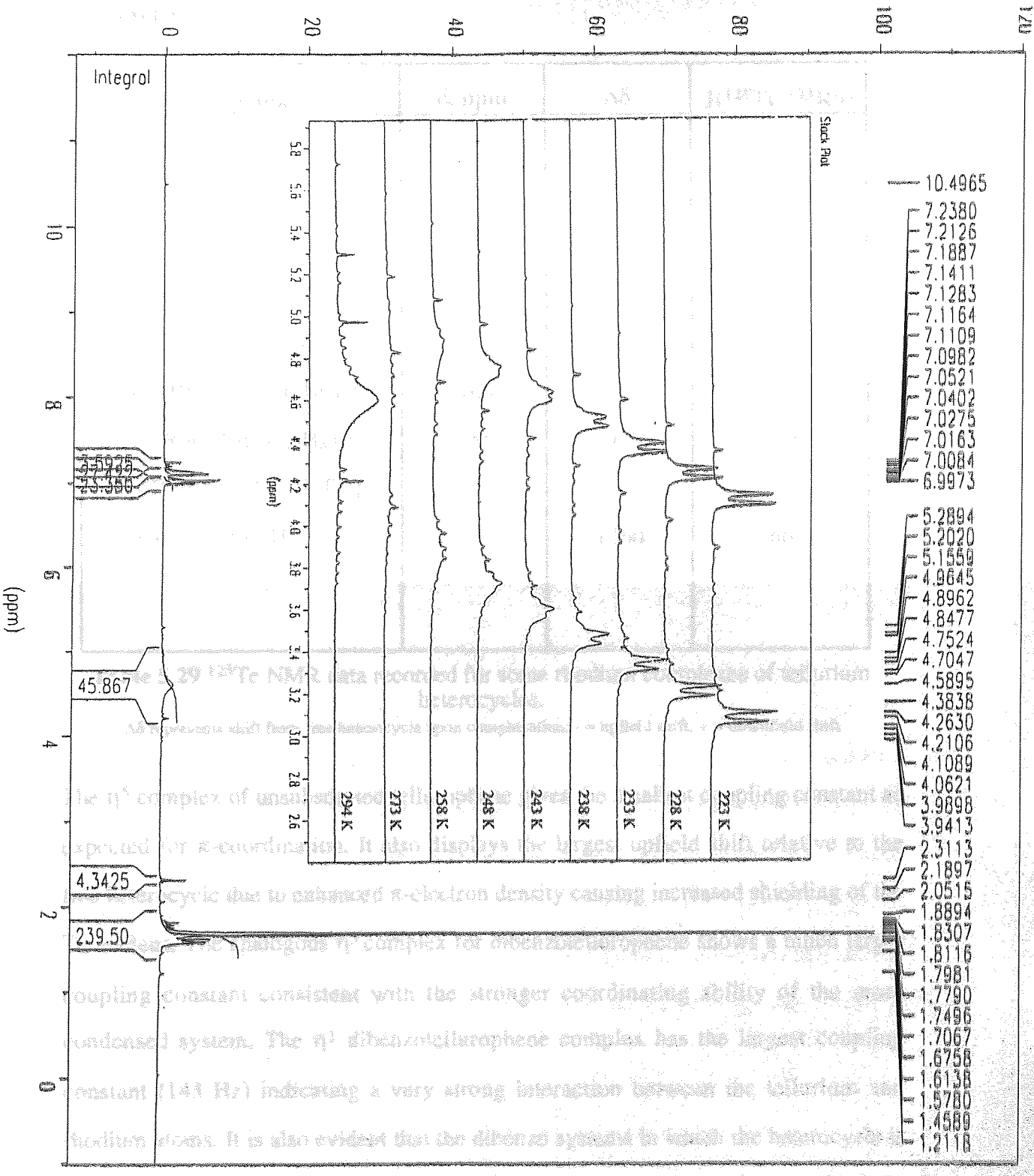

Figure 5.18 ^{1}H NMR spectrum of $[Cp^*RhCl_2(C_8H_8Te)]$ (13)

Inset shows temperature dependence of ^{1}H NMR signal for saturated ring protons

5.3.16 Summary of ^{125}Te NMR data for rhodium complexes of tellurium heterocycles

Table 5.29 summarises the data collected for some rhodium complexes of tellurium heterocycles.

compound	δ, ppm	Δδ	J(^{125}Te-^{103}Rh)
Free C_4H_4Te	325	-	-
Free $C_{12}H_8Te$	220	-	-
Free C_8H_8Te[92]	-185	-	-
$[Cp^*Rh(\eta^5\text{-}C_4H_4Te)]^{2+}$	121	-204	20
$[Cp^*Rh(\eta^5\text{-}C_{12}H_8Te)]^{2+}$	166	-54	87
$Cp^*RhCl2(\eta^1\text{-}C_{12}H_8Te)$	155	-67	143
$[Cp^*RhPPh_3(\eta^4\text{-}C_4H_4Te)]^{2+}$	-	-	-
$[Cp^*Rh(\eta^1\text{-}C_8H_8Te)]^{2+}$	75	+260	66

Table 5.29 ^{125}Te NMR data recorded for some rhodium complexes of tellurium heterocycles.

Δδ represents shift from free heterocycle upon complexation; - = upfield shift, + = downfield shift

The η^5 complex of unsubstituted tellurophene gives the smallest coupling constant as expected for π-coordination. It also displays the largest upfield shift relative to the free heterocycle due to enhanced π-electron density causing increased shielding of the Te nucleus. The analogous η^5 complex for dibenzotellurophene shows a much larger coupling constant consistent with the stronger coordinating ability of the more condensed system. The η^1 dibenzotellurophene complex has the largest coupling constant (143 Hz) indicating a very strong interaction between the tellurium and rhodium atoms. It is also evident that the dibenzo systems in which the heterocycle is bonded predominantly through the tellurium experience much smaller upfield shifts upon complexation compared to analogous unsubstituted tellurophene complexes.

Although no data is available for the η^4 complex of tellurophene it is fully expected that its ^{125}Te signal will not be split by coupling with rhodium since the tellurium is bent out of the plane of the heterocycle away from the metal.

Similar results have been observed by Angelici[64,65] for selenophene complexes who has demonstrated that η^5 compounds absorb further upfield than η^1 compounds with the free selenophenes absorbing furthest downfield. However, the use of coupling constants for studying binding modes has not been previously reported.

In contrast to complexes of the aromatic heterocycles, 2-telluraindane in which the tellurium is in a non-aromatic environment, gives a ^{125}Te NMR signal on complexation, which is *downfield* relative to that of the free heterocycle. Furthermore, the coupling constant of this η^1 complex is roughly half the value of η^1-dibenzotellurophene. This suggests a weaker coordination for the saturated system arising from lesser back-donation from rhodium to tellurium.

These results demonstrate that ^{125}Te NMR provides a valuable tool for studying the nature of bonding between tellurium heterocycles and rhodium. Hence, by observations of both the coupling constants and coordination shifts it should be possible to predict the types of interactions present particularly in instances where X-ray crystallography is not available. This could be further used to establish the modes of binding of tellurophene adsorbed on HDS catalysts thereby providing some mechanistic insight into the process of HDS. It should be noted however, that factors such as the charge of the complex as well as the presence of other ligands will have some influence on the NMR parameters.

5.4 X-RAY CRYSTALLOGRAPHY

The crystal structures of compounds (**8**), (**9**) and (**10**) were established and the crystal parameters are included in Table 5.30.

Data for all three structures were collected on a Rigaku R-Axis II area-detector diffractometer at 293(2)K using graphite monochromated MoKa radiation, λ = 0.71069 Å. For (**8**), (**9**) and (**10**) respectively, sixty 3°, thirty-six 5° and thirty 6° oscillation exposures were made with crystal to detector distances 80, 105, and 80 mm. Absorption corrections were not applied as the crystals were nearly equi-dimensional (see Table 5.30).

The structures were determined[99] by direct methods and refined[100] on F^2 by full-matrix least squares using anisotropic displacement parameters for the non-hydrogen atoms. H atoms were placed in calculated positions with isotropic displacement parameters. ORTEP[113] plots of the complexes (**8**), (**9**) and (**10**) are shown in Figures 5.19-5.22. Atomic coordinates are listed in Tables 5.31-5.33 and selected bond lengths and angles are in Tables 5.34 - 5.38.

	(8)	(9)	(10)
Molecular formula	$C_{23}H_{23}ORh$	$C_{34}H_{31}RhTe$	$C_{22}H_{23}Cl_2RhTe$
Molecular weight	418.3	670.1	588.8
Crystal system	orthorhombic	monoclinic	monoclinic
Space group	Pbca	$P2_1/n$	$P2_1/n$
Cell constants			
(Å) a	16.437(2)	14.891(6)	10.296(2)
b	14.741(2)	20.451(9)	15.660(5)
c	31.450(4)	9.488(4)	13.755(4)
(°) β	-	108.57(1)	102.20(2)
Cell Volume (Å^3)	7620(2)	2739(2)	216.7(10)
Density (g cm-3)	1.459	1.625	1.804
Z	16	4	4
$\mu(MoK_\alpha)$ mm^{-1}	0.903	1.688	2.357
crystal size, mm	0.5 x 0.3 x 0.25	0.25 x 0.2 x 0.2	0.2 x 0.15 x 0.1
hkl range	+/-16, +/-14, -27,31	-16,17, +/-24, +/-11	+/-12, +/-18, +/-16
Data collection			
Angular range (°)	2-21	2-25	2-25
Unique reflns [I>σ(I)]	3768	4744	3842
variables	451	325	235
Δ/σ (max)	0.004	0.001	0.009
Δρ, eÅ^{-3}	+0.31 to -0.32	+0.49 to -0.66	+0.52 to -0.63
R, wR[a]	0.0285, 0.0783	0.0487, 0.0908	0.0554, 0.0671
Observed reflns [I>σ(I)]	3657	4482	2818
R, wR[a] obs reflns	0.0257, 0.0770	0.0441, 0.0880	0.0313, 0.0582
w(a, b)[b]	0.041, 4.92	0.024, 8.35	0.018, 0.25

[a] $wR = [\Sigma w(Fo^2-Fc^2)^2/\Sigma w(Fo^2)^2]^{1/2}$

[b] $w = 1/[\sigma^2(Fo^2) + (aP)^2 + bP]$ where $P = (Fo^2 + 2Fc^2)/3$

Table 5.30 Crystal and experimental parameters for compounds (8), (9) and (10)

Atom	x	y	z
Rh(1)	6675(1)	3379(1)	9921(1)
Rh(2)	4093(1)	3311(1)	7447(1)
O(1)	5886(2)	5186(2)	9985(1)
O(31)	3438(2)	5130(2)	7216(1)
C(1)	6907(2)	1951(2)	9717(1)
C(2)	6133(2)	2211(2)	9546(1)
C(3)	5614(2)	2398(2)	9895(1)
C(4)	6062(2)	2244(2)	10280(1)
C(5)	6852(2)	1960(2)	10165(1)
C(6)	7626(3)	1646(3)	9461(2)
C(7)	5886(4)	2182(3)	9089(2)
C(8)	4733(3)	2658(4)	9864(3)
C(9)	5714(4)	2281(4)	10725(2)
C(10)	7505(3)	1638(3)	10466(2)
C(11)	7436(2)	3955(2)	9476(1)
C(12)	8168(2)	4309(2)	9632(1)
C(13)	8740(2)	4662(2)	9348(1)
C(14)	8579(3)	4680(3)	8920(1)
C(15)	7848(3)	4374(3)	8768(1)
C(16)	7285(2)	4014(2)	9044(1)
C(17)	7570(2)	3916(2)	10304(1)
C(18)	8238(2)	4299(2)	10096(1)
C(19)	8880(2)	4653(3)	10334(1)
C(20)	8870(2)	4631(3)	10767(1)
C(21)	8213(3)	4267(3)	10971(1)
C(22)	7564(2)	3919(2)	10747(1)
C(23)	6173(2)	4489(3)	9964(1)
C(31)	3896(2)	2132(2)	6992(1)
C(32)	3161(2)	2262(2)	7233(1)
C(33)	3339(2)	2114(2)	7670(1)
C(34)	4188(2)	1910(2)	7703(1)
C(35)	4523(2)	1901(2)	7285(1)
C(36)	3957(3)	2132(3)	6517(1)
C(37)	2334(2)	2455(3)	7052(2)
C(38)	2726(3)	2106(3)	8022(1)
C(39)	4627(3)	1621(3)	8098(1)
C(40)	5370(3)	1624(3)	7171(2)
C(41)	4403(2)	3917(2)	8016(1)
C(42)	5196(2)	4292(2)	8031(1)
C(43)	5477(2)	4670(3)	8408(1)
C(44)	4990(3)	4702(3)	8763(1)
C(45)	4211(3)	4366(3)	8746(1)
C(46)	3914(2)	3977(3)	8374(1)
C(47)	5197(2)	3860(2)	7296(1)
C(48)	5633(2)	4268(2)	7626(1)
C(49)	6405(3)	4621(3)	7545(1)
C(50)	6749(2)	4555(3)	7147(2)
C(51)	6326(2)	4165(3)	6819(1)
C(52)	5551(2)	3838(2)	6889(1)
C(53)	3660(2)	4427(3)	7297(1)

Table 5.31 Atomic coordinates (x 10^4) for complex (8)

Atom	x	y	z
Te(1)	1518(1)	2370(1)	1962(1)
Rh(1)	2881(1)	3082(1)	3425(1)
C(1)	1387(4)	1599(3)	3351(6)
C(2)	1043(4)	1654(3)	4562(7)
C(3)	982(5)	1103(4)	5341(8)
C(4)	1250(6)	501(4)	4951(8)
C(5)	1597(5)	446(3)	3759(8)
C(6)	1668(4)	1000(3)	2947(6)
C(7)	2037(4)	999(3)	1669(6)
C(8)	2354(4)	452(3)	1105(7)
C(9)	2694(5)	510(3)	-87(8)
C(10)	2718(5)	1109(3)	-743(7)
C(11)	2398(4)	1659(3)	-216(7)
C(12)	2062(3)	1603(3)	995(6)
C(13)	1783(3)	3567(2)	3834(6)
C(14)	1463(4)	3479(3)	5053(6)
C(15)	685(4)	3819(3)	5189(7)
C(16)	216(4)	4261(3)	4105(8)
C(17)	508(4)	4358(3)	2894(7)
C(18)	1280(3)	4013(2)	2731(6)
C(19)	1628(3)	4057(2)	1446(6)
C(20)	2396(3)	3644(2)	1537(6)
C(21)	2730(4)	3622(3)	328(6)
C(22)	2339(5)	4018(3)	-909(6)
C(23)	1612(5)	4439(3)	-949(7)
C(24)	1259(4)	4458(3)	213(7)
C(25)	3848(4)	2756(3)	5665(6)
C(26)	4031(3)	3419(3)	5396(6)
C(27)	4362(3)	3436(3)	4145(6)
C(28)	4367(4)	2783(3)	3622(6)
C(29)	4052(4)	2365(3)	4558(7)
C(30)	3601(5)	2503(4)	6984(8)
C(31)	3982(4)	3994(3)	6342(7)
C(32)	4711(4)	4029(3)	3561(8)
C(33)	4777(5)	2562(4)	2439(8)
C(34)	4033(5)	1637(3)	4502(10)

Table 5.32 Atomic coordinates (x 10^4) for complex (**9**)

Atom	x	y	z
Te(1)	3330(1)	2538(1)	1782(1)
Rh(1)	4668(1)	2456(1)	377(1)
Cl(1)	5642(1)	1279(1)	1430(1)
Cl(2)	5970(1)	3510(1)	1455(1)
C(1)	1869(4)	3496(3)	1514(3)
C(2)	2103(5)	4368(3)	1523(4)
C(3)	1045(6)	4919(4)	1422(5)
C(4)	-216(6)	4603(4)	1338(5)
C(5)	-481(5)	3750(4)	1318(4)
C(6)	585(4)	3158(3)	1399(3)
C(7)	1645(4)	1747(3)	1461(3)
C(8)	1626(5)	869(3)	1414(4)
C(9)	403(6)	446(4)	1307(4)
C(10)	-748(6)	921(5)	1256(5)
C(11)	-744(4)	1786(4)	1287(4)
C(12)	454(4)	2229(3)	1375(3)
C(13)	3114(4)	2565(3)	-950(3)
C(14)	4061(4)	3233(3)	-927(3)
C(15)	5322(5)	2837(3)	-956(3)
C(16)	5153(4)	1944(3)	-965(3)
C(17)	3783(4)	1760(3)	-943(3)
C(18)	1658(4)	2692(4)	-1011(4)
C(19)	3785(5)	4168(3)	-962(4)
C(20)	6582(5)	3315(4)	-957(4)
C(21)	6191(5)	1270(4)	-989(4)
C(22)	3142(5)	906(3)	-1004(4)

Table 5.33 Atomic coordinates (x 10^4) for complex (**10**)

Rh(1)-C(23)	1.837(4)	C(4)-C(5)	1.412(5)
Rh(1)-C(17)	2.059(3)	C(4)-C(9)	1.511(6)
Rh(1)-C(11)	2.059(3)	C(5)-C(10)	1.508(6)
Rh(1)-C(1)	2.232(3)	C(11)-C(16)	1.382(5)
Rh(1)-C(5)	2.248(4)	C(11)-C(12)	1.401(4)
Rh(1)-C(4)	2.256(3)	C(12)-C(13)	1.394(5)
Rh(1)-C(3)	2.266(4)	C(12)-C(18)	1.464(5)
Rh(1)-C(2)	2.270(3)	C(13)-C(14)	1.375(5)
O(1)-C(23)	1.132(4)	C(14)-C(15)	1.370(5)
C(1)-C(5)	1.410(5)	C(15)-C(16)	1.378(5)
C(1)-C(2)	1.434(5)	C(17)-C(22)	1.394(5)
C(1)-C(6)	1.500(5)	C(17)-C(18)	1.397(5)
C(2)-C(3)	1.417(5)	C(18)-C(19)	1.395(5)
C(2)-C(7)	1.493(6)	C(19)-C(20)	1.362(5)
C(3)-C(4)	1.436(5)	C(20)-C(21)	1.366(6)
C(3)-C(8)	1.502(6)	C(21)-C(22)	1.379(5)
O(1)-C(23)-Rh(1)	177.8(3)	C(1)-C(2)-C(3)	107.0(3)
Rh(1)-C(11)-C(12)	116.0(2)	C(3)-C(4)-C(5)	107.5(3)
Rh(1)-C(17)-C(18)	116.3(2)	C(1)-C(2)-C(7)	126.6(4)
C(11)-C(12)-C(18)	114.3(3)	C(1)-Rh(1)-C(11)	95.2(1)
C(12)-C(18)-C(17)	114.2(3)	C(5)-Rh(1)-C(17)	93.8(1)
C(12)-C(11)-C(16)	118.3(3)	C(1)-Rh(1)-C(23)	159.6(2)
C(18)-C(17)-C(22)	118.2(3)	C(5)-Rh(1)-C(23)	149.5(2)
C(17)-C(18)-C(19)	119.6(3)	C(6)-C(1)-Rh(1)	124.9(2)
C(11)-C(12)-C(13)	119.7(3)	C(10)-C(5)-Rh(1)	126.8(3)

Table 5.34 Bond lengths (Å) and selected angles (°) for complex (8) (structure a)

Rh(2)-C(53)	1.853(4)	C(34)-C(35)	1.425(5)
Rh(2)-C(47)	2.045(3)	C(34)-C(39)	1.501(5)
Rh(2)-C(41)	2.064(3)	C(35)-C(40)	1.494(5)
Rh(2)-C(34)	2.221(4)	C(41)-C(46)	1.386(5)
Rh(2)-C(35)	2.255(3)	C(41)-C(42)	1.415(5)
Rh(2)-C(33)	2.268(3)	C(42)-C(43)	1.390(5)
Rh(2)-C(31)	2.274(3)	C(42)-C(48)	1.463(5)
Rh(2)-C(32)	2.279(3)	C(43)-C(44)	1.374(6)
O(31)-C(53)	1.128(4)	C(44)-C(45)	1.374(6)
C(31)-C(35)	1.423(5)	C(45)-C(46)	1.392(5)
C(31)-C(32)	1.437(5)	C(47)-C(52)	1.396(5)
C(31)-C(36)	1.499(5)	C(47)-C(48)	1.406(5)
C(32)-C(33)	1.421(5)	C(48)-C(49)	1.396(6)
C(32)-C(37)	1.501(5)	C(49)-C(50)	1.376(6)
C(33)-C(34)	1.431(5)	C(50)-C(51)	1.370(6)
C(33)-C(38)	1.497(5)	C(51)-C(52)	1.379(5)
O(31)-C(53)-Rh(2)	175.7(3)	C(32)-C(33)-C(34)	107.6(3)
Rh(2)-C(41)-C(42)	114.1(2)	C(32)-C(31)-C(35)	107.4(3)
Rh(2)-C(47)-C(48)	116.3(3)	C(34)-C(33)-C(38)	127.0(3)
C(41)-C(42)-C(48)	114.4(3)	C(34)-Rh(2)-C(41)	94.1(1)
C(42)-C(48)-C(47)	114.2(3)	C(35)-Rh(2)-C(47)	91.9(1)
C(42)-C(41)-C(46)	118.8(3)	C(34)-Rh(2)-C(53)	160.8(1)
C(48)-C(57)-C(52)	118.4(3)	C(35)-Rh(2)-C(53)	151.73(1)
C(47)-C(48)-C(49)	119.1(3)	C(39)-C(34)-Rh(2)	126.7(3)
C(41)-C(42)-C(43)	119.4(3)	C(40)-C(35)-Rh(2)	126.7(2)

Table 5.35 Bond lengths (Å) and selected angles (°) for complex (8) (structure b)

Te(1)-C(1)	2.103(6)	C(13)-C(14)	1.396(7)
Te(1)-C(12)	2.105(5)	C(13)-C(18)	1.410(7)
Te(1)-Rh(1)	2.525(6)	C(14)-C(15)	1.392(8)
Rh(1)-C(13)	2.052(5)	C(15)-C(16)	1.380(9)
Rh(1)-C(20)	2.057(5)	C(16)-C(17)	1.367(8)
Rh(1)-C(26)	2.206(5)	C(17)-C(18)	1.398(7)
Rh(1)-C(27)	2.212(5)	C(18)-C(19)	1.472(7)
Rh(1)-C(28)	2.245(5)	C(19)-C(24)	1.390(7)
Rh(1)-C(25)	2.255(5)	C(19)-C(20)	1.402(7)
Rh(1)-C(29)	2.269(5)	C(20)-C(21)	1.388(7)
C(1)-C(6)	1.388(8)	C(21)-C(22)	1.391(8)
C(1)-C(2)	1.404(8)	C(22)-C(23)	1.375(9)
C(2)-C(3)	1.366(9)	C(23)-C(24)	1.365(8)
C(3)-C(4)	1.379(10)	C(25)-C(26)	1.422(8)
C(4)-C(5)	1.389(9)	C(25)-C(29)	1.428(9)
C(5)-C(6)	1.394(8)	C(25)-C(30)	1.504(9)
C(6)-C(7)	1.482(8)	C(26)-C(27)	1.424(7)
C(7)-C(8)	1.387(8)	C(26)-C(31)	1.495(8)
C(7)-C(12)	1.397(7)	C(27)-C(28)	1.426(8)
C(8)-C(9)	1.384(9)	C(27)-C(32)	1.493(8)
C(9)-C(10)	1.380(9)	C(28)-C(29)	1.415(8)
C(10)-C(11)	1.378(9)	C(28)-C(33)	1.508(9)
C(11)-C(12)	1.396(7)	C(29)-C(34)	1.490(9)

Table 5.36 Bond lengths (Å) for complex (**9**)

C(1)-Te(1)-C(12)	80.8(2)	C(7)-C(12)-Te(1)	112.9(4)
C(1)-Te(1)-Rh(1)	107.8(2)	C(6)-C(7)-C(12)	116.4(5)
C(12)-Te(1)-Rh(1)	108.4(1)	C(1)-C(6)-C(7)	116.8(5)
C(13)-Rh(1)-Te(1)	80.4(1)	C(7)-C(12)-C(11)	121.3(5)
C(20)-Rh(1)-Te(1)	81.1(1)	C(2)-C(1)-C(6)	121.1(6)
C(25)-Rh(1)-Te(1)	156.6(2)	C(20)-Rh(1)-C(13)	79.3(2)
C(26)-Rh(1)-Te(1)	155.0(1)	C(20)-C(19)-C(18)	114.1(4)
C(27)-Rh(1)-Te(1)	119.1(2)	C(13)-C(18)-C(19)	114.3(4)
C(28)-Rh(1)-Te(1)	120.5(2)	C(21)-C(20)-C(19)	117.9(5)
C(29)-Rh(1)-Te(1)	104.5(2)	C(14)-C(13)-C(18)	117.2(5)
C(6)-C(1)-Te(1)	113.1(4)	C(13)-Rh(1)-C(28)	159.9(2)
C(2)-C(1)-Te(1)	125.8(4)	Rh(1)-C(28)-C(33)	129.9(4)
C(11)-C(12)-Te(1)	125.9(4)		

Table 5.37 Selected bond angles (°) for complex (**9**)

Te(1)-C(1)	2.101(4)	C(7)-C(8)	1.378(6)
Te(1)-C(7)	2.101(4)	C(7)-C(12)	1.423(6)
Te(1)-Rh(1)	2.6033(7)	C(8)-C(9)	1.402(7)
Rh(1)-C(14)	2.148(4)	C(9)-C(10)	1.388(7)
Rh(1)-C(17)	2.148(4)	C(10)-C(11)	1.355(8)
Rh(1)-C(13)	2.165(4)	C(11)-C(12)	1.397(6)
Rh(1)-C(16)	2.165(5)	C(13)-C(14)	1.425(6)
Rh(1)-C(15)	2.166(5)	C(13)-C(17)	1.435(6)
Rh(1)-Cl(2)	2.425(1)	C(13)-C(18)	1.496(6)
Rh(1)-Cl(1)	2.426(1)	C(14)-C(15)	1.446(6)
C(1)-C(2)	1.387(6)	C(14)-C(19)	1.491(6)
C(1)-C(6)	1.402(5)	C(15)-C(16)	1.409(6)
C(2)-C(3)	1.373(6)	C(15)-C(20)	1.498(6)
C(3)-C(4)	1.371(7)	C(16)-C(17)	1.447(6)
C(4)-C(5)	1.362(7)	C(16)-C(21)	1.508(6)
C(5)-C(6)	1.423(6)	C(17)-C(22)	1.486(6)
C(6)-C(12)	1.461(6)		
C(1)-Te(1)-C(7)	81.6(2)	Cl(2)-Rh(1)-Te(1)	79.8(4)
C(1)-Te(1)-Rh(1)	112.1(1)	C(2)-C(1)-Te(1)	125.8(3)
C(7)-Te(1)-Rh(1)	111.0(1)	C(6)-C(1)-Te(1)	111.9(3)
C(13)-Rh(1)-Te(1)	102.08(1)	C(8)-C(7)-Te(1)	127.0(4)
C(14)-Rh(1)-Te(1)	119.1(1)	C(12)-C(7)-Te(1)	111.4(3)
C(15)-Rh(1)-Te(1)	157.3(1)	C(1)-C(6)-C(12)	117.3(4)
C(16)-Rh(1)-Te(1)	154.8(1)	C(2)-C(1)-C(6)	122.1(4)
C(17)-Rh(1)-Te(1)	117.1(1)	C(15)-Rh(1)-Cl(1)	123.5(1)
Cl(1)-Rh(1)-Te(1)	79.1(4)	C(15)-Rh(1)-Cl(2)	95.7(1)

Table 5.38 Bond lengths (Å) and selected angles (º) for complex (10)

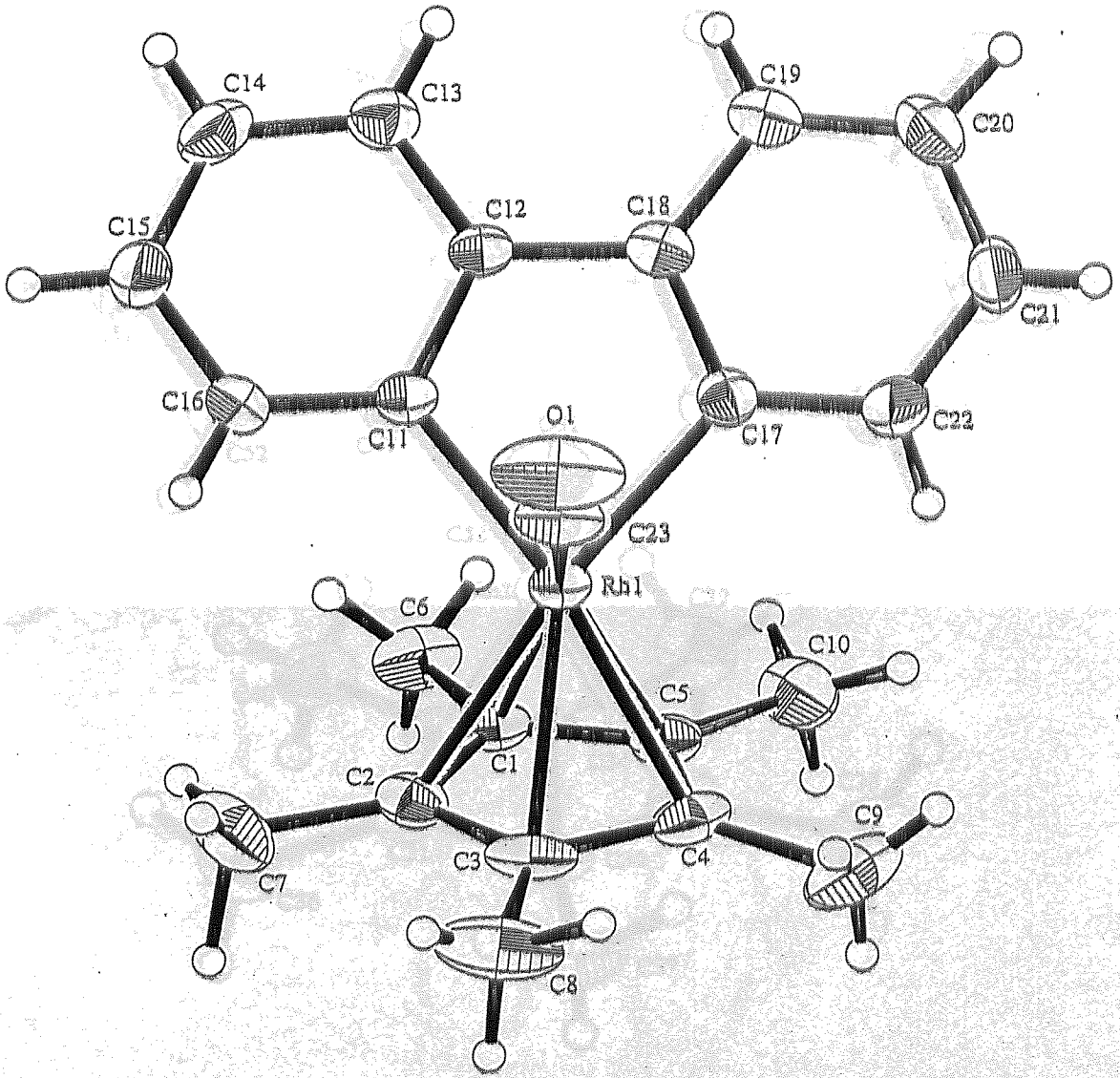

Figure 5.19 The molecular structure of $C_{12}H_8Rh(CO)Cp^*$ (8) (structure a)

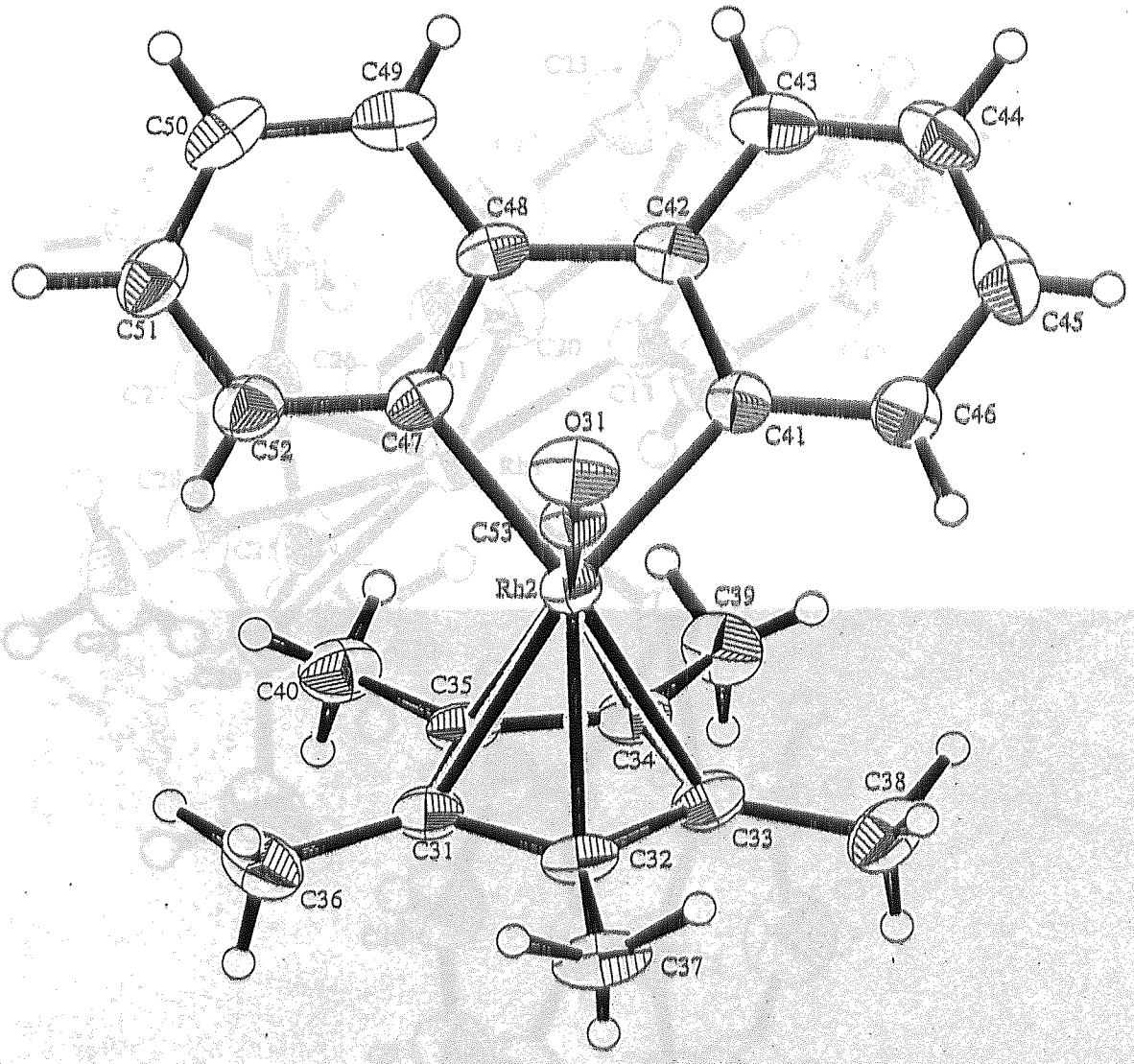

Figure 5.20 The molecular structure of $C_{12}H_8Rh(CO)Cp^*$ (8) (structure b)

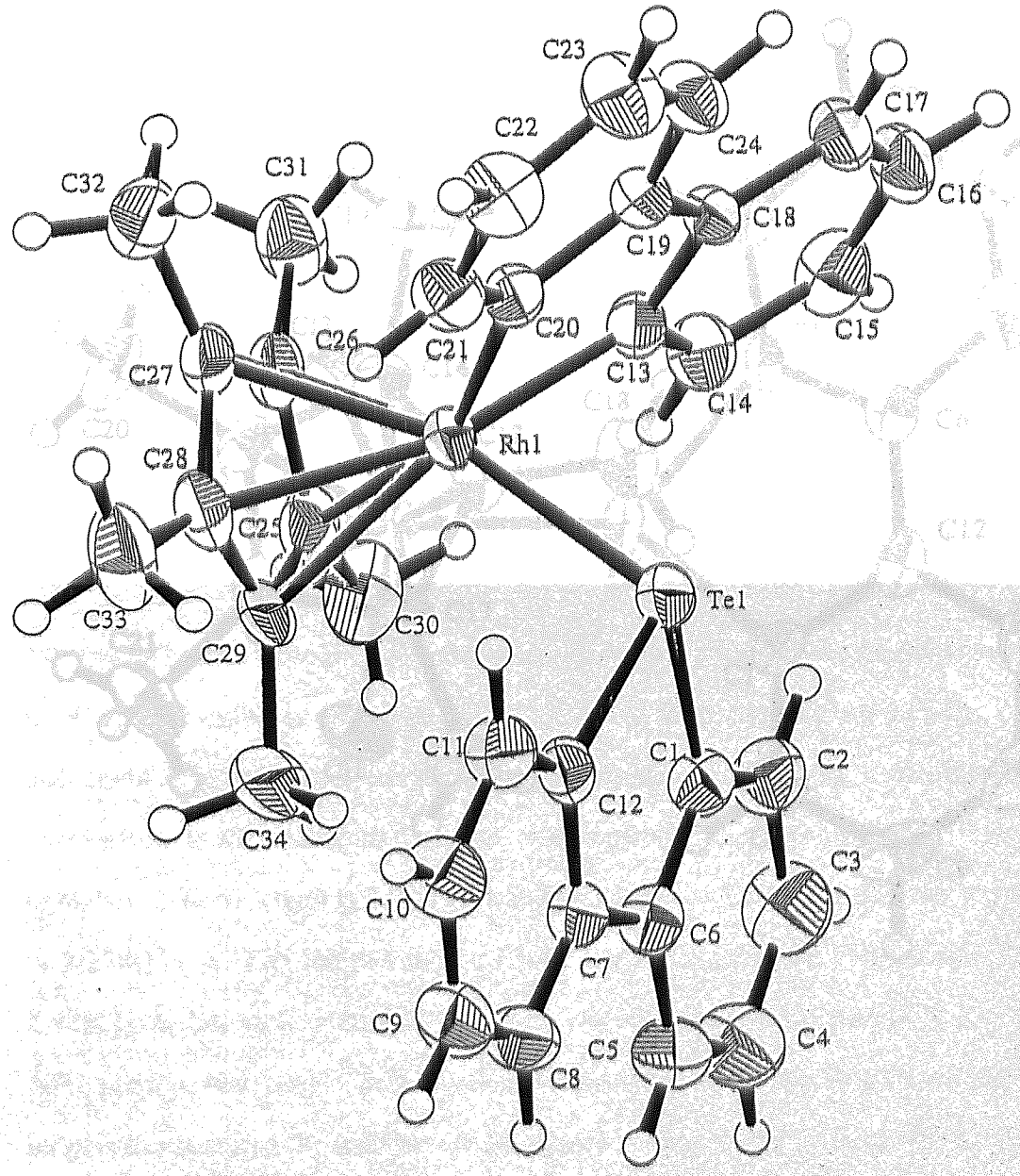

Figure 5.21 The molecular structure of $C_{12}H_8RhCp^*(\eta^1\text{-}C_{12}H_8Te)$ (**9**)

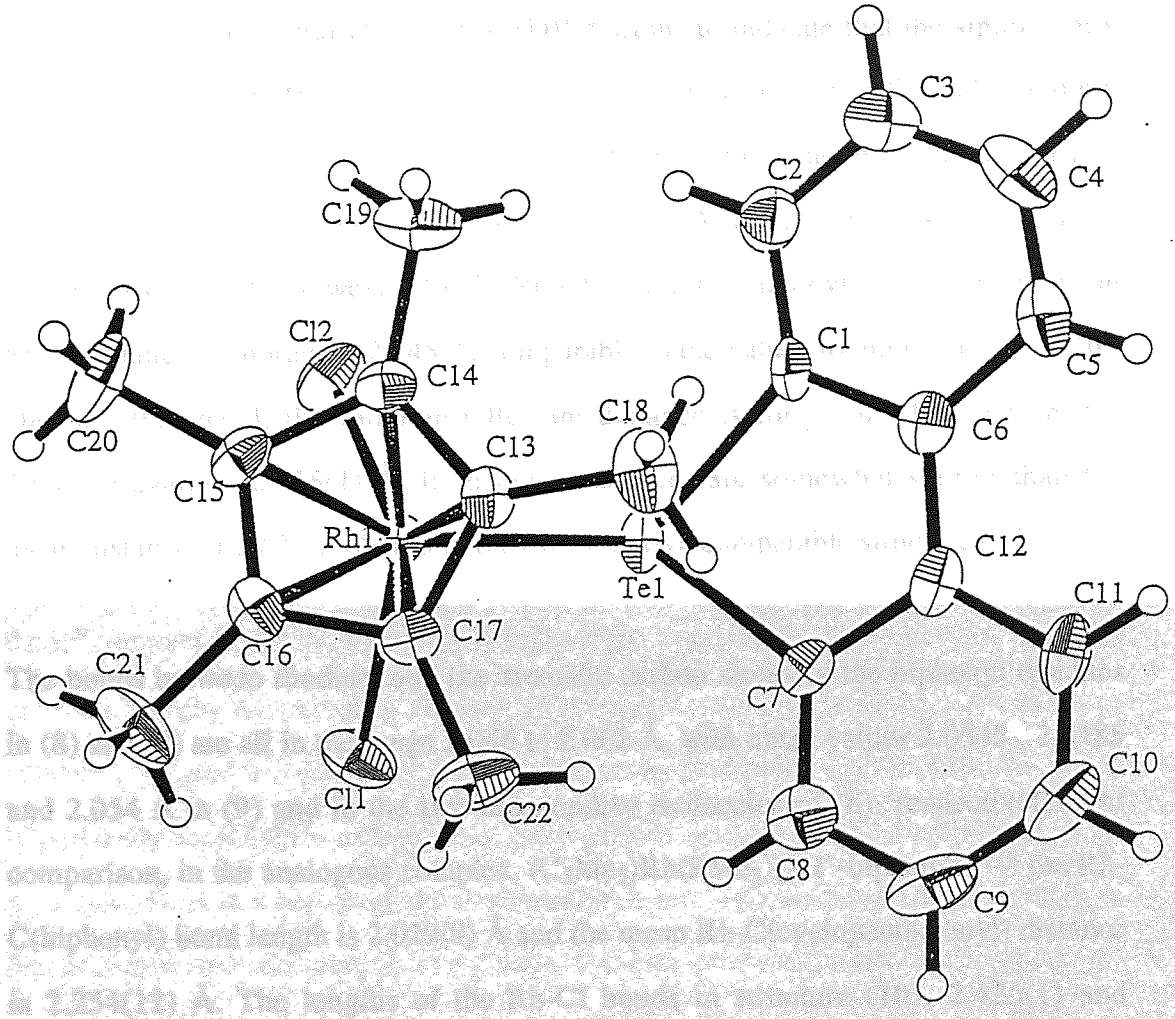

Figure 5.22 The molecular structure of $Cp^*RhCl_2(\eta^1\text{-}C_{12}H_8Te)$ (**10**)

5.4.1 Structural studies of rhodium/tellurium complexes

Each of the three structures contains a π-bonded Rh-pentamethylcyclopentadienyl residue. Rh-C distances are 2.232-2.270, 2.223-2.280, 2.207-2.269 and 2.148-2.166 Å, in structures (**8**) (two independent molecules), (**9**) and (**10**), respectively. The mean distances are 2.255(7), 2.260(10), 2.238(12) and 2.158(4) Å, respectively. A search of the Cambridge Structural Database (CSD)[114] seems to indicate that the significantly shorter distances in (**10**) may be due to the presence of two sterically undemanding, electronegative chlorine atoms bonded to rhodium in this structure. The mean Rh-C distance in 515 cyclopentadienyl structures is 2.23 Å, in agreement with the values found in (**8**) and (**9**). However, for 25 $Rh(Cl_2)$-cyclopentadienyl structures the mean Rh-C distance is shorter, at 2.145 Å, comparable to the values found in structure (**10**). On the other hand, the rhodium-tellurium distance is longer in (**10**) than in (**9**), 2.603(1) against 2.525(1) Å. Both these distances are somewhat shorter than the mean distance of 2.622(2) Å found for Rh-Te in five comparable structures .[115-117]

The bonds between rhodium and the aromatic carbon atoms of the biphenyl residues in (**8**) and (**9**) are all in the range 2.046 to 2.062 Å, with mean values 2.0545 , 2.0585 and 2.054 Å in (**9**) and in the two independent molecules of (**8**), respectively. For comparison, in the analogous complex, $(C_5Me_5)Rh(PMe_3)$(2,2'-biphenyl),[118] the Rh-C(biphenyl) bond length is 2.029(9) Å and the mean Rh-C(cyclopentadienyl) distance is 2.254(12) Å. The lengths of the Rh-Cl bonds in structure (**10**), 2.425(1) and 2.426(1) Å, fall well within the range of lengths found for this bond, 2.225-2.615 Å[114], but the mean length, 2.381(2) Å, is somewhat shorter. The Te-C(biphenyl) bond lengths in structures (**9**) and (**10**) are all closely similar, range 2.101-2.105 Å, in good agreement with the lengths found in dibenzotellurophene,[119] 2.084 and 2.089 Å, and with the value given by Allen *et al*[120] for Te-C (aromatic), 2.116 Å.

The cyclopentadienyl rings are essentially planar, maximum atomic deviation +/- 0.017 Å for the ring of structure (**10**). In all three structures the methyl substituents are

displaced by distances of up to 0.175 Å from the ring plane on the side remote from the metal atom.

5.5 CONCLUSIONS

The $[Cp^*RhCl_2]_2$ dimer represents a useful system for the synthesis of rhodium complexes of tellurium heterocycles. Thus, reaction with tellurophene in the presence of silver triflate gives, as expected, the η^5 complex, $[Cp^*Rh(\eta^5\text{-}C_4H_4Te)](OTf)_2$, in good yield, thereby following the precedent established by related thiophene species.[39] A similar reaction using dibenzotellurophene as the ligand, again results in the formation of an η^5 complex although a stronger interaction between tellurium and rhodium has been postulated. Repeating the reaction with the exclusion of silver triflate yields, almost quantitatively, $[Cp^*RhCl_2(\eta^1\text{-}C_{12}H_8Te)]$ in which the dibenzotellurophene is coordinated to the rhodium via the tellurium atom only. Reaction of $Cp^*RhPPh_3Cl_2$ with tellurophene in the presence of silver triflate affords the η^4 complex $[Cp^*RhPPh_3(\eta^4\text{-}C_4H_4Te)](OTf)_2$, in which the unlabile PPh_3 ligand is retained thereby encouraging a lesser coordination to the heterocycle. Attempts to synthesise η^4 and η^2 complexes of tellurophene by employing $Cp^*Rh(diphos)Cl_2$ and $[Cp^*Rh(diphos)Cl]PF_6$ respectively have proved unsuccessful. 2-telluraindane in which the Te is in a non-aromatic environment reacts with the rhodium dimer both in the presence and absence of silver salts, the end product invariably being an η^1 complex. Telluracyclopentane, rather surprisingly, does not coordinate to rhodium under any conditions.

The synthesised complexes have been studied wherever possible by ^{125}Te NMR spectroscopy and some useful conclusions can be drawn by observing both chemical shifts and $^{103}Rh\text{-}^{125}Te$ coupling constants. Hence, η^5 complexes tend to absorb furthest upfield, relative to the free heterocycle, whilst giving the smallest value for the coupling constant. η^1 complexes, in contrast, give smaller upfield coordination

shifts whilst having the largest coupling constants. These observations lead to the belief that ^{125}Te NMR spectroscopy may be valuable for studying the mode of binding of group 16 heterocycles to HDS catalyst surfaces particularly in instances where X-ray crystallography is not available.

A further objective was to investigate whether, once activated by the rhodium, it would be possible to achieve removal of the heteroatom by subsequent reaction with an organometallic reagent. This work was limited to the $[Cp^*Rh(\eta^5\text{-}C_4H_4Te)](OTf)_2$ and $[Cp^*Rh(\eta^5\text{-}C_{12}H_8Te)](OTf)_2$ systems and initial reaction with Cp_2Co was carried out in order to reduce the 2+ complexes. In the case of $[Cp^*Rh(\eta^5\text{-}C_4H_4Te)](OTf)_2$, treatment with Cp_2Co is expected to produce an η^4 complex as observed for the analogous thiophenes. However due to the greater reactivity of the tellurophene system no η^4 complex is observed, instead the detellurated compound $Cp^*Rh(\eta^5\text{-}C_4H_4RhCp^*)$ is isolated. As suggested in Scheme 5.1 this is thought to have arisen from an η^4 intermediate which undergoes further reactions prior to yielding the end product. Further reaction with $Fe_3(CO)_{12}$ affords the known complex (**3**) depicted in Scheme 5.1.

Similar reactions with $[Cp^*Rh(\eta^5\text{-}C_{12}H_8Te)](OTf)_2$ provides a greater spectrum of new compounds as depicted in Scheme 5.2. The reduction product upon treatment with Cp_2Co is thought to be the novel η^1 complex (**9**) in which the rhodium is inserted into a dibenzo ring and also η^1-coordinated to dibenzotellurophene. Further reaction with $Fe_3(CO)_{12}$ leads to the formation of detellurated products (**6**) (dibenzoferrole) and the novel organometallic complex (**8**). Analogous systems of dibenzothiophene are unreactive under similar conditions, hence the observations with the more reactive tellurium compound enable us to at least examine the *mechanistic feasibility* of dechalcogenation reactions with the more conjugated heterocycles *via* the rhodium chemistry. A further advantage enjoyed by the tellurium systems is that access to numerous novel organometallics is obtained from this chemistry.

CHAPTER 6

THE REACTIONS OF NITROGEN-CONTAINING TELLURIUM AND SELENIUM HETEROCYCLES WITH ORGANOMETALLIC REAGENTS

6.1 INTRODUCTION

As a variation on previously studied systems it was thought to be interesting to investigate the reactions of heterocycles containing both tellurium and nitrogen heteroatoms. To maintain the theme of "modelling desulfurisation", the reactivity of these systems towards $Fe_3(CO)_{12}$ and $[Cp^*RhCl_2]_2$ were studied. Previous observations have led to the thought that the relatively facile detelluration of heterocyclic organotellurium compounds enables these materials to be seen as potential precursors of novel organometallic compounds. Hence it is speculated that if the tellurium heterocycle contains an additional heteroatom such as nitrogen, access to new areas of organometallic chemistry should be possible. The presence of nitrogen in the heterocycle provides an attractive feature for these reactions and it is interesting to see whether the organometallic reagent will be reactive towards the nitrogen as well as tellurium. An additional consideration is that the reactions of these heterocycles may be regarded as models for the removal of nitrogen from fossil fuels

6.2 EXPERIMENTAL

6.2.1 Preparation of N-containing heterocycles

Schemes 6.1-6.4 illustrate synthetic routes to some N-containing selenium and tellurium heterocycles which were prepared according to published literature methods. The identities and purities of these compounds were confirmed by observation of melting points and spectral data.

(i) 2,1,3-Benzoselenadiazole[121]

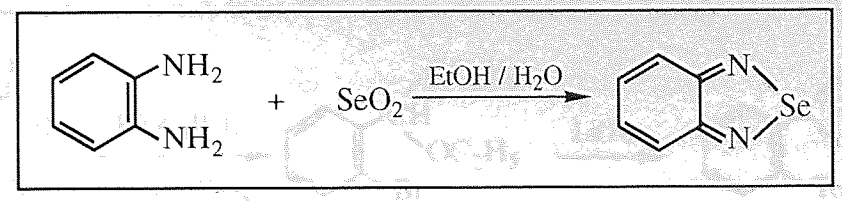

Scheme 6.1

2,1,3-Benzoselenadiazole was prepared in almost quantitative yields. The infrared spectrum was in good agreement with the reported spectral data.

(ii) 3,4-Quinoxalino-1-telluracyclopentane[122]

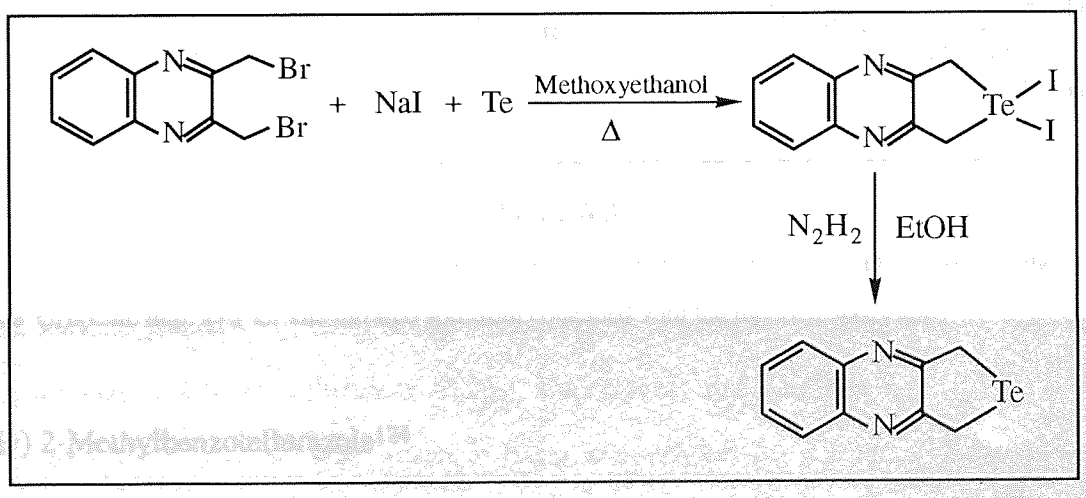

Scheme 6.2

3,4-Quinoxalino-1-telluracyclopentane was prepared in 25% yield (based on Te). Comparison of the infrared spectrum with the reported spectrum confirmed the identity of the heterocycle.

(iii) Benzisotellurazole[123]

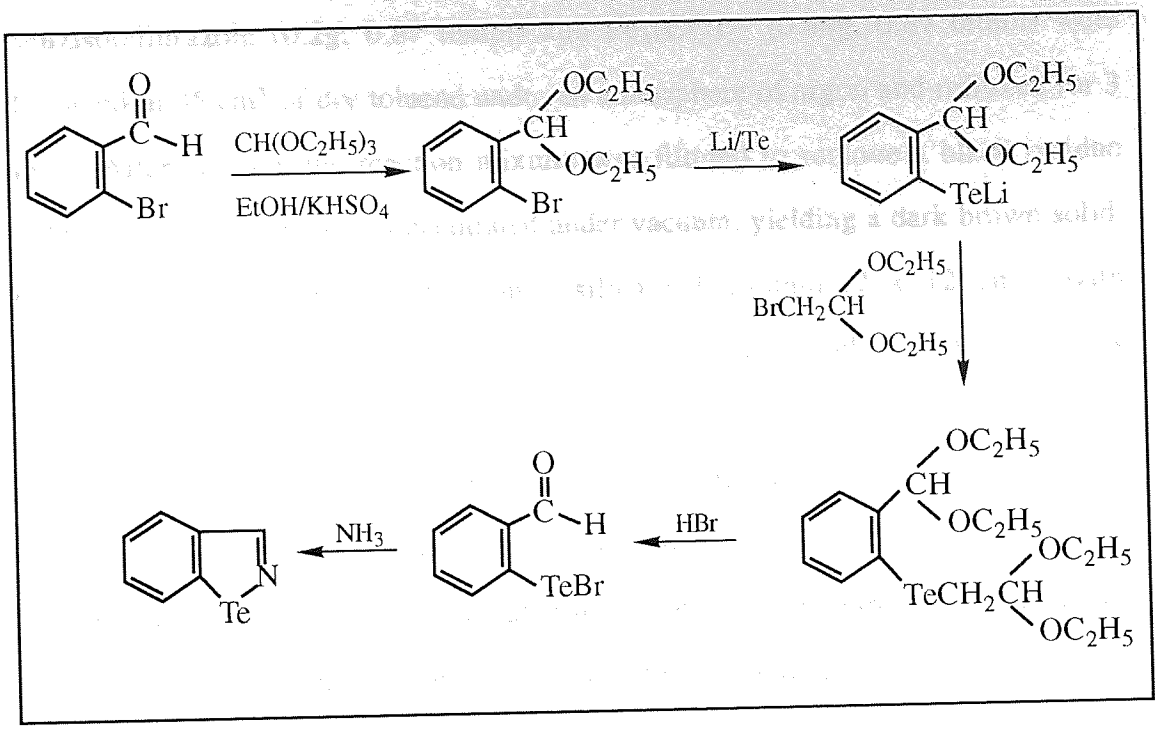

Scheme 6.3

Benzisotellurazole was obatained in 22% yield (based on Te). The melting point was determined as 168°C, c.f. lit. m.p. 173°C. The infrared spectrum coincided with the reported spectrum.

(iv) 2-Methylbenzotellurazole[124]

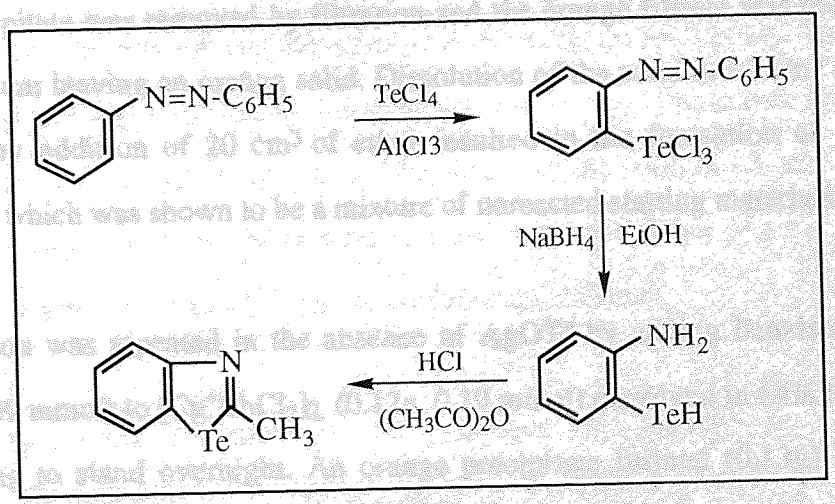

Scheme 6.4

The overall yield of 2-methylbenzotellurazole was 27% (based on $TeCl_4$). The melting point was determined as 93°C, in good agreement with the reported m.p, 93-95°C. ^{13}C and ^{1}H NMR spectra were both satisfactory and are shown in Figures 6.6 and 6.9 respectively.

6.2.2 Reaction of benzisotellurazole with $Fe_3(CO)_{12}$

Benzisotellurazole (0.2g, 0.87 mmol) and $Fe_3(CO)_{12}$ (0.44g, 0.87 mmol) were dissolved in 35 cm^3 of dry toluene under an atmosphere of argon and refluxed for 3 hours. After cooling, the reaction mixture was filtered to remove a black residue (0.18g) and the filtrate was concentrated under vacuum, yielding a dark brown solid. The solid was chromatographed on a silica gel column (2 x 12 cm) with hexane/CH_2Cl_2 (2:1) as the eluting solvent, thus revealing a purple band succeeded by a green band. Collection of the two fractions followed by evaporation of the solvent yielded dark purple crystals from the first eluate (15mg) which were shown to be the cluster compound, $Fe_3Te_2(CO)_9$, and a dark green solid from the second eluate. Crystals of the dark green solid suitable for X-ray crystallography were grown by slowly cooling a concentrated toluene solution of the compound.

6.2.3 Reaction of benzisotellurazole with $[Cp^*RhCl_2]_2$

An acetone solution (10 cm^3) of AgOTf (0.42g, 1.63 mmol) was added to an acetone suspension of benzisotellurazole (0.25g, 1.40 mmol) and $[Cp^*RhCl_2]_2$ (0.25g, 0.40 mmol) and the mixture was stirred at room temperature for 2 hours. The resulting AgCl precipitate was removed by filtration and the orange filtrate was concentrated under vacuum leaving an orange solid. Dissolution of the solid in ~2 cm^3 of CH_2Cl_2 followed by addition of 20 cm^3 of ether resulted in the formation of an orange precipitate which was shown to be a mixture of unreacted starting materials.

The reaction was repeated in the absence of AgOTf by adding benzisotellurazole (0.09g, 0.39 mmol) to $[Cp^*RhCl_2]_2$ (0.12g, 0.19 mmol) dissolved in $CHCl_3$ (2.5 cm^3) and leaving to stand overnight. An orange precipitate formed (0.13g) which was removed by filtration and washed with ether.

6.2.4 Reaction of 2-methylbenzotellurazole with $Fe_3(CO)_{12}$

2-methylbenzotellurazole (0.5g, 2.04 mmol) and $Fe_3(CO)_{12}$ (1.06g, 2.10 mmol) were dissolved in 50 cm^3 of dry toluene and refluxed for 3 hours. After cooling, the reaction mixture was filtered to remove a brown residue (0.62g) and the filtrate was concentrated under vacuum, yielding a dark brown solid. The solid was chromatographed on a silica gel column (2 x 15 cm) with hexane/CH_2Cl_2 (2:1) as the eluting solvent, thereby giving a red band preceded by a brown band and a fast eluting purple band. Collection of the three fractions followed by evaporation of the solvent gave purple crystals from the first eluate, identified as the cluster compound $Fe_3Te_2(CO)_9$ (60mg, 12.7% based on $Fe_3(CO)_{12}$), a dark purple solid from the second eluate and a dark red solid from the third. Crystals of the latter two compounds suitable for X-ray crystallography were grown by slowly cooling concentrated hexane solutions of the solids.

6.2.5 Reaction of 2-methylbenzotellurazole with $[Cp^*RhCl_2]_2$

An acetone solution (10 cm^3) of AgOTf (0.41g, 1.60 mmol) was added to an acetone suspension of 2-methylbenzotellurazole (0.34g, 1.40 mmol) and $[Cp^*RhCl_2]_2$ (0.25g, 0.40 mmol) and the mixture was stirred at room temperature for 2 hours. The resulting AgCl precipitate was removed by filtration and the orange filtrate was concentrated under vacuum leaving an orange solid. Dissolution of the solid in ~3 cm^3 of CH_2Cl_2 followed by addition of 20 cm^3 of ether resulted in the formation of a red precipitate (0.43g), which was shown to be a mixture of starting materials.

The reaction was repeated in the absence of AgOTf by adding 2-methylbenzotellurazole (0.24g, 0.98 mmol) to $[Cp^*RhCl_2]_2$ (0.25g, 0.40 mmol) dissolved in $CHCl_3$ (2.5 cm^3) and leaving to stand overnight. No reaction product was isolated using this procedure.

6.2.6 Reaction of 2,1,3-benzoselenadiazole with $Fe_3(CO)_{12}$

2,1,3-Benzoselenadiazole (1.00g, 5.46 mmol) and $Fe_3(CO)_{12}$ (2.7g, 5.46 mmol) were dissolved in toluene (50 cm^3) and heated under reflux for 3 hours, during which time the solution changed from dark green to colourless. Filtration of the reaction mixture afforded a brown residue (0.39g) and a colourless filtrate which did not contain any involatile material after evaporation under vacuum. The residue was analysed for the presence of Se by ESCA while the fate of the organic fragment of the heterocycle was not established.

6.2.7 Reaction of 2,1,3-benzoselenadiazole with molybdenum hexacarbonyl

2,1,3-Benzoselenadiazole (0.5g, 2.73 mmol) and $Mo(CO)_6$ (0.72g, 2.73 mmol) were heated in toluene (50 cm^3) under reflux for 30 minutes during which time an intense purple colour formed in solution. The solution was filtered and evaporated to dryness under vacuum to give a purple solid (0.57g).

6.2.8 Reaction of 3,4-quinoxalino-1-telluracyclopentane with $Fe_3(CO)_{12}$

3,4-quinoxalino-1-telluracyclopentane (0.15g, 0.6 mmol) and $Fe_3(CO)_{12}$ (0.31g, 0.6 mmol) were heated in refluxing heptane (30 cm^3) for 3 hours. Filtration afforded a brown residue (0.47mg) and a dark green solution which after evaporation to dryness under vacuum yielded a black solid. The solid was chromatographed on a TLC-grade silica column (2 x 15 cm) giving a purple band followed by a green band. Elution with pentane followed by evaporation of solvent gave dark purple crystals from the first eluate and a green solid from the second which was identified as unreacted iron carbonyl.

6.3 RESULTS AND DISCUSSION

Infrared and NMR spectra for selected compounds are displayed in Figures 6.1-6.11 on pages 232-242.

6.3.1 Reaction of benzisotellurazole with $Fe_3(CO)_{12}$

Two major components were recovered after chromatography from this reaction. The first fraction yielded 15mg of dark purple crystals which were identified as the previously reported cluster compound, $Fe_3Te_2(CO)_9$ (**1**).[97] The second fraction afforded a dark green solid and this was shown to be a novel compound of formula $(C_6H_4CHNTe)_2Fe_3(CO)_7$ (**2**); yield 55mg, 15.3% based on benzisotellurazole.

Requires (%)	C, 30.5;	H, 1.2;	N, 3.4	$C_{21}H_{10}N_2Te_2Fe_3O_7$
Found (%)	C, 30.9;	H, 1.4;	N, 3.3	

The structure of (**2**) is shown below.

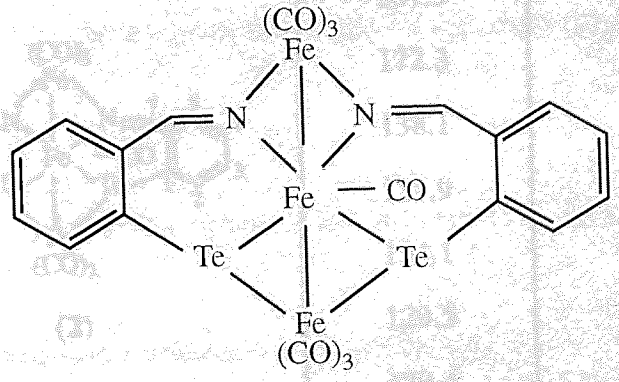

(**2**)

Peaks found in the carbonyl region of the infrared spectrum of (**2**) are recorded in Table 6.1 while NMR data is displayed in Tables 6.2 and 6.3.

KBr, ν(CO) cm^{-1}
2060
2021
2008
1998
1985
1964
1941
1922
1906

Table 6.1 Infrared peaks in the carbonyl region of compound (**2**)

compound	^{13}C δ, ppm ($CDCl_3$)	assignment
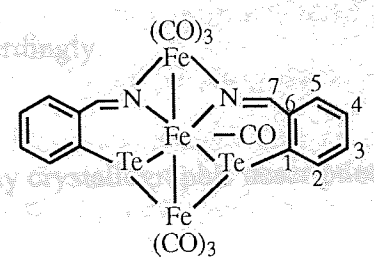 (**2**)	213.6	CO
	207.9	CO
	172.3	C7
	138.1	C2
	137.9	C6
	134.1	C5
	129.5	C3
	129.4	C4
	104.5	C1

Table 6.2 ^{13}C NMR data for compound (**2**)

compound	^{1}H δ, ppm ($CDCl_3$)	assignment
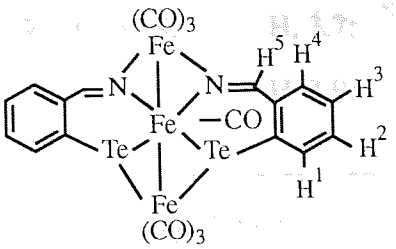 (2)	9.12 (s, 1H) 8.05 (m, 1H) 7.46 (m, 1H) 7.32 (m, 1H) 7.22 (m, 1H)	H5 H1 H4 H2 H3

Table 6.3 ^{1}H NMR data for compound (**2**)

The infrared spectrum of compound (**2**) (Figure 6.1) shows a very rich absorption in the carbonyl region. The presence of the carbonyl groups is also evident in the ^{13}C NMR spectrum (Figure 6.4)) indicated by the two absorptions at 213.6 and 207.9 ppm. Further assignments have been made by considerations of electronegativities of adjacent atoms as well as peak intensities. Hence, the carbon adjacent to N absorbs low field at 172.3 ppm while the quarternary carbon adjacent to the electropositive tellurium displays a relatively upfield absorption for aromatic carbons (104 ppm vs 128 ppm for benzene). The assignments for the ^{1}H spectrum (Figure 6.5) have been made accordingly.

A full x-ray crystallographic description of this structure is explained in section 6.4.

6.3.2 Reaction of benzisotellurazole with $[Cp^*RhCl_2]_2$

No reaction occurred when silver triflate was present and a mixture of starting materials was recovered. However, when the reaction was carried out in the absence of silver triflate an orange precipitate formed which was shown by infrared spectroscopy to be a reaction product. Precedent from the reactions of tellurophenes with $[Cp^*RhCl_2]_2$, the expected formula of this product is $Cp^*RhCl_2(\eta^1\text{-}C_7H_5NTe)$

and good evidence for this is provided by elemental analysis and mass spectrometry (Table 6.4)

Requires (%)	C, 37.8;	H, 3.7;	N, 2.6	$C_{17}H_{20}RhCl_2NTe$
Found (%)	C, 37.9;	H, 3.9;	N, 2.2	

m/z (FAB)	assignment
541	$[Cp^*RhCl_2(C_7H_5NTe)]^+$
506	$[Cp^*RhCl(C_7H_5NTe)]^+$

Table 6.4 FAB-MS (NOBA matrix) peaks for $[Cp^*RhCl_2(C_7H_5NTe)]$

Due to the very low solubility of this compound suitable NMR data was not obtained hence the expected η^1 coordination mode of the heterocycle to the metal was not confirmed.

6.3.3 Reaction of 2-methylbenzotellurazole with $Fe_3(CO)_{12}$

Three major fractions were collected from this reaction after chromatography. The first fraction afforded purple crystals, identified as the cluster compound $Fe_3Te_2(CO)_9$ formed in 12% yield based on $Fe_3(CO)_{12}$. The dark purple solid recovered from the second eluate was shown to have the formula $C_8H_7NFe_3(CO)_{10}$ (**3**); yield 25mg, 6.3% based on $Fe_3(CO)_{12}$.

Requires (%)	C, 38.2;	H, 1.2;	N, 2.5	$C_{18}H_7NFe_3O_{10}$
Found (%)	C, 38.8;	H, 1.3;	N, 2.6	

The dark red solid obtained from the second eluate was shown to have the formula $C_8H_7NFe_2(CO)_6$ (**4**); yield 28mg, 10.1% based on $Fe_3(CO)_{12}$.

Requires (%)	C, 42.3;	H, 1.8;	N, 3.5	$C_{14}H_7NFe_2O_6$
Found (%)	C, 43.4;	H, 1.6;	N, 3.7	

The structures of (**3**) and (**4**) are shown below.

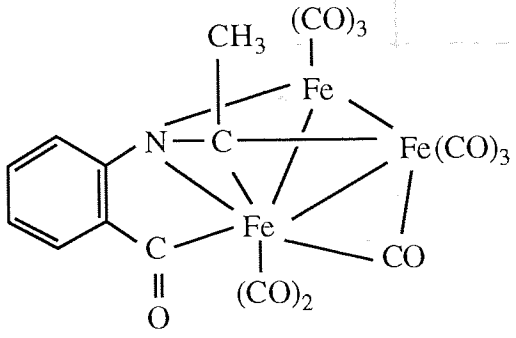

(**3**)

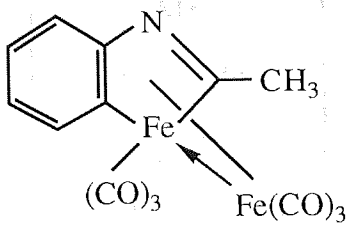

(**4**)

Infrared peaks in the carbonyl region for compounds (**3**) and (**4**) are recorded in Table 6.5. Mass spectral data is displayed in Table 6.6 while NMR data is shown in Tables 6.7 and 6.8.

KBr, ν(CO) cm^{-1}	
compound (3)	**compound (4)**
2083	2071
2036	2038
2015	2015
1978	1985
1870	1919
1856	1881
1690	
1649	

Table 6.5 Infrared peaks in the carbonyl region of compounds (**3**) and (**4**)

compound	m/z (FAB)	assignment
$C_8H_7NFe_3(CO)_{10}$ (**3**)	565	M^+
	481	M^+ - 3CO
	425	M^+ - 5CO
	341	M^+ - 8CO
$C_8H_7NFe_2(CO)_6$ (**4**)	397	M^+
	313	M^+ - 3CO
	229	M^+ - 6CO

Table 6.6 FAB-MS (NOBA matrix) peaks for compounds (**3**) and (**4**)

compound	^{13}C δ, ppm ($CDCl_3$)	assignment
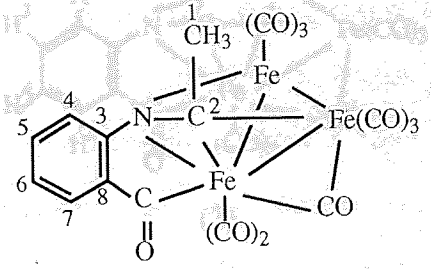 (**3**)	204.5-202.6	CO
	161.4	C3
	140.5	C8
	134.0	C5
	128.7	C6
	124.3	C7
	121.4	C2
	121.3	C4
	33.4	C1

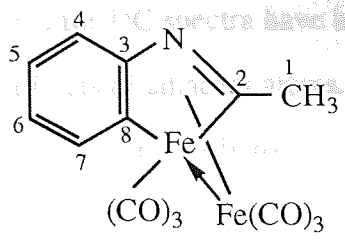 (**4**)	211.8-206.9	CO
	149.0	C4
	143.0	C3
	142.2	C8
	133.3	C7
	126.3	C6
	126.0	C5
	--	C2
	36.3	C1

Table 6.7 ^{13}C NMR data for compounds (**3**) and (**4**)

compound	^{1}H δ, ppm ($CDCl_3$)	assignment
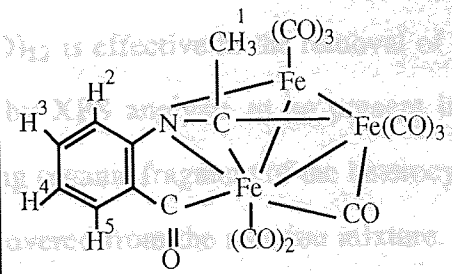 (**3**)	7.72 (m, 1H)	H2
	7.62 (m, 1H)	H5
	7.34 (m, 1H)	H3
	7.24 (m, 1H)	H4
	2.60 (s, 3H)	H1
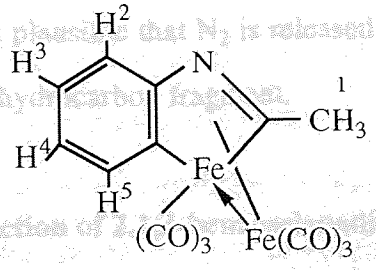 (**4**)	7.91 (m, 1H)	H2
	7.70 (m, 1H)	H5
	7.50 (m, 1H)	H3
	7.05 (m, 1H)	H4
	2.66 (s, 3H)	H1

Table 6.8 ^{1}H NMR data for compounds (**3**) and (**4**)

The ^{13}C NMR spectra of compounds (**3**) and (**4**) are shown in Figures 6.7 and 6.8 respectively, while ^{1}H NMR spectra are displayed in Figures 6.10 and 6.11. Assignments for ^{13}C spectra have been made by consideration of peak intensities and inductive effects of adjacent atoms. Anisotropic effects have also been considered for assignment of the aryl carbons.

The X-ray crystallographic structures of (**3**) and (**4**) have been elucidated and are discussed in section 6.4.

6.3.4 Reaction of 2-methylbenzotellurazole with $[Cp^*RhCl_2]_2$

2-methylbenzotellurazole did not react with $[Cp^*RhCl_2]_2$ under any conditions. This is in contrast to benzisotellurazole which reacts with the rhodium dimer in the absence of silver triflate to give an η^1 complex.

6.3.5 Reaction of 2,1,3-benzoselenadiazole with $Fe_3(CO)_{12}$

$Fe_3(CO)_{12}$ is effective in the removal of Se from 2,1,3-benzoselenadiazole, which is found by XPS analysis to be present in the reaction residue after filtration. The resulting organic fragment of the heterocycle appears to be a volatile material and was not recovered from the reaction mixture. It is possible that once selenium is removed from the heterocycle the remaining organic fragment, which is expected to be highly unstable, either rapidly decomposes or dimerises thereby affording a volatile organic liquid. Furthermore, the presence of nitrogen was not detected in the reaction residue, hence it is plausible that N_2 is released during the reaction together with the selenium leaving a hydrocarbon fragment.

6.3.6 Reaction of 2,1,3-benzoselenadiazole with molybdenum hexacarbonyl

A purple solid was recovered from this reaction and its infrared spectrum showed the presence of a rich carbonyl region which was not coincident with carbonyl peaks

observed for molybdenum hexacarbonyl (see Table 6.9). Further analysis (NMR spectroscopy and mass spectrometry) proved inconclusive as to the identity of this product.

KBr, ν(CO) cm^{-1}	
purple solid	**$Mo(CO)_6$**
2073	2116
2001	2002
1968	1980
1918	1955
1807	

Table 6.9 Infrared bands in the carbonyl region of the product from the reaction of $Mo(CO)_6$ and 2,1,3-benzoselenadiazole

6.3.7 Reaction of 3,4-quinoxalino-1-telluracyclopentane with $Fe_3(CO)_{12}$

The dark purple crystals obtained after chromatography from this reaction were shown by infrared spectroscopy to be the previously reported cluster compound, $Fe_3Te_2(CO)_9$. Hence, it is clear that the iron carbonyl is effective in accomplishing the removal tellurium from the heterocycle. The other material recovered from chromatography was unreacted iron carbonyl, however, no product containing the organic residue of the heterocycle was recovered suggesting it is either a volatile liquid or a highly unstable compound. This contrasts with the products obtained from the reaction of 2-telluraindane with $Fe_3(CO)_{12}$ (see chapter 3) in which the $Fe_3Te_2(CO)_9$ cluster is also obtained, but in addition the organic residue is recovered in the form of an unsymmetric dimer stabilised by an $Fe(CO)_3$ fragment. This suggests that the inclusion of two nitrogens into the heterocycle appears to hinder the formation of a stable organometallic complex once the tellurium heteroatom has been extruded.

6.3.8 Summary of reactions of N-containing tellurium and selenium heterocycles with $Fe_3(CO)_{12}$

The reactions of nitrogen containing tellurium heterocycles with $Fe_3(CO)_{12}$ have been summarised in Scheme 6.5 on page 17.

The reaction of benzisotellurazole with $Fe_3(CO)_{12}$ results in the dimerisation of the heterocycle leading to the formation of the symmetrical complex (**2**) as demonstrated by reaction (i) in Scheme 6.5. This product has arisen by the regioselective insertion of Fe into the Te-N bond of the heterocyclic ring. Hence, the initial attack occurs at the Te-N bond of the heterocycle and this mimics the reaction in which benzothiophene is the substrate where the S-C bond remote from the benzene ring undergoes cleavage.[53] The Te-C bond is retained, again demonstrating the greater strength and resistance to attack of heteroatom-benzene ring carbon bonds. A further feature of this structure is the almost linear arrangement of Fe atoms which must have emerged from the rupture of one of the Fe-Fe bonds in the iron carbonyl. It is also interesting to note that the tellurium is retained in the heterocycle even after prolonged reaction times, although small traces of the cluster compound $Fe_3Te_2(CO)_9$ are recovered. This is in contrast to dibenzotellurophene, which on reaction with $Fe_3(CO)_{12}$, is readily detellurated to yield the dibenzoferrole as discussed in chapter 3.

In contrast to benzisotellurazole, the reaction of 2-methylbenzotellurazole with $Fe_3(CO)_{12}$ (reaction (ii) in Scheme 6.5) results in the removal of tellurium to afford two novel organometallic compounds of iron, (**3**) and (**4**), formed in similar yields. Hence, where the nitrogen atom is not adjacent to the tellurium, rather it is two atoms away, the tellurium is removed from the heterocycle relatively easily by the cleavage of both C-Te bonds. The location of the initial attack of the iron carbonyl is less predictable than for benzisotellurazole, but it emerges from both sets of reactions that Fe has a particular affinity for N. The position of the nitrogen atom in the heterocycle

also has a marked effect on the reaction by influencing the stability of the tellurium atom within the organometallic system.

Complex (**3**) has an interesting structure in that both an organic carbonyl and an Fe atom have inserted into the heterocycle, replacing the tellurium. It is possible that initial carbonyl insertion may facilitate interaction between iron and nitrogen. A further feature of note is the fact that the triangular arrangement of iron atoms has been retained within the structure, contrasting with the linear arrangement observed for complex (**2**). Complex (**4**) can be compared to the ferroles obtained from the reactions of tellurophenes with $Fe_3(CO)_{12}$ (see chapter 3). This is perhaps the more expected product from this reaction since the environment of the tellurium atom in 2-methylbenzotellurazole closely resembles that found in benzotellurophene. It is unclear as to whether the formation of compounds (**3**) and (**4**) are related or whether two separate reactions occur in parallel. In both cases, however, the tellurium is recovered in the form of $Fe_3Te_2(CO)_9$.

A common feature for both reactions (i) and (ii) is that the nitrogen atom is retained within the heterocycle even with prolonged reaction times. The presence of excess iron carbonyl in the reaction mixture also has no effect on the final products.

Reactions (iii) and (iv) in Scheme 6.5 both result in the removal of the heteroatom but in each case no product containing the organic fragment is observed. This is possibly due to the presence of two nitrogen atoms within the heterocycle, which may combine once the group 16 atom has been eliminated, resulting in the release of dinitrogen. The accompanying hydrocarbon residue would then be expected to exist in the form of a volatile organic liquid which could possibly be recovered chromatographically. Alternatively, the hydrocarbon residue may be extremely unstable making recovery very difficult.

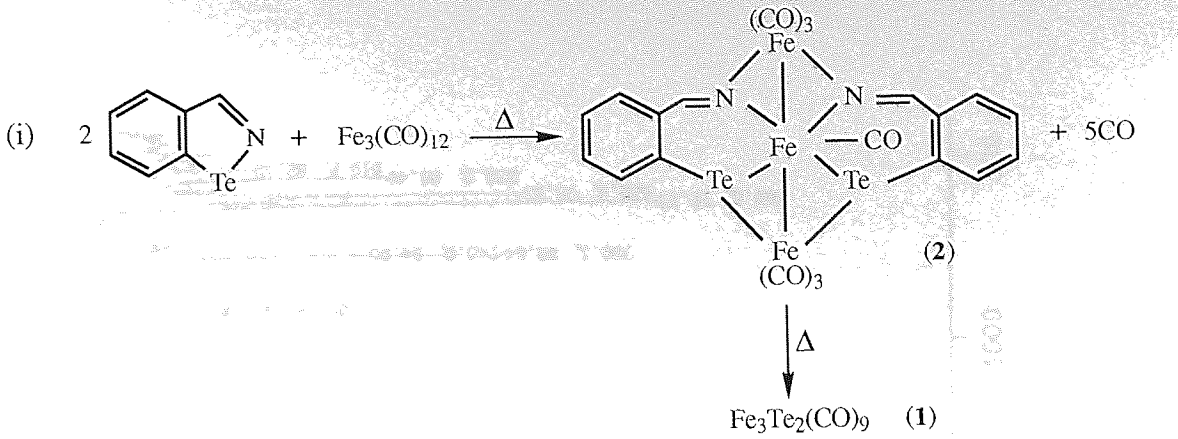

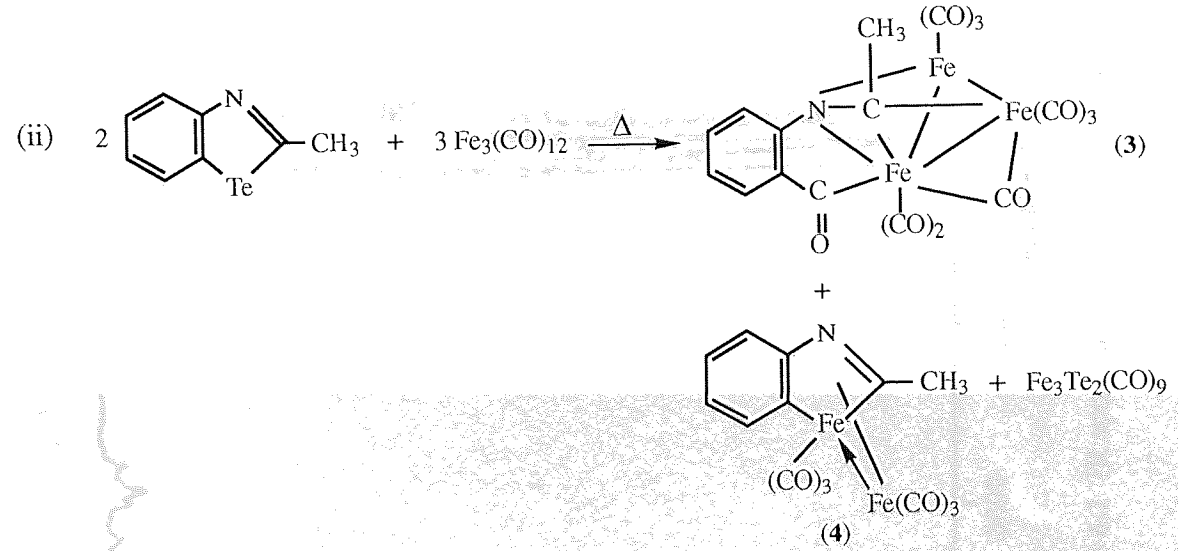

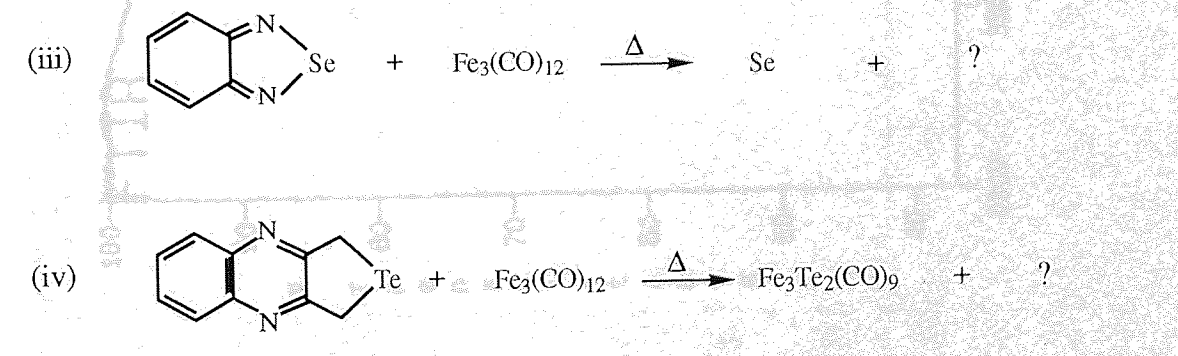

Scheme 6.5 Reactions of N-containing tellurium heterocycles with $Fe_3(CO)_{12}$

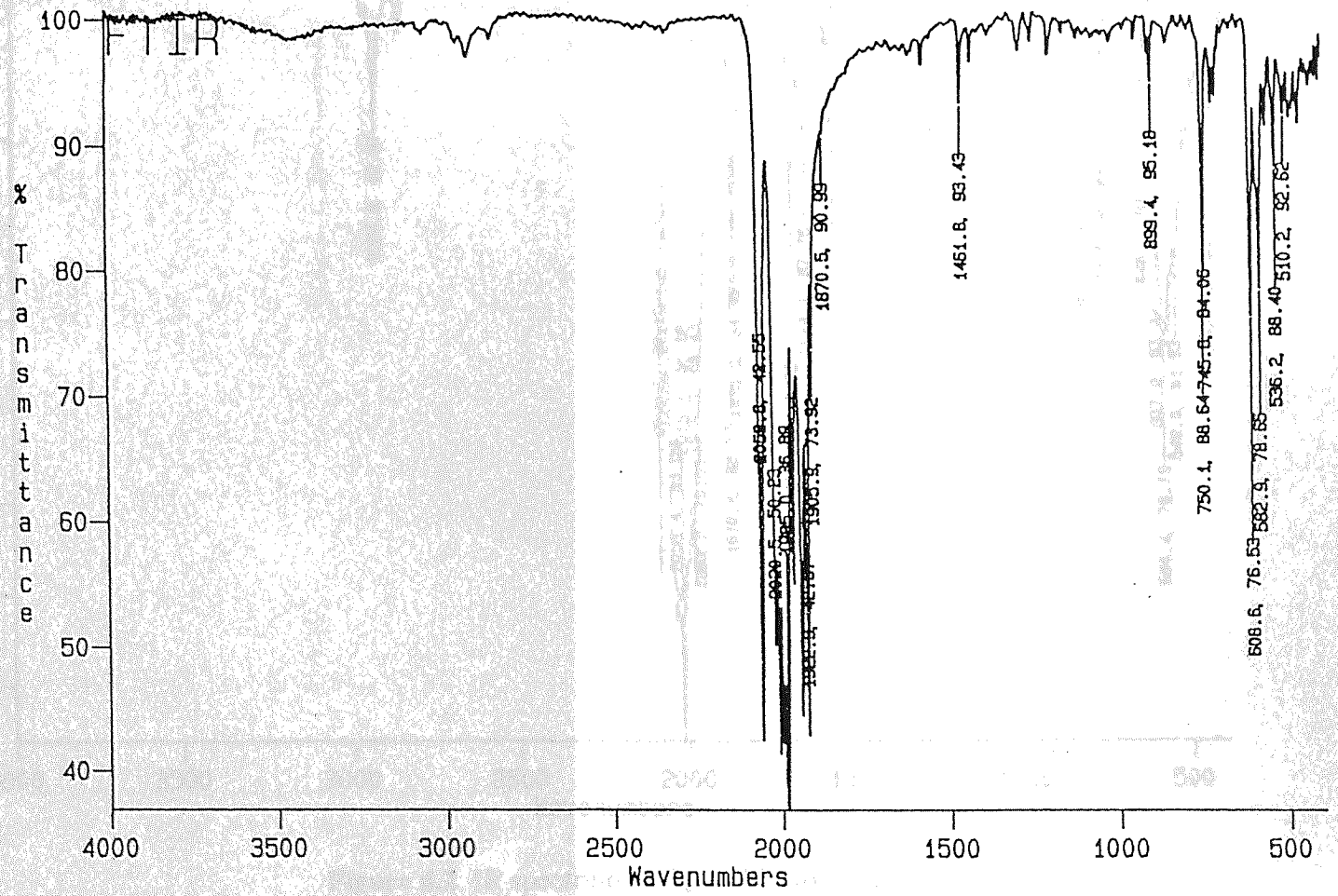

Figure 6.1 IR spectrum of $(C_6H_4CHNTe)_2.Fe_3(CO)_7$ (**2**)

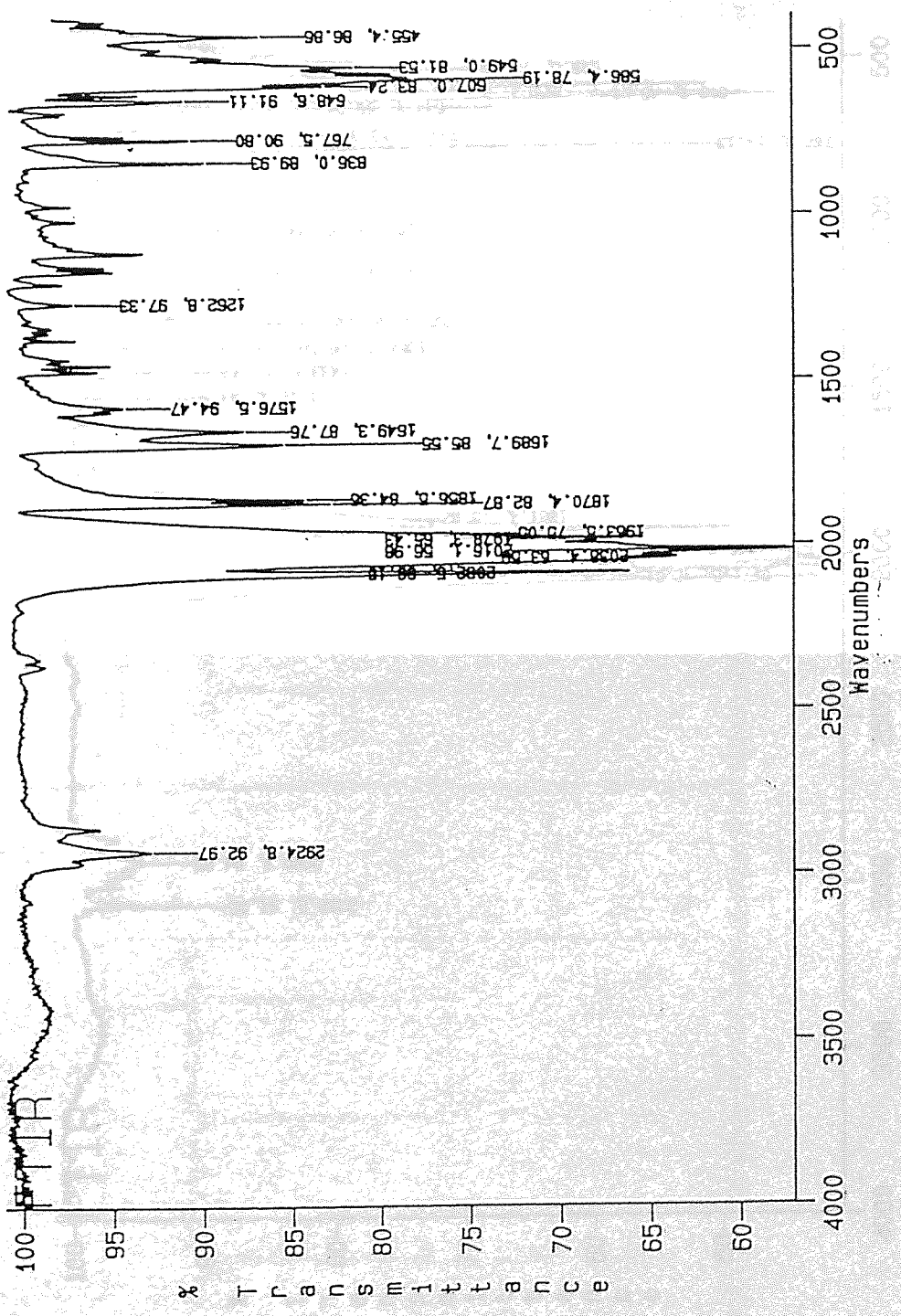

Figure 6.2 IR spectrum of $C_8H_7N.Fe_3(CO)_{10}$ (**3**)

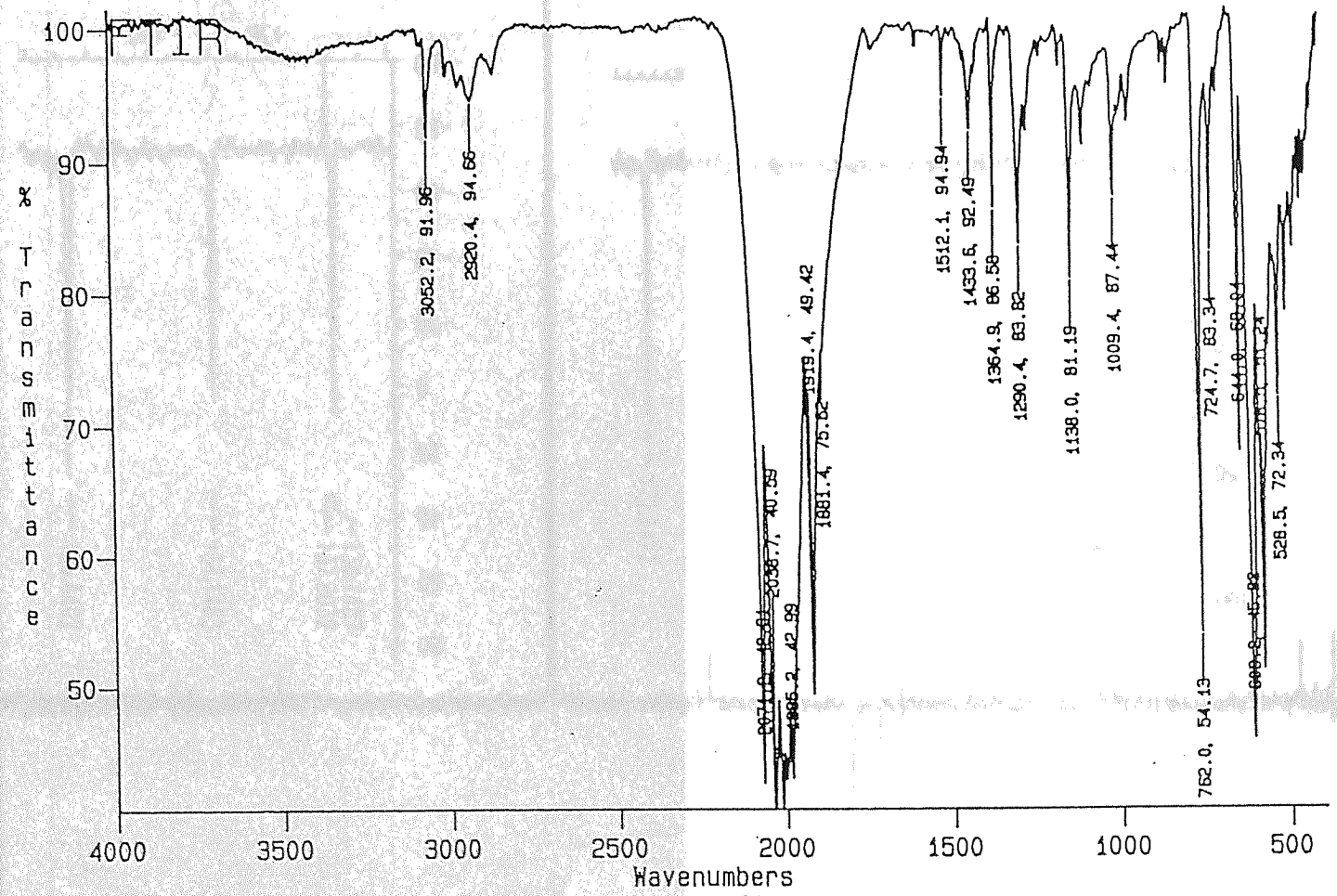

Figure 6.3 IR spectrum of $C_8H_7N.Fe_2(CO)_6$ (**4**)

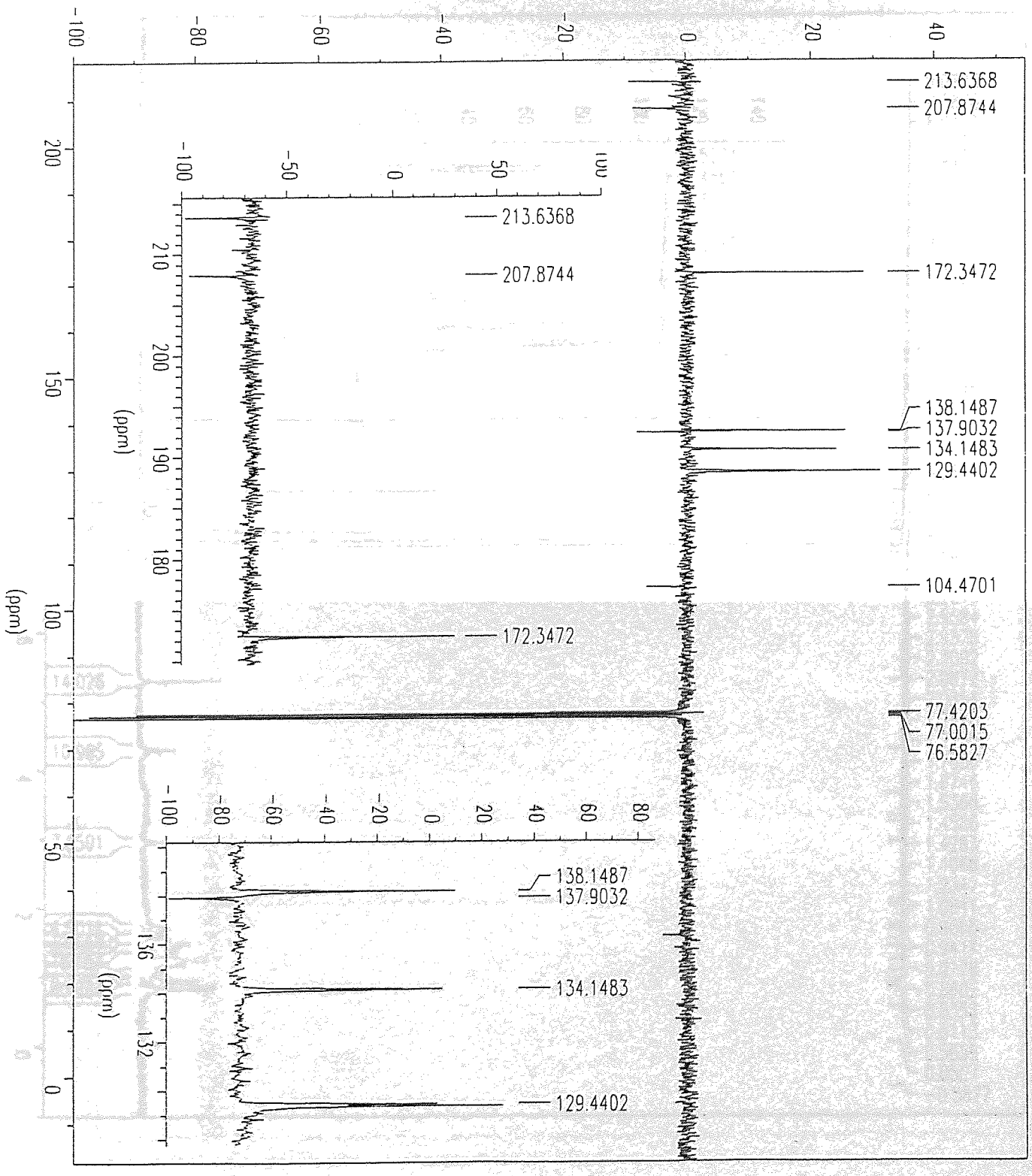

Figure 6.4 ^{13}C NMR spectrum of $(C_6H_4CHNTe)_2.Fe_3(CO)_7$ (**2**)

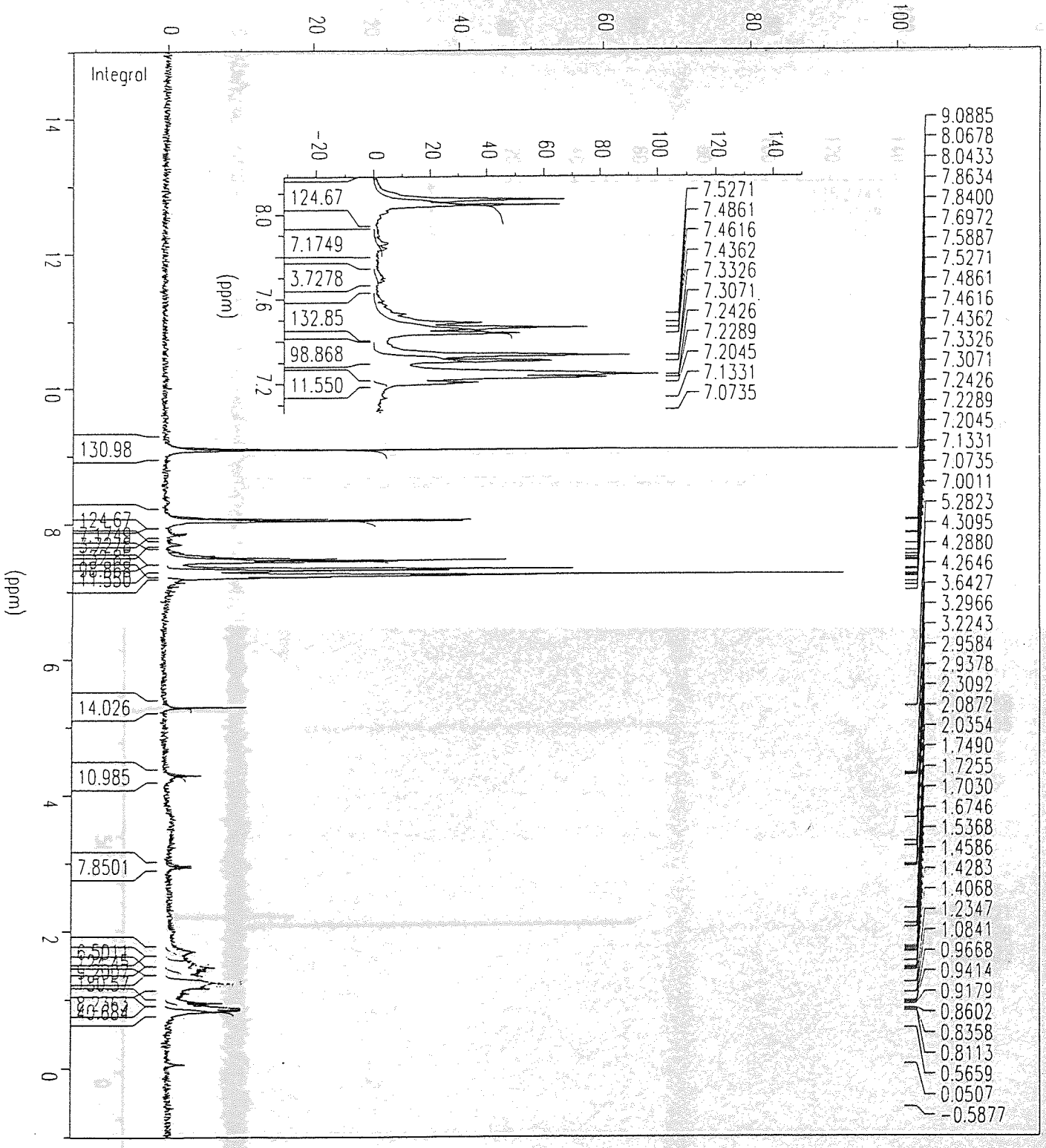

Figure 6.5 ^{1}H NMR spectrum of $(C_6H_4CHNTe)_2.Fe_3(CO)_7$ (2)

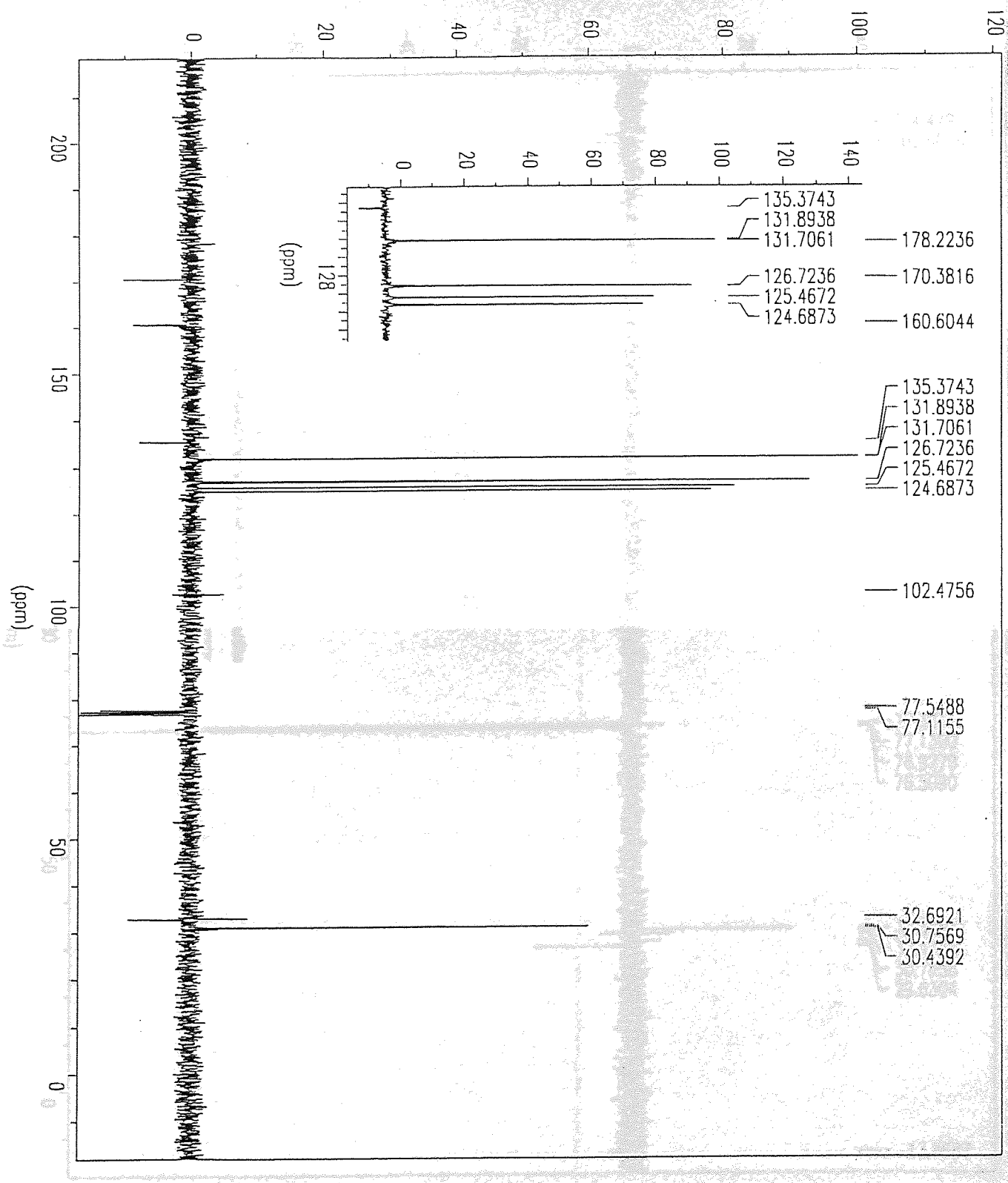

Figure 6.6 ^{13}C NMR spectrum of 2-methylbenzotellurazole

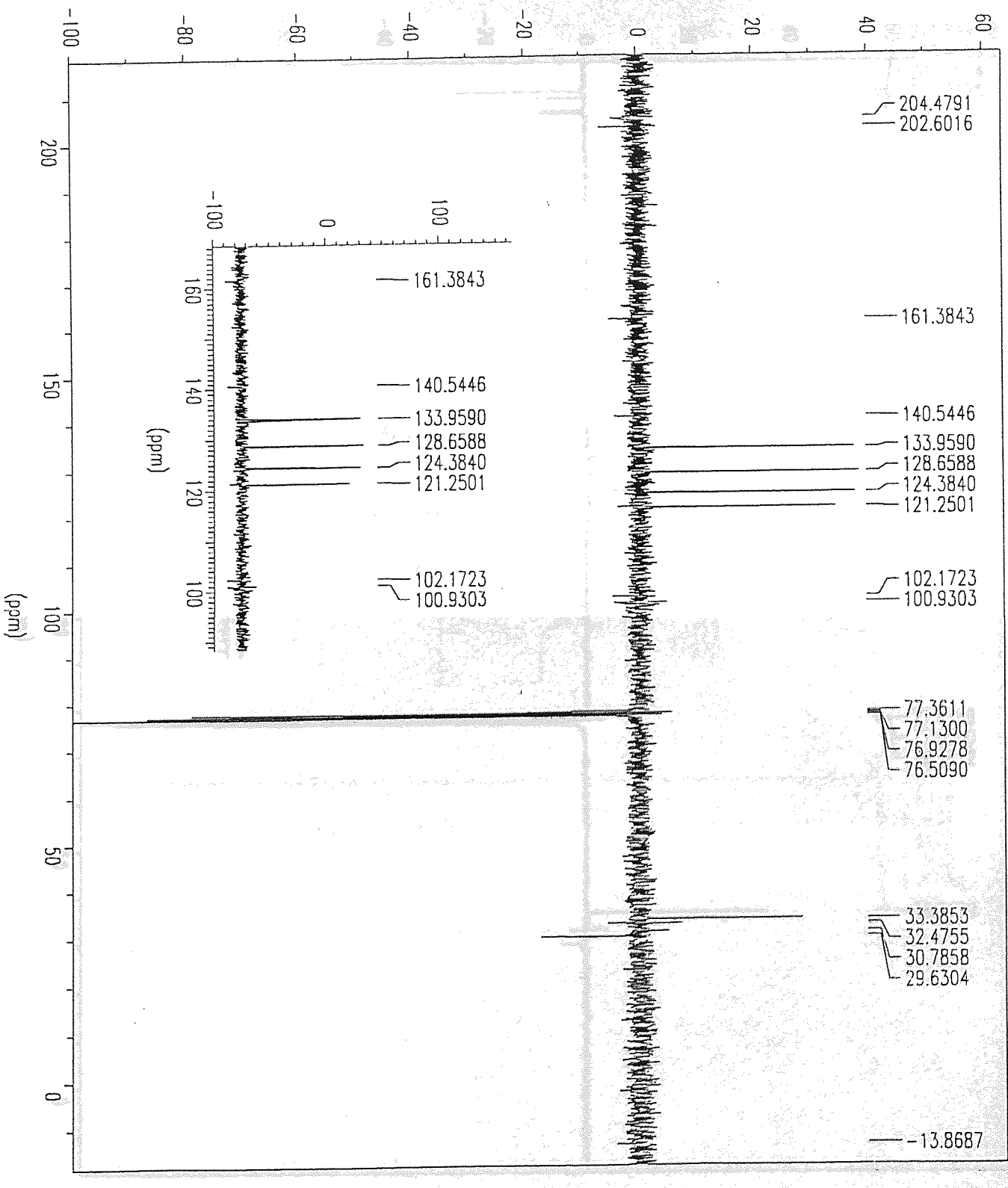

Figure 6.7 ^{13}C NMR spectrum of $C_8H_7N.Fe_3(CO)_{10}$ (3)

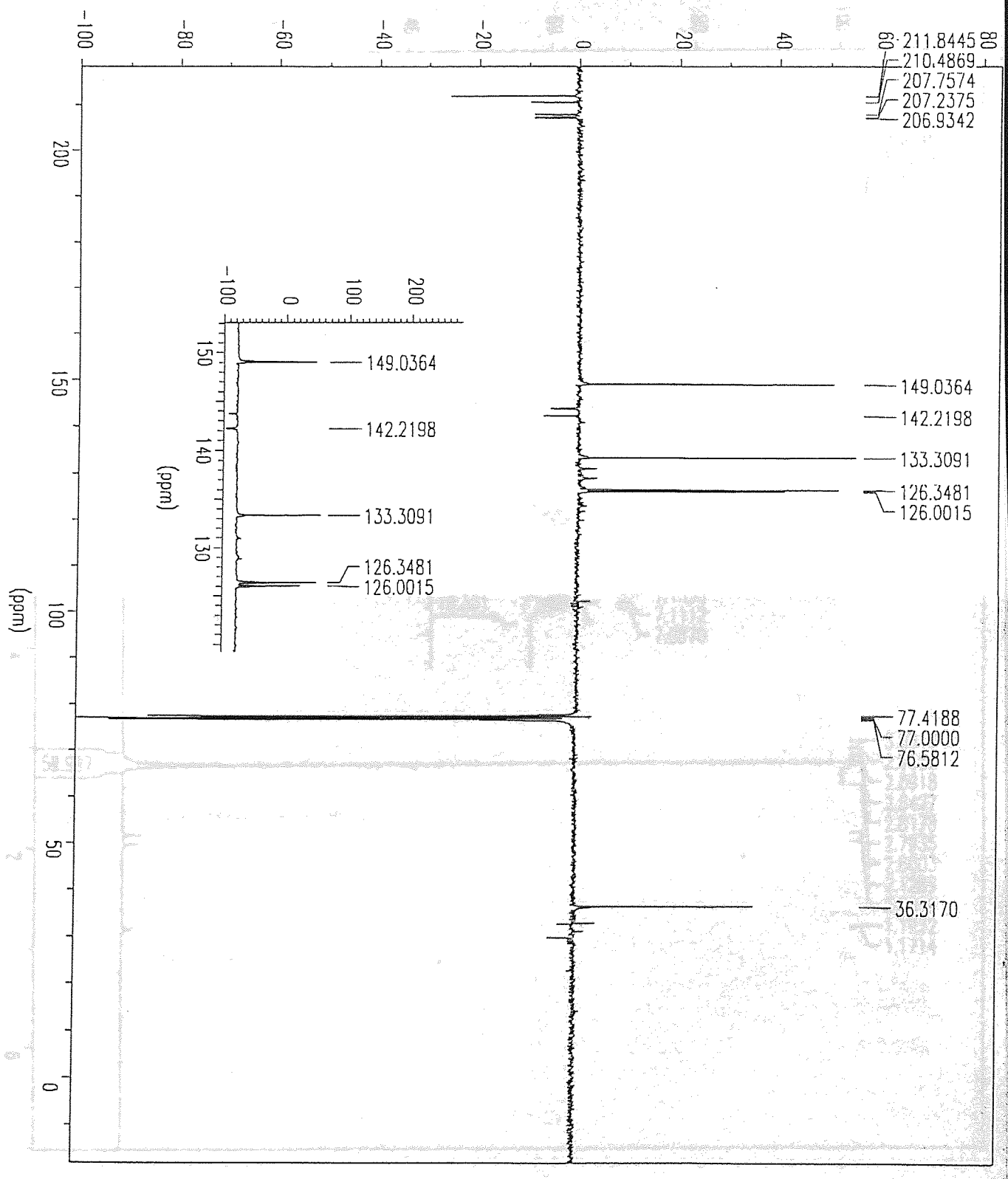

Figure 6.8 ^{13}C NMR spectrum of $C_8H_7N.Fe_2(CO)_6$ (**4**)

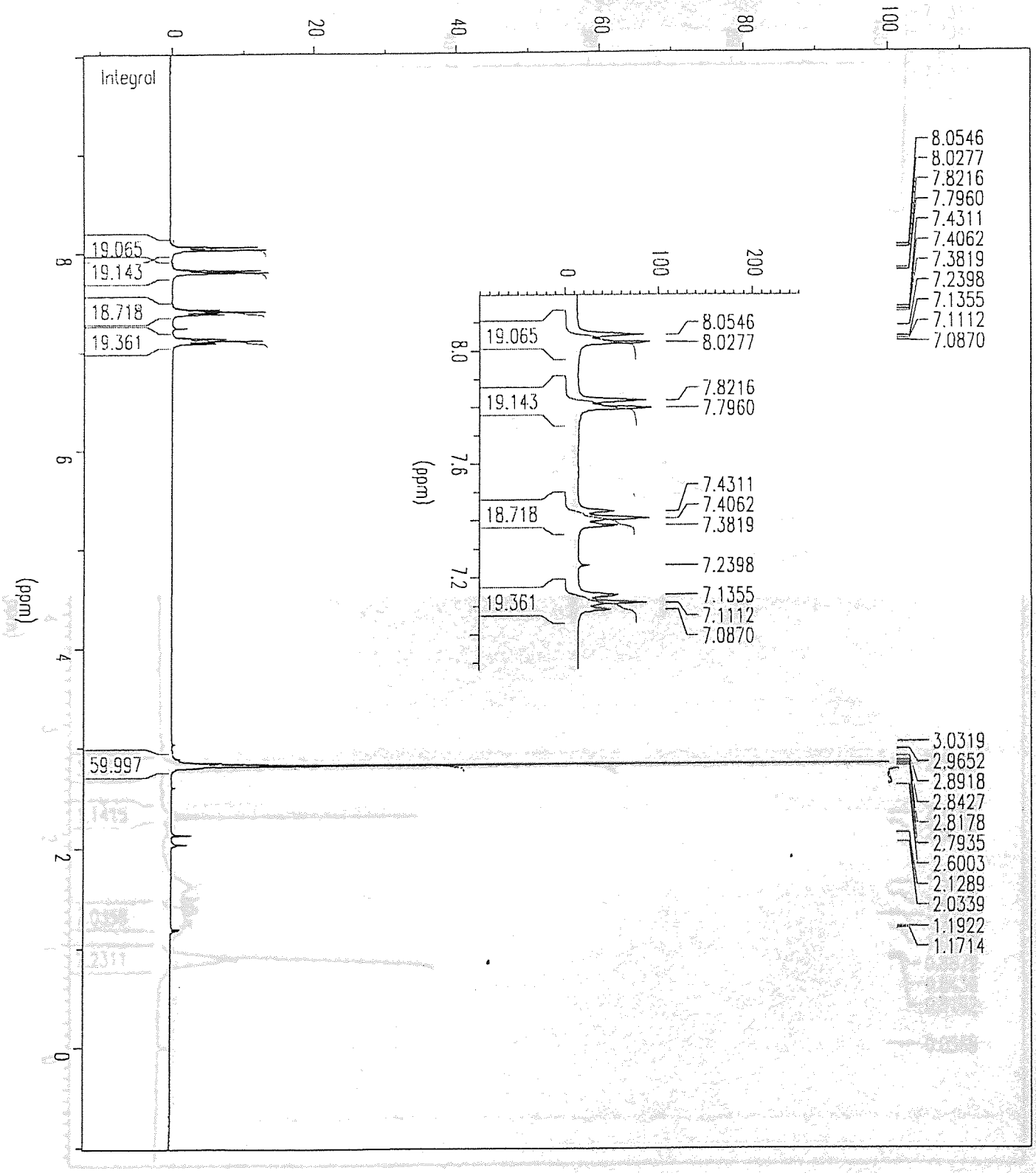

Figure 6.9 ^{1}H NMR spectrum of 2-methylbenzotellurazole

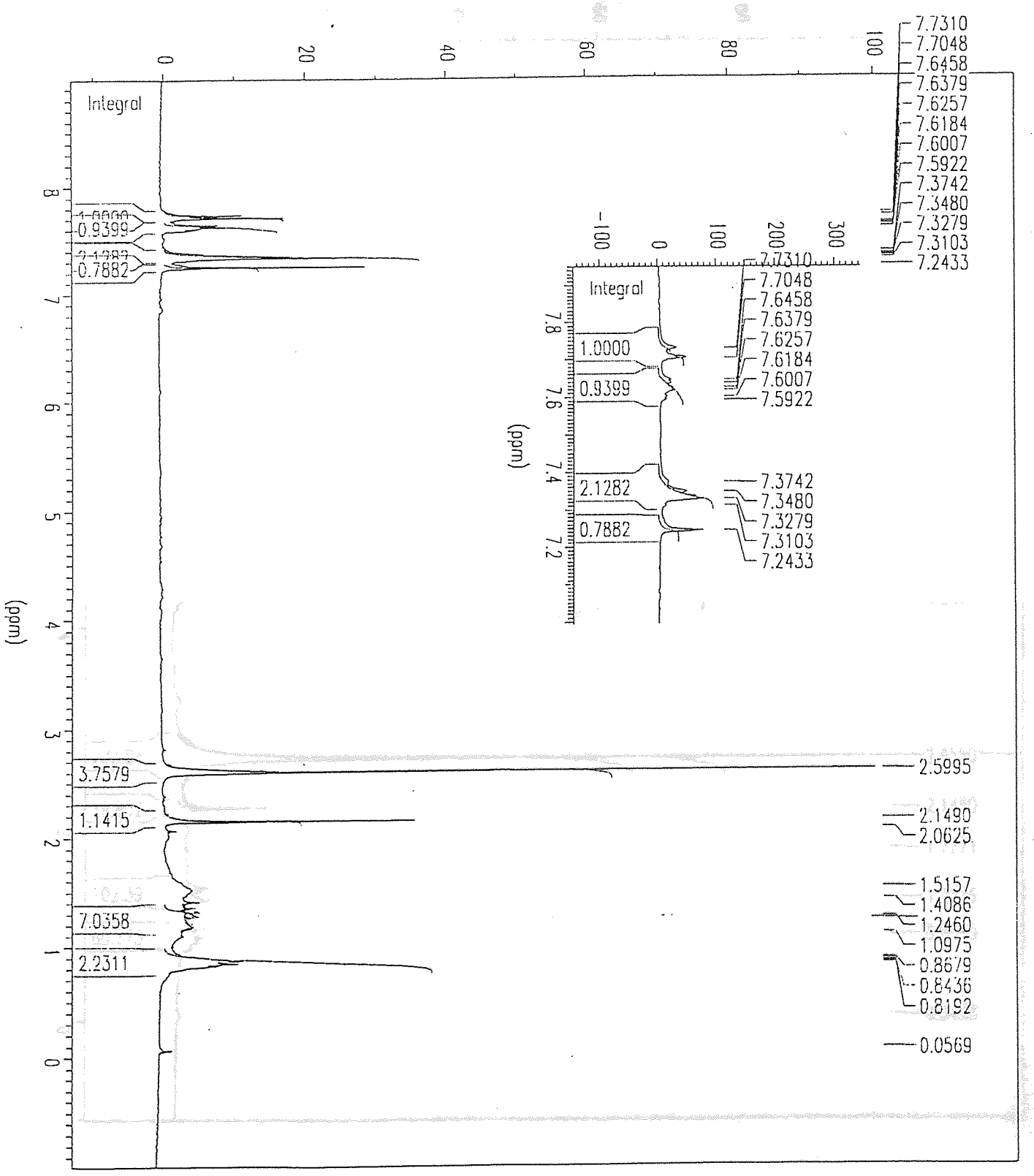

Figure 6.10 ^{1}H NMR spectrum of $C_8H_7N.Fe_3(CO)_{10}$ (3)

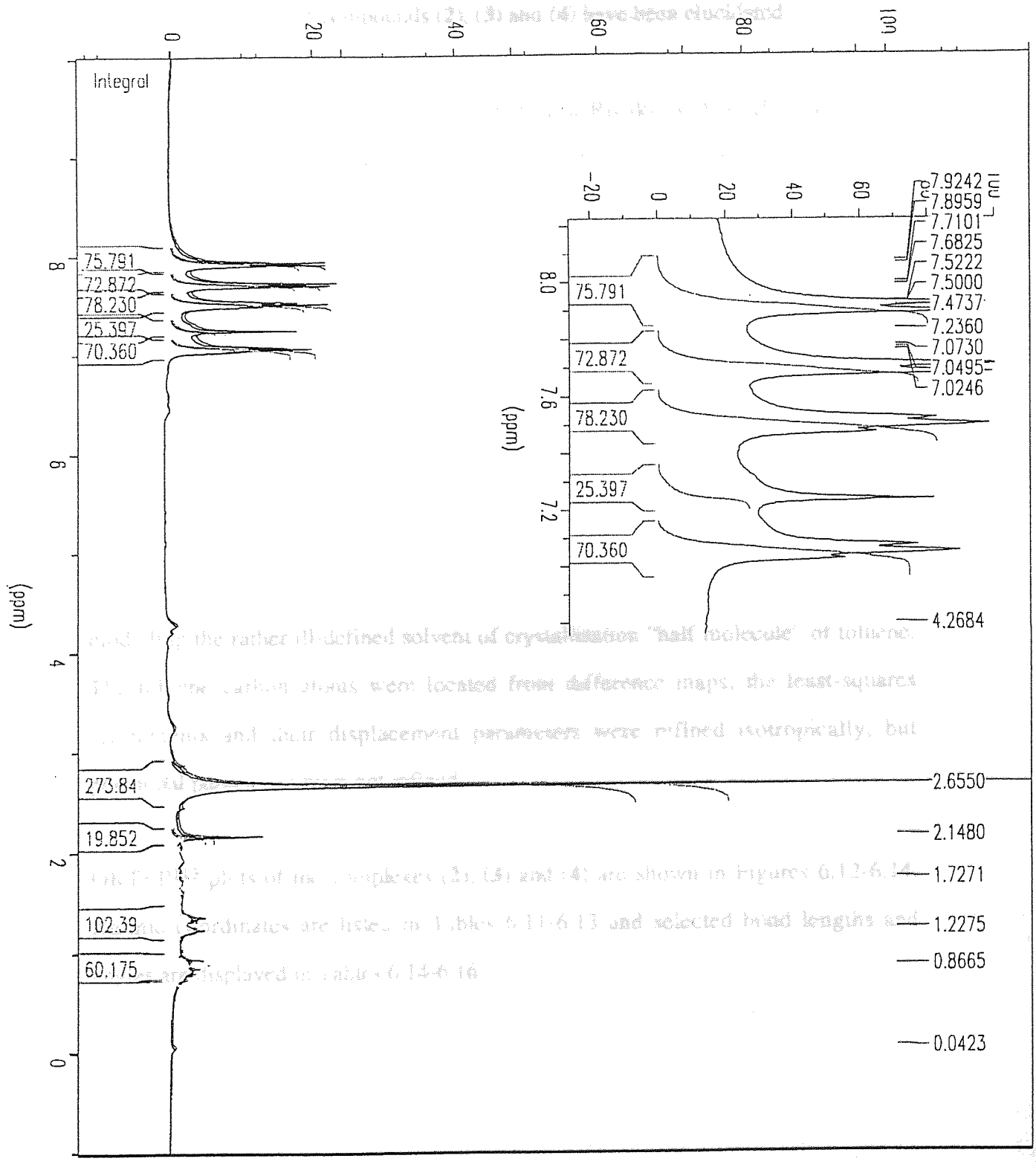

Figure 6.11 ^{1}H NMR spectrum of $C_8H_7N.Fe_2(CO)_6$ (4)

6.4 X-RAY CRYSTALLOGRAPHY

The crystal structures of compounds (**2**), (**3**) and (**4**) have been elucidated.

Data for all three structures were collected on a Rigaku R-Axis II area-detector diffractometer at 293(2)K using graphite monochromated MoK_α radiation, λ=0.71069 Å. For (**2**), (**3**) and (**4**), respectively, sixty 3°, twenty-four 8° and forty-six 4° oscillation exposures were made (f range > 180°) with crystal to detector distances of 80 mm. Absorption corrections were not applied as the crystals were nearly equi-dimensional (see Table 6.10).

The structures were determined[99] by direct methods and refined[100] on F^2 by full-matrix least squares using anisotropic displacement parameters for the non-hydrogen atoms. H atoms were placed in calculated positions. The relatively high R values and large residual electron density of structure (**2**) are probably due to difficulties in modelling the rather ill-defined solvent of crystallisation "half-molecule" of toluene. The toluene carbon atoms were located from difference maps; the least-squares refinements and their displacement parameters were refined isotropically, but positional parameters were not refined.

ORTEP[113] plots of the complexes (**2**), (**3**) and (**4**) are shown in Figures 6.12-6.14. Atomic coordinates are listed in Tables 6.11-6.13 and selected bond lengths and angles are displayed in Tables 6.14-6.16.

	(2)	(3)	(4)
Molecular formula	$C_{21}H_{10}Fe_3N_2O_7Te_2$	$C_{18}H_7Fe_3NO_{10}$	$C_{14}H_7Fe_2NO_6$
Molecular weight	825.2	564.8	396.9
Crystal system	monoclinic	triclinic	monoclinic
Space group	C2/c	P1	$P2_1/n$
Cell constants			
(Å) a	21.063(2)	10.587(3)	14.801(3)
b	15.350(1)	11.722(3)	7.148(2)
c	19.000(2)	8.640(2)	15.289(4)
(°) α	90	105.59(2)	90
β	98.49(1)	96.54(2)	109.41(2)
γ	90	90.83(2)	90
Cell Volume ($Å^3$)	6075.7(9)	1024.9(5)	1525.6(7)
Density (g cm-3)	1.905	1.830	1.728
Z	8	2	4
$\mu(MoK_\alpha)$ mm^{-1}	3.338	2.152	1.930
crystal size, mm	0.2 x 0.2 x 0.25	0.2 x 0.3 x 0.3	0.25 x 0.25 x 0.35
hkl range	+/-25, -18,17, +/-22	+/-12, +/-13, +/-10	+/-17, -7,8, -18,17
Data collection			
Angular range (°)	2-25	2-25	2-25
Unique reflns [$I>\sigma(I)$]	5221	3266	2471
variables	323	289	209
Δ/σ (max)	0.001	0.001	0.017
$\Delta\rho$, $eÅ^{-3}$	+1.54 to -1.75	+0.51 to -0.55	+0.46 to -0.67
R, wR[a]	0.1056, 0.2112	0.0561, 0.1425	0.0719, 0.1832
R, wR[a] obsd data [$I>2\sigma(I)$]	0.0686, 0.1899	0.0520, 0.1386	0.0630, 0.1672
w(a, b)[b]	0.105, 0	0.064, 2.05	0.122, 0

Table 6.10 Crystal and experimental parameters for compounds (**2**), (**3**) and (**4**)

[a]$wR = [\Sigma w(Fo^2-Fc^2)^2/\Sigma w(Fo^2)^2]^{1/2}$

[b]$w = 1/[\sigma^2(Fo^2) + (aP)^2 + bP]$ where $P = (Fo^2 + 2Fc^2)/3$

Atom	x	y	z
Te(1)	5807(1)	380(1)	5552(1)
Te(2)	5851(4)	370(1)	3773(1)
Fe(1)	7845(1)	-265(1)	5048(1)
Fe(2)	6686(1)	84(1)	4828(1)
Fe(3)	6026(1)	1584(1)	4692(1)
O(1)	8966(5)	886(8)	5257(6)
O(2)	8243(6)	-1521(7)	4041(6)
O(3)	8289(5)	-511(7)	6195(6)
O(4)	6537(6)	-1824(6)	4794(6)
O(5)	6810(7)	2577(7)	5794(6)
O(6)	4797(6)	2482(8)	4616(8)
O(7)	6578(7)	2702(7)	3711(7)
N(1)	7325(5)	341(6)	5629(5)
N(2)	7341(5)	364(6)	4286(5)
C(1)	6274(7)	853(8)	6538(6)
C(2)	5879(6)	1158(8)	7008(6)
C(3)	6137(7)	1487(9)	7644(7)
C(4)	6792(8)	21546(9)	7831(6)
C(5)	7208(6)	1259(8)	7378(6)
C(6)	6952(6)	910(7)	6705(6)
C(7)	7418(6)	617(7)	6263(6)
C(8)	6376(6)	869(8)	2996(6)
C(9)	6001(7)	1144(9)	2355(6)
C(10)	6312(7)	1533(9)	1832(7)
C(11)	6946(7)	1593(9)	1896(7)
C(12)	7326(7)	1318(9)	2512(7)
C(13)	7035(6)	929(8)	3076(6)
C(14)	7476(6)	646(7)	3699(6)
C(15)	8543(7)	415(8)	5176(7)
C(16)	8084(6)	-1028(8)	4425(7)
C(17)	8090(7)	-1031(9)	5740(7)
C(18)	6605(7)	-1074(9)	4816(7)
C(19)	6500(7)	2171(9)	5369(8)
C(20)	5268(7)	2111(9)	4627(8)
C(21)	6363(8)	2234(9)	4079(9)
C(22)	690	-345	2021
C(23)	289	-110	1146
C(24)	251	483	1095
C(25)	290	1234	1368
C(26)	650	1148	1859
C(27)	857	406	2345
C(28)	773	-944	2120

Table 6.11 Atomic coordinates (x 10^4) for complex (**2**)

Atom	x	y	z
Fe(1)	7414(1)	1717(1)	2241(1)
Fe(2)	7676(1)	3868(1)	2406(1)
Fe(3)	6502(1)	2389(1)	-264(1)
O(1)	4636(4)	1185(4)	1178(6)
O(2)	8739(5)	1149(5)	5070(6)
O(3)	5989(5)	2508(5)	5053(6)
O(4)	7381(5)	-879(4)	1655(7)
O(5)	8784(5)	5913(5)	1581(7)
O(6)	8915(5)	4604(4)	5778(5)
O(7)	5242(5)	4908(6)	3197(7)
O(8)	5854(7)	462(5)	-3286(6)
O(9)	4110(5)	3629(6)	507(9)
O(10)	7800(6)	4004(6)	-1712(7)
N(1)	8779(4)	2604(4)	1560(5)
C(1)	10035(5)	2473(5)	2290(7)
C(2)	11152(6)	2892(6)	1866(9)
C(3)	12285(6)	2778(7)	2741(10)
C(4)	12341(6)	2255(7)	3992(10)
C(5)	11249(6)	1843(6)	4441(8)
C(6)	10097(5)	1955(5)	3577(7)
C(7)	8224(5)	1826(5)	196(6)
C(8)	8946(7)	942(6)	-940(7)
C(9)	5622(6)	1568(5)	1025(7)
C(10)	8832(5)	1543(5)	3926(7)
C(11)	6555(6)	2227(5)	3964(7)
C(12)	7379(5)	127(5)	1840(7)
C(13)	8332(6)	5114(5)	1869(7)
C(14)	8426(5)	4329(5)	4474(7)
C(15)	6191(6)	4495(6)	2864(8)
C(16)	6100(7)	1198(6)	-2122(8)
C(17)	5030(7)	3158(6)	-412(9)
C(18)	7312(7)	3418(6)	-1077(7)

Table 6.12 Atomic coordinates (x 10^4) for complex (**3**)

Atom	x	y	z
Fe(1)	-1818(1)	-1680(1)	-88(1)
Fe(2)	-3339(1)	-3505(1)	-468(1)
O(1)	-124(3)	-3871(9)	994(4)
O(2)	-1098(4)	-108(11)	-1646(4)
O(3)	-1281(4)	1930(7)	804(3)
O(4)	-4948(2)	-4118(8)	-2176(3)
O(5)	-2023(3)	-5687(6)	-1118(3)
O(6)	-3882(3)	-6648(6)	482(3)
N(1)	-3781(2)	-698(6)	-366(2)
C(1)	-2500(3)	-2232(6)	796(3)
C(2)	-2170(3)	-3069(7)	1707(3)
C(3)	-2707(3)	-3074(8)	2251(3)
C(4)	-3648(3)	-2245(8)	1966(3)
C(5)	-4012(3)	-1479(7)	1117(3)
C(6)	-3434(3)	-1452(6)	528(3)
C(7)	-3106(3)	-710(7)	-784(3)
C(8)	-3423(4)	198(9)	-1730(4)
C(9)	-776(4)	-3048(9)	579(4)
C(10)	-1391(4)	-1314(11)	-1051(5)
C(11)	-1473(4)	529(9)	446(3)
C(12)	-4313(3)	-3911(8)	-1509(3)
C(13)	-2432(3)	-4642(7)	-819(3)
C(14)	-3675(3)	-5436(8)	100(3)

Table 6.13 Atomic coordinates (x 10^4) for complex (**4**)

Te(1)-C(1)	2.11(1)	Fe(2)-Fe(3)	2.68(2)
Te(1)-Fe(2)	2.506(2)	Fe(3)-C(19)	1.76(2)
Te(1)-Fe(3)	2.553(2)	Fe(3)-C(21)	1.76(2)
Te(2)-C(8)	2.11(1)	Fe(3)-C(20)	1.78(2)
Te(2)-Fe(2)	2.504(2)	O(1)-C(15)	1.14(2)
Te(2)-Fe(3)	2.543(2)	O(4)-C(18)	1.16(2)
Fe(1)-C(17)	1.78(1)	O(5)-C(19)	1.14(2)
Fe(1)-C(16)	1.79(1)	N(1)-C(7)	1.27(1)
Fe(1)-C(15)	1.79(2)	N(2)-C(14)	1.27(1)
Fe(1)-N(1)	1.907(9)	C(1)-C(2)	1.39(2)
Fe(1)-N(2)	1.92(1)	C(2)-C(3)	1.35(2)
Fe(1)-Fe(2)	2.472(2)	C(3)-C(4)	1.38(2)
Fe(2)-C(18)	1.78(1)	C(4)-C(5)	1.39(2)
Fe(2)-N(2)	1.89(1)	C(5)-C(6)	1.42(2)
Fe(2)-N(1)	1.92(1)	C(6)-C(7)	1.45(2)
C(1)-Te(1)-Fe(2)	105.3(4)	N(1)-Fe(2)-Te(1)	90.9(3)
C(1)-Te(1)-Fe(3)	102.4(3)	Te(2)-Fe(2)-Te(1)	85.30(6)
Fe(2)-Te(1)-Fe(3)	64.04(6)	Fe(1)-Fe(2)-Fe(3)	133.40(9)
C(8)-Te(2)-Fe(2)	104.1(3)	Te(2)-Fe(3)-Te(1)	83.52(6)
C(8)-Te(2)-Fe(3)	100.1(3)	C(7)-N(1)-Fe(1)	134.0(9)
N(1)-Fe(1)-N(2)	64.21(6)	C(7)-N(1)-Fe(2)	144.7(9)
N(2)-Fe(2)-N(2)	83.8(4)	Fe(1)-N(1)-Fe(2)	80.6(4)
N(2)-Fe(2)-N(1)	84.4(4)	C(14)-N(2)-Fe(2)	146.5(9)
N(2)-Fe(2)-Te(2)	90.4(3)	C(14)-N(2)-Fe(1)	131.6(9)
N(1)-Fe(2)-Te(2)	158.1(3)	Fe(2)-N(2)-Fe(1)	80.8(4)
N(2)-Fe(2)-Te(1)	156.4(3)		

Table 6.14 Selected bond lengths (Å) and angles (°) for complex(**2**)

Fe(1)-C(12)	1.801(6)	Fe(3)-C(16)	1.825(7)
Fe(1)-C(11)	1.802(6)	Fe(3)-C(9)	1.955(6)
Fe(1)-N(1)	1.999(4)	Fe(3)-C(7)	1.983(6)
Fe(2)-C(10)	2.021(6)	O(1)-C(9)	1.166(7)
Fe(2)-C(9)	2.043(6)	O(2)-C(10)	1.217(7)
Fe(2)-C(7)	2.082(5)	O(3)-C(11)	1.149(7)
Fe(1)-Fe(2)	2.496(1)	O(5)-C(13)	1.144(7)
Fe(1)-Fe(3)	2.589(1)	O(10)-C(18)	1.139(7)
Fe(2)-C(15)	1.785(6)	N(1)-C(7)	1.348(7)
Fe(2)-C(13)	1.800(6)	N(1)-C(1)	1.435(7)
Fe(2)-C(14)	1.805(6)	C(1)-C(2)	1.397(8)
Fe(2)-N(1)	1.936(4)	C(1)-C(6)	1.399(8)
Fe(2)-Fe(3)	2.647(1)	C(5)-C(6)	1.383(8)
Fe(3)-C(18)	1.801(6)	C(6)-C(10)	1.506(8)
Fe(3)-C(17)	1.820(7)	C(7)-C(8)	1.506(8)
N(1)-Fe(1)-C(7)	38.5(2)	Fe(1)-Fe(3)-Fe(2)	56.9(3)
N(1)-Fe(1)-Fe(2)	49.5(1)	C(7)-N(1)-C(1)	122.5(4)
C(7)-Fe(1)-Fe(2)	73.1(2)	C(7)-N(1)-Fe(2)	112.3(3)
N(1)-Fe(1)-Fe(3)	70.6(1)	C(1)-N(1)-Fe(2)	125.2(3)
C(7)-Fe(1)-Fe(3)	48.8(2)	C(7)-N(1)-Fe(1)	74.1(3)
Fe(2)-Fe(1)-Fe(3)	62.7(4)	C(1)-N(1)-Fe(1)	113.8(3)
N(1)-Fe(2)-Fe(1)	51.8(1)	Fe(2)-N(1)-Fe(1)	78.7(2)
N(1)-Fe(2)-Fe(3)	70.1(1)	O(1)-C(9)-Fe(3)	144.1(5)
Fe(1)-Fe(2)-Fe(3)	60.4(3)	O(1)-C(9)-Fe(1)	135.2(5)
C(7)-Fe(3)-Fe(1)	52.2(1)	O(2)-C(10)-Fe(1)	127.1(5)
C(7)-Fe(3)-Fe(2)	71.2(2)		

Table 6.15 Selected bond lengths (Å) and angles (°) for complex(**3**)

Fe(1)-C(11)	1.773(6)	O(2)-C(10)	1.140(8)
Fe(1)-C(10)	1.804(7)	O(3)-C(11)	1.131(7)
Fe(1)-C(9)	1.825(6)	O(4)-C(12)	1.144(6)
Fe(1)-C(7)	1.974(5)	O(5)-C(13)	1.147(6)
Fe(1)-C(1)	1.977(4)	O(6)-C(14)	1.143(6)
Fe(1)-C(13)	2.426(5)	N(1)-C(7)	1.354(6)
Fe(1)-Fe(2)	2.497(1)	N(1)-C(6)	1.398(6)
Fe(2)-C(12)	1.781(5)	C(1)-C(6)	1.420(6)
Fe(2)-C(14)	1.787(6)	C(1)-C(2)	1.442(6)
Fe(2)-C(13)	1.798(5)	C(2)-C(3)	1.327(7)
Fe(2)-C(7)	2.111(5)	C(3)-C(4)	1.442(7)
Fe(2)-C(1)	2.124(4)	C(4)-C(5)	1.346(7)
Fe(2)-N(1)	2.132(4)	C(5)-C(6)	1.432(7)
Fe(2)-C(6)	2.153(4)	C(7)-C(8)	1.511(7)
O(1)-C(9)	1.128(7)		
C(7)-Fe(1)-C(1)	79.5(2)	C(7)-N(1)-C(6)	111.7(4)
C(7)-Fe(1)-Fe(2)	54.8(1)	C(7)-N(1)-Fe(2)	70.5(3)
C(1)-Fe(1)-Fe(2)	55.2(1)	C(6)-N(1)-Fe(2)	71.7(2)
C(7)-Fe(2)-N(1)	37.2(2)	C(6)-C(1)-Fe(1)	113.2(3)
C(1)-Fe(2)-C(6)	38.8(2)	N(1)-C(6)-C(1)	116.1(4)
N(1)-Fe(2)-C(6)	38.1(2)	N(1)-C(7)-Fe(1)	118.7(3)
C(7)-Fe(2)-Fe(1)	49.9(1)	O(5)-C(13)-Fe(2)	163.5(4)
C(1)-Fe(2)-Fe(1)	49.9(1)	O(5)-C(13)-Fe(1)	125.8(4)

Table 6.16 Bond lengths (Å) and selected angles (°) for complex(**4**)

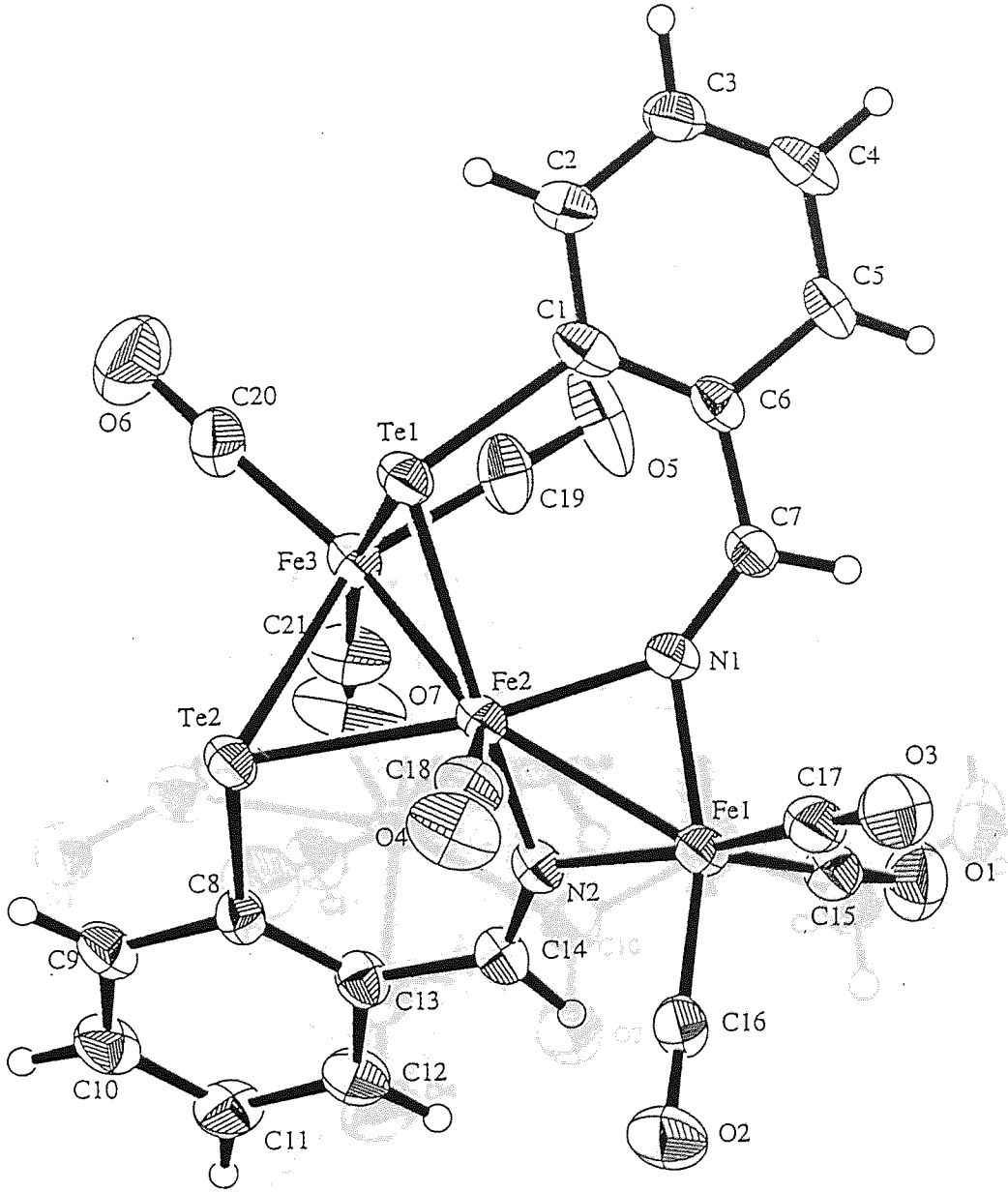

Figure 6.12 The molecular structure of $(C_6H_4CHNTe)_2.Fe_3(CO)_7$ (**2**)

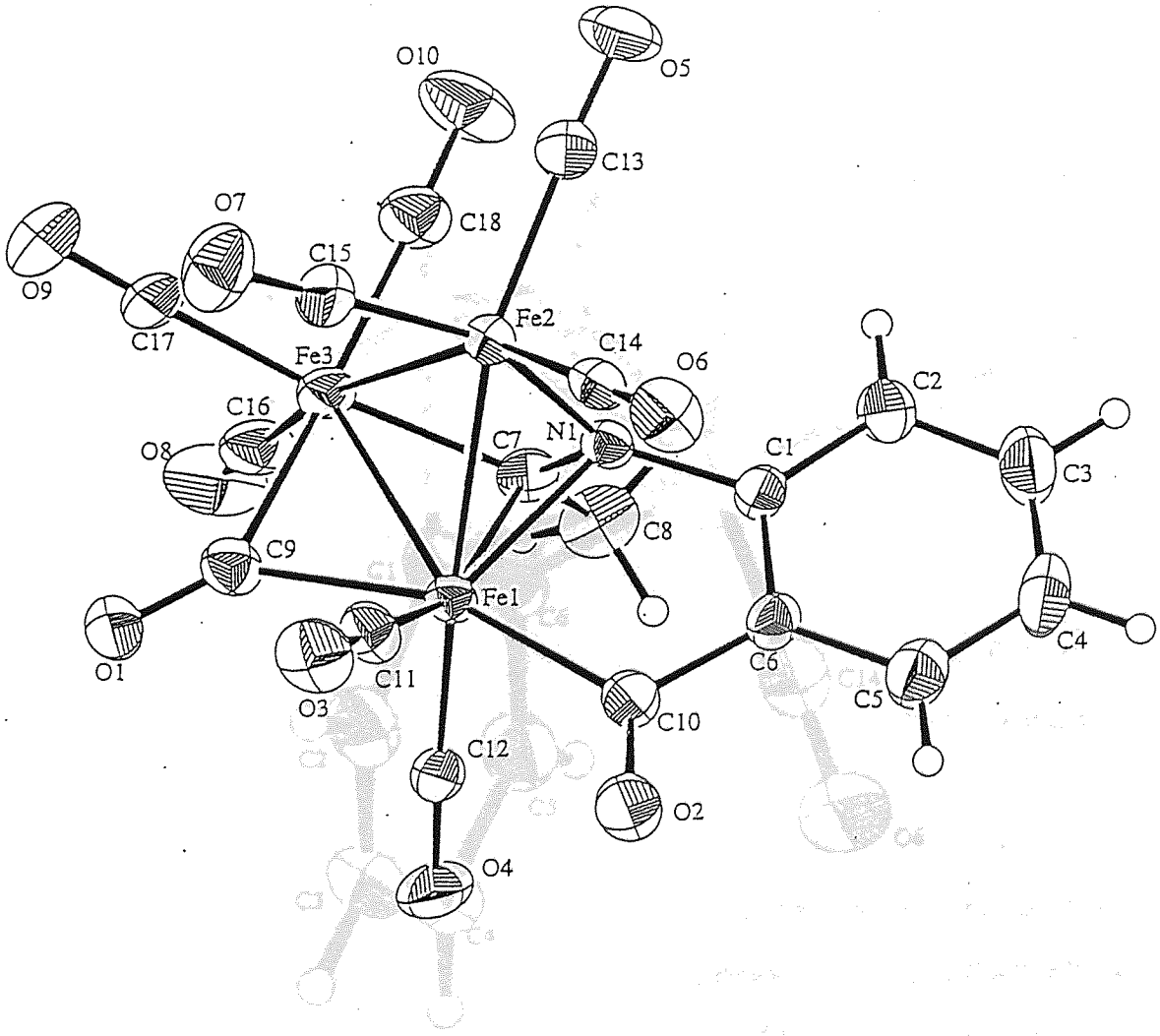

Figure 6.13 The molecular structure of $C_8H_7N.Fe_3(CO)_{10}$ (3)

Figure 6.14 The molecular structure of $C_8H_7N.Fe_2(CO)_6$ (4)

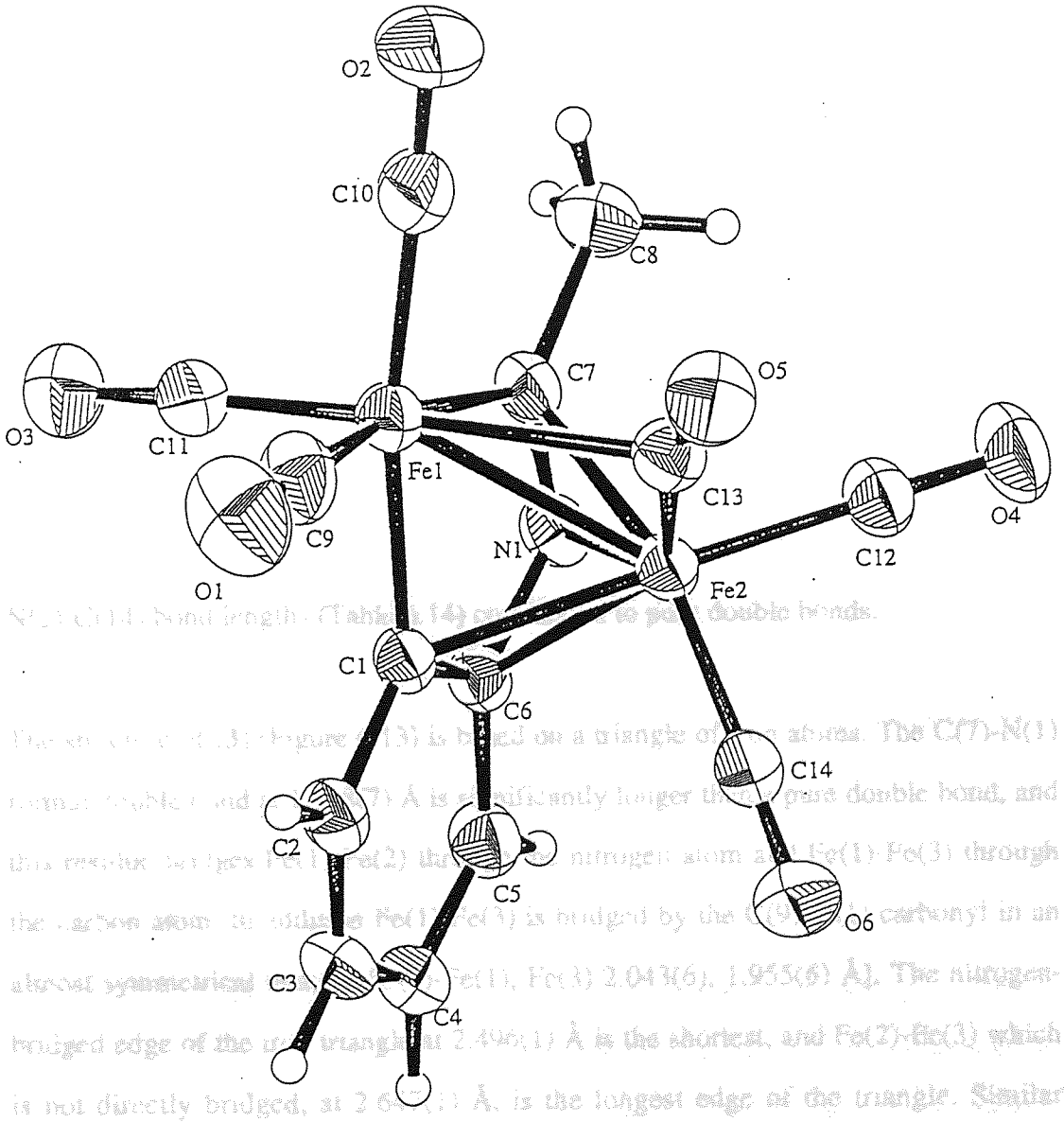

Figure 6.14 The molecular structure of $C_8H_7N.Fe_2(CO)_6$ (**4**)

6.4.1 Structural studies of complexes (2), (3) and (4)

The molecular structure of (**2**) (Figure 6.12) contains a non-linear chain of three iron atoms, angle Fe(1)-Fe(2)-Fe(3) 133.4(1)°, Fe(1)-Fe(2), length 2.472(2) Å, doubly bridged by nitrogen and Fe(2)-Fe(3), length 2.683(2) Å, doubly bridged by tellurium. Fe(1) and Fe(3) show 6-coordination, whereas the central iron, Fe(2), is 7-coordinate. There is no comparable system in the structural literature[125] involving single or double bridging by nitrogen and tellurium of adjacent iron atoms of a three-atom chain. In an example of single bridging by tellurium in $Fe_3(CO)_8(\mu_3\text{-}^iPrP)[\mu_2\text{-}Te(PhMe_3)]_2$,[126] the Fe-Fe distances are 2.666(2) and 2.768(2) Å with Fe-Te in the range 2.527-2.571 Å. Here however, the Fe-Fe-Fe angle is 94.2°, presumably to allow (μ_3-^{i}PrP) coordination. A selection of 11 Fe-Fe bonds doubly bridged by tellurium, extracted from the CSD,[125] show a mean length of 2.611(7) Å with Fe-Te 2.549(2) Å, and 23 Fe-Fe bonds doubly bridged by nitrogen average 2.498(29) Å with Fe-N 1.939(11) Å. These values are comparable to those found in (**2**). The N(1)-C(7) and N(2)-C(14) bond lengths (Table 6.14) correspond to pure double bonds.

The structure of (**3**) (Figure 6.13) is based on a triangle of iron atoms. The C(7)-N(1) formal double bond at 1.348(7) Å is significantly longer than a pure double bond, and this residue bridges Fe(1)-Fe(2) through the nitrogen atom and Fe(1)-Fe(3) through the carbon atom. In addition Fe(1)-Fe(3) is bridged by the C(9)-O(1) carbonyl in an almost symmetrical manner [C(9)-Fe(1), Fe(3) 2.043(6), 1.955(6) Å]. The nitrogen-bridged edge of the iron triangle at 2.496(1) Å is the shortest, and Fe(2)-Fe(3) which is not directly bridged, at 2.647(1) Å, is the longest edge of the triangle. Similar variations in Fe-Fe bond distances have been noted in other Fe_3 triangles.[127,128] Fe(1) shows apparent 8-fold coordination, involving two iron atoms, a nitrogen and five carbon atoms (relevant distances in Table 6.15). Of these the C(7)=N(1) residue may be considered to be π-bonded, whereas the other six atoms are essentially σ-bonded. Seven-coordination of iron, via five σ-bonds to two iron atoms, a bridging nitrogen

and two bridging carbonyls, and two π-bonds to a 1,3-cyclohexadiene residue occurs in $Fe_3(\mu_3\text{-NPh})(\eta^4\text{-}C_6H_8)(CO)_8$.[129]

In (**4**) (Figure 6.14), one iron atom, Fe(1), forms part of a benzoferrazole system, and the second iron, Fe(2), is π-bonded to the C(1)-C(6)-N(1)-C(7) residue of the ferrazole. Here the C(1)-C(6) aromatic bond is lengthened to 1.420(6) Å, the central C-N single bond is shortened to 1.398(6) Å and the N(1)-C(7) formal double bond lengthened to 1.354(6) Å. The Fe-Fe distance is relatively short at 2.498(1) Å. In addition the Fe(2)-C(13)-O(5) carbonyl group forms a weak bridge to Fe(1) [Fe(1)-C(13) 2.426(5), Fe(2)-C(13) 1.798(5) Å, angles O(5)-C(13)-Fe(1), Fe(2) 125.8(4), 163.5(4)°]. If the Fe(1)-C(13) interaction is considered to be significant, Fe(1) exhibits 7-coordination. A search of the CSD[125] indicates no examples of previous X-ray structure determinations of benzoferrazole systems. However in two analogous ferrole complexes[130] and a dibenzoferrole,[96] Fe-C(σ) bond lengths are in the range 1.921-2.039, mean 1.984(19) Å, Fe-C(π) lengths are 2.035-2.216, mean 2.125(15) Å, and Fe-Fe 2.466(1), 2.567(1) and 2.468(1) Å, similar to the lengths found in (**4**), and in the 3-ferra-4-pyrrolin-2-one complex, $Fe_2(\mu\text{-CH=CHNPhC\{O\}})(CO)_6$, Fe-Fe is 2.597 Å.[131]

6.5 CONCLUSIONS

The reactions of N-containing tellurium heterocycles with iron carbonyl give access to novel organometallic compounds which possess some unique structural features, as determined crystallographically. Reactions with rhodium and molybdenum organometallics appear to be less successful in yielding new organometallics than previously observed with the tellurophenes.

Benzisotellurazole reacts with $Fe_3(CO)_{12}$ to afford a novel dimeric compound (**2**) in which the tellurium is retained and the central iron atom is located in a unique seven coordinate environment. No comparable system in the structural literature can be

found involving nitrogen, tellurium and iron. The formation of this dimer is comparable to the formation of benzothiaferrole from the reaction of benzothiophene with $Fe_3(CO)_{12}$.[53] In both cases the heterocycle is attacked at the heteroatom-carbon bond remote from the aryl ring. Furthermore, as previously noted, the reaction of 2-telluraindane with the iron carbonyl also leads to a dimerisation reaction but in contrast to benzisotellurazole, tellurium is eliminated leading to *unsymmetric* coupling of the two C_8H_8 fragments.[96]

2-methylbenzotellurazole behaves more like the tellurophenes, in both cases the tellurium atom being bonded to two carbons as part of an aromatic system. Hence, reaction with $Fe_3(CO)_{12}$ leads to detelluration of the heterocycle with the end product (**4**) resembling the ferroles obtained from the tellurophenes. In addition, a second product (**3**) is also obtained in which the triangular arrangement of iron atoms is retained. This again displays some unprecedented structural features, of particular note being the coordination environments of the three iron atoms. Fe(1) shows apparent eight-fold coordination, involving two iron atoms, a nitrogen and five carbons, while Fe(2) and Fe(3) exhibit six and seven-fold coordination environments respectively. It is therefore clear that these heterocycles containing both tellurium and nitrogen act as precursors for novel organometallic systems of iron.

Heterocycles containing more than one nitrogen atom are less successful in producing new organometallic compounds. Although detelluration (and deselenation) reactions are observed, recovery of the organic residue of the heterocycle is difficult. One reason suggested for this is that following detelluration, the close proximity of two nitrogens may lead to the release of dinitrogen from the heterocyclic ring resulting in the formation of volatile or unstable organic liquids.

REFERENCES

References

1. W. S. Kyte, "Desulfurisation of coal combustion systems", Hemisphere Publishing Corp., New York, 1989, p. 19.
2. W. S. Kyte, "Desulfurisation of coal combustion systems", Hemisphere Publishing Corp., New York, 1977, p. 19-24.
3. R. A. Meyers, "Coal desulfurisation", Marcell Decker, New York, 1977, p. 3.
4. British Standards Institution, BS 1016: Part 6, 1977.
5. British Standards Institution, BS 1016: Part 11, 1977.
6. American Society for Testing and Materials, D2492, 1988.
7. American Society for Testing and Materials, D3177, 1988.
8. L. M. Stock, R. Wolny and B Bal, "Sulfur distribution in American bituminous coals", *Energy and Fuels*, 1989 3, 651-661.
9. W. Mellors, " A Comprehensive Treatise on Inorganic and Theoretical Chemistry, 14, Wiley, New York, 1961.
10. H. J. Gluskoter and J. A. Simon, *American Chemical Society, Division of Fuel Chemistry, Preprints,* 1964, 8, 159.
11. H. H. Scobert, "Chemical utilisation of coal", Ed. Y. Yurum. NATO ASI Series C, 1992, 370.
12. X. D. Hu, L. Zhang, S. M. Cui, Z. H. Whang and J. S. Gao, "Study on chemical stability of organic sulfur in coal and its structure", *Fuel Science and Technology International*, 1995, 13(2) 161-177.
13. S. Lee, P. Vishnubhatt and C. J. Kulik, "Selective removal of sulfur from coal by trichloroethane extraction", *Fuel Science and Technology International*, 1994, 12(2), 211-228.
14. G. González Benito, G. Osario and D. Bonilla, "Biological sulfur removal by *Thiobacillus thioxidans* in fine coal coming from a flotation washing plant", *Coal Science*, 1995, 24, 1745-1748.

15 G. Olsson, O. Holst and H. T. Karlson, "Microbial desulfurisation of different coal types", *Coal Science*, 1995, 24, 1741-1744.

16 G. D. Galpern, "Thiophene and its derivatives", S. Gronowitz (Ed), Wiley, New York, 1986, 44(1), p. 325.

17. S. Harris and R. R. Chianelli, "Catalysis by transition metal sulfides - the relationship between calculated electronic trends and hydrodesulfurisation reactivity", *J. Catal*, 1984, 86, 400-412.

18. M. G. Choi and R. J. Angelici, "Reaction of sulfur-coordinated thiophene in $Cp^*Re(CO)_2(C_4H_4S)$ to give the thiophene-bridged $Cp^*Re(CO)_2(\mu\text{-}C_4H_4S)Fe(CO)_3$", *J. Am. Chem. Soc.*, 1989, 111, 8753-8754.

19. N. Kuhn and H. Schumann, "Cyclopentadienyl-iron complexes with R_2E ligands (E = S, Se, Te) - synthesis and spectroscopic classification", *J. Organomet. Chem.*, 1984, 276, 55-66.

20. J. Goodrich, P. N. Nickias and J. P. Selegue, "Synthesis, structure and reactivity of $CpFe(CO)_2(DBT)(BF_4)$ and related S-bonded thiophene complexes", *Inorg. Chem.* 1987, 26, 3424-3426.

21. R. J. Angelici and J. W. Benson, "Equilibrium and kinetic studies of sulfur-coordinated thiophenes (Th) in $Cp(CO)_2Ru(\eta^1\text{-}(S)\text{-}Th)^+$ and $Cp(CO)_2Ru(\eta^1\text{-}(S)\text{-}Th)^+$ - models for thiophene adsorption on HDS catalysts", *Organometallics*, 1993, 12, 680-687.

22. R. J. Angelici and J. W. Benson, "Reactions of 2-benzothienyl complexes with acid to give $Cp(PMe_3)_2Ru(\eta^1\text{-}(S)\text{-}BT)^+$ and $Cp(CO)(PPh_3)Ru(\eta^1\text{-}(S)\text{-}BT)^+$ - a model for benzothiophene deuterium exchange in HDS catalysts", *Inorg. Chem.*, 1993, 32, 1871-1874.

23. D. Lingzehn, B. Duckett. K. F. Ohman and W. D. Jones, "A model for homogeneous HDS - the importance of η^2-coordination and sulfur coordination in C-H and C-S bond cleavage reactions of thiophene", *J. Am. Chem. Soc.*, 1992, 114, 151-160.

24. M. H. Chisolm, S. T. Haubrich, J. D. Martin and W. E. Streib, "Stepwise activation of σ-thienyl ligands at ditungsten centres", *J. Chem. Soc., Chem. Commun.*, 1994, 683-684.

25. E. O. Fischer and K. Öfele, *Chem. Ber.*, 1958, 91, 2395.

26. H. Singer, *J. Organomet. Chem.*, "Thiophene-manganesetricarbonyl complex", 1967, 9, 135-140.

27. C. C. Lee, M. Iqbal, and R. G. Sutherland, "Ligand exchange reactions with η^6-arene-η^5-cyclopentadienyliron cations under thermal or photochemical conditions", *J. Organomet. Chem*, 1985, 288, 89-96.

28. M. Draganjac, C. J. Ruffing and T. B. Rauchfuss, "A model for chemisorption - A stabilised η^1-S-thiophene complex and its relationship to η^5-coordination", *Organometallics*, 1985, 4, 1909-1911.

29. (a) M. J. H. Russel, C. WhiteA. Yates and P. M. Maitlis, "Tetramethylthiophene complexes of rhodium, iridium, palladium and ruthenium", *J. Chem. Soc., Dalton Trans.*, 1978, 857-861.
(b) R. Sanchez-Delgaldo, R. L. Marquez-Silva, J. Puga, A. Tripicchio and M. Camellini, "Organometallic models for the HDS reaction - synthesis of [(η-thiophene)M(PPh_3)$_2$] (M = Rh, Ir) and X-ray structure of the Rh derivatives; the first example of a fully characterised π-thiophene complex of an HDS active metal", *J. Organomet. Chem.*, 1986, 316, C35-C38.

30. R. Cordone, W. B. Harman, and H. Taube, "π-heterocyclic complexes of pentammineosmium(II) and the metal-induced cycloaddition of pyrrole and maleic anhydride", *J. Am. Chem. Soc.*, 1989, 111, 5969-5970.

31. (a) T. A. Manuel and T. J. Meyer, "Iron carbonyl derivatives of 2,2'-dithienyl and o-aminobenzenethiol", *Inorg. Chem.*, 1964, 3, 1049-1051.

32. W. D. Jones and L. Dong, "Insertion of rhodium into the C-S bond of thiophene - mechanism of a model for the HDS reaction", *J. Am. Chem. Soc.*, 1991, 113, 559-564.

33. J. Chen, L. M. Daniels and R. J. Angelici, "New modes of thiophene coordination and reactivity - structures of $Cp^*Ir(\eta^2$-thiophene), and iridathiabenzene and $Cp^*Ir(\eta^4$-thiophene.$BH_3)$", *J. Am. Chem. Soc.*, 1990, 112, 199-204.

34. S. C. Huckett and R. J. Angelici, "HDS model complexes - nucleophilic addition to π-coordinated benzothiophene and thiophene", *Organometallics*, 1988, 7, 1491-1500.

35. A. E. Ogilvy, A. E. Skaugset and T. B. Rauchfuss, "Electron transfer activation of coordinated thiophene - preparation and desulfurisation of $Cp^*Rh(\eta^4$-$C_4Me_4S)$", *Organometallics*, 1989, 8, 2739-2741.

36. J. Chen and R. J. Angelici, "An η^4-thiophene ligand - a new mode of thiophene coordination in $Cp^*Rh(\eta^4$-2,5-dimethylthiophene)", *Organometallics*, 1989, 8, 2277-2279.

37. D. A. Lesch, J. W. Richardson, R. A. Jacobson and R. J. Angelici, "Reactions of the π-thiophene ligand in $(\eta^4$-$C_4H_4S)Mn(CO)_3$ - mechanistic possibilities for catalytic HDS", *J. Am. Chem. Soc.*, 1984, 106, 2901-2906.

38. G. H. Spies and R. J. Angelici, "Model studies of thiophene HDS using (η-thiophene)$Ru(\eta^5$-$C_5H_5)$ - reactions leading to C-S bond-cleavage", *Organometallics*, 1987, 6, 1897-1903.

39. S. Luo, A. E. Ogilvy, T. B. Rauchfuss, A. L. Rheingold and S. R. Wilson, "Thermolysis of $Cp^*Rh\{\eta^4:\eta^1$-$C_4Me_4S)Fe(CO)_4\}$: A case study in thiophene desulfurisation", *Organometallics*, 1991, 10, 1002-1009.

40. X. Ma, K. Sakanishi, T. Isoda and I. Mochida, "Quantum chemical calculation on the desulfurisation reactivities of heterocyclic sulfur compounds", *Energy and fuels*, 1995, 9, 33-37.

41. J. R. Gillespie, A. E. A. Porter and W. E. Willmont, "Reaction of activated arenes with 2,5-dichlorothiophenium bis(methoxycarbonylmethylide), *J. Chem. Soc., Chem. Commun.*, 1979, 50-51.

42. S. M. Bucknor, M. Draganjac, T. B. Rauchfuss, C. J. Ruffing, W. C. Fultz and A. L. Rheingold, "Synthesis and structure of a stable complex featuring an S-bound dibenzothiophene ligand - $[RuCl_2(4\text{-}R_2P)(DBT)]_2$", *J. Am. Chem. Soc.*, 1984, 106, 5379-5381.

43. M. G. Choi and R. J. Angelici, "Kinetic studies of PPh_3 substitution of sulfur-coordinated thiophene in $Cp'(CO)_2Re(Th)$ - a model for adsorption onto HDS catalysts", *Inorg. Chem.*, 1991, 30, 1417-1419.

44. K. M. Rao, C. L. Day, R. A. Jacobson and R. J. Angelici, "η^1(S)- and η^6-coordination of dibenzothiophene (DBT) in $Cp^*MCl_2[\eta^1(S)\text{-DBT}]$ and $Cp^*M(\eta^6\text{-DBT})^{2+}$ (M = Ir, Rh)", *Inorg. Chem.*, 1991, 30, 5046-5049.

45. E. O. Fischer, H. A. Goodwind, C. G. Kreiter, H. D. Simmons, K. Sonogashira and S. B. Wild, "Aromatic complexes of chromium tricarbonyl,",*J. Organomet. Chem.*, 1968, 14, 359-374.

46. C. C. Lee, B. R. Steele and R. G. Sutherland, "Ligand exchange of some heterocyclic analogues of fluorene and anthracene with ferrocene", *J. Organomet. Chem.*, 1980, 186, 265-270.

47. C. M. J. Wang and R. J. Angelici, "Synthesis and reactivity of ruthenium complexes with dibenzothiophene and hexahydrodibenzothiophene ligands - models for catalytic HDS", *Organometallics*, 1990, 9, 1770-1777.

48. W. Hieber and C. Scharfenberg, *Ber.* 1940, 73, 1012.

49. S. A. Khattab, L. Markó, G. Bor and B. Markó, "Sulfur-containing metal carbonyls - a mixed cobalt-iron carbonyl sulfide", *J. Organomet. Chem.*, 1964, 1, 373-376.

50. H. D. Kaesz, R. B. King, T. A. Manuel, L. D. Nichols and F. G. A. Stone, "Chemistry of the metal carbonyls: The desulfurisation of thiophene", *J. Am. Chem. Soc.*, 1960, 82, 4749.

51 G. Dettlof and E. Weiss, "Crystal structure, ^1H NMR and mass spectrum of tricarbonylferracyclopentadiene-tricarbonyl", *J. Organomet. Chem.*, 1976, 108, 213-223.

52. P. Hübener and E. Weiss, "Crystal structure and spectroscopic study of tricarbonylmethylferrathiacyclohexadiene-tricarbonyl", *J. Organomet. Chem.*, 1977, 129, 105-115.

53. A. E. Ogilvy, M. Draganjac, T. B. Rauchfuss and S. R. Wilson, "Activation and deactivation of thiophene and benzothiophene by iron carbonyls", *Organometallics,* 1988, 7, 1171-1178.

54. A. J. Arce, P. Arrojo, A. J. Deeming, Y. De Sanctis, "Desulfurisation of thiophenes with ruthenium clusters", *J. Chem. Soc., Dalton Trans.*, 1992, 2423-2424.

55. A. J. Arce, Y. De Sanctis, M. W. Day, K. I. Hardcastle and A. J. Deeming, "Triosmium clusters formed by oxidative addition and decarbonylation of 2-formylpyrrole - crystal structures of 3 triosmium clusters containing aromatic and non-aromatic heterocyclic ligands derived from pyrrole", *Organometallics,* 1990, 9, 6-12.

56. J. Chen, V. G. Young, R. J. Angelici, "Reactions of the iridathiabenzene complex Cp^*Ir(2,5-dimethylthiophene) with $Co_2(CO)_8$, $Co_4(CO)_{12}$, and $(\eta^6$-$C_6H_3Me_3)Co_4(CO)_9$", *Organometallics,* 1996, 15, 1414-1421.

57. W. D. Jones and R. M. Chin, "Hydrodesulfurisation of thiophene to butadiene and butane by a homogeneous iridium complex", *J. Am. Chem. Soc.*, 1994, 116, 198-203.

58. H. Alper and C. Blais, "Removal of sulfur from fuels by molybdenum hexacarbonyl on silica", *Fuel*, 1980, 59, 670.

59. J. J. Eisch, L. E. Hallenbeck and K. I. Han, "Organic chemistry of subvalent transition metal complexes - HDS of organosulfur heterocycles by metal hydride nickel(0) complexes - accelerated single-electron transfer in C-S bond cleavage", *J. Am. Chem. Soc.*, 1986, 108, 7763-7767.

60. A. J. Arce, Y. De Sanctis, A. Karam and A. J. Deeming, "Desulfurisation of benzothiophene by S/Ru exchange: Formation and structure of the cluster $[Ru_3(CO)_8(C_8H_6)]$", *Angew. Chem. Int. Ed. Engl.*, 1994, 33, No. 13, 1381-1383.

61. W. D. Jones and R. M. Chin, "Carbon-sulfur bond cleavage by cobalt. Reaction of $Cp^*Co(C_2H_4)_2$ with dibenzothiophene", *J. Organomet. Chem.*, 1994, 472, 311-316.

62. F. Fringuelli and A. Taticchi, "Tellurophene and some of its derivatives", *J. Chem. Soc., Perkin Trans. 1*, 1972, 199-203.

63. G. Pilcher and H. A. Skinner, Ed. F. R. Hartley and S. Patai, "The Chemistry of the metal-carbon bond, Vol 1", John Wiley and Sons, 1982, 69.

64. M-G, Choi and R. J. Angelici, "Synthesis, reactivity and ^{77}Se NMR studies of the η^2- and η^1(Se)-selenophene complexes $Cp'(CO)_2Re(Sel)$", *J. Am. Chem. Soc.*, 1991, 113, 5651-5657.

65. C. J. White, T. Wang, R. A. Jacobson and R. J. Angelici, "Synthesis, equilibrium binding and ^{77}Se NMR studies of η^1-selenophene complexes", *Organometallics*, 1994, 13, 4474-4480.

66. N. Pozdeev, O. Akulinin, A. Shapkin and N. Magdesieva, *Dokl. Akad. Nauk SSSR*, 1969, 1851, 384.

67 R. Brown and J. Crofts, *Chem. Phys.*, 1973, 1, 217.

68. G. Marino, *Chem. Scripta*, 1975, 8A, 23.

69. F. Fringuelli, G. Marino and A. Taticchi, "A comparative study of the aromatic character of furan, thiophene, selenophene and tellurophene", *J. Chem. Soc., Perkin Trans. 2*, 1974, 332-337.

70. F. Fringuelli, G. Marino, G. Savelli and A. Taticchi, *J. Chem. Soc., Chem. Commun.*, 1971, 1441.

71. H. J. Gysling, "The ligand chemistry of tellurium", *Coord. Chem. Rev.*, 1982, 42, 133-239.

72. G. T. Morgan and F. H. Burstall, "Cyclotellurobutane", *J. Organomet. Chem.*, 1931, 180-184.

73. E. H. Braye, W. Hübel and I. Caplier, "New unsaturated heterocyclic systems", *J. Am. Chem. Soc.*, 1961, 83, 4406-4413.

74. R. Pettit, "Metal complexes with 2,2,1-bicycloheptadiene", *J. Am. Chem. Soc.*, 1959, 81, 1266-12669.

75. W. Hieber and T. Kruck, "Telluroganyl-haltige metallcarbonyle", *Chem. Ber.*, 1962, 95, 2027-2041.

76. K. Öfele and E. Dotzauer, "Metal complexes of tellurophenes", *J. Organomet. Chem.*, 1972, 42, C87-C90.

77. K. Öfele, *Chem. Ber.*, 1966, 99, 1732.

78. K. Öfele and E. Dotzauer, "$Cr(CO)_3$-π-complex of pyrrole and pyrrole derivatives", *J. Organomet. Chem.*, 1971, 30, 211-220.

79. S. E. Livingstone, "Metal complexes of ligands containing sulfur, selenium or tellurium donor atoms, *Quart. Rev.*, 1965, 19, 386-425.

80. R. B. King, P. M. Treichel and F. G. A. Stone, "Chemistry of the metal carbonyls. New Organosulfur derivatives of iron and cobalt", *J. Am. Chem. Soc.*, 1961, 83, 3600-3604.

81. W. Mack, *Angew. Chem (Ger),* 1965, 77, 260.

82. K. Akashi, Y. Hayashi, T. Arakawa, T. Kimura, H. Kobayashi, "Photothermographic photosensitive materials", Japanese Patent 78, 143, 216, Asahi Chemical Industry, 1978; *Chem. Abstr.*, 1979, 90, 596-597, ref. 195607s.

83. Y. Hayashi, T. Arakawa, T. Shiga, M. Ozaki, H. Kobayashi, "Organic tellurium-silver complexes", Japanese Patent 78, 65, 827, Asahi Chemical Industry, 1978; *Chem. Abstr.*, 1978, 89, 580, ref. 146588g.

84. O. Haas and A. Von Zelewsky, "Formation of adducts of O-, S,- Se-, Te-, N- and P-bases with a planar low-spin cobalt (II) complex", *J. Chem. Res.* (M), 1980, 1201.

85. A. J. Arce, R. Machado, C. Rivas and Y. De Sanctis, "Extrusion of selenium and tellurium atoms from selenophene and tellurophene by reaction with trinuclear iron, ruthenium and osmium clusters", *J. Organomet. Chem.*, 1991, 419, 63-75.

86. D. Himmelreich and G. Müller, "Oxidative addition of furan to a triosmium cluster - the crystal structure of $[(HOs(CO)_{10}(\mu, \eta^2\text{-}C_4H_3O)]$", *J. Organomet. Chem.*, 1985, 297, 341-348.

87. P. Monsef-Mirzai, N. T. Bailey and G. J. Lawson, "The use of microwave heating in the acetylation of coals", *Fuel,* 1990, 69, 533-534.

88. P. Monsef-Mirzai, M. Ravindran, W. R. McWhinnie and P. Burchill, "The use of microwave heating for the pyrolysis of coal via inorganic receptors of microwave energy", *Fuel*, 1992, 71, 716-717.

89. W. Lohner and K. Praefcke, "An improved synthesis of tellurophene", *Chem. Ber.*, 1978, 111, 3745-3746.

90. J. D. McCullough, "Dibenzotellurophene. A new synthesis by way of 2-biphenyltellurium trichloride", *Inorg. Chem.*, 1975, 14, 2285-2286.

91. A. Yanagisawa and S. Suga, "Syntheses of dibenzo[1,2]diselenin and related novel chalcogenide heterocyclic compounds", *J. Heterocyclic Chem.*, 1991, 28, 433-438.

92. (a) R. F. Ziolo and W. H. H. Gunther, "The synthesis and characterisation of α and β-1,1-diido-3,4-benzo-1-telluracyclopentane", *J. Organomet. Chem.*, 1978, 146, 245-251.

(b) A. Z. Al-Rubaie and W. R. McWhinnie, "The syntheses and spectroscopic examination of telluronium salts based on the 1-organo-3,4-benzo-1-telluracyclopentane cation", 1982, 234, 287-298.

93. H. D. K. Drew, "Cyclic Organometallic compounds", *J. Chem. Soc.*, 1926, 223-231.

94. (a) W. Hübel and E. Weiss, "New organo-iron carbonyls", *Chemistry and Industry*, 1959, 703.

(b) W. Hübel and E. H. Braye, *J. Inorg. Nucl. Chem.*, 1959, 10, 250.

95 M. L. H. Green, L. Pratt and G. Wilkinson, "Spectroscopic studies of some organo-iron compounds", *J. Chem. Soc.*, 1960, 989-997.

96. K. Singh, W. R. McWhinnie, H. L. Chen, M. Sun and T. A. Hamor, "Reactions of heterocyclic organotellurium compounds with triiron dodecacarbonyl: reactions of thiophenes revisited", *J. Chem. Soc., Dalton Trans.*, 1995, 1545-1549.

97. (a) W. Hieber and J. J. Gruber, *Z. Aorg. Allg. Chem.*, 1958, 296, 91.

(b) D. A. Lesch and T. B. Rauchfuss, "Isolation and characterisation of $Fe_2(\mu\text{-}Te_2)(CO)_6$ and its conversion to $Fe_3(\mu_3\text{-}Te)_2(CO)_x$ (x = 9, 10)", *Inorg. Chem.*, 1981, 20, 3583-3585.

98. G. M. Sheldrick, "Foundations of crystallography", *Acta Cryst., Sect. A*, 1990, 46, 467-473.

99. TEXSAN, Single Crystal Analysis Software, version 1.6, Molecular Structure Corporation, 3200 Research Forest Drive, TX 77381, USA, 1993.

100. G. M. Sheldrick, SHELXL-93, Program for Crystal Structure Refinement, University of Göttingen, 1993.

101. N. Walker and D. Stewart, "An empirical method for correcting diffractometer data for absorption effects", *Acta. Cryst. Sect. A*, 1983, 39, 158-166.

102. W. D. S. Motherwell and W. Clegg, University of Cambridge, 1988.

103. H. B. Chin and R. Bau, "Molecular structure of (1,7-cyclododecadiyne) hexacarbonyl diiron", *J. Am. chem. Soc.*, 1973, 95, 5068-5070.

104. F. H. Allen, J. E. Davies, J. J. Galloy, O. Johnson, O. Kennard, C. F. Macrae, E. M. Mitchell, G. F. Mitchell, J. M. Smith and D. G. Watson, "The development of version 3 and version 4 of the CSD system", *J. Chem. Inf. Comp. Sci.*, 1991, 31, 187-204.

105. F. A. Cotton, V. W. Day, B. A. Frenz, K. I. Hardcastle and J. M. Troup, "Conformations of fused cycloalkanes in organometallic complexes", *J. Am. Chem. Soc.*, 1973, 95, 4522-4528.

106. M. R. Churchill and R. Mason, *Proc. R. Soc., London, Ser. A*, 1967, 301, 433.

107. E. Cuthbertson and D. D. MacNicol, "Tellurium extrusion: synthesis of benzocyclobutene and naphtho[b]cyclobutene", *Tetrahedron Lett.*, 1975, No. 24, 1893-1894.

108. P. Monsef-Mirzai, W. R. McWhinnie, M. C. Perry and P. Burchill, "Measurement of-OH groups in coal of different rank using microwave technology", *Fuel*, 1995, 74, 674-683.

109. D. M. P. Mingos and D. R. Braghurst, "The applications of microwave dielectric effects to synthetic problems in chemistry", *Chem. Soc. Rev.*, 1991, 20, 1-47.

110. S. Luo, A. E. Skaugset, T. B. Rauchfuss and S. R. Wilson, "Redistribution of reduced thiophene ligands in the conversion of $(C_5R_5)Rh(\eta^4\text{-}C_4Me_4S)$ to $[(C_5R_5)Rh]_3(\eta^4,\eta^1\text{-}C_4Me_4S)_2$", *J. Am. Chem. Soc.*, 1992, 114, 1732-1735.

111. J. W. Kang, K. Moseley, P. M. Maitlis, "Penatamethylcyclopentadienyl-rhodium and -iridium halides. Synthesis and properties", *J. Am. Chem. Soc.*, 1969, 91, 5970-5977.

112. M. H. Chisolm and S. Godleski, "Application of C-13 NMR in inorganic chemistry", *Prog. Inorg. Chem.*, 1976, 20, 299-436.

113. C. K. Johnson, ORTEP, Report ORNL-5138, Oak Ridge National Laboratory, Oak Ridge, TN, USA, 1976.

114. Cambridge Structural Database System, April 1996 release, Cambridge Crystallographic Data Centre, 12 Union Road, Cambridge, UK.

115. S. Schulz, M. Andruh, T. Pape, T. Heinze, H. W. Roesky, L. Haming, A. Kuhn and R, Herbst-Irmer, "Facile synthesis of selenium containing and tellurium containing metal cubanes", *Organometallics*, 1994, 13, 4004-4007.

116. M. D. Vaira, M. Peruzzini and P. Stoppioni, "Synthesis and structure of dirhodium compounds featuring an end-on bridging ditellurium", *Inorg. Chem.*, 1989, 28, 4614-4619.

117. M. Divaira, M. Peruzzini and P. Stoppioni, "Hydrochalcogenide and hydride hydrochalcogenide derivatives of rhodium", *Inorg. Chem.*, 1991, 30, 1001-1007.

118. C. Perthuisot and W. D. Jones, "Catalytic hydrogenolysis of an aryl-aryl carbon-carbon bond with a rhodium complex", *J. Am. Chem. Soc.*, 1994, 116, 3647-3648.

119. J. D. McCullough, "Crystal and molecular structure of dibenzotellurophene", *Inorg. Chem.*, 1975, 14, 2639-2643.

120. F. H. Allen, D. G. Watson, L. Brammer, D. G. Orpen and R. Taylor, "Tables of bond lengths determined by X-ray and neutron diffraction", *J. Chem. Soc., Perkin Trans.* 2, 1987, S1-S19.

121. (a) C. W. Bird, G. W. H. Cheeseman and A. A. Sarsfield, *J. Chem. Soc. Pt 4,* "2,1,3-Benzoselenadiazoles as intermediates in o-phenylenediamine synthesis", 1963, 4767-4770.

(b) C. W. Bird and G. W. H. Cheeseman, "The infrared spectra and structure of 2,1,3-benzoselenadiazoles", *Tetrahedron*, 1964, 20, 1701-1705.

122. H. B. Singh, "Charge transfer in organotellurium chemistry", Ph.D. Thesis, 1983, 95-96.

123. (a) R. Weber, J. Piette and M. Renson, "A novel heterocycle of tellurium: the 1,2-benzisotellurazole", *J. Heterocyclic Chem.*, 1977, 15, 865-867.

(b) J. Piette, R. Lysy and M. Renson, "Halogens of aromatic tellurenyls and tellurocyanates", *Bull. Soc. Chim. France*, 1972, No. 559, 3559-3561.

(c) A. G. Maslakov, W. R. McWhinnie, M. C. Perry, N. Shaikh, S. L. W. McWhinnie and T. A. Hamor, "Reactions of some ortho-tellurated compounds with intramolecular co-ordinate bonds", *J. Chem. Soc., Dalton Trans.*, 1993, 619-623.

124. (a) T. Junk and K. J. Irgolic, "2-methylareno[d]-3-azatellurophenes", *Phosphorus and Sulfur and the related elements*, 1988, 38, 121-135.
(b) R. Przyklek-Elling and W. H. H. Gunther, Eastman Kodak Co., U. S. Patent 4,661,438, 28 Apr. 1987.

125. Cambridge Structural Database, October 1995 release, Cambridge Crystallographic Data Centre, 12 Union Road, Cambridge, UK.

126. D. Bucholz, G. Huttner, L. Zsolnai and W. J. Imhof, "New methods for the introduction of μ_3-chalcogen elements in metallic carbonyl clusters", *J. Organomet. Chem.*, 1989, 377, 25-41.

127. D. Lentz and R. Marschall, "New mechanism for fluxionality in triiron carbonyl clusters", *Organometallics*, 1991, 10, 1487-1496.

128. F. Ragaini, J. S. Song, D. L. Ramage, G. L. Geoffroy, G. A. P. Yap and A. L. Rheingold, "Radical processes in the reduction of nitrobenzene promoted by iron carbony;l clusters", *Organometallics*, 1995, 14, 387-400.

129. J. S. Song, S. H. Han, S. T. Nguyen, G. L. Geoffroy and A. L. Rheingold, "Reactivity of Fe_3 and Ru_3 μ_3-phenylimide clusters with alkynes, allene and 1,3-cyclohexadiene", *Organometallics*, 1990, 9, 2386-2395.

130. (a) M. Tasi, A. K. Powell and H. Vahrenkamp, "2 Ferrole isomers in equilibrium - experimental confirmation of an old hypothesis", *Angew. Chem. Int. Ed. Engl.*, 1989, 28, 318-319.
(b) M. Tasi, A. K. Powell and H. Vahrenkamp, "Conversion of the clusters $Fe_3(CO)_9(\mu_3,\eta^2\text{-}N_2Et_2)$ and $Fe_3(CO)_9(\mu_3\text{-}NEt)_2$ into organic products", *Chem. Ber.*, 1991, 124, 1549-1557.

131. C. A. Mirkin, K. L. Lu, T. E. Snead, B. A. Young, G. L. Geoffroy, A. L. Rheingold and B. S. Haggerty, "Preparation and interconversion of binuclear 2-ferrazetine and isomeric ferrapyrrolinone complexes", *J. Am. Chem. Soc.*, 1991, 113, 3800-3810.

132. R. G. Teller, J. M. Williams, "Crystal and molecular structure of bis[dicarbonyl(p-pentamethylcyclopentadienyl)iron] and structural comparisons with the non-methylated analogue", *Inorg. Chem.* , 1980, 19, 2770-2773.